Investigating *Zfhx3* function in the mouse brain: Characterising dopamine-related behavioural and molecular functions

A thesis submitted for the degree of Doctor of Philosophy by

Paige Street

Mammalian Genetics Unit, MRC Harwell

Department of Physiology, Anatomy, and Genetics

Wolfson College Oxford

Abstract

Zinc finger homeobox 3 (*Zfhx3*) is a brain-region enriched transcription factor that binds to AT motifs in promoter and enhancer regions. *Zfhx3* has been shown, using mouse models, to have an important role in transcriptional regulation of neuropeptides and their receptors within the suprachiasmatic nucleus (SCN), allowing for the maintenance of typical circadian rhythms. In humans, coding sequence mutations have been linked to a range of diseases, including schizophrenia.

In addition to the SCN, data from the Allen Brain Atlas show *Zfhx3* expression within dopaminergic regions in the mouse midbrain. Given the dopaminergic hypothesis of schizophrenia, and the genetic associations, we wish to elucidate the contribution of *Zfhx3* to schizophrenia-related behavioural changes in mice.

We established a DAT-*Cre* (dopamine active transporter) driven *Zfhx3* knockout mouse – a conditional knockout mouse model which deletes *Zfhx3* in dopaminergic cells only. We also generated a *Zfhx3* knockout mouse cohort via injection of *Cre*-expressing adeno-associated virus (AAV) into the ventral tegmental area of *Zfhx3*-floxed mice – targeting the origin of key dopaminergic pathways.

These mice have been subject to a behavioural phenotype pipeline focused on schizophrenia-related endophenotypes, then sub-dissected midbrain and dopamine pathway terminus brain regions have undergone molecular analysis to investigate changes in gene expression.

We discuss the biological relevance of these findings, particularly in how they relate to dopaminergic function in physiology and disease.

Acknowledgements

This DPhil has been a…challenge. The fact that I am even sitting here writing an acknowledgements page at all is an honest-to-god miracle, thanks almost entirely to the amazing people I have around me.

First and foremost I would like to thank my two supervisors, Dr Patrick Nolan and Dr Gareth Banks, for so many things. Thank you for giving me the chance to work on this project, through which I've learned so much, and for giving me unending support and kindness in my most turbulent moments.

I am immensely grateful for all of the Nolan Lab post-docs - the expertise they imparted, and the time they gave to me and my training: (Dr.) Nora Bourbia, Petrina Lau, Minghui Yin, Akanksha Bafna, and Nicole Morrissey. I count myself as very fortunate to have been part of such a talented and generous team. I would like to give special thanks to Akanksha, who guided me through so many unfamiliar areas with unrelenting patience, when we were the only Nolans left post-closure and stress was high for us both.

It is impossible to pin down only a few people to thank from the Mary Lyon Centre, as working with the wonderful and dedicated people there was both a pleasure and a privilege. However as promised I would like to give a specific shout-out to Eddie Chambers, the best rodent anaesthetist of all time, and an impressive dancer.

I could write a whole chapter on how much my friends have uplifted me during this time, all of the 'girls' (a loose term for the range of genders involved) of the 'Bae Bay' who would make so much noise, even in the middle of the workday. I don't

think I would've even bothered coming in most days if you weren't all there to say (or hear me say) something completely unprofessional, at an exceptional volume.

A special note to the hilarious, creative, and all-round fantastic adventurers and DMs I played Dungeons and Dragons with during this time (even the ones that nagged me to write my thesis and stop messaging about lore). Anyone who plays D&D knows how special the game, and your party, are to your life. Thank you to my current character Sunny Le Clay, the no-good, gun-toting, bath-dodging steampunk, who accompanied me throughout my thesis writing and kept me sane.

My spectacular partner of 6 years does not want to be mentioned, completely ignoring how terrible that makes me look. Thank you for not murdering me during these last few months.

Ultimately, I would like to express how grateful I am to my family. To my parents Trudi and Christine, thank you from the bottom of my heart for literally everything. To my brother Connor, thank you for being the family life coach, and for never failing to make me laugh with your antics. To Bonnie, a dog who is more of a person than most people I know, thank you for comforting me when no human could.

This thesis is dedicated to my late granddad Brian 'Bill' Street, an eccentric man who was loved by all. Thank you for always believing in me.

Contents

Figure List

Table List

List of abbreviations

6-OHDA	6-hydroxydopamine
AAV	Adeno-associated virus
ADHD	Attention Deficit/Hyperactivity Disorder
AFP	Human α-fetoprotein
ALS	Amyotrophic lateral sclerosis
APP	Amyloid-β protein precursor
Atbf1	AT-motif binding factor 1
ATM	Ataxia telangiectasia mutated
ATP	Adenosine triphosphate
Au1	Primary auditory cortex
Avp	Arginine vasopressin
cAMP	Cyclic adenosine monophosphate
Cre	Cre recombinase
DAT	Dopamine active transporter
ENU	N-ethyl-N-nitrosourea
FASTQ	Sample pair sequence files
fTIR	Frustrated total internal reflection
GABA	Gamma-Aminobutyric Acid
GABBR2	Gamma-Aminobutyric Acid Type B Receptor Subunit 2
Gpcr50	G protein-coupled receptor 50
GRIN2A	Glutamate Ionotropic Receptor NMDA Type Subunit 2A
HA	Hibernate-A
hSyn	Human synapsin 1
HTT	Huntingtin
ISH	in-situ hybridisation
MPTP	1-methyl-4-phenyl-1,2,3,6-tetrahydropyridine
MUC5AC	Mucin 5AC
NADH	Nicotinamide adenine dinucleotide
NB-A	Neurobasal A medium complete
NDUFA	NADH:ubiquinone oxidoreductase
NMDA	N-methyl-D-aspartate
NOR	Novel object recognition
Npy	Orexigenic neuropeptide Y
PDGFRB	Platelet derived growth factor receptor beta
PIAS3	Protein inhibitor of activated STAT 3
PLL	Poly-L-lysine hydrobromide
PQ	Paraquat
Rbm39	RNA-binding protein 39

RNA-STAR	Spliced Transcripts Alignment to a Reference
ROS	Reactive oxygen species
rRNA	Ribosomal RNA
SCN	Suprachiasmatic nucleus
SG	SYBR Green I
SN	Substantia nigra
SNc	Substantia nigra pars compacta
SNP	Single nucleotide polymorphism
SNV	Single nucleotide variant
STAT3	Signal transducer and activator of transcription 3
STG	Superior temporal gyrus
STRING	Search Tool for the Retrieval of Interacting Genes/Proteins
SynGO	Synaptic Gene Ontologies
TH	Tyrosine hydroxylase
tRNA	Transfer RNA
Tshr	Thyroid-stimulating hormone receptor
UBC CreERT2	Human ubiquitin C promoter
Vip	Vasoactive intestinal peptide
VTA	Ventral tegmental area
Zfhx3	Zinc finger homeobox 3
$Zfhx3^{Sci}$/Sci	Short-circuit
τDD	Circadian period

1

Introduction

1

Introduction

1.1 Zinc Finger Homeobox 3

1.1.1 Discovery

Zinc finger homeobox 3 (*Zfhx3*) – otherwise historically known as AT-motif binding factor 1 (*Atbf1*) - is a large transcription factor that has been reported to bind to AT-rich core sequences in both gene promotor and enhancer regions. *Zfhx3* was initially identified as a transcriptional regulator of the human α-fetoprotein gene (AFP) by binding to the gene enhancer AT-motif, supressing transcriptional activation of AFP (Morinaga, Yasuda et al. 1991, Yasuda, Mizuno et al. 1994).

Zfhx3 expresses two protein isoforms, a long 404kDa protein (ZFHX3-A), and a short 306kDa protein (ZHFX3-B). The shorter protein isoform ZFHX3-B was the first to be discovered, as transcriptional regulator to AFP expression, and contains 4 homeodomains and 18 zinc fingers. The longer isoform ZFHX3-A was discovered later, containing 4 homeodomains, 23 zinc fingers, and a pseudo zinc finger (Miura, Tam et al. 1995).

Expression of the two isoforms is controlled by alternative promoter usage, to produce two splice variants. ZFHX3-A has a neuron-specific promotor, and ZFHX3-A has been reported to be preferentially expressed in the developing rat brain over ZFHX3-B. Therefore in this study, which is centred on the mouse brain,

only the ZFHX3-A isoform will be discussed (Miura, Tam et al. 1995, Ishii, Kawaguchi et al. 2003).

Figure 1.1.1.1. shows the structure of ZFHX3-A, highlighted with multiple loci of interest, in both humans and mouse models, that are expanded upon further in this chapter.

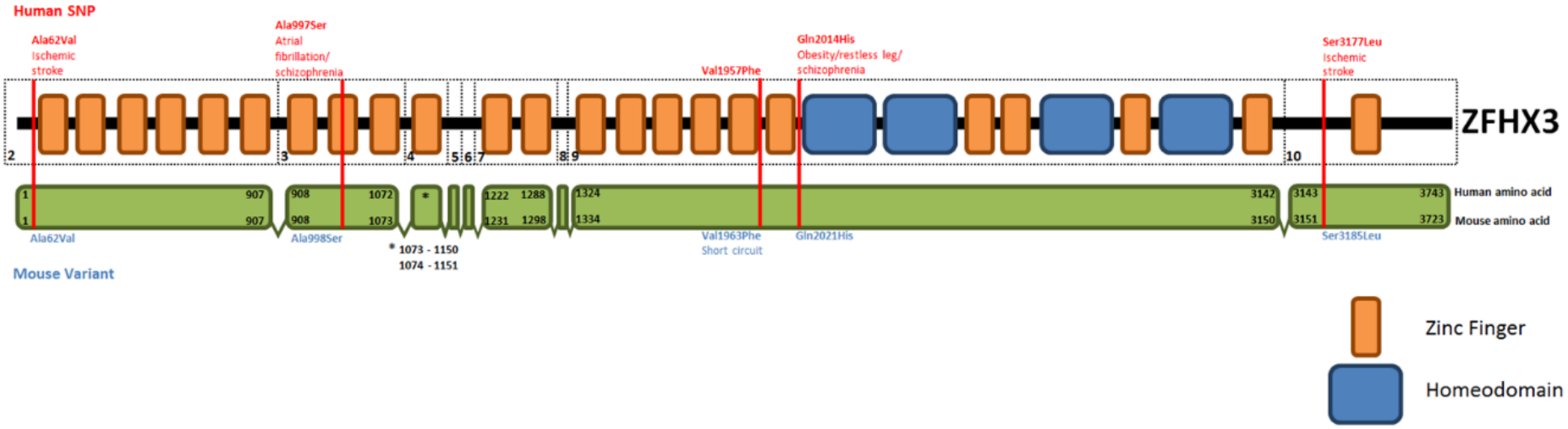

Figure 1.1.1.1.: A schematic of the ZFHX3-A protein, taken from UniProtKB - Q15911 (ZFHX3_HUMAN). Orange boxes represent zinc finger motifs and blue boxes represent homeodomains. The map is split into coding exons, marked by the dotted boxes labelled with black numbers. The green map shows the amino acid numbers associated with the beginning and end of each coding exon in both the human and mouse ZFHX3. The red markers show the locations of several disease-associated SNP variants found via GWA studies, with the human variation shown in red text above the map and the corresponding amino acid change on the mouse protein shown below the map in blue. Also included is the position of the 'short circuit' mutation found in mice that leads to a circadian phenotype, and the corresponding human amino acid position.

1.1.2 Developmental Role

Zfhx3 has many roles in development – heterozygous deletion of *Zfhx3* in mice can cause preweaning mortality (Sun, Fu et al. 2012). Some developmental roles include: enterocyte differentiation in the villi crypts (Kataoka, Joh et al. 2000); regulating the differentiation of myoblasts (Berry, Miura et al. 2001); regulating differentiation of pituitary cell types via *Pit1* (Qi, Ranish et al. 2008); and development of post-pubertal mammary glands (Li, Fu et al. 2012). Recently, a Six3-*Cre*; *Zfhx3*-Flox line – which deletes *Zfhx3* in the suprachiasmatic nucleus (SCN) from early stages in its development – has shown a completely arrhythmic circadian phenotype, and further investigation uncovered that neurons within the SCN lacked typical SCN-neuron identity markers (*Introduction 1.1.4.2.*)(Wilcox, Bains et al. 2021).

Spatio-temporal expression studies in the mouse CNS reports that *Zfhx3* expression is both temporally and spatially regulated. It is regionally expressed in the developing mouse brain, with a peak of expression at E13-15 and a decline until post-natal day 28, when expression is dramatically reduced while retaining discrete regions of high expression (Watanabe, Miura et al. 1996). Expression is reported in this study to be regionally restricted, with highest levels of expression in the thalamus and inferior colliculus, and no expression observed in the olfactory bulb, hippocampus, or cerebral cortex. However, when considering this data it is worth noting that a reliable antibody for ZFHX3 is a more recent development than this study.

There is evidence to show that *Zfhx3* plays a role in regulation of neuronal cell differentiation. One study suggests that ZFHX3 is initially expressed in the

cytoplasm where it supresses nestin, and as the cell engages with the developing extracellular matrix ZFHX3 localises in the nucleus, where it promotes expression of the *Neurod1* gene. This mechanism induces cell cycle arrest, which is a key stage of neuronal differentiation. (Jung, Kim et al. 2005).

Together these findings suggest that not only does *Zfhx3* have a role in regulating neuron differentiation, but that the region-specific nature of expression indicates that *Zfhx3* is involved in the differentiation and maintenance of region-specific neuronal subpopulations.

1.1.3 Adult function and dysfunction

1.1.3.1 Cancer

Changes in ZFHX3 expression levels and cellular distribution have been linked to a variety of cancer types – with reduced expression and non-nuclear localisation being biomarkers for poor prognosis. *Zfhx3* has therefore been classified as a tumour suppressor gene, and identified as one of multiple tumour suppressor genes at chromosomal location 16q22:

- *Gastric cancer*: ZFHX3 is reported to be absent in gastric cancer cells that show high levels of AFP expression – as ZFHX3 is a transcriptional regulator of AFP. AFP-producing gastric cancer cells have higher malignancy, and patients with AFP^{+} cancer cells show poorer rates of survival (Kataoka, Miura et al. 2001). ZFHX3 shows a similar mechanism in regards to mucin 5AC - gastric cancers that express MU5AC have a poorer

prognosis, and the presence of ZFHX3 expression in cancer cell nuclei significantly suppressed MUC5AC expression (Mori, Kataoka et al. 2007).

- *Cervical cancer*: expression of ZFHX3 is reported in cervical cancer cells, however it is absent in typical cells. It is theorised that *Zfhx3* is involved in the pathogenesis process of the cancer (Li, Huang et al. 2002).
- *Breast cancer*: high *Zfhx3* mRNA expression levels were correlated with better prognosis, with high levels reported in patients without metastasis to the lymph nodes (Zhang, Yamashita et al. 2005).
- *Prostate cancer*: downregulation and deleterious mutations are observed in in *Zfhx3* in cancerous cells, especially in higher-grade tumours (Sun, Frierson et al. 2005).
- *Lung cancer*: in non-small cell lung cancer, low ZFHX3 expression in cancer cells has been shown to be a predictor of lower 5-year survival rate, and is positively correlated to metastasis to lymph nodes (Minamiya, Saito et al. 2012). Mutations in *Zfhx3* have also been shown to predict longer overall survival of non-small cell lung cancer patients undergoing immune checkpoint inhibitor treatment (Zhang, Zhou et al. 2021).
- *Skin cancer: Zfhx3* has been proposed to be a potential prognostic marker for skin cancer, as nuclear expression of ZFHX3 in cells indicates lower rates of malignancy. This is because ZFHX3 is a non-direct inhibitor of signal transducer and activator of transcription 3 (STAT3) – which is key to the survival and proliferation of skin cancer cells (Nishio, Miura et al. 2012).
- *Head and neck squamous cell cancer:* decreased nuclear localisation, and increased cytoplasmic localisation of ZFHX3 was seen in more invasive tumours (Sun, Li et al. 2013).

- *Endometrial cancer:* deleterious *Zfhx3* mutations were found in a statistically significant proportion of tumours. These tumours were of higher grade than tumours without mutations, and patients showed more frequent lymphatic metastasis, and reduced overall survival (Walker, Miranda et al. 2015).
- *Urothelial bladder cancer:* expression of ZFHX3 in the cytoplasm, as opposed to the nucleus, was correlated to higher cancer malignancy and worse prognosis (Kawaguchi, Hara et al. 2016).
- *Mucinous salivary adenocarcinoma:* a missense mutation on the 22nd zinc finger of *Zfhx3* was found in mucinous salivary adenocarcinoma cells, amongst other deleterious mutations in many other tumour suppressor genes (Panaccione, Zhang et al. 2017).

1.1.3.2 Protein-protein interaction

Alongside being a DNA-binding protein, ZFHX3 also interacts with other proteins: binding to both the retroviral (v-) and cellular (c-) MYB oncoproteins, repressing the transcriptional activity of v-Myb (Kaspar, Dvoráková et al. 1999); binding to protein inhibitor of activated STAT 3 (PIAS3), enhancing its inhibition of STAT3 (Nojiri, Joh et al. 2004); and binding to amyloid-β protein precursor (APP) (Uhm, Kim et al. 2015).

1.1.3.3 Oxidative Stress

ZFHX3 knockdown may indirectly affect mitochondrial function, leading to an increase in reactive oxygen species (ROS) in the cell.

Zfhx3 has been implicated in atrial fibrillation via GWAS – a condition which is associated with mitochondrial dysfunction, leading to increased ROS (Youn, Zhang et al. 2013). ZFHX3 knockdown in cardiomyocytes leads to increased arrhythmogenesis, alongside dysregulation of calcium homeostasis - which is essential to typical mitochondrial function (Kao, Hsu et al. 2016).

Zfhx3 has also been implicated in the protection of cerebellar neurons from oxidative stress. ROS caused by neuron excitation have been shown to play a factor in the pathology of neurodegenerative diseases (Coyle and Puttfarcken 1993). For example, the neurodegenerative disorder ataxia telangiectasia, characterised by degeneration of the cerebellum, is caused by mutations in ataxia telangiectasia mutated (ATM) gene (Savitsky, Bar-Shira et al. 1995). Oxidative stress in neurons, caused by excessive excitation, activates ATM in the cytoplasm, and downregulation of ATM has been shown to lead to excessive ROS in the cell (Alexander, Cai et al. 2010). It has been reported that ATM indirectly positively regulates ZFHX3 expression, which regulates platelet derived growth factor receptor beta (PDGFRB) expression, which PDGFRB then in turn activates the neuroprotective ATM.

1.1.3.4 Genome-wide association studies

Zfhx3 is expressed in other tissues in addition to the brain. It has been extensively studied as part of GWAS, linking *Zfhx3* variants to a range of human diseases, including:

- *Kawasaki disease*; which is a childhood vascular inflammatory condition induced by infection in genetically vulnerable children. In a Japanese population study, multiple intronic SNPs of *Zfhx3* were associated with the disease, with 3 SNPs found to be protective (Burgner, Davila et al. 2009).
- *Ischemic and cardioembolic stroke*; are where there is an interruption of blood flow to the brain. Variants were often closely associated or overlapping between the two stroke types, with multiple variants found in Icelandic, Nordic, North American, German, and British population cohorts (Gudbjartsson, Holm et al. 2009, Bevan, Traylor et al. 2012) – and additionally in a multi-national database of Caucasian and South Asian subjects (Malik, Traylor et al. 2016).
- *Atrial fibrillation*; a condition where the heart has an irregular rhythm, affecting the upper chambers. 1 intronic variant and 2 exonic missense variants were found to be associated with atrial fibrillation, in multiple genetic databases (Benjamin, Rice et al. 2009, Tsai, Hsieh et al. 2015).
- *Atherosclerosis*; which is the hardening of the arteries with plaque deposits. 1 SNP in *Zfhx3* has been found in a study of cohorts from the USA (Chou, Shulman et al. 2013).
- *Cardiovascular disease*; which is a term that encompasses multiple diseases of the heart, including myocardial infarction. Multiple studies in Asian populations found a range of *Zfhx3* variants associated with cardiovascular disease, including an insertion/deletion polymorphism (Sun, Zhang et al. 2015), a CAA repeat polymorphism (Sun, Zhang et al. 2015), and 2 DNA methylation sites (Nakatochi, Ichihara et al. 2017).

- *Obesity*; in a study on a cohort of Korean subjects, 7 SNPs of *Zfhx3* were found to be associated with susceptibility to obesity (Yang 2017), in addition to a rare single nucleotide coding sequence variant (SNV) - Gln2014His - found within a large population cohort consisting of multiple ancestries (Turcot, Lu et al. 2018).
- *Restless leg syndrome*; a disorder characterised by the overwhelming urge to move one's legs, often at bedtime, causing sleep disruption. Further phenome-wise association study analysis by Turcot and Lu et al. (2018) of the *Zfhx3* SNV (Gln2014His) associated to obesity, using electronic medical record data, found this SNV to also be associated with restless leg syndrome.

1.1.4 Circadian Rhythms

Circadian rhythms are 24 hour cycles found in all organisms, from the macro (behaviour) to the micro (cellular and molecular) level (Dunlap 1999). As previously discussed, while *Zfhx3* is not highly expressed in the adult brain, there is spatially restricted enrichment of expression in the SCN – the master clock of the body (Lein, Hawrylycz et al. 2007). Along with these findings, there has been mounting evidence implicating *Zfhx3* in mammalian circadian rhythms.

1.1.4.1 Short Circuit (*Sci*)

Research into the circadian function of *Zfhx3* began with the discovery of the short-circuit (*Zfhx3*^{Sci}) mutation in mice (Parsons, Brancaccio et al. 2015). An N-ethyl-N-nitrosourea (ENU) mutagenesis screen was carried out in mice with the

intention of elucidating genetic factors behind mammalian circadian rhythms. This screen generated a mouse with a shortened circadian period (τDD) (Parsons, Brancaccio et al. 2015).

Termed 'short-circuit' (*Sci*) these mice had a circadian period shorter than the population norm - between 21.4 and 23 hours. The *Sci* mutation was a dominant missense mutation (Val1963Phe), and homozygous lethal, meaning only heterozygous animals could undergo behavioural phenotyping.

Zfhx3 is a transcription factor, and molecular analysis of SCN tissue uncovered that RNA for multiple key circadian neuropeptides and receptors involved in intercellular signalling in the SCN were significantly downregulated e.g. arginine vasopressin (*Avp*) and vasoactive intestinal peptide (*Vip*).

ZFHX3^{Sci} had a decreased ability to bind a consensus AT motif in the promotor regions of circadian neuropeptides and other factors, leading to a shortened circadian period, including disruption of the core transcriptional-translational feedback loop and its outputs - key mechanisms of the molecular clock and maintaining a typical circadian rhythm.

1.1.4.2 Six3-Cre mediated conditional deletion of *Zfhx3*

The *Six3* promotor is active in the ventral hypothalamus - which includes the SCN - from E9.0 (Furuta, Lagutin et al. 2000). This study investigated the effect of *Zfhx3* knockout in the SCN, from development, using a conditional knockout line *Zfhx3*-Flox; Six3-*Cre* (Wilcox, Bains et al. 2021).

Analysis of their circadian behaviour revealed that *Zfhx3*-Flox; Six3-*Cre* homozygous knockout mice displayed complete arrhythmicity in their circadian

locomotive behaviour in constant dark conditions, and showed no rhythmic response to light input – either as part of a 12:12 light-dark cycle or light pulses during the dark phase. In addition to light, homozygous knockout mice showed no social entrainment, failing to entrain to the typical circadian behaviour of two control cage-mates.

Alongside arrhythmicity in locomotive behaviour, homozygous knockout mice also displayed arrhythmicity in metabolic output, although overall output (e.g. CO_2 and O_2) and body mass (fat and lean) remained the same between homozygotes and controls.

Histological investigation of the suprachiasmatic hypothalamus of homozygous knockout mice revealed a complete absence of SCN regional definition, including the lack of neuropeptide expression (*Vip* and *Avp*) that typically define the core and the dorsomedial shell of internal SCN cellular structures, respectively (Yan, Karatsoreos et al. 2007).

The findings of this study show that *Zfhx3* is essential to the development of the SCN, and the absence of *Zfhx3* during development causes genetic ablation of the region, leading to circadian arrhythmicity and loss of SCN regional identity.

1.1.4.3 Inducible-Cre mediated *Zfhx3* knockout

Zhx3 is understood to play a key role in neuronal development, particularly in the development of the regional identity of SCN and its internal cellular structures. To investigate to the adult-only effect of *Zfhx3* knockout, this study (Wilcox, Vizor et al. 2017) utilised a tamoxifen-inducible transgenic line expressing *Cre* from the

human ubiquitin C promoter (UBC CreERT2) (Ruzankina, Pinzon-Guzman et al. 2007).

Post-tamoxifen treatment, homozygous induced knockout mice demonstrated a significant shortening of τDD by approximately an hour from typical circadian rhythms. In addition, approximately 30% of homozygous knockout mice displayed complete arrhythmicity in circadian behaviour when in constant darkness. These findings add to the evidence that the *Zfhx3* gene is essential to the maintenance of typical circadian rhythms in the adult mouse.

1.1.5 Metabolism

RNA-Seq analysis of *Zfhx3*$^{Sci/+}$ (*Introduction 1.1.4.1.*) hypothalamus sub-dissections reveals altered expression of multiple genes involved in growth and metabolism. These findings suggest the possibility of *Zfhx3* playing a key transcriptional role in the regulation of body energy expenditure (Nolan, Banks et al. 2022).

Zfhx3$^{Sci/+}$ mutant mice were smaller in size and had lower body mass, and had supressed food intake compared to their wildtype littermates. Analysis of circulating anabolic hormones revealed that *Zfhx3*$^{Sci/+}$ mice had lower levels of fasted serum leptin and insulin. Analysis of mRNA levels in the arcuate nucleus – the hypothalamic centre in control of appetite – revealed decreased expression of orexigenic neuropeptide Y (*Npy*) and G protein-coupled receptor 50 (*Gpcr50*), which may explain the reported reduced appetite and reduced energy expenditure, respectively. These findings suggest the *Sci* mutation has a protective metabolic effect, and that *Zfhx3* plays a role in body energy balance.

1.1.6 Expression in the Brain – Dopaminergic System

As previously discussed, *Zfhx3* is not widely expressed in the adult brain. There are however discrete regions of expression enrichment.

In addition to the SCN, *Zfhx3* has been found to be highly expressed in the dopaminergic regions. Ishii et al. observed that immunoreactivity for ZFHX3 in the brain decreased post-nataly, however a cell sub-population that retained ZFHX3 expression were dopaminergic neurons of the substantia nigra pars compacta (SNc)(Ishii, Kawaguchi et al. 2003). Lein et al. also recorded expression of ZFHX3 in the central dopaminergic regions in the midbrain - the ventral tegmental area (VTA) and SNc via *in-situ* hybridisation (ISH) on adult mice (Lein, Hawrylycz et al. 2007)(**Figure 1.1.7.1.**).

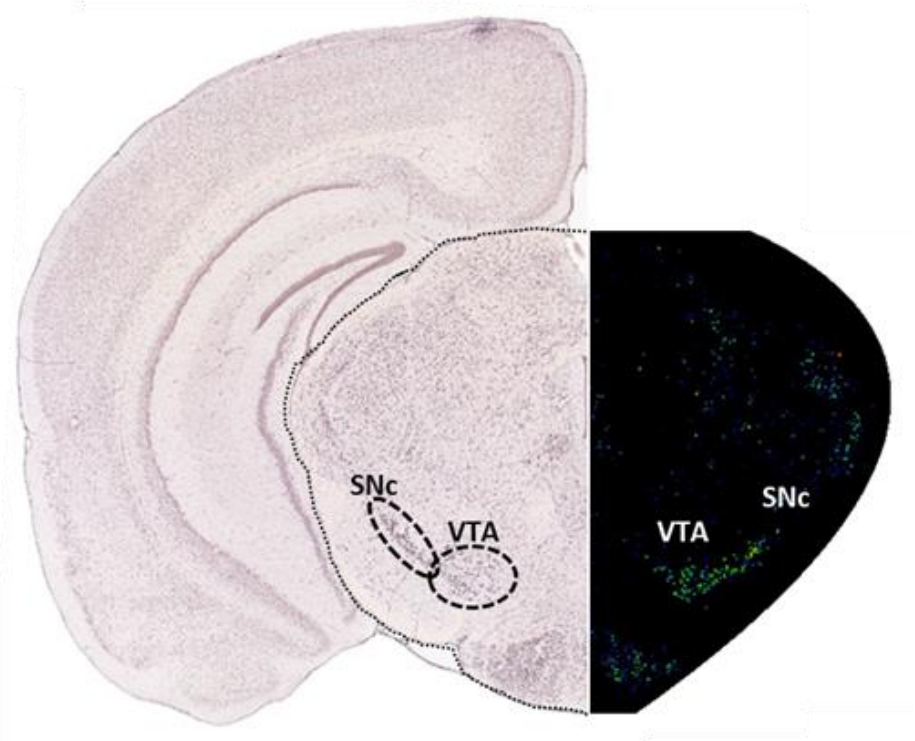

Figure 1.1.7.1. ZFHX3 expression in the adult mouse brain coronal section, showing the VTA and SNc; with VTA and SNc labelled. Image left shows ISH data, image right illustrates expression levels. Images modified from the Allen Brain Atlas (Lein, Hawrylycz et al. 2007)

One region with high *Zfhx3* expression in the adult brain is the SCN, which is the master clock of the body. *Zfhx3* has demonstrated a key role in both the regional development and adult function of the SCN, through the use of multiple conditional knockouts. The question of the role of *Zfhx3* in the development and adult function of dopaminergic regions however, has not previously been investigated.

1.2 Dopaminergic System

Dopamine is a monoamine neurotransmitter that is key to intercellular communication in central nervous system (Carlsson 1959). The dopaminergic

signalling system is divided into multiple pathways, and is involved in motor control, reward, and learning (Arias-Carrión, Stamelou et al. 2010).

The topic of the dopaminergic system is vast, with a wealth of research into the function, dysfunction, pharmacology, and more. For the purposes of this thesis, many areas have been summarised in order to focus on dopaminergic disease, primarily schizophrenia.

1.2.1 Functional Overview

1.2.1.1 Dopaminergic Pathways

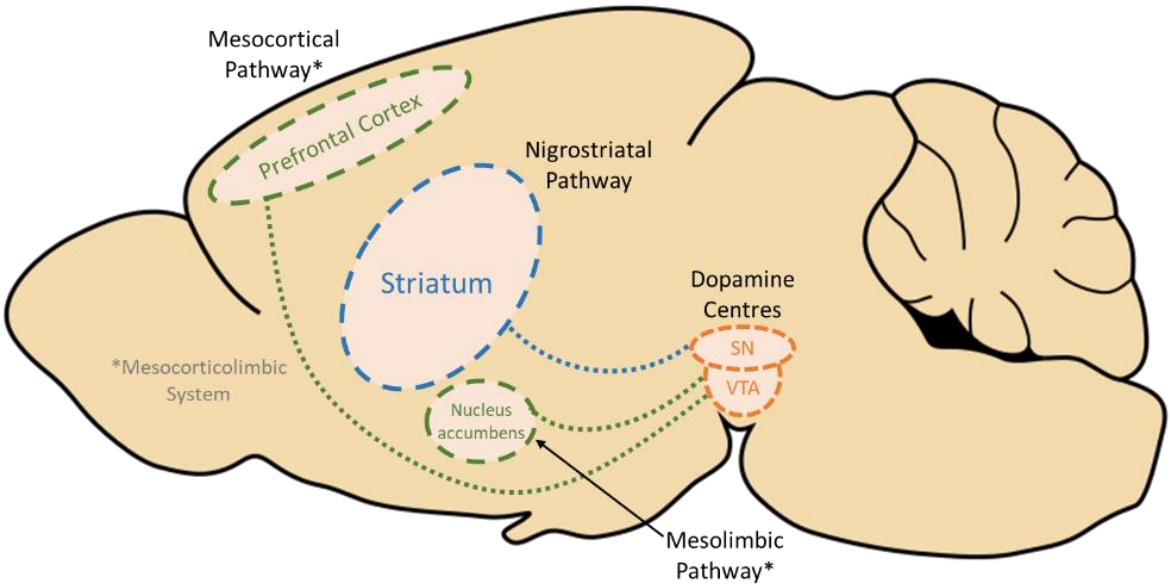

Figure 1.2.1.1.1. Key dopaminergic pathways in the mouse brain; including the nigrostriatal pathway, the mesocortical pathway, and the mesolimbic pathway – the latter two of which form the mesocorticolimbic system. Image modified from (Töle 2014).

The dopaminergic system consists of multiple pathways, projecting from the dopaminergic regions (VTA and SN – ventral tegmental area and substantia nigra) in the midbrain to multiple target brain regions. Discussed here are the 3 major

pathways: the nigrostriatal pathway, the mesocortical pathway, and the mesolimbic pathway – the latter two of which form the mesocorticolimbic system (**Figure 1.2.1.1.1**)

The nigrostriatal pathway consists of projections from the SN region in the midbrain to the striatum. The most well defined function of the nigrostriatal pathway is its role in motor function. It has been implicated in motor learning, for example monkeys with dopamine depletion in the SN display significant deficits in learning and performing in sequential motor tasks (Matsumoto, Hanakawa et al. 1999). It is linked to response initiation, which is the initiation of movement as a response to an external cue, as dopamine depletion in this pathway impairs this response (Carli, Evenden et al. 1985). It is also involved in pain modulation, as the stimulation (via apomorphine) of D_2 receptors expressed in the pathway provides an analgesic affect (Michael-Titus, Bousselmame et al. 1990).

The mesocorticolimbic system consists of two key dopamine pathways, the mesocortical pathway and the mesolimbic pathway, which together are involved in the functions of reward and motivation (Kelley and Berridge 2002). Both mesocortical and mesolimbic pathways consists of projections from the VTA region in the midbrain, to the prefrontal cortex and the nucleus accumbens respectively. The mesocortical pathway alone serves in a mostly modulatory role, acting in an inhibitory manner to sub-cortical dopamine signalling, as suggested by studies reporting that dopamine depletion in the prefrontal cortex alone does not cause any overt behavioural phenotype. However, there is evidence to indicate that this pathway has a key role in working memory (Tzschentke 2001, Marié and Defer 2003). The mesolimbic pathway is the main driver of the reward-seeking function of the mesocorticolimbic system, and - pertinent to this study – it

is reported that these motivational responses are linked to vigilance in animals, and therefore to the sleep/wake cycle (Alcaro, Huber et al. 2007, Eban-Rothschild, Rothschild et al. 2016, Oishi and Lazarus 2017).

1.2.1.2 Dopaminergic Receptors

There are two categories of dopamine receptors – D_1-like and D_2-like. D_1-like receptors include D_1 and D_5 receptors, and D_2-like includes D_2, D_3, and D_4 receptors (Missale, Nash et al. 1998). D_1-like receptors generally promote production of cyclic adenosine monophosphate (cAMP) secondary messenger, while D_2-like receptors downregulate cAMP production (Kebabian and Calne 1979, Enjalbert and Bockaert 1983).

- *Locomotion:* D_1, D_2, and D_3 function together to control locomotor activity. D_1 receptors are post-synaptic and have an excitatory effect on locomotive behaviour, while D_2 and D_3 receptors have both pre and post-synaptic functions and act as moderators of dopamine transmission (Missale, Nash et al. 1998, Sibley 1999, Joseph, Wang et al. 2002).
- *Reward:* D_1 and D_2 are the primary receptors involved in reward mechanisms. In mouse studies using cocaine, both D_1 and D_2 receptors are involved in drug-induced locomotor behaviour. Human studies however report the importance of D_2 receptors only, through study of the regulation of food reward (Baik 2013).
- *Working Memory:* Working memory specifically is reported to be executed primarily by the prefrontal cortex via the mesocortical pathway. D_1 receptors are of notably high concentration in the prefrontal cortex, and are the primary mediators of working memory (Lidow, Goldman-Rakic et al. 1991). However,

D_2 receptors also play a role - blockade of D_2 receptors in monkeys downregulates D_1 receptor expression, causing working memory deficits (Castner, Williams et al. 2000). D_4 are also highly expressed in the prefrontal cortex - with mRNA levels comparable to that of D_1 receptors - and have been found to have a differential role in working memory regulation. Rats with above average performance in a working memory task had their performance dampened by a D_4 antagonist, with the opposite effect observed in mice with poor working memory performance (Meador-Woodruff, Damask et al. 1996, Zhang, Grady et al. 2004).

- *Sleep:* Dopaminergic neurons in the VTA are essential to the maintenance of the 'awake' state of animals – and mice treated with D_1 and D_2 antagonists showed disruption of the wake-maintenance and sleep-suppression mechanism mediated by VTA dopaminergic signalling (Eban-Rothschild, Rothschild et al. 2016). D_2 receptors in the basolateral amygdala are also reported to play a vital role in the transition from non-REM to REM sleep (Hasegawa, Miyasaka et al. 2022).
- *Pain:* In the mesolimbic pathway, chronic pain has been linked to reduced receptor availability of D_2 and D_3 receptors (Martikainen, Nuechterlein et al. 2015). Stimulation of D_1 and D_2 receptors in the prefrontal cortex has been shown to reduce neuropathic pain behaviours in mice (Huang, Zhang et al. 2020). In addition, as mentioned previously the stimulation of D_2 receptors in the nigrostriatal pathway reduces pain sensation. Male D_5 receptor knockout mice have been reported to exhibit reduced sensitivity to formalin and heat-induced pain (Megat, Shiers et al. 2018).

1.2.2 Dopaminergic Dysfunction and Disease

Discussed here is an overview of clinical presentation and pathology of selected dopaminergic diseases.

1.2.2.1 Parkinson's Disease

Parkinson's disease is a chronic neurodegenerative disorder, demonstrating a range of motor and non-motor symptoms, seen primarily in older adults. (Beitz 2014). The diagnosis of Parkinson's is based on the presentation of three central motor symptoms: bradykinesia - with tremor, rigidity, or both (Postuma, Berg et al. 2015). Bradykinesia is the slowing of movement, with progressive hesitation and decrease in speed - this can be assessed through observing hand movement, gait, voice, and/or face movements. Tremor is defined as a 4-6 Hz tremor observed in a limb at rest. Rigidity is the slow movement, and resistance against movement, of major joints when passively moved. Non-motor symptoms – some of which may appear years before onset of motor symptoms – include but are not limited to: hyposmia/anosmia; visual hallucinations; double vision; heightened nociceptive and neuropathic pain; anxiety, including panic attacks and social phobia; depression; fatigue; cognitive decline; impulse control deficits; and sleep disorder (Schapira, Chaudhuri et al. 2017, Ruitenberg, Wu et al. 2018)

Parkinson's pathology is defined by formation of Lewy Bodies (abnormal protein aggregates including α- synuclein and ubiquitin) in dopaminergic neurons of the SN, causing neuron loss and degeneration (Beitz 2014). SNPs on genes encoding D_2 dopamine receptor and dopamine active transporter (DAT) gene have also

been associated with higher dyskinesia and greater susceptibility to the disease, respectively (Wang, Liu et al. 2001, Kaiser, Hofer et al. 2003).

Mitochondrial dysfunction - with defects in the electron transport chain - has also been observed in Parkinson's pathology. Exposure to human MPTP neurotoxin has also been shown to generate Parkinsonian symptoms, through inhibition of Complex I of the electron transport chain (Ramsay, Salach et al. 1986, Parker, Boyson et al. 1989).

Pharmacological treatment of Parkinsonian symptoms is primarily through the use of dopamine receptor agonists such as levodopa, intended to relieve the dopamine deficit behind the pathology of the disease.

1.2.2.2 Huntington's Disease

Huntington's disease is a fatal neurodegenerative disorder caused by a CAG repeat expansion on exon 1 of the huntingtin (*HTT*) gene (MacDonald, Ambrose et al. 1993). Huntington's is characterised by progressive movement disorder 'chorea' – which is random, involuntary movement – coupled with psychiatric symptoms and cognitive decline. Motor symptoms begin with small involuntary movements in the face and fingers, but progress to a 'drunken' gait, then further to bradykinesia as seen in Parkinson's disease (Roos 2010). Psychiatric symptoms can appear earlier than motor decline and have a wide scope, including: anxiety, depression, obsessive-compulsive behaviours, aggression, and (at late-stage) psychosis (van Duijn, Kingma et al. 2007). Cognitive decline can happen at any stage of the disease, and can also range in severity even in the late stages of the disease (Bates, Dorsey et al. 2015).

Huntington's pathology is defined by atrophy of the striatum, and a decrease in SN neurons - by about 40% (Vonsattel, Myers et al. 1985, Oyanagi, Takeda et al. 1989). Considering dopaminergic neurons, post-mortem brain sections of late-stage Huntington's patients show decreased tyrosine hydroxylase (dopaminergic marker) expression, and reduced dopaminergic innervation of the striatum. It is theorised that this breakdown of the nigrostriatal pathway contributes to the characteristic motor dysfunction of the disease (Bédard, Wallman et al. 2011). Analysing dopamine signalling of the nigrostriatal pathway in patients, it was found that late-stage patients had reduced levels of dopamine, however early-stage patients had increased levels of dopamine. This demonstrated that Huntington's disease has a complex dopamine pathology, progressing from upregulated to downregulated dopamine levels, causing the progressive presentation of motor symptoms seen in patients (Kish, Shannak et al. 1987, Garrett and Soares-da-Silva 1992).

1.2.2.3 Attention Deficit/Hyperactivity Disorder

Attention Deficit/Hyperactivity Disorder (ADHD) is a chronic neurodevelopmental disorder, with a heterogeneous presentation amongst patients. It is characterised by childhood (17 years of age or younger) presentation of inattentive, hyperactive, and/or impulsive behaviour that is more pronounced than their peers, that impairs normal function (Austerman 2015). Inattentive symptoms include the inability to follow instructions, a dislike of schoolwork (and other focused activities), and high distractibility. Hyperactive/impulsive symptoms include fidgeting, the inability to sit still, excessive talking, and frequently interrupting others. The combination of

presented symptoms give three subcategories of the condition: predominantly inattentive, predominantly hyperactive/impulsive, and combined (American Psychiatric Association 2013).

Investigation into the pathophysiology behind ADHD have reported multiple links to the dopaminergic system. Imaging studies on children with ADHD have shown a delay in the development of the prefrontal cortex, and dysfunction in the mesocorticolimbic system and frontostriatal circuits - all of which are either directly or indirectly involved in dopaminergic signalling (Castellanos, Giedd et al. 1996, Posner, Rauh et al. 2013). ADHD is also highly heritable with multiple genes having been linked to the disorder, including genes involved in the dopamine synapse: DAT, D_4, and D_5 (Hawi, Cummins et al. 2015). It has also been found that patients with ADHD have lower D_2/D_3 receptor and DAT availability in the midbrain and nucleus accumbens (Volkow, Wang et al. 2009).

Treatments for ADHD symptoms are often founded in the pharmacological correction of dopamine and noradrenaline (a product of dopamine) dysfunction. Theories on the nature of dopamine dysfunction in ADHD include rapid re-uptake of dopamine at the synapse, low levels of dopamine release, and low density of dopamine receptors. Effective treatment of ADHD symptoms uses stimulant drugs, which increase the availability of dopamine and noradrenaline in the synapse by blocking re-uptake, with evidence to suggest that prolonged use of stimulants increases dopamine transporter density (Caye, Swanson et al. 2019).

1.2.2.4 Schizophrenia

Schizophrenia is a severe, chronic psychiatric condition that is characterised by the presence of two or more of the following: ‘positive’ symptoms such as hallucinations, delusions, disorganised speech, disorganised or catatonic behaviour; and negative symptoms such as avolition, apathy, and social withdrawal (American Psychiatric Association 2013). Additional cognitive symptoms include emotional dysregulation and disorganised thinking. Outside of the diagnostic criteria, schizophrenia pathology has been reported to include cognitive impairments in: working memory, visual learning, attention, problem solving, and social cognition (Alkan, Davies et al. 2021).

Schizophrenia is classed as a neurodevelopmental disorder. At the point of illness onset, patients show abnormal brain structural development, with decreased overall brain and hippocampal volume, and increased ventricular volume (Steen, Mull et al. 2006). There is conflicting evidence as to whether schizophrenia is also a progressive illness. Significant decrease is seen in the volume in multiple grey and white matter regions of the brain, most severely during the early post-onset years (Andreasen, Nopoulos et al. 2011). However, it has been theorised that these changes are not caused by the disease itself, but by drug abuse, poor lifestyle, stress, and the prolonged use of antipsychotic medication, which are all factors that are closely linked with schizophrenia pathology (Zipursky, Reilly et al. 2013).

The ‘dopamine hypothesis of schizophrenia’ postulates that the pathophysiology of schizophrenia is through dopamine dysfunction, however the theories to the nature of this dysfunction have progressed in complexity since its conception. The current state of the hypothesis postulates that psychosis and other positive symptoms are caused by presynaptic striatal hyperdopaminergia (Howes and

Kapur 2009). The theory of presynaptic striatal hyperdopaminergia is supported by reports of schizophrenic patients having been found to have increased dopamine synthesis in the presynaptic striatum, and increased dopamine synaptic release. Dopaminergic receptors in the striatum also show differences: an increase in D_2 and D_3 receptor density, and an increased baseline occupancy of D_2 receptors. Outside of psychosis and positive symptoms, there is evidence to suggest that negative symptoms are caused by reduced dopaminergic signalling along the mesocortical pathway, and reduced stimulation of D_1, D_3, and D_4 receptors in the prefrontal cortex (Stępnicki, Kondej et al. 2018).

Pharmacological treatment for schizophrenia primarily relies on D_2 antagonists, reducing signalling in the overactive striatum. The first antipsychotics were D_2 antagonists only, however more modern treatments have additional targets. 'Second generation' drugs are also serotonin $5HT_{2A}$ receptor antagonists, which decrease dopaminergic signalling of the mesolimbic pathway, and also reduce negative symptoms. 'Third generation' drugs target further more receptors, including having an agonist effect on $5HT_{1A}$, D_2, and D_3 receptors, to reduce negative symptoms (Orzelska-Górka, Mikulska et al. 2022).

Dopamine signalling exhibits two basic modes – in 'phasic' signalling, typically associated with reward, and in 'tonic' extrasynaptic levels (Floresco, West et al. 2003). Glutamate is one of the signalling molecules that modulates the phasic dopamine signalling states, with GABA being the primary dopaminergic tonic signalling regulator alongside glutamate (Overton and Clark 1992). Since glutamate regulates dopamine signalling, it is implicated in the dopamine hypothesis of schizophrenia through both phasic and tonic dopamine signalling, as part of the NMDA-R hypofunction hypothesis (Olney and Farber 1995).

There are 5 glutamate circuits in the brain, leading from the frontal cortex and projecting to the brainstem, limbic areas, and midbrain. Circuits leading to the midbrain and limbic areas are likely involved in mediating dopamine signalling, however it is the projection to the brainstem that mediates dopamine signalling, via the mesolimbic pathway (Schwartz, Sachdeva et al. 2012).

The NMDA-R hypofunction hypothesis of schizophrenia pathophysiology postulates that schizophrenia arises from hypoactive glutamatergic signalling from the anterior hippocampus, triggering dysfunction in multiple circuits and brain regions to give rise to different symptoms. This theory asserts that positive schizophrenia symptoms arise from a hyperresponsive dopaminergic system, as a direct response from the hypoactive glutamatergic signalling of the anterior hippocampus observed in schizophrenic patients. The hyperresponsive state of the dopaminergic system leads patients to have characteristic 'aberrant salience', which is ascribing undue motivational importance to neutral stimuli, as well as psychotic symptoms. Cognitive and negative symptoms arise from the same hyperactive signalling, but to the prefrontal cortex and the cingulate cortex respectively (Grace and Gomes 2019). This circuit disruption of glutamatergic signalling to dopamine activity arises from the dysregulation of the GLU-GABA-GLU-DA neurocircuit loop – this is where a pyramidal glutamate neuron fires upon a GABA interneuron, which in turn fires upon a secondary glutamate pyramidal neuron, which finally fires upon dopaminergic neurons. Hypoactivity of glutamate neurons disrupts this circuit and causes hyperactivity on dopamine neurons (Schwartz, Sachdeva et al. 2012).

Additional NMDA receptor-based evidence from animal studies support the theory that glutamate dysfunction is linked to schizophrenia. The N-methyl-D-aspartate

(NMDA) receptor is a glutamate receptor, and multiple antagonist and agonist interactions are linked to schizophrenia. Mice treated with ketamine – an NMDA receptor antagonist - exhibit hippocampal hypermetabolism and size reduction, both of which are associated with schizophrenia and psychotic disorder (Schobel, Chaudhury et al. 2013). In addition, genetic mouse model - $SR^{-/-}$ (serine racemase) - with reduced levels of an NMDA co-agonist D-serine - displayed multiple schizophrenia biological indicators, such as reduced dendritic spines and hippocampal volume (Balu, Li et al. 2013).

In addition to dopaminergic and glutamatergic circuitry, changes are seen in the cortex in schizophrenic patients. The superior temporal gyrus (STG) is a region in the brain that consists of the primary auditory cortex. Regional dysfunction is involved in auditory hallucinations and disorder of thought, symptoms both associated with schizophrenia, with the volume of the region being negatively correlated with severity of symptoms (Rajarethinam, DeQuardo et al. 2000).

Changes in gene expression in the STG of schizophrenic patients was investigated using microarray and real-time PCR to measure mRNA expression in post-mortem STG tissue from schizophrenic patients. Amongst other genes, *Zfhx3* was identified as being significantly upregulated. As *Zfhx3* plays a key role in development in the CNS, it was hypothesised that this upregulation correlated to the dysfunction in neurodevelopment and neurodifferentiation seen in schizophrenia (Bowden, Scott et al. 2008).

1.2.2.5 Schizophrenia SNPs in *Zfhx3*

In a personal communication from Maya Bucan (University of Pennsylvania) in 2017, Dr Bucan reported that multiple exonic *Zfhx3* variants – 8 SNPs and 1 insertion - have been linked to schizophrenia, from the study of schizophrenic

Begin	End	Variant Type	Reference	Alternative	Exon	Effect	Cross-references	Zygosity	Polyphen-2 impact prediction
72787993	72787994	SNP	G	C	10	Missense	Novel	Het	Tolerated
72788423	72788424	SNP	G	T	10	Missense	Novel	Het	Tolerated
72796640	72796641	SNP	C	G	9	Missense	rs62051555	Het	Possibly damaging
72797252	72797253	SNP	G	T	9	Missense	Novel	Het	Deleterious
72797359	72797360	SNP	T	A	9	Missense	Novel	Het	Tolerated
72797656	72797657	SNP	T	C	9	Missense	Novel	Het	Tolerated
72950696	72950697	SNP	C	A	3	Missense	rs2213978	Het	Probably damaging
72957798	72957798	Ins	-	CCC	2	Insert	Novel	Het	NA
72957816	72957817	SNP	A	G	2	Missense	rs4788682	Hom	Tolerated

Table 1.2.2.4.1.1. Exonic *Zfhx3* variants associated with schizophrenia; showing the chromosomal location of the SNP or insertion, the base(s) change, exonic location of variation, mutation type, whether the variant has been identified in other GWAS, zygosity of effect, and prediction of the impact of the variation using Polyphen-2 (Polymorphism Phenotyping) impact tool (SNPs only).

patients of the Amish populations in Pennsylvania, USA (**Table 1.2.2.4.1.1**). It is of note that the same variant (Gln2014His, or rs62051555) found associated to obesity and restless leg syndrome, is also found here. It is likely that this SNP has a significant effect on the functionality of ZFHX3.

1.2.2.6 Sexual Dimorphism in Dopamine and Dysfunction

There is notable sexual dimorphism reported in the presentation and pathophysiology of multiple dopamine-based diseases and disorders. This is something that should be taken into account when investigating an animal model of disease, in order to draw more accurate conclusions:

- *Parkinson's disease*: In female patients, motor symptoms tend to have a later onset, with less rigidity and more instability in their posture. They are more likely to experience severe pain, inflammation of the bowel leading to gastrointestinal difficulties, and are more likely to experience anxiety. (Haaxma, Bloem et al. 2007, Colombo, Abbruzzese et al. 2015, Broen, Leentjens et al.

2018, Houser, Chang et al. 2018, Silverdale, Kobylecki et al. 2018). In male patients, while motor symptoms have earlier onset, males tend to have a later onset of 'freezing gait'. They have lower cognitive function, with more rapid cognitive deterioration, and more commonly demonstrate impulse control dysfunction (Bhattacharjee 2018, Cholerton, Johnson et al. 2018, Kim, Lee et al. 2018). Regarding pathophysiology, dopaminergic neurons in the Parkinson's midbrain show different changes in gene expression between female and male patients. Female Parkinson's neurons show upregulations in genes involved in neuronal maturation and neuron signal transduction, which is not seen in males (Cantuti-Castelvetri, Keller-McGandy et al. 2007). Female patients also show a higher D_1:D_2 receptor ratio in the striatum but not the cortex, giving possible explanation as to why female patients are more resilient to impulse control disorder, but more susceptible to anxiety (Cullity, Madsen et al. 2019).

- *Huntington's Disease*: Unfortunately there have been few studies into the sexual dimorphism of Huntington's presentation or pathophysiology. However, female patients have been reported to experience more severe motor, psychiatric, and cognitive symptoms than male patients, however age progression of these symptoms showed no difference between the genders (Hentosh, Zhu et al. 2021).
- *Attention Deficit/Hyperactivity Disorder:* Girls and boys diagnosed with ADHD are more likely to manifest different symptoms and disorder subtypes. Girls are more likely to be recorded as demonstrating inattentive behaviours, while boys are more likely to be recorded showing impulsive behaviours. Boys were also

more likely to be reported as demonstrating poor behaviour, and anxiety/depressive symptoms (Slobodin and Davidovitch 2019).

- *Schizophrenia:* Male patients have more pronounced cognitive dysfunction compared to women in multiple areas, including attention and executive function (Goldstein, Seidman et al. 1998). Male patients also had significantly reduced volume in the bilateral amygdala compared to healthy controls (Niu, Matsui et al. 2004). While both male and female patients show enlarged hypothalamus, this positively correlated to more pronounced anxiety in female patients (Goldstein, Seidman et al. 2007). Sexual dimorphism in behaviour also exists in animal models. In models of schizophrenia, males show better performance in working memory and spatial memory tasks, while females show advantages in visual memory e.g. in novel object recognition tests. Male rodent models also displayed abnormal social behaviour, including social withdrawal (Leger and Neill 2016). In human schizophrenia brain morphology, male patients have greater reduction in volume of the frontal lobe (including the prefrontal cortex, a dopamine circuit terminus region) and the temporal lobe, which is associated with auditory processing (Andreasen, Ehrhardt et al. 1990, Bryant, Buchanan et al. 1999). In rodent models, examining the effect of antipsychotic drugs on models of schizophrenia showed that there are likely differences in function of D_2 receptors in the pathophysiology, although differences in receptor expression are yet to be investigated (Williams, Coppolino et al. 2021).

1.2.2.7 Dopamine Disorders and Behavioural Phenotyping

In *Chapter 4* we discuss a behavioural phenotyping pipeline for the mouse models involved in this study. These mouse models exhibit dopamine dysfunction, and

therefore the endophenotypes investigated in these mice are related to the four dopamine disorders discussed here: Parkinson's disease, Huntington's disease, ADHD, and schizophrenia. The tests included in this pipeline assess: Parkinson's using anxiety, motor, social, sleep, pain, and memory tests; Huntington's using anxiety, motor, social, and memory tests; ADHD using anxiety tests to assess impulsivity; and schizophrenia using social, memory, and pre-pulse inhibition tests.

1.3 Project Overview: *Zfhx3*, Dopamine, and Dopaminergic Disorders

There are multiple links tying together *Zfhx3*, dopamine, and dopaminergic disorders i.e. schizophrenia. The foundation of this study assumes on the validity of the dopaminergic hypothesis of schizophrenia, which is a long-standing hypothesis with much evidence to support it.

Zfhx3 expression has been observed in the mouse adult brain in a highly regional pattern in multiple studies, with two of those regions being the dopaminergic regions VTA and SNc.

Zfhx3 has been linked to schizophrenia in human studies. Upregulation of *Zfhx3* is seen in the STG of schizophrenic patients, and multiple variants of *Zfhx3* have been associated with schizophrenia in a population study.

With this evidence there is precedent for the investigation of the role of *Zfhx3* in the dopaminergic system, and the role of *Zfhx3* in the presentation of schizophrenia-related behaviours and molecular changes.

1.4 Cre-Lox Conditional Knockout Models

This study uses the principle of the Cre-LoxP conditional knockout animal model. These models rely on the mechanism of Cre-LoxP recombination, where *Cre* recombinase enzyme induces site-specific deletion of nucleotide sequences that are flanked by LoxP sites. This can be used to create a null allele, generating specific gene knockout animal models (Murray, Eppig et al. 2012). This study uses two knockout mouse models using this system, details of which can be found in *Methods*.

Both knockout models use the same 'floxed' animal, where exons 7 and 8 of *Zfhx3* are flanked by LoxP sites, and recombination with *Cre* leads to the formation of a premature stop codon and nonsense-mediated decay of the gene product – producing a null allele (Sun, Fu et al. 2012). The two lines with conditional knockout of *Zfhx3* induce recombination using two methods of *Cre* introduction.

The first conditional knockout line is DAT-*Cre*, *Zfhx3*-Flox, which has *Zfhx3* knocked out only in dopaminergic neurons, from embryonal day 13 (Kadkhodaei, Ito et al. 2009). This model is created from crossing the *Zfhx3*-Floxed line with a *Cre*-driver line – where *Cre* recombinase is under the control of the DAT promotor, which is active from development onwards (Zhuang, Masson et al. 2005).

The second conditional knockout model uses the intracranial injection of *Cre*-expressing adeno-associated virus (AAV). This line uses intracranial injection of AAV-Cre into the midbrain of adult *Zfhx3*-Floxed mice, creating a spatial-temporal specific knockout (Kaspar, Vissel et al. 2002).

1.5 Thesis Aims

This thesis aims to investigate both the developmental and adult role of *Zfhx3* within the dopaminergic system.

This was achieved by first exploring the expression pattern of ZFHX3 in neuronal populations present in the midbrain, through immunofluorescent co-staining for ZFHX3 and neuronal identity markers.

Two conditional *Zfhx3* knockout models were generated: one targeting dopaminergic neurons from development onwards (DAT-*Cre*; *Zfhx3*-Flox), another targeting all neuronal subpopulations the VTA in adulthood only (intracranial injection of *Cre*-expressing virus). These mice underwent a behavioural phenotyping pipeline, designed to assess dopamine disorder-specific endophenotypes, before post-mortem molecular analysis of dissected brains.

This molecular analysis included the investigation of ZFHX3 expression in the midbrain of these two knockout cohorts, including the evaluation of any changes in dopaminergic region development in the DAT-*Cre*; *Zfhx3*-Flox line.

Changes in gene expression in the midbrain and dopaminergic circuit target regions in the DAT-*Cre*; *Zfhx3*-Flox line was then carried out using RNA-Seq analysis.

The changes seen in each of these mouse lines could then be used to elucidate the differences in the role of *Zfhx3* during development, and during adulthood only, in addition to the role of *Zfhx3* in non-dopaminergic neurons also present in the midbrain.

2

Materials and Methods

2

Materials and Methods

2.1 Mice

2.1.1 C57BL/6N

For investigating *Zfhx3* expression in the brain, wildtype C57BL/6N female and male mice were sourced from the Mary Lyon Centre.

2.1.2 *Zfhx3*-Floxed

The primary mouse line used in this project was a floxed *Zfhx3* line on a C57BL/6N background (*Zfhx3*$^{Tm1.1Jtd}$), originally provided to the group by Dr Jin-Tang Dong (Emory University) and has since been re-derived by the Mary Lyon Centre for this study. These mice have LoxP sites flanking exons 7 and 8 of the *Zfhx3* gene, which upon recombination leads to an introduction of an early STOP codon – resulting in RNA degradation via nonsense-mediated decay (Sun, Fu et al. 2012).

2.1.3 DAT-Cre

These mice express the Cre-recombinase gene knocked into the 5′-UTR upstream of the dopamine active transporter (DAT) translational start codon - under the DAT

promoter - meaning *Cre* is expressed exclusively in dopaminergic neurons. This system was developed by Zhuang et al. to allow for study of gene function within the dopaminergic system (Zhuang, Masson et al. 2005). This line was derived from sperm obtained from Edgar Kramer at the University of Plymouth.

2.1.4 DAT-*Cre*; *Zfhx3*-Flox

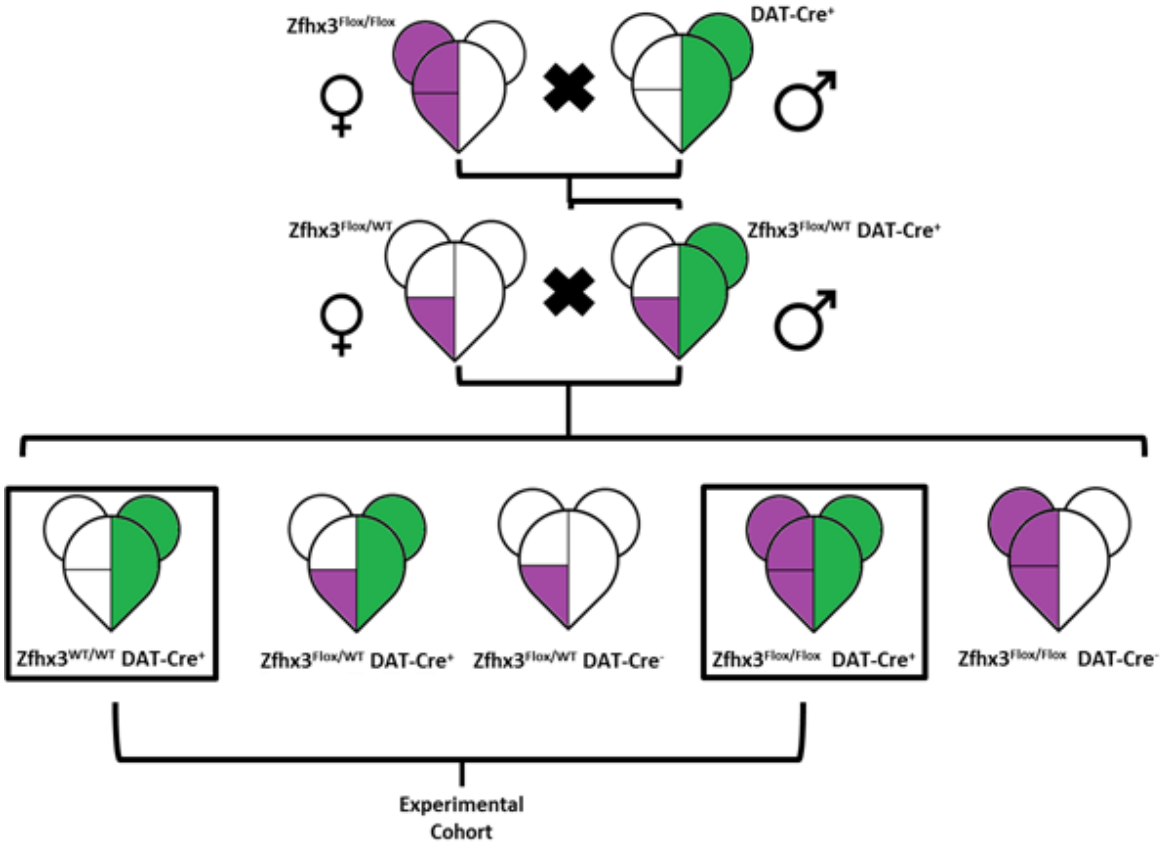

Figure 2.1.4.1. DAT-*Cre*; *Zfhx3*-Flox breeding plan

Figure 2.1.4.1. illustrates the breeding plan for the DAT-*Cre*; *Zfhx3*-Flox experimental cohort. Mice with *Zfhx3*$^{Flox/Flox}$ DAT-*Cre*$^{+}$ genotype were the experimental group, with *Zfhx3*$^{WT/WT}$ DAT-*Cre*$^{+}$ mice as the control.

2.1.5 Housing and welfare

All non-surgery mice were group-housed, with a maximum of 5 animals per cage, with the following exceptions: behavioural cohort male mice were individually housed following motor function testing; and mice of both sexes undergoing surgical procedures were individually housed from three days prior to surgery, then indefinitely post-surgery.

All mice were housed in individually ventilated cages (L36.5cm x W20.7cm x H140cm Techniplast 1284) with food (Rm(3)e supplied by SBS) and water available *ad libitum,* and were under 12:12hr light/dark cycle (lights on at 07:00). Cages contained aspen and shred bedding, including a cardboard enrichment tunnel, and were cleaned by 'spot checking' for cleanliness – and cleaned no more than once a week.

When possible, mice were handled using the 'tube' method, where mice are handled exclusively inside a tube. However when this was not possible, 'supportive' handling techniques were used, where mice are never allowed to 'dangle' and are always supported by a hand.

Animals were kept and studied in compliance of the ASPA Act 1986 (Amended 2012) and under guidance of the Medical Research Council 2013.

License Numbers	
Establishment License	X9BFFDAE2
Project License Reference	30/4303
Personal License Number (PIL)	IB22890B8

Table 2.1.5.1. License numbers permitting animal research

2.1.6 Genotyping

Genotyping of mice was carried out using TaqMan qPCR assay to measure relative amplification of target gene sequences using fluorescent probe sequences. Ear notches for genotyping and identification were taken at P14.

Genotyping Primers		
Wildtype *Zfhx3*	Forward	AAGAAGCGATAAGCTAACACCAGG
	Reverse	ACGCCAAAGGTTGAGGAGAATG
***Zfhx3*-Flox**	Forward	GCCATAACTTCGTATAATGTATGCTATACG
	Reverse	ACGCCAAAGGTTGAGGAGAATG
DAT-*Cre*	Forward	GCGGTCTGGCAGTAAAAACTATC
	Reverse	GTGAAACAGCATTGCTGTCACTT

Table 2.1.6.1. Primer sequences used for mouse genotyping

Genotyping Probes	
Wildtype *Zfhx3*	TTAAAGGAATTCACGGGGTTAGGGC
***Zfhx3*-Flox**	TTATAAGCTTACGGGGTTAGGGCTGT
DAT-*Cre*	AAACATGCTTCATCGTCGGTCCGG

Table 2.1.6.2. Probe sequences used for mouse genotyping

2.2 Antibodies and Immunofluorescent Staining

2.2.1 Antibodies and Reagents

Blocking Solutions and Detergents			
Type	Producer	ID	Lot Number
Normal Donkey Serum	abcam	ab7475	GR3238H1-22
Normal Goat Serum	abcam	ab7481	-
Triton X-100	Fisher Scientific	BP151-500	110012

Table 2.2.1.1. Blocking solutions and detergent for immunofluorescent staining

Primary Antibodies Antigen Target	Type	Supplier	ID	Lot Number	Concentration	Additional Detail
ZFHX3	Rabbit polyclonal	MRC Harwell	E6153-IC	1655C	1:500	-
TH	Sheep polyclonal	abcam	ab113	GR284187-41	1:500	-
GAT1 (SLC6A1)	Guinea Pig polyclonal	Frontier Institute	GAT-GP-Af260	-	1:500	-
Anti-GAD67	Mouse monoclonal	abcam	ab26116	GR3233478-1	1:250	-
GABA	Mouse monoclonal	Sigma Aldrich	A0310	-	1:200	-
GAD67	Mouse monoclonal	Sigma Aldrich	MAB5406	2726806	1:1000	-
GAD67	Chicken polyclonal	abcam	ab75712	-	1:250	-
VGLUT2	Mouse monoclonal	abcam	ab79157	GR3205581-1	1:500	-
GAD-65/67	Mouse monoclonal	Santa Cruz	sc-365180	D2318	1:1000	Conjugated Alexa Fluor 488
GAD-65/67	Mouse monoclonal	Santa Cruz	sc-377145	C3117 A0722	1:1000	Conjugated Alexa Fluor 488

Table 2.2.1.2. Primary antibodies for immunofluorescent staining

Secondary Antibodies Specificity	Fluorophore	Supplier	ID	Lot	Concentration
Donkey Anti-Rabbit	Alexa Fluor 647	LifeTech	A31573	1693297	1:300
Donkey Anti-Rabbit	Alexa Fluor 647	abcam	ab150075	GR282734-1	1:200
Donkey Anti-Sheep	Alexa Fluor 488	abcam	ab150177	GR3210700-1 GR3232735-1	1:300
Donkey Anti-Sheep	DyLight 650	abcam	ab96942	GR267510-1	1:300
Goat Anti-Guinea Pig	Alexa Fluor 488	abcam	ab150185	GR3205565-1	1:300
Goat Anti-Mouse	Alexa Fluor 594	Invitrogen	A11005	1524907	1:300
Donkey Anti-Mouse	Alexa Fluor 594	Invitrogen	A21202	1890861	1:300
Goat Anti-Chicken	Alexa Fluor 488	abcam	ab150169	-	1:200
Goat Anti-Mouse	Alexa Fluor 488	abcam	ab150113	GR3373409-3	1:200
Goat Anti-Mouse	Alexa Fluor 488	Invitrogen	A10684	1986972	1:1000

Table 2.2.1.3. Secondary antibodies for immunofluorescent staining

2.2.2 Immunofluorescent staining protocol

2.2.2.1 Slide preparation

Brains were dissected fresh and then frozen in OCT (stored at -80ºC), before cryosectioning in the coronal plane to 20 µm thickness and mounted on SuperFrost Plus Adhesion slides (Thermo Scientific). Slides were then stored at -20ºC until staining.

Frozen slides were defrosted for 30 minutes, then fixed in 4% PFA for 10 minutes at 4ºC. Post-fixing, sections were washed in PBS/0.3% Triton-X on a rocker for 5 minutes at room temperature. Sections were then blocked with 20% Normal Donkey or Goat Serum (NDS/NGS) in PBS/0.3% Triton-X for 2 hours at room temperature, before brief PBS washing on a rocker for 5 minutes.

For primary antibody incubation, antibody solution using 1% NDS/NGS in PBS/0.3% Triton-X was prepared (600 µl per slide). Slides were incubated at 4ºC for 48 hours, with 400 µL of PBS/0.3% Triton-X added to slides after 24 hours to prevent sections from drying out.

After 48 hours, slides were washed three times in PBS/0.3% Triton on a rocker, for 20 minutes (per wash) at room temperature. For secondary incubation, 600 µL of antibody solution was used per slide using 1% NDS/NGS in PBS/0.3% Triton-X. Slides were then incubated overnight at 4ºC, and then for 45 minutes at room temperature. Slides were washed three times in PBS/0.3% Triton on rocker, for 20 minutes (per wash) at room temperature, before being mounted using ProLong

Gold anti-fade mountant with DAPI (Life Technologies). Slides were then stored in darkness at 4ºC.

2.2.2.2 Viral Vector-Transduced Primary Cell Culture

4% PFA was added to the wells of the cell culture plate for 10 minutes at room temperature, to fix the cells. Wells were then washed out with PBS three times to halt fixing, before cells were mounted onto slides using ProLong Gold anti-fade mountant with DAPI.

2.2.3 Confocal Imaging

Immunofluorescent imaging of samples was carried out by the LSM 710 laser scanning confocal microscope, and Zeiss Zen Black image acquisition software. Any further image analysis was carried out using Zen Blue 3.3 (Zen Lite).

For cell counting, images were taken using x20 magnification with 1024 x 1024 pixels/320.09 x 320.09 µm image size. Images were captured using the Z-stack function and Maximum Intensity Projection application on Zen Black.

Cell counting was performed using ImageJ (Fiji) software (Schindelin, Arganda-Carreras et al. 2012).

6 animals were imaged for each brain region, with 3-6 images taken through the anterior-posterior plane. Images were selected by the quality of staining, which may have introduced some bias onto sections with more clearly defined TH^+ neurons. Borders for the imaging frame were focused on TH^+ neurons since the

investigation was looking for ZFHX3 expression in TH+ neurons, however all cells within the frame were counted.

For this method, the advantage is its simplicity – it involves only a 2D image of a maximum intensity projection of a simple Z-stack, and the cells can be counted either manually or with cell counting software. The disadvantages include: inconsistency of imaging position between samples; bias in imaging frame position; and difficulty distinguishing cells that are stacked in the Z-frame.

As opposed to the manual method stated here, a stereological method would give more advantages, taking random samples across the entire region to reduce bias, and taking data from 3D chambers in the tissue to differentiate stacked or ‘long’ cells – ensuring each cell is counted only once (Woodruff-Pak 2010, Bjerke, Yates et al. 2023).

2.3 Behavioural Phenotyping

All behavioural phenotyping was carried out in the Mary Lyon Centre (*Establishment Licence Number X9BFFDAE2*) according to standard operating procedures consistent across the centre.

To mitigate possible circadian effects on behaviour, all tests were carried out between 1pm-6pm - with the exception of Fear Conditioning, where the ‘conditioning’ and ‘context’ trials must be carried out in the morning.

All tests were carried out genotype-blinded, and testing was carried out in computer-randomised order.

2.3.1 Power Calculation

G*Power software (RRID:SCR_013726) was used to determine the minimum number of DAT-*Cre*; *Zfhx3*-Flox mice needed to reach statistical significance in behavioural phenotyping (Cohen 1988). Mean and standard deviation values were taken from preliminary behavioural data, the desired p-value was set at 0.05 and the desired power was set at 0.8. 'Cohen's d' – used to describe the magnitude of the effect expected – was set at 0.5, which is advised in the case of lab animals. The minimum n-number to reach statistical power was determined to be n=7.

2.3.2 Anxiety

All anxiety tests require mice to be left to habituate for 30 minutes in their home cages before being removed for testing.

2.3.2.1 Open Field

The apparatus consists of four open-top square arenas (44x44 cm) under 150-200 lux lighting conditions, with live video feed from an overhead camera above the arenas. The test runs over 20 minutes, with two to four same-sex mice undergoing testing at once, one mouse per arena (ensuring that male mice from different cages are not in the same run). Mice are placed along the edge of the arena.

The ambulatory behaviour of each mouse is measured and recorded by Ethovision XT 8.5 software (Noldus, Netherlands), and is defined by movement through and within three zones: periphery (8cm from arena walls), centre (11cm central square), and the intermediary zone.

2.3.2.2 Light-dark Box

The light-dark box is a Perspex arena comprised of a ‘light’ zone (open top) and a ‘dark’ zone (removable closed top) with a small opening between the two. A test run lasts for 10 minutes and is carried out under 100 lux light level. Two light-dark arenas are run simultaneously, with two mice of the same sex (one mouse per arena). Mice are placed in the open ‘light’ zone.

The ambulatory behaviour of each mouse is measured and recorded by Ethovision XT 8.5 software. Zones are defined as the ‘light’ zone, the ‘dark’ zone – which is hidden from the view of the camera – and the ‘entry’ zone, which reaches into the light zone for a short distance around the opening between ‘light’ and ‘dark’ zones. Parameter measurements are limited for the ‘dark’ zone, as ambulatory behaviour while in this zone cannot be recorded.

2.3.2.3 Elevated O-Maze

The elevated o-maze consists of a narrow circular track, with two ‘open’ zones, and two opposite ‘closed’ zones defined by walls each side of the track. A test run uses one maze for one mouse, is carried out at 50 lux light level, and lasts for 15 minutes.

The ambulatory behaviour of each mouse is measured and recorded by Ethovision XT 8.5 software, and is defined by movement through and within the two ‘open’ and two ‘closed’ zones.

2.3.2.4 Marble Burying

Marble burying consists of a standard home cage with three times the standard volume of bedding chips, and the food hopper removed. Nine marbles are placed in the cage, arranged into three rows of three. Mice are placed in a cage for 30 minutes, and once the mouse is returned to their home cage the number of marbles ≤2/3rd buried are counted.

2.3.3 Motor

2.3.3.1 Rotarod

The Rotarod apparatus is a rotating rod sectioned into five tracks, and can therefore test five same-sex mice in one run (ensuring that male mice from different cages are not in the same run). This test uses the accelerating rod protocol, with the Rotarod running for 300 s from 4 to 400 rpm.

The apparatus is placed in a laminar air flow cabinet, and each mouse is weighed before being placed in a lane. The test starts with a fixed-speed rotation, and once all mice are facing the same direction the accelerating protocol can begin. Mice are returned to their home cage once they fall from the rod, or begin to passively rotate.

Recorded parameters are: weight, walking duration on the rod, and method of test failure:

- Jump – the mouse jumps off the rod.
- Fall – the mouse falls without control.

- Controlled Drop – the mouse controls their fall by gripping the rod with their forepaws.
- Passive Rotation – the mouse stops walking and clings to the rod as it rotates.

2.3.3.2 Locotronic

The Locotronic apparatus (Intellibio) is a horizontal ladder run, with sensors beneath the rungs to detect any errors or slips in paw placement, while time taken to cross the length of the ladder is also recorded.

Each mouse undertakes three runs over two consecutive days – two on day one, with at least 30 minutes between runs, and one run on day two. Each run lasts a maximum of 5 minutes, or until the mouse completes the run. Results are calculated as an average of measurements across the three trials.

2.3.3.3 Gait Analysis (MouseWalker)

Mouse gait parameters are measured using the MouseWalker apparatus system (Mendes, Bartos et al. 2015). The apparatus consists of a transparent glass walkway and (removable) Perspex walls, with an angled mirror beneath the

Figure 2.3.3.3.1. Graphic illustration of MouseWalker view Image modified from BioRender.com.

walkway to allow for viewing and recording of paw placement. Two lights are situated around the walkway: red light shining above, and green light projected into the transparent walkway. Each time a paw comes into contact with the walkway, the effect of frustrated total internal reflection (fTIR) created by the green light means that paw placement can be easily seen by a camera, against the red light overhead the mouse (**Figure 2.3.3.3.1.**). The camera feeds into a computer running StreamPix 7 software (NorPix), for video recording and analysis.

This test is conducted in darkness to mitigate any effect of anxiety on their ambulation. Mice are habituated for 30 minutes in the testing room with all the lights switched off excluding the red and green walkway lights, and the computer monitor. The phenotyper is provided a head torch to allow for handling mice and equipment without the need to switch on the main lights.

One mouse is tested per run. The mouse is placed on the walkway (with the removable walls in position) and allowed to walk for 5 minutes. After 5 minutes the mouse is removed and the walkway is cleaned with Trigene and soft white tissue, taking exceptional care to remove any smudges to the walkway as this will interfere with data analysis. If the mouse does not move for 2 minutes after the start of the test, it is returned to its home cage

Video analysis of gait parameters was carried out at the Mary Lyon Centre by Dr Sonia Bains, using DeepLabCut software (Mathis, Mamidanna et al. 2018).

2.3.3.4 Grip Strength

This test uses a force sensor apparatus to measure the force of the mouse's grip on a metal grid – fore paws, and fore with hind paws together. One mouse is tested per run.

The force sensor is placed in a laminar flow cabinet for the test. Mice are first weighed, and then pulled steadily over the metal grid by the fore paws only, and then again with their fore and hind paws gripping the grid. Grip strength is measured in grams, and measurements are weight-corrected for each mouse.

2.3.3.5 Motor Function Test

Mice were tested for between one and two weeks. The motor function test involves mice being individually housed in cages with a running wheel connected to a desktop running TSE Systems PhenoMaster software, in order to record and assess activity under multiple parameters.

As with standard home cages, mice have access to food and a water *ab libitum* and are subject to a 12:12 light/dark cycle.

2.3.4 Memory

2.3.4.1 Forced Alternation

This test uses a Y-shaped arena, with different black-and-white patterns decorating the end wall of each arm. Each arm has a slot near the entrance to allow for a Perspex gate to be fitted, blocking off an arm. The arena is set under

an overhead camera, under 90-110 lux lighting conditions. One mouse is tested per run.

For the first run, one arm (deemed the ‘novel’ arm) is blocked off by a Perspex gate. The mouse is placed in the ‘start’ arm, and can explore one additional arm of the Y-maze, the ‘familiar’ arm. The first run lasts ten minutes. At the end of the run, the mouse is returned to the home cage for no more than 2 minutes while the arena is cleaned with Trigene and the gate is removed. For the second run, the mouse is then returned to the ‘start’ arm, and allowed to explore both the ‘familiar’ and ‘novel’ arms for five minutes.

The ambulatory behaviour of each mouse is measured and recorded by Ethovision XT 8.5 software, with behavioural parameters defined by movement between and within the three arms of the maze.

2.3.4.2 Novel Object Recognition

Novel Object Recognition is carried out in circadian cabinets, where each cabinet is single sex and home cages are open-top. Cages use bespoke metal cage lids and metal dividers, to allow for effective in-case recording from overhead cameras – one camera per cage. As with standard home cages, mice have access to food and a water *ab libitum* and are subject to a 12:12 light/dark cycle.

Two different objects (‘familiar’ objects’) are placed along the short edge of each cage (opposite from the food hopper) and left for 10 minutes. The objects are then removed for 30 minutes, and one object is replaced with a novel object. One

‘familiar’ and one ‘novel’ object are then placed back into the cage for 5 minutes. All objects are then removed and the test ends.

Mouse behaviour in relation to the objects is recorded and analysed using ANY-maze software (RRID:SCR_014289).

2.3.4.3 Fear Conditioning

Fear Conditioning test uses two arenas: a square arena with a metal grid floor, which delivers a foot shock during the ‘conditioning’ trial; and a circular Perspex arena with a black-and-white stripe pattern decorating the wall, and a Perspex floor. The test consists of three trials, and takes place over two consecutive days. ‘Conditioning’ and ‘context’ trials are carried out under 23-26 lux lighting conditions, while the ‘cue’ trial uses 15-18 lux light level. Freezing behaviour is recorded via overhead cameras.

Trial one is the ‘conditioning’ trial. The trial runs for 281 seconds, with a 20 second tone followed by a one second foot shock. Mice are returned to their home cages after the trial until the following day.

Trial two is the ‘context’ trial, and must be carried out 24 hours after the ‘conditioning’ trial. Mice are returned to the same square foot shock apparatus, however no tone sounds and no foot shock is administered. The test runs for 300 seconds, then mice are returned to their home cages.

Trial three is the ‘cue’ trial, which must be run at least 4 hours after the ‘context’ trial. This trial is run using the circular apparatus, with vanillin solution applied

around the top of the apparatus wall. This trial also runs for 300 seconds, with two 20 second tones sounding during the trial with no foot shock.

The freezing and ambulatory behaviour of each mouse is measured and recorded by Ethovision XT 8.5 software.

2.3.5 Sleep – Non-Invasive Sleep Screening

24 hour sleep recording and analysis takes place in circadian cabinets (*detailed in 2.3.3.2.*). Cameras above each cage record mouse activity in the cage, and locomotor activity over a 24 hour period (ZT0-ZT23) is analysed with ANY-maze software. Sleep is scored as periods of 40 seconds or more of immobility (Fisher, Godinho et al. 2012). In addition to the total amount of time spent asleep, the number and duration of sleep bouts was recorded. A sleep bout is defined as the period between the onset of sleep to waking.

2.3.6 Social Dominance

Mice pairs are matched against each other in dominance ‘bouts’ according to multiple criteria: one mouse is a control and the other is a mutant genotype, they must be the same sex, and they must not be litter- or cage-mates. Each mouse undergoes three dominance bouts against different mice who meet these same criteria.

The dominance apparatus consists of a red Perspex tube in a frame, with a slot in the centre of the tube to allow for fitting a red Perspex gate to block across the tube lumen. Each mouse is randomly assigned to enter opposite ends of the tube,

and once both mice are close to and oriented towards the gate, it is removed and the mice are allowed to interact. The mouse that backs off and out of their end of the tube is the ‘loser’, and the other the ‘winner’ of the dominance bout.

2.3.7 Startle and Pre-Pulse Inhibition

Mice must be left for 30 minutes after transport to the testing suite to allow for habituation.

Testing apparatus are comprised of a transparent Perspex tube with removable end plates, with holes bored into the side to allow sound to enter the tube (Med Associates Inc Equipment). These holders are inserted into custom-built sound cabinets - which are fitted foam soundproofing material and sound speakers - and screwed on to vibration plates that measure mouse startle responses.

One mouse is placed in each tube, and one tube is inserted into its own cabinet. The test programme runs from 45-50 minutes, where mice were subject to 15 110-db 40ms sound pulses, either alone or preceded by 65dB, 70dB or 75dB sound ‘pre-pulses’ in pseudorandom order (Nolan, Peters et al. 2000).

Vibration plates measure the mouse’s startle responses, which are recorded with Startle Reflex software.

2.3.8 Pain – Von Frey Filament Test

Von Frey Filaments are a standardised set of retractable silicone rods of increasing thickness/force application (0.008-300 g), used to test the reflexive pain

threshold of rodent hind paws. The pain reflex test is carried out over three trials, one trial per day.

This test is carried out inside of a laminar flow cabinet. Mice are placed on top of a metal grid inside individual black Perspex chambers, with a transparent ceiling, no floor, and a removable door plate. Up to 16 mice can be tested at once, with separate runs for female and male mice.

Mice are placed in individual chambers on the raised grid, and are habituated for one hour before testing begins.

A hind paw is initially poked with the 0.6 g rod in the centre, for no longer than two seconds. If there is no reflex, move up the filament pack to increase the thickness of the rod by one increment, and test again. Conversely if there was a reflex in the previous trial, decrease the rod thickness by one increment. The intention of the test is to determine the lowest thickness filament that causes a reflexive foot retraction.

One trial uses five paw pokes, with a minimum of two minutes between each paw poke. Repeat for both hind paws.

This trial is then repeated twice over two more days, to determine a pain threshold measurement for each paw.

2.4 Intracranial Injection Surgery

2.4.1 Final Experimental Protocol

Before the surgical procedure is carried out, stereotaxic co-ordinates of the target brain region are determined using a mouse brain atlas.

Prior to surgery, mice are individually housed for 72 hours and provided with condensed milk. 24 hours before surgery, mice are provided with Rimadyl analgesic mixed with condensed milk.

Before the procedure, the surgery area and all equipment are prepared and sterilised. The drill adaptor is attached to the stereotaxic frame micromanipulator (Kopf Instruments, Model 940 with digital display console), then all areas and apparatus are sterilised with Distel solution. All areas of the frame that will be touched during surgery are covered with cling film, and an autoclaved surgical drape is laid out on the adjacent table to create an aseptic field.

Surgical equipment and consumables are laid out in the aseptic field: an autoclaved surgery kit, autoclaved cotton buds and swabs, sterile sutures (Ethicon 5-0), a single-use sterile scalpel (15 blade disposable Swann Morton), sterile surgical gloves, a 25 g needle, and two small (2 x 2 cm) squares of Parafilm sterilised with Distel.

Non-sterile equipment is placed nearby, making sure not to touch the sterile surgical drape: 1% Virkon solution, AAV solution (on wet ice), a 1-10 µl Gilson pipette and tip box, ophthalmic ointment, a small pot containing 10% Hibiscrub, a 1 ml syringe containing Vetergesic, and a cling film box.

The glass syringes are prepared (Hamilton 7000 Series) and micropipettes attached (Biomedical Instruments ICSI Pipette, bevelled, straight, ID: 7 µm, BA: 0°, BL: 0 mm, TL: ~ 8 mm, PL: 55 mm, glass: BM100T-10P, VICbv-7-0-0-55) to the glass syringe using the Hamilton compression fitting (RN Compression Fitting

1 mm, 55750-01). Syringes and micropipettes are then primed with mineral oil (Thermo Scientific) using the Hamilton priming kit. Two prepared syringe-pipettes (if injecting bilaterally) are placed next to the sterile drape, with the glass micropipettes resting within their storage cases to both keep the micropipette tips sterile and the syringes stable on the table surface.

The mouse is then prepared for surgery. The mouse is weighed then anesthetised using 5% isoflurane. Once there is loss of pedal reflex, the isofluorane feed is switched to the face mask and reduced to 1-2% to allow for the mouse's scalp to be shaved. The mouse is then transferred over to the stereotaxic frame face mask (1-2% isofluorane).

The mouse's head is secured to the frame using Kopf ear bars – one end of each bar in an ear, with the other end attached to the stereotaxic frame. Ophthalmic ointment is then applied to both eyes on both eyes, the rectal thermometer is inserted, and the head sterilised by applying 10% Hibiscrub to the shaved area. Cling film is placed over the mouse as a surgical drape, then wiped above the head with a Steret swab to sterilise.

Nitrile gloves are removed and replaced with sterile surgical gloves, following correct aseptic technique.

A square opening is made in the cling film over the head using sterile surgical scissors. Using a scalpel, an incision is made down the middle of the skull dorsal, making an approximately 1 cm rostral-caudal incision, and fixed open using surgery clips. The fine layer of membrane under the scalp is gently scraped away to clearly expose the skull and skull bone markers - the Bregma marker is used to measure stereotaxic co-ordinates.

The drill (with an autoclaved drill piece) is fixed into the holder on the frame. The stereotaxic co-ordinates for the target brain region are then measured using the micromanipulator against the Bregma marker, to reach the X and Y co-ordinates on the skull corresponding to the target region. The drill is then used to make holes in the skull above the target brain regions, stopping short of the dura, which is then incised using the 25g needle.

After the drill-holes are made, the syringe-pipette is fixed into the micromanipulator on the frame.

To withdraw virus into the micropipette tip, an indent is pushed into the centre of a square of Parafilm which is placed atop the skull, with the sterile paper-fixed side touching the skull. The Gilson pipette is then used to pipette a small bead of AAV injection solution onto the Parafilm, and the end of the micropipette is lowered into the bead of solution. Using the micropump (UMP3 UltraMicroPump), virus solution (AAV5 10^{12} vg/ml, 800 nl) is withdrawn into the micropipette. The Parafilm square is then discarded into the Virkon solution.

Using the same process as with the drill, the syringe-pipette is adjusted to the required X and Y co-ordinates (over the drilled holes) for the target region, before lowering the pipette to the correct Z co-ordinates.

Once at the correct Z co-ordinates, the injection is carried out by the at a rate of 200 nl a minute). After the injection is complete the micropipette must be left in place for 10 minutes, before either removing the pipette or moving up to the next Z co-ordinate target in the region (to a maximum of 4 injections per hemisphere). If injecting bi-laterally, the syringe-pipette is replaced before repeating the withdraw-inject steps in the second region.

Once injections are complete, the scalp is sutured closed, ensuring the loose ends are cut fairly close to the skin to prevent the mouse from pulling the sutures. Between 0.08-0.1 ml of Vetergesic dilution (0.1 mg/kg) is administered via subcutaneous injection, and the mouse is placed into the recovery ‘hot box’ until fully recovered from anaesthesia. The mouse can then be returned to home cage and placed back on the ward. Mice that have not recovered from anaesthesia within two hours are euthanised.

Re-useable surgical equipment and the surgical drape are sealed into autoclave bags and taken to be autoclaved. Any consumables that have come into contact with viral solution must be left in Virkon solution for at least 24 hours before disposal.

Mice are subject to daily welfare checks to assess healing and general health, with a number of humane endpoints in place:

1. **Appearance**

- Weight loss exceeding 15%
- Piloerect coat showing no improvement over 24 hours
- Skin lesions showing no improvement within 48 hours
- Increases in urination leading to dehydration for more than 24 hours.

2. **Posture**

- Hunched appearance, not improving within a working day
- Tremors or abnormal gait impinging on the ability to feed

3. **Behaviour**

- Abnormal response to handling impinging on the welfare of the animal (lethargy, extreme hyperactivity)
- Unprovoked vocalisation
- Head tilt not improving within 24 hours

Post-mortem brain tissue is required to be submerged in 4% PFA for at least 48 hours prior to further experiments, to ensure the absence of active viral particles. Mice that have undergone intracranial injection of virus solution are not to be perfused, as this would cause live viral particles to contaminate the perfusion equipment.

2.4.2 Initial Protocol

The original protocol used by the centre differed in the following ways:

- Instead of a glass micropipette, a metal 25g Hamilton needle (260µm I.D.) was used.
- Syringes were primed with sterile water, as opposed to mineral oil.
- An air bubble was introduced into the water priming the syringe to track injection volume.
- Virus solution was withdrawn into the Hamilton syringe directly from the virus storage Eppendorf, held up to the needle by hand.
- The syringe-needle was attached to the micromanipulator from the beginning of surgery.
- X- and Y-co-ordinates were measured using the mounted syringe-needle, and a 25 g needle was used to mark the skull for drilling.

- Drills were used by hand.
- AAV2 virus was used as opposed to AAV5 (**Table 2.4.3.1.**)

2.4.3 Viruses

Serotype	Vector Promotor	Cre	Fluorescent Reporter	Delivery Titre (vg/ml)	Applied Titre (vg/ml)	Supplier
AAV2	Syn	+	Venus	1.77E+13	10E+11 and 10E+12	University Medical Centre Hamburg-Eppendorf (UKE)
		-	Venus	2.33E+13		
AAV5	Syn	+	dTomato	7.00E+12	7.00E+12	Addgene
		-	mCherry			

Table 2.4.3.1. Viruses used for intracranial injection

Viruses are stored at -80°C in 2 µl aliquots, with each aliquot permitted 2 freeze/thaw cycles. Virus solution is kept on wet ice at all times when not in storage.

2.5 Molecular Analysis

2.5.1 RNA Extraction

RNA extraction for qPCR and RNASeq was carried out using Invitrogen RNAqueous-4PCR Kit, which uses a phenol-free method. Before proceeding, all surfaces were been cleaned with Ambion RNaseZap solution to remove any RNase enzymes that could degrade samples. Similarly, all plastics used in this protocol were RNase-free, and gloves were be changed often to avoid contamination of samples.

Firstly an aliquot of elution solution (approximately 50-200 µl per prep) was warmed on a heat block to 70-80°C, to use later in the elution step. Tissue samples – in this case fresh frozen brain sub-dissections (cortex, striatum, and midbrain) - were disrupted using an RNase-free pestle and lysis solution (10–12 volumes per tissue mass). The homogenised solution was then mixed with an equal volume of 64% ethanol solution, and the tube inverted until mixed thoroughly.

The lysis-ethanol mixture was drawn through a filter cartridge using a centrifuge set at 10,000–14,000 rpm for up to 1 minute, which captures the sample RNA while the remainder of the mixture passes through into a collection tube to be discarded. The filter cartridge was then washed multiple times, to remove RNases and other proteins caught in the cell cartridge. The RNA sample was then eluted from the filter cartridge using the pre-heated elution solution.

RNA samples were then stored at -20°C for short-term storage, or -80°C for long-term storage.

2.5.2 Quantitative PCR

2.5.2.1 Primers

Gene	Protein	Direction	Sequence
Drd1	**Dopamine receptor D1**	Forward	GTCTCCCAGATCGGGCATT
		Reverse	AGTCACTTTTCGGGGATGCT
Drd2	**Dopamine (auto)receptor D2**	Forward	GACACCACTCAAGGGCAACT

		Reverse	TCCATTCTCCGCCTGTTCAC
Drd3	**Dopamine receptor D3**	Forward	ACGGGACAAATGGAGCACAT
		Reverse	TGGCAGATGCTGTAGTAGCG

Table 2.5.2.1.1. Primers for qPCR

2.5.2.2 Method

Before carrying out the complete qPCR experiment, standard curves for each primer pair were generated. This used one RNA sample, run in 10-fold serial dilution with each primer pair. Once standard curves are generated, all samples were analysed using these primers. Both of these steps were carried out using the same protocol.

qPCR was carried out using the PrecisionPLUS OneStep RT-qPCR Master Mix, containing SYBR Green I (SG) for DNA detection. 'Housekeeping' gene RNA-binding protein 39 (Rbm39) was used as a control.

A master mix was created for each primer pair, using the following volumes per well:

- 10 µl RT-qPCR Master Mix
- 0.4 µl of 10 µmol Forward Primer
- 0.4 µl of 10 µmol Reverse Primer
- 8.2 µl DEPC-treated water
- 1 µl (50 ng) of RNA template

The PCR plate was covered in in acetate film, and spun for a few seconds before the plate was loaded into the thermocycler with the following settings:

1. **Step 1** - 55°C, 10 minutes
2. **Step 2** - 95°C, 8 minutes
3. **Step 3** - (40 cycles)
    - 95°C, 10 seconds (denaturation)
    - 60°C, 1 minute (annealing and elongation)
4. **Step 4** – Melt curve
    - 95°C, 15 seconds
    - 60°C 1 minute
    - 95°C 30 seconds

qPCR analysis was carried out using Applied Biosystems 7500 Real-Time PCR Software v.2.3 (ThermoFisher Scientific).

Relative quantification of target genes was calculated using the Pfaffl method, which is used when qPCR experiments use primers of varying efficiency (Pfaffl 2001).

2.5.3 RNA Sequencing

2.5.3.1 Sample Preparation and Sequencing

Tissue samples were from both female and male mice, from cortex, midbrain, and striatum brain sub-dissections. Mice were *Zfhx3*$^{Flox/Flox}$ DAT-*Cre*$^{+}$ experimental genotype, with *Zfhx3*$^{WT/WT}$ DAT-*Cre*$^{+}$ as controls. RNA samples (*Methods 2.5.1.*) were quality controlled using Nanodrop.

Libraries were generated by The Oxford Genomics Centre using Poly(A) RNASeq on NovaSeq6000 (Illumina) platform.

2.5.3.2 Analysis and Comparisons

Sample pair sequence files (FASTQ) were uploaded onto Galaxy Europe web platform (https://usegalaxy.eu), which contains free-to-use RNASeq analysis tools (Afgan, Baker et al. 2018). Sequence files were first subject to quality control using FastQC (version 0.11.9), before adapter trimming using Trim Galore! software and re-running FastQC sequence analysis. RNA-STAR (Spliced Transcripts Alignment to a Reference) aligns each sequence pair to a reference genome file (*Mus musculus*), then featureCounts quantifies RNASeq reads to allow for comparison of expression levels between samples. Comparisons were then generated using limma software, and differential gene lists were defined as having statistical significance $p \leq 0.1$.

2.5.3.3 Post-Comparison Analysis

Protein interaction networking analysis of differential gene lists was carried out using the STRING database (https://string-db.org) of known and predicted protein-protein interactions (Szklarczyk, Gable et al. 2021) and biological function/disease associations using the KEGG database – also on string-db.org (Kanehisa and Goto 2000, Kanehisa 2019, Kanehisa, Furumichi et al. 2023). Networks were generated using only experiments and databases as active interaction sources, and using the highest confidence setting (0.900).

Enrichment and function of differential genes across the synapse were analysed SynGO (Synaptic Gene Ontologies) (https://www.syngoportal.org), which analyses

gene/protein function and localisation of synaptic proteins within the synapse (Koopmans, van Nierop et al. 2019).

2.5.4 Primary Cell Culture and Viral Vector Transduction

Solutions:

- 1:500 in ddH_2O, Poly-L-lysine hydrobromide (PLL) solution (Sigma-Aldrich)
- 1:500 in ddH_2O, Laminin (Sigma-Aldrich)
- HABG:
    - Hibernate-A (HA) medium (Fisher Scientific)
    - Glutamax (Thermo Fisher)
    - B27 (Invitrogen)
    - Penicillin-Streptomycin solution (Sigma Aldrich)
- Papapin solution
    - Papain (Worthington Biochemical)
    - Hibernate-A medium
- Neurobasal A medium complete (NB-A)
    - Neurobasal A (Invitrogen)
    - B27
    - Glutamax
    - Penicillin-Streptomycin solution

Primary neuronal cells were grown in a 12-well plate on 19 mm glass cover slips. To prepare, glass cover slips (Thermo Scientific) in 12-well plates were treated with 70% ethanol overnight, then exposed to UV light. Coverslips were then coated in PLL solution and incubated overnight at 37°C. PLL was then removed

from the wells and coverslips allowed to dry. Laminin-PLL solution (3:7 ratio) was then added to the wells – enough to coat the coverslips - and cultured overnight at 37°C. After washing plate wells twice with NB-A solution (Invitrogen), 1 ml NB-A was added to each well. The plate was then ready for use in primary cell culture.

Cortical and hippocampal tissue (P0 male C57BL/6N) were dissected and collected into tubes containing 1 ml HABG on ice, and once all tissue was collected tubes were incubated at 30°C for 8 minutes. HABG was removed from the tubes, and the tissue was washed twice with warm HA medium before being incubated at 30°C for 15-20 minutes in 1:1 HA-papain solution. After incubation, tissue was washed 5 times with HABG, and then allowed to rest for 5 minutes at room temperature.

3 ml of HABG was added to each tube, and tissue was triturated with a p1000 Gilson pipette, then a fine polished glass pipette. Cells were allowed to settle for one minute, then passed through a 40 µm cell strainer (Scientific Laboratory Supplies). The strained solution was then centrifuged at 1000 rpm at 4°C, until a pellet formed. The supernatant was discarded, and the pellet re-suspended in 3 ml of pre-warmed (30°C) NB-A.

Wells were seeded with 75k cells each, which is optimal for confocal imaging. NB-A solution was changed every 7 days, by removing half of the solution in the well and replacing with fresh NB-A.

5 days after plating, wells were inoculated with 1 µl each of either 10^{12} or 10^{13} vg/ml, of either AAV2-*Cre*-Venus or AAV2-Venus. Transfected cells were then incubated for a further 14 days before mounting for imaging.

2.6 Statistics

Unless otherwise specified, statistical analysis of data was carried out using Microsoft Excel (2016) and GraphPad Prism (v.9).

Statistical tests used were: T-test for discrete variables; 2-way ANOVA for multiple variables; and Chi^2 for categorical variables.

Statistical tests carried out for each behavioural test:

- Unpaired T-Test – all anxiety tests, all motor tests, Y-maze, novel object recognition, sleep, Von Frey, pre-pulse inhibition
- 2-way ANOVA with Šídák's multiple comparison – rotarod, motor function test, Y-maze, fear conditioning, sleep
- 2-way ANOVA with mixed-effects analysis with multiple comparisons - sleep
- Chi^2 test – Y-maze, novel object recognition, social dominance

Assumptions:

- T-Test: normality was visually inspected on quantile-quantile plots; similarity of variance was tested using the F-test; sample data was not randomly sampled from a population due to low n-numbers; and the data was continuous.
- 2-way ANOVA: normality was visually inspected on quantile-quantile plots; similarity of variance was tested using the F-test; samples were independent (mice); the Greenhouse–Geisser correction was applied in order to compensate for any lack of Sphericity; however the groups did not have the same sample size due to low n-numbers.

- Chi^2: assumptions were met by having counts of cases (mice) as opposed to percentages, the categories were mutually exclusive, and each subject (mouse) contributed data to only one cell in the test.

For 2-way ANOVA, multiple test corrections were carried out using either/both Šídák's multiple comparison, or mixed-effects analysis with multiple comparisons. See details on which tests these were used on, above.

2.7 Statement on n-numbers

It is notable that in this study, that the n-numbers in Chapters 4, 5, and are low – and therefore statistical significance is difficult to achieve. This was due to multiple factors, including personal illness (meaning mice aged out of certain age categories) and COVID - where we were both unable to use the animal centre, and all experimental cohorts were culled due to welfare concerns; and severe phenotypes leading to welfare culls. Please keep these factors in mind when reading Chapters 4, 5, 6 and the Discussion, and consider this study to be a pilot study that needs further expansion with a higher n-number.

3

Results I: Expression study of ZFHX3 in midbrain dopaminergic regions and in cortex

3

Results I: Expression study of ZFHX3 in midbrain dopaminergic regions and in cortex

3.1 Introduction

Zfhx3 has been implicated in dopaminergic function and disorders, and enrichment of expression of *Zfhx3* in dopaminergic centres is detailed in the Allen Brain Atlas (*Introduction 1.1.5.).* However, the pattern of ZFHX3 expression across neuron identities in dopaminergic centres – the ventral tegmental area (VTA) and substantia nigra pars compacta (SNc) – are unreported. The Allen Brain Atlas also reports gene expression using *in-situ* hybridisation, and does not directly measure ZFHX3 protein expression levels.

This project uses two conditional knockout mouse models to examine the effects of ZFHX3 deletion in dopaminergic regions (*Introduction 1.3.1.*). Considering neuron target identities, the DAT-*Cre; Zfhx3*-Flox line knocks out *Zfhx3* in dopaminergic neurons only, while the injection AAV-*Cre* knockout line has *Zfhx3* knocked out in all neuron sub-populations around the target injection site (VTA).

Therefore in order to discuss the behavioural phenotype and molecular changes in the knockout mutants, it is imperative to characterise ZFHX3 expression in these regions - most pertinently, the pattern of expression amongst neuronal sub-populations.

Upon discovery of ZFHX3 expression in the mouse cortex, this study included investigation of expression in the primary auditory cortex (Au1) as upregulation of ZFHX3 expression is seen in the superior temporal gyrus of schizophrenic patients – for which the Au1 is the mouse analogous region (*Introduction 1.1.4.5.*). As the behavioural study of the conditional knockout lines of this project was focused on schizophrenia endophenotypes, defining ZFHX3 expression levels in the Au1 would be a pertinent line of inquiry.

3.2 Neuronal identities in dopaminergic centres

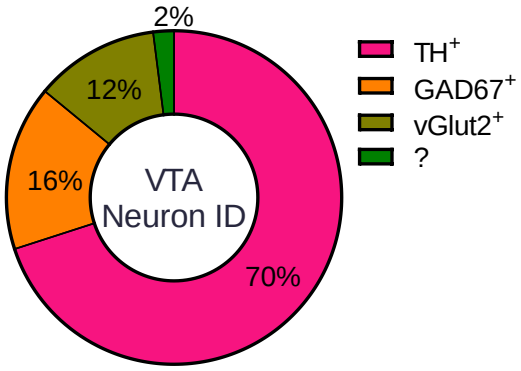

Figure 3.2.1. Distribution of neuronal identities in the VTA VTA chart modified from (Kim, Kim et al. 2019)

The VTA consists of multiple neuron subpopulations, including dopaminergic (TH^+), GABA-ergic ($GAD67^+$) and glutamatergic ($vGlut2^+$) neurons (Kim, Kim et al. 2019)(**Figure 3.2.1.**), while the SNc consists mostly of dopaminergic neurons, with a diverse population of other neuronal identities, most notably GABA-ergic neurons (Yung, Häusser et al. 1991)

This study characterises ZFHX3 expression in all cell identities cells (DAPI-stained), and in TH^+ neurons, in these regions.

3.3 Aims

The aim of this study is to confirm expression of ZFHX3 in dopaminergic centres in the wildtype C57BL/6N (B6N) mouse brain, and to define its expression profile in dopaminergic neurons within these centres - the VTA and SNc.

3.4 Expression in dopaminergic centres

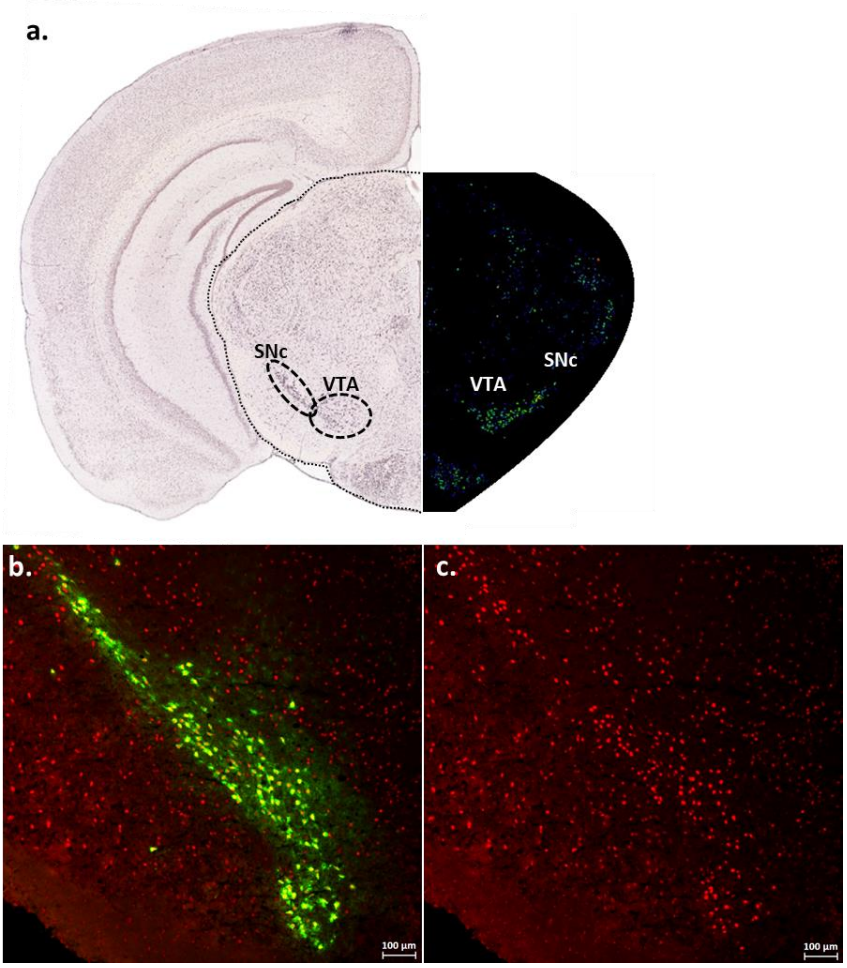

Figure 3.4.1. *Zfhx3* expression in the VTA and SNc (a) a composite image showing *in-situ* hybridisation (left) and expression data (right) of *Zfhx3* localisation in the midbrain (images modified from the Allen Brain Atlas (Lein, Hawrylycz et al. 2007)); (b) immunofluorescent staining of wildtype B6N midbrain sections, with the VTA and SNc labelled with TH in green, and *Zfhx3* in red; (c) single-channel image of (b), showing red *Zfhx3* expression in the VTA and SNc. Images taken at x5 magnification.

It was initially reported in the Allen Brain Atlas that *Zfhx3* is expressed in the dopamine centres in the midbrain – the VTA and the SNc – using ISH (**Figure 3.4.1. a)**. The intention of this line of inquiry was to confirm the expression of ZFHX3 in these regions using an anti-ZFHX3 antibody co-labelled with tyrosine hydroxylase (TH) – a dopaminergic marker (**b, c**).

Primary results confirm that ZHFX3 is expressed in the VTA and SNc, in line with ISH data from the Allen Brain Atlas. While the neuron population in the SNc is

comprised of solely dopaminergic neurons, the VTA is comprised of multiple neuron identities (*Chapter 3, 3.2.*). This project utilises both a dopaminergic neuron-only *Zfhx3* knockout line, and an intracranial AAV-*Cre* injection line that induces knockout in all neurons in the VTA, therefore the neuronal localisation of ZFHX3 expression within these regions should be characterised in order to assess the extent of *Zfhx3* knockout in these two lines.

3.4.1 Ventral Tegmental Area

ZFHX3 expression can be seen throughout the VTA and specifically in dopaminergic neurons, in both females and males (**Figure 3.4.1.1.**). From double-labelling IF antibodies, staining with DAPI, and cell counting in the VTA (*Methods 2.2*)(**Figure 3.4.1.2.**), the proportion of cells in this region expressing ZFHX3 is 29.5% in females and 29.6% in males, with no significant difference between sexes (a; p= 0.7588).

Out of all ZFHX3-expressing cells in the region, the proportion of cells that are dopaminergic neurons is 43.1% in females and 41.7% in males, with no significant difference between the sexes (b; p=0.9688).

Looking solely at dopaminergic neurons, the proportion of neurons expressing ZFHX3 is 94.7% in females and 91.5% in males, with no significant difference between the sexes (c; p= 0.4626). Statistical analysis was performed using unpaired t-test. Data are shown as mean ± standard error of mean.

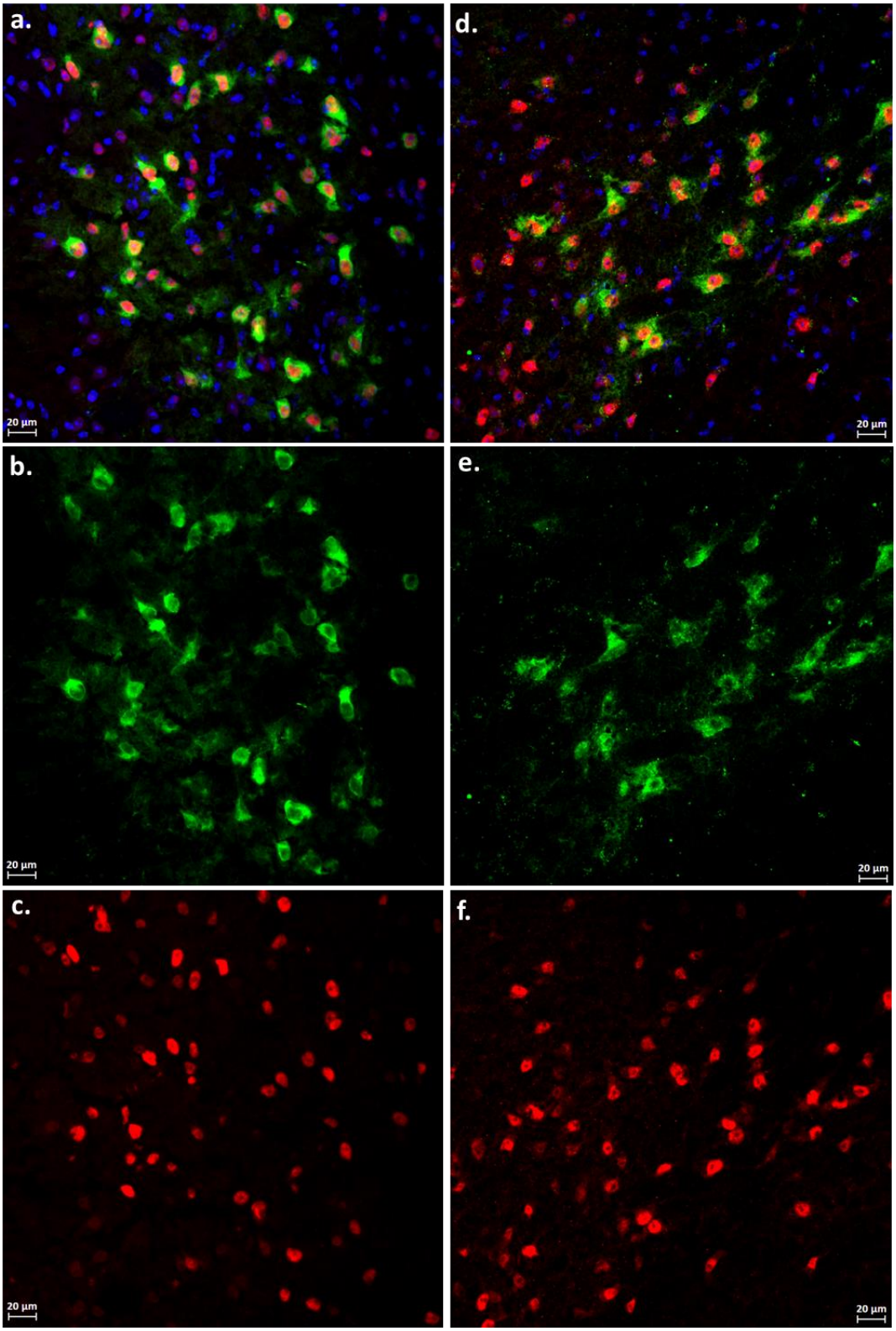

Figure 3.4.1.1. Immunofluorescence - *Zfhx3* expression in the VTA (a) immunofluorescent staining of female wildtype B6N midbrain sections, with the VTA labelled with TH in green, *Zfhx3* in red, and DAPI in blue; (b) TH only; (c) *Zfhx3* only; (d) staining of male wildtype B6N midbrain sections, with the VTA labelled with the same antibodies; (e) TH only: (f) *Zfhx3* only. Images taken at x20 magnification.

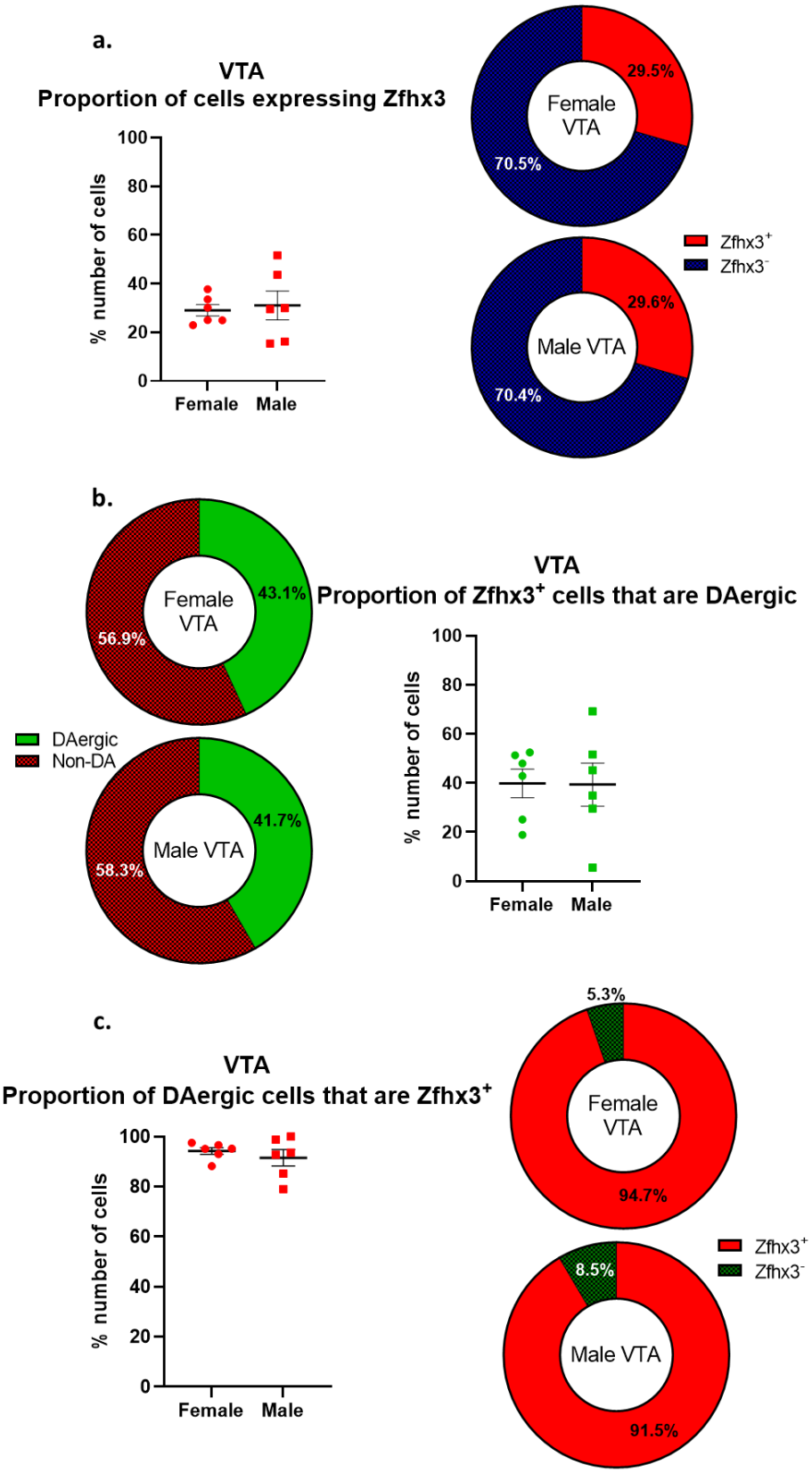

Figure 3.4.1.2. Cell Counting – *Zfhx3* expression in the VTA (a) proportion of cells expressing *Zfhx3;* (b) proportion of *Zfhx3*-expressing cells that are dopaminergic neurons; (c) proportion of dopaminergic neurons that express *Zfhx3*. n=6 for both females and males.

3.4.2 Substantia Nigra Pars Compacta

ZFHX3 expression can be seen in across the entire region and also specifically in dopaminergic neurons, in both females and males (**Figure 3.4.2.1.**). From counting cells and co-fluorescence In the SNc (**Figure 3.4.2.2.**), the proportion of cells in this region expressing ZFHX3 is 24.5% in females and 27.2% in males, with no significant difference between sexes (a; p= 0.3799).

Out of all ZFHX3-expressing cells in the region, the proportion of cells that are dopaminergic neurons is 36.4% in females and 29% in males, with no significant difference between the sexes (b; p= 0.2641). Since not all neurons in the SNc are dopaminergic, these results imply that there is either a population of non-dopaminergic cells expressing ZFHX3 in this region, or that confocal images of the area included $ZFHX3^{+}$ (TH^{-}) neurons from other regions outside of the SNc. Further investigation is needed to clarify these numbers, including a more precise ruling on the spatial boundaries of the SNc region.

Looking solely at dopaminergic neurons, the proportion of neurons expressing ZFHX3 is 91% in females and 88.7% in males, with no significant difference between the sexes (c; p= 0.4357). Statistical analysis was performed using unpaired t-test. Data are shown as mean ± standard error of mean.

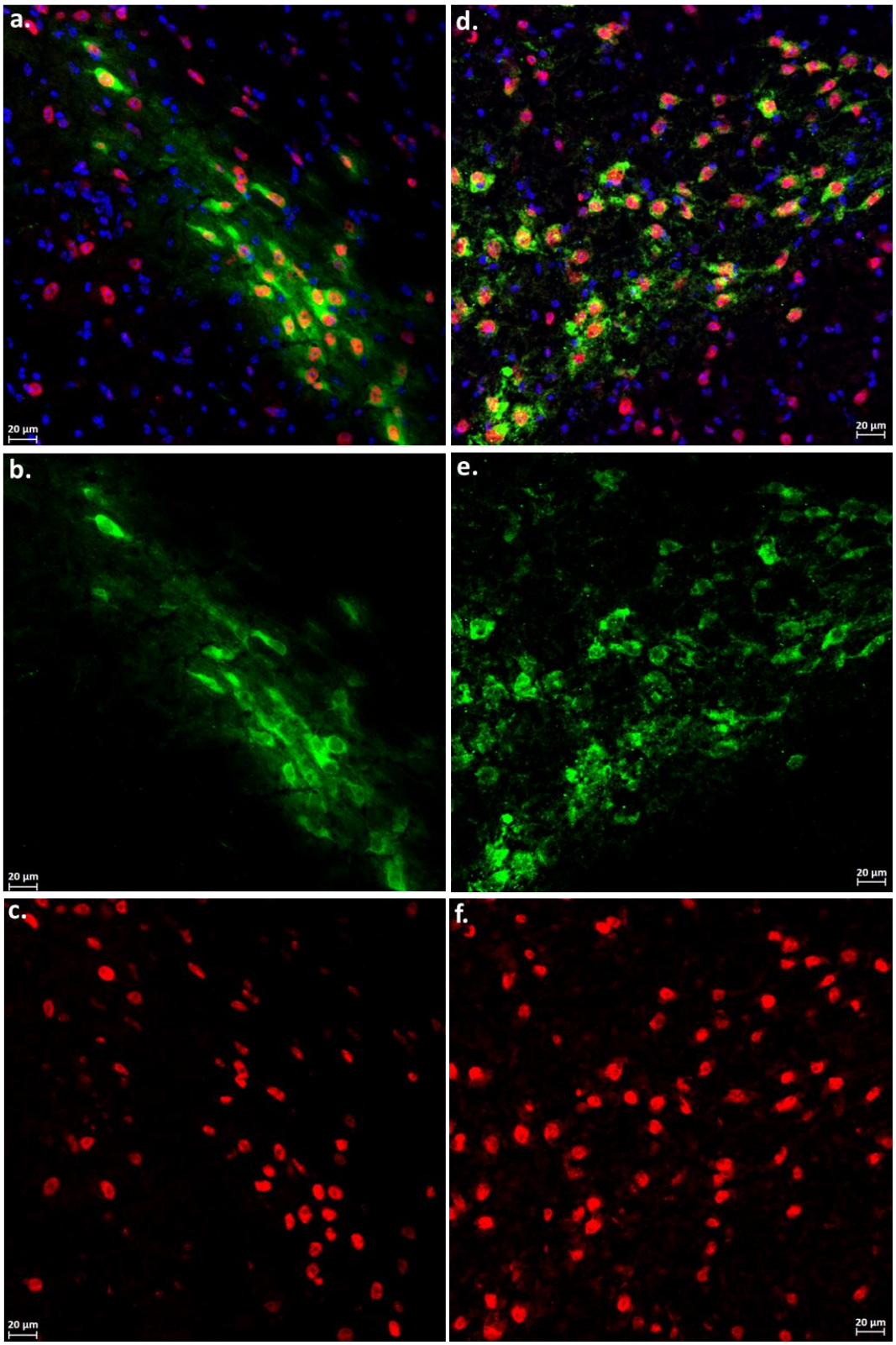

Figure 3.4.2.1. Immunofluorescence - *Zfhx3* expression in the SNc (a) immunofluorescent staining of female wildtype B6N midbrain sections, with the SNc labelled with TH in green, and *Zfhx3* in red; (b) TH only; (c) *Zfhx3* only; (d) staining of male wildtype B6N midbrain sections, with the SNc labelled with the same antibodies; (e) TH only: (f) *Zfhx3* only. Images taken at x20 magnification.

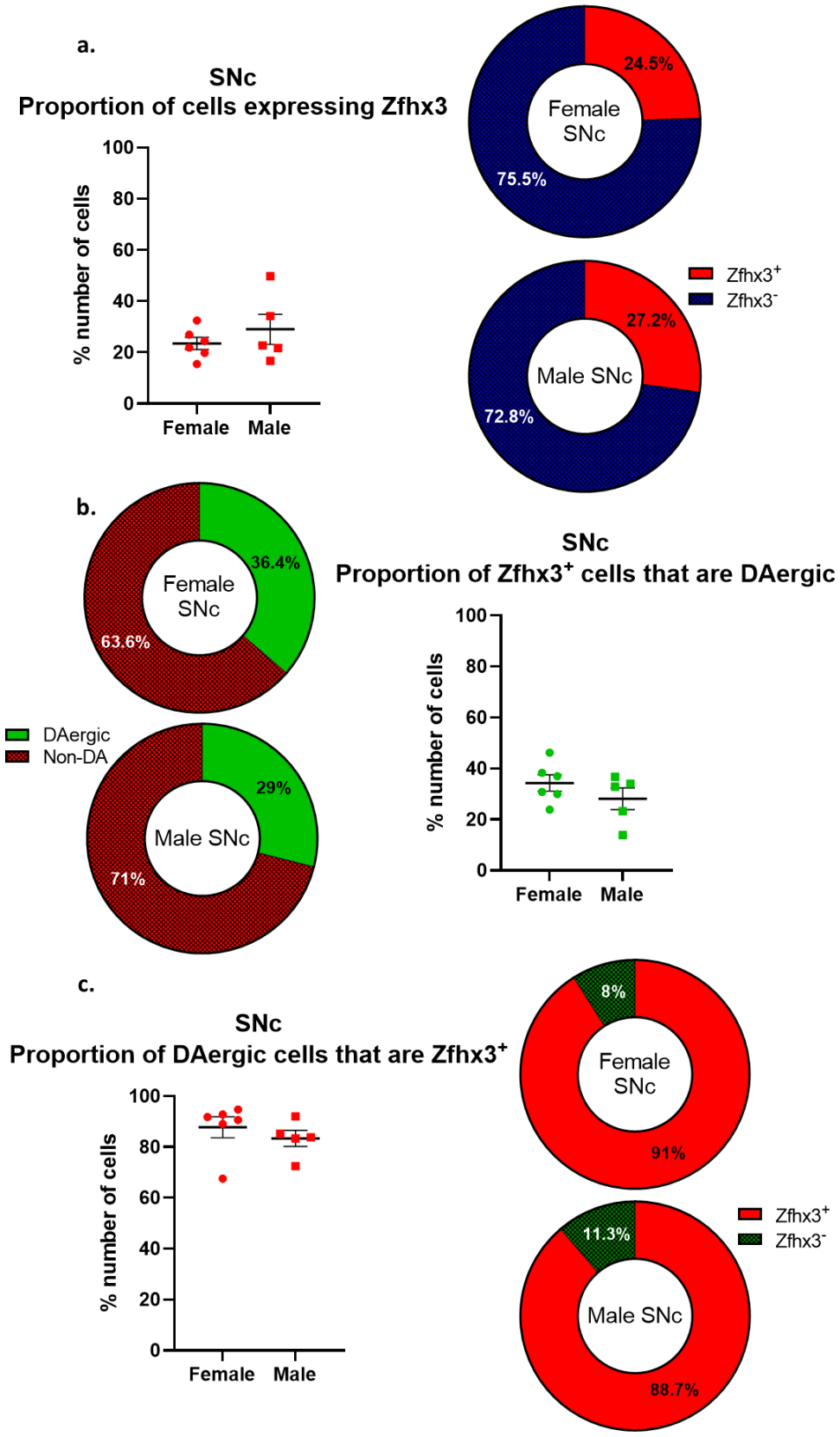

Figure 3.4.2.2. Cell Counting – *Zfhx3* expression in the SNc (a) proportion of cells expressing *Zfhx3;* (b) proportion of *Zfhx3*-expressing cells that are dopaminergic neurons; (c) proportion of dopaminergic neurons that express *Zfhx3*. n=6 for females, n=5 for males.

3.5 ZFHX3 expression pattern comparison between dopamine centres

When comparing ZFHX3 expression between the VTA and SNc – via counting ZFHX3^{+} cells- there are measureable differences in the expression patterns between female and male wildtype mice (**Figure 3.5.1.**).

In overall number of cells expressing ZFHX3, male mice show no significant difference in expression between the VTA and SNc (d; p= 0.5085), however female mice show significantly higher ZFHX3 expression in the VTA compared to the SNc (a; p= 0.0043). Neither female nor male show differences in the proportion of ZFHX3^{+} cells that are dopaminergic neurons, however males display a trend towards a greater proportion in the VTA over the SNc (b; p= 0.2941)(e; p= 0.0529). In addition, neither female nor male mice show significant differences in the proportion of dopaminergic neurons expressing ZFHX3 (c; p=0. 0.0849) (f; p= 0.1466). Statistical analysis was performed using paired t-test. Data are shown as mean ± standard error of mean.

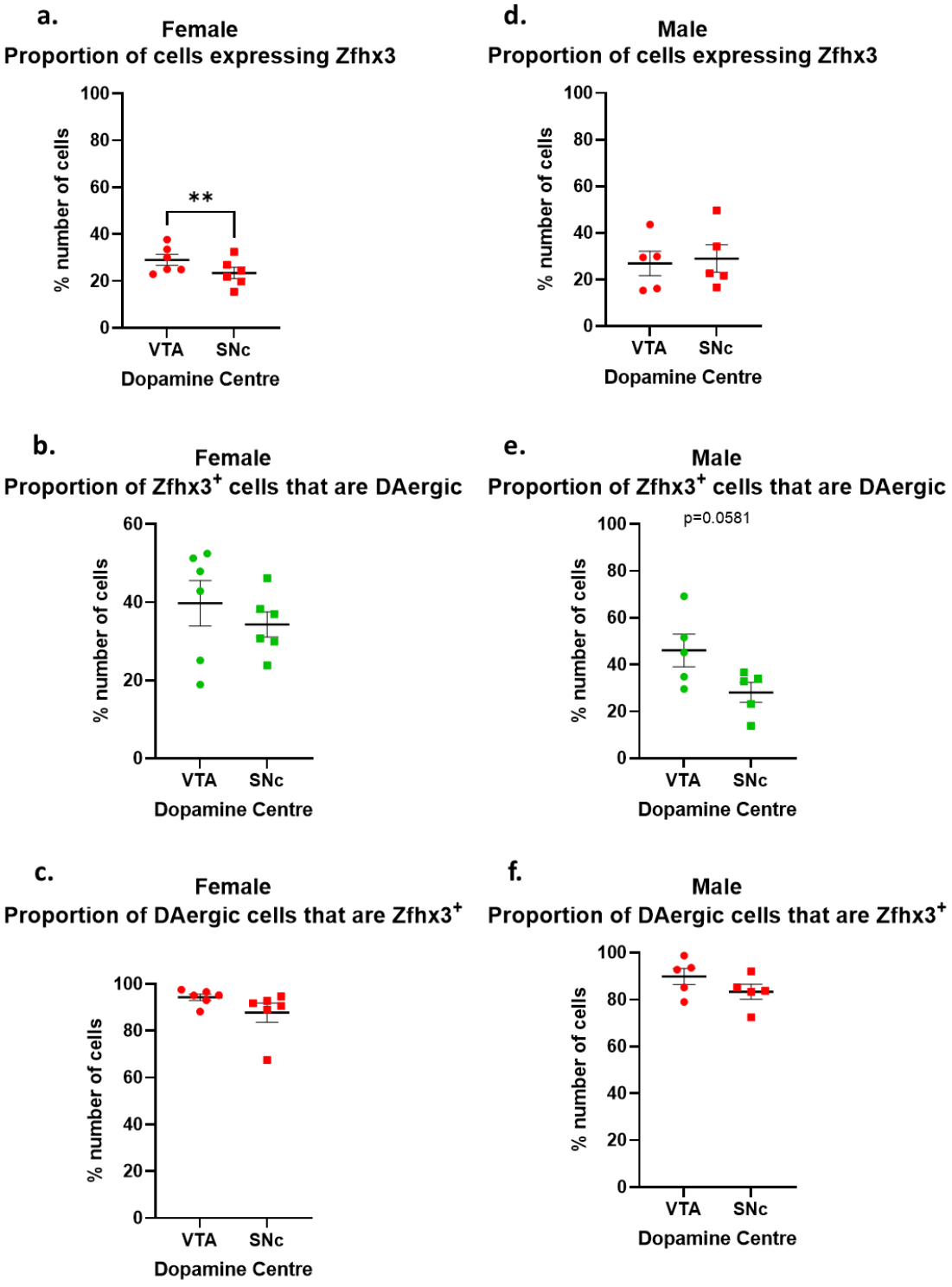

Figure 3.5.1. *Zfhx3* expression pattern comparison between dopamine centres analysing differences in expression levels between the VTA and SNc: (a)(d) proportion of cells expressing *Zfhx3*, (b)(e) proportion of *Zfhx3+* cells that are dopaminergic neurons, and (c)(f) proportion of dopaminergic neurons that are *Zfhx3+*, in female and male coronal sections respectively. Significance is represented by: ** $p \leq 0.01$.

3.6 ZFHX3 and the Primary Auditory Cortex

According to Allen Brain Atlas ISH data, there is no notable enrichment of *Zfhx3* expression in the cortex. However from immunofluorescent staining of wildtype sections with this custom generated ZFHX3 antibody, expression was seen across the cortex, most pertinently in the Au1. In the Au1, proportion of cells expressing ZFHX3 is 54.3% in females and 57.7% in males, with no significant difference between the sexes ($p = 0.4691$)(**Figure 3.6.1.**). Statistical analysis was performed using unpaired t-test. Data are shown as mean ± standard error of mean.

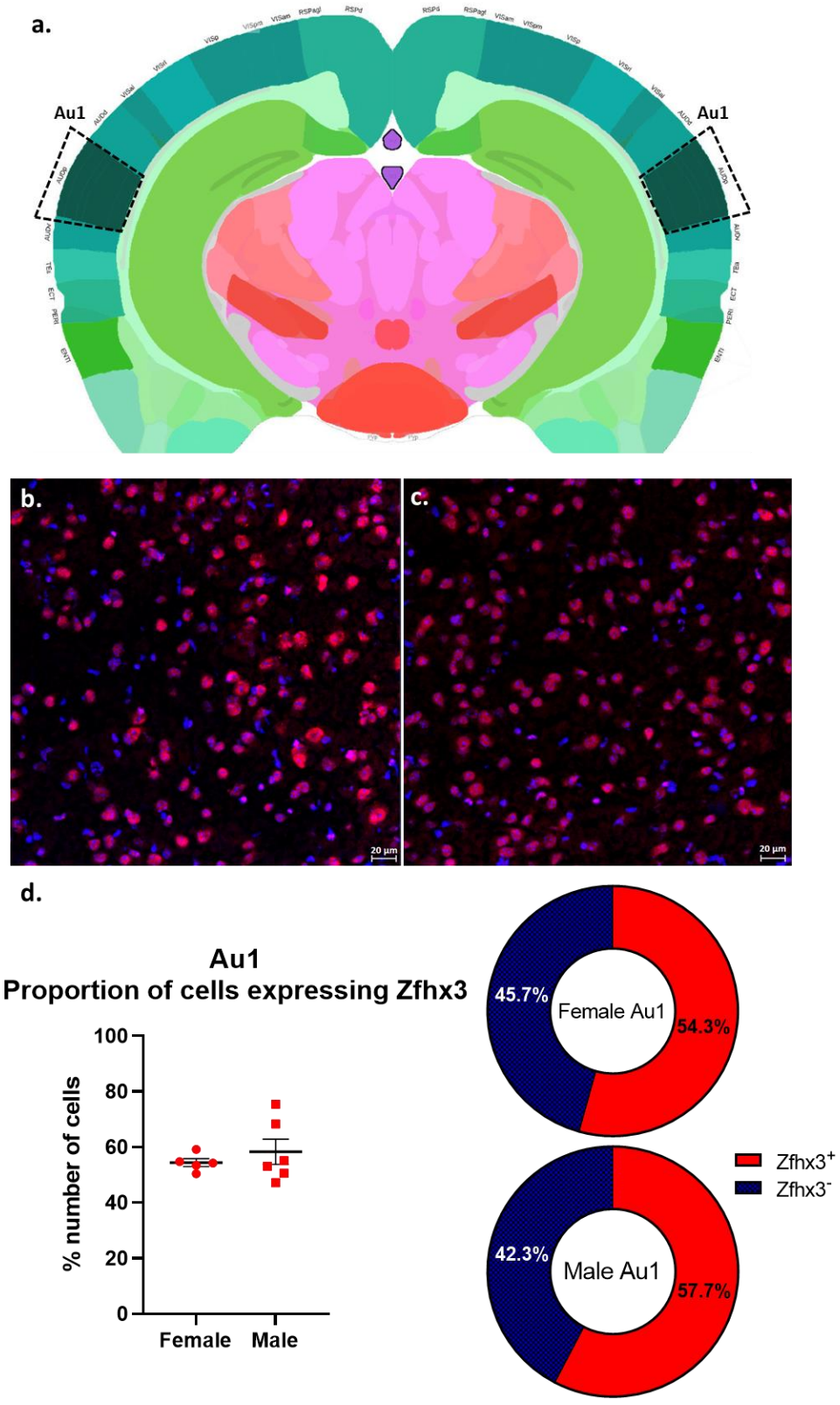

Figure 3.6.1. Immunofluorescence and Cell Counting - *Zfhx3* expression in the Au1 (a) location of Au1 in coronal mouse brain section (Image modified from the Allen Brain Atlas (Lein, Hawrylycz et al. 2007)); (b) immunofluorescent staining of female wildtype B6N cortical sections, with the Au1 labelled with DAPI in blue, and *Zfhx3* in red; (c) staining of male wildtype B6N cortical sections, with the Au1 also labelled with DAPI and *Zfhx3*; (d) proportion of cells in the Au1 expressing *Zfhx3*. Images taken at x20 magnification. n=5 for females, n=6 for males.

3.7 Discussion

In line with ISH data from the Allen Brain Atlas, there is enrichment of ZFHX3 expression in the dopaminergic centres of both female and male wildtype mice.

In both the VTA and SNc, there is no significant difference in expression pattern between female and male mice. In overall levels of ZFHX3 expression, the proportion of all cells (DAPI-stained) expressing ZFHX3 is around 30% in the VTA and 25% in the SNc (although as previously mentioned the SNc needs to be more thoroughly examined). Amongst ZFHX3^{+} cells, the proportion that are dopaminergic neurons is around 40% in the VTA and around 30% in the SNc. However, in both regions the proportion of dopaminergic neurons that express ZFHX3 is around 90%. These results suggest that ZFHX3 plays a key role within the dopaminergic centres, in both dopaminergic neurons and other cell types in the regions.

There are however differences in ZFHX3 expression patterns in females and males, when comparing expression between dopaminergic centres. Females show significantly more overall ZFHX3 expression in the VTA compared to the SNc, while males do not show this contrast in regions. Males show a trend towards the VTA having a greater proportion of ZFHX3^{+} cells being dopaminergic neurons than the SNc, while females do not show this trend. These differences in regional expression ratios may contribute to the sexual dimorphism seen in both the behavioural and molecular phenotype of the DAT-*Cre*; *Zfhx3*-Flox knockout line (*Chapters 4, Results 2 & Chapter 5, Results 3*).

These results indicate that ZFHX3 is expressed in more cell types than only dopaminergic neurons. Attempts were made to investigate these cell identities,

with a focus on identifying the distribution of ZFHX3 expression in the array of different neuronal identities found the in the dopaminergic centres – both GABA-ergic and glutamatergic neurons (**Figure 3.2.1.**). This was primarily intended to inform on the effect of non-specific neuronal knockout of *Zfhx3* induced by intracranial injection of AAV-*Cre* into the midbrain, at the cellular level (*Chapter 6, Results 4*). However, many antibodies went through rounds of troubleshooting, and none could be found that showed consistent staining while passing control tests (*Methods 2.2.1*). This line of inquiry can continue with more time to troubleshoot antibodies and staining methods.

In the Au1, overall expression of ZFHX3 is seen in around 55% of cells – more than in dopaminergic centres - and show no significant difference between females and males. These results imply that *Zfhx3* has a role in the cortex - in the Au1, and possibly other regions. The next step of this experiment would be to investigate ZFHX3 expression across further cortical regions, and co-stain for specific identifiers of cortical layers.

3.7.1 Concluding Remarks

ZFHX3 expression is seen in dopaminergic regions the VTA and SNc, and most pertinently in TH^+ (dopaminergic) neurons. It is also expressed in the cortex – where expression had not been previously reported.

There is no significant difference in the pattern nor proportion of ZFHX3-expressing cells in these regions, between females and males. In female mice, there is significantly lower expression of ZFHX3 in SNc cells compared to the VTA – a difference that is not seen in males. However in males, there is a trend

towards more ZFHX3^{+} cells having a dopaminergic neuron identity in the VTA than the SNc, which is not seen in females.

For this study it was essential to investigate the pattern and amount of expression of ZFHX3 in cells of dopaminergic regions, in order to contextualise the findings seen in the investigation of the two conditional *Zfhx3* knockout mouse models – as each model induces deletion of ZFHX3 in different neuronal sub-populations within the VTA and SNc. This relationship, and in turn the role of *Zfhx3* in these regions, will be expanded upon in the *Discussion* chapter.

4

Results II: Behavioural characterisation of conditional knockout mice – DAT-*Cre*; *Zfhx3*-Flox

4

Results II: Behavioural characterisation of conditional knockout mice – DAT-Cre; Zfhx3-Flox

4.1 Introduction

Zfhx3 has been reported as having a key role in neuronal development (*Introduction 1.1.2.*). It has been found that targeted developmental knockout of *Zfhx3* in the suprachiasmatic nucleus (SCN) – the central mammalian pacemaker – using a *Six3* promoter-driven *Cre* mouse line, causes SCN neurons to lose their neuronal identity. Specifically, neuropeptides *Vip* (vasoactive intestinal polypeptide) and *Avp* (arginine vasopressin)-expressing cells (Wilcox, Bains et al. 2021). Alongside the failure of the SCN to develop neuronal identities, these mice consequently displayed total circadian arrhythmia.

Zfhx3 has also been shown to have a role in adulthood, separate from its developmental role. When *Zfhx3* is ubiquitously deleted in adult mice via tamoxifen-induced *Cre* expression, homozygous mice exhibited a shortening in circadian period, with 30% of mice displaying circadian arrhythmicity (Wilcox, Vizor et al. 2017).

In summary - developmental region-specific knockout of *Zfhx3* can cause neuron identity changes and a significant behavioural phenotype, and adult-only knockout can also induce a behavioural phenotype.

We have developed a region-specific knockout of *Zfhx3* using a DAT-promoter driven *Cre* line to induce knockout only in dopaminergic neurons, from development (*Methods 2.1.4.*).

As DAT is expressed during development, knockout mouse cohorts will express both developmental and adult effects. To separate out these two distinct gene mechanisms, we later carried out intracranial injection of *Cre*-expressing adeno-associated virus into dopaminergic centres of adult *Zfhx3*$^{Flox/Flox}$ mice (*Chapter 6*)

Initial investigation of the DAT-*Cre*; *Zfhx3*-Flox line was behavioural characterisation, comparing *Zfhx3*$^{Flox/Flox}$ *Cre*$^{+}$ homozygous knockout mice to *Zfhx3*$^{-/-}$ *Cre*$^{+}$ controls.

The development of this behavioural phenotyping pipeline was based on endophenotypes of schizophrenia and other dopaminergic functions, disorders, and diseases (*Introduction 1.2.2.*):

- Anxiety
- Motor
- Memory
- Sleep
- Social Dominance
- Startle and Pre-Pulse Inhibition
- Pain Threshold

This behavioural phenotyping pipeline was then followed by molecular analysis, through immunofluorescent imaging of dopaminergic centres (*Chapter 4, 4.2.*); and qPCR and RNASeq (*Chapter 5*) of dopaminergic centres and dopamine circuit-terminus brain regions.

4.2 Immunofluorescent Validation of DAT-*Cre*; *Zfhx3*-Flox Mice

In DAT-*Cre*; Zfhx3-*Flox* homozygous knockout mice, we see a knockdown of *Zfhx3* (stained red) in dopaminergic neurons, in both the VTA and the SNc (**Figures 4.2.1.** and **4.2.2.**). Dopaminergic neuron sub-population identity remains in these dopaminergic centres, staining positive for marker tyrosine hydroxylase (stained green).

From qualitative assessment, *Zfhx3* expression is noticeably reduced in both the male and female Cre^{+} Flox-Hom animals, in both the VTA and the SNc. Homozygous knockout mice have a sporadic distribution of *Zfhx3* expression within dopaminergic neurons in the VTA and SNc, with some sections showing no *Zfhx3* expression at all, compared to wildtypes where *Zfhx3* expression in dopaminergic neurons is consistent through coronal sections (rostral-caudal) of the regions (*Chapter 3*).

Future characterisation of the sections will involve quantifying expression of *Zfhx3* in the dopaminergic centres through cell counting, and quantifying fluorescence within $ZFHX3^{+}$ cells. This will involve co-staining with tyrosine hydroxylase and anti-ZFHX3 to identify: number of dopaminergic neurons, number of *Zfhx3*-expressing cells, number of co-expressing neurons, and levels of *Zfhx3* expression distributed amongst cell types.

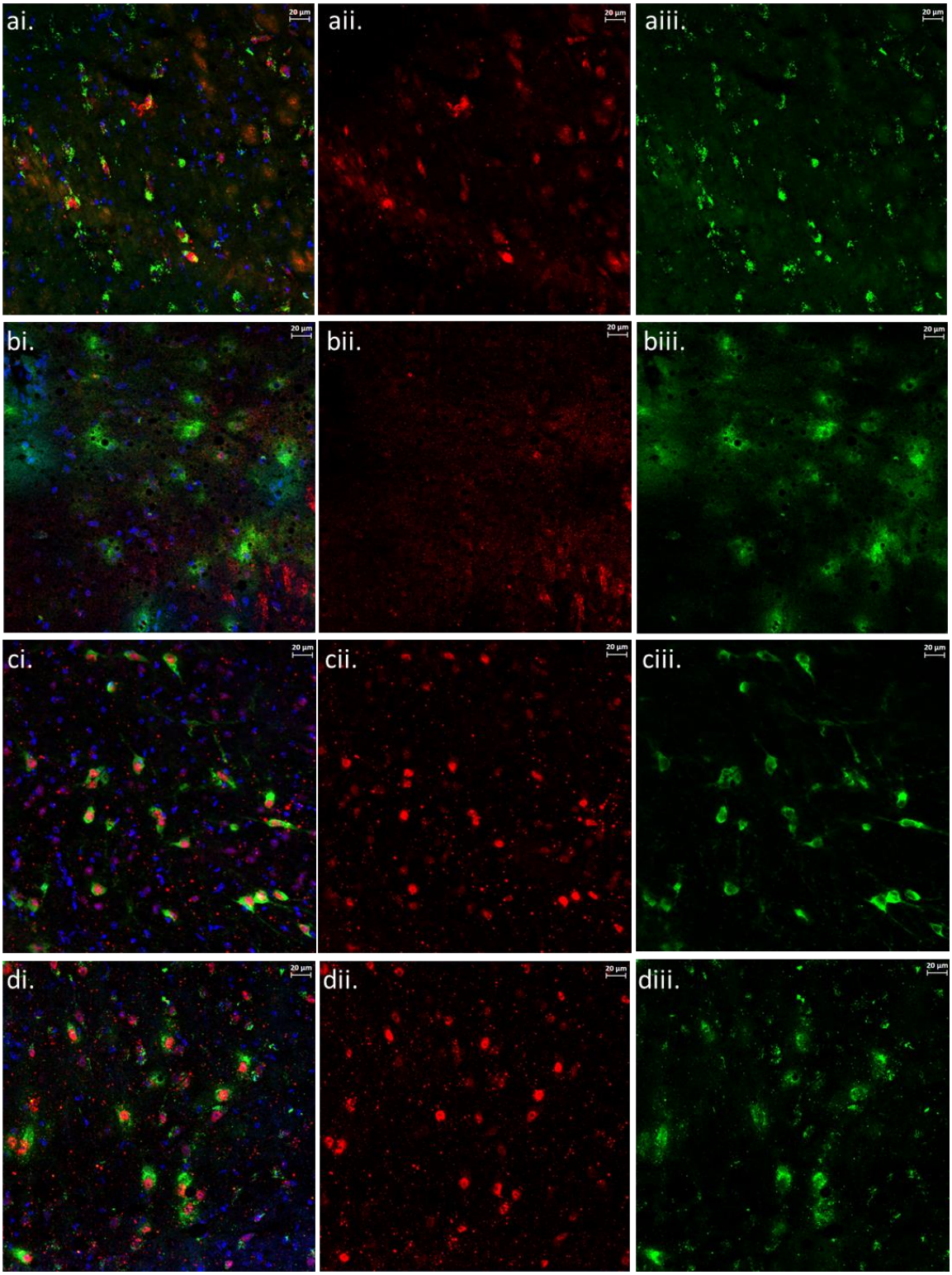

Figure 4.2.1. DAT-Cre; Zfhx3-Flox ventral tegmental area showing *Zfhx3* expression in red, tyrosine hydroxylase in green, and DAPI nuclear stain in blue. (ai) female *Cre*$^{+}$ Flox-Hom; (bi) male *Cre*$^{+}$ Flox-Hom; (ci) female *Cre*$^{+}$ Flox-WT; (di) male *Cre*$^{+}$ Flox-WT; (ii) ZFHX3^{+} cells only (iii) TH^{+} cells only

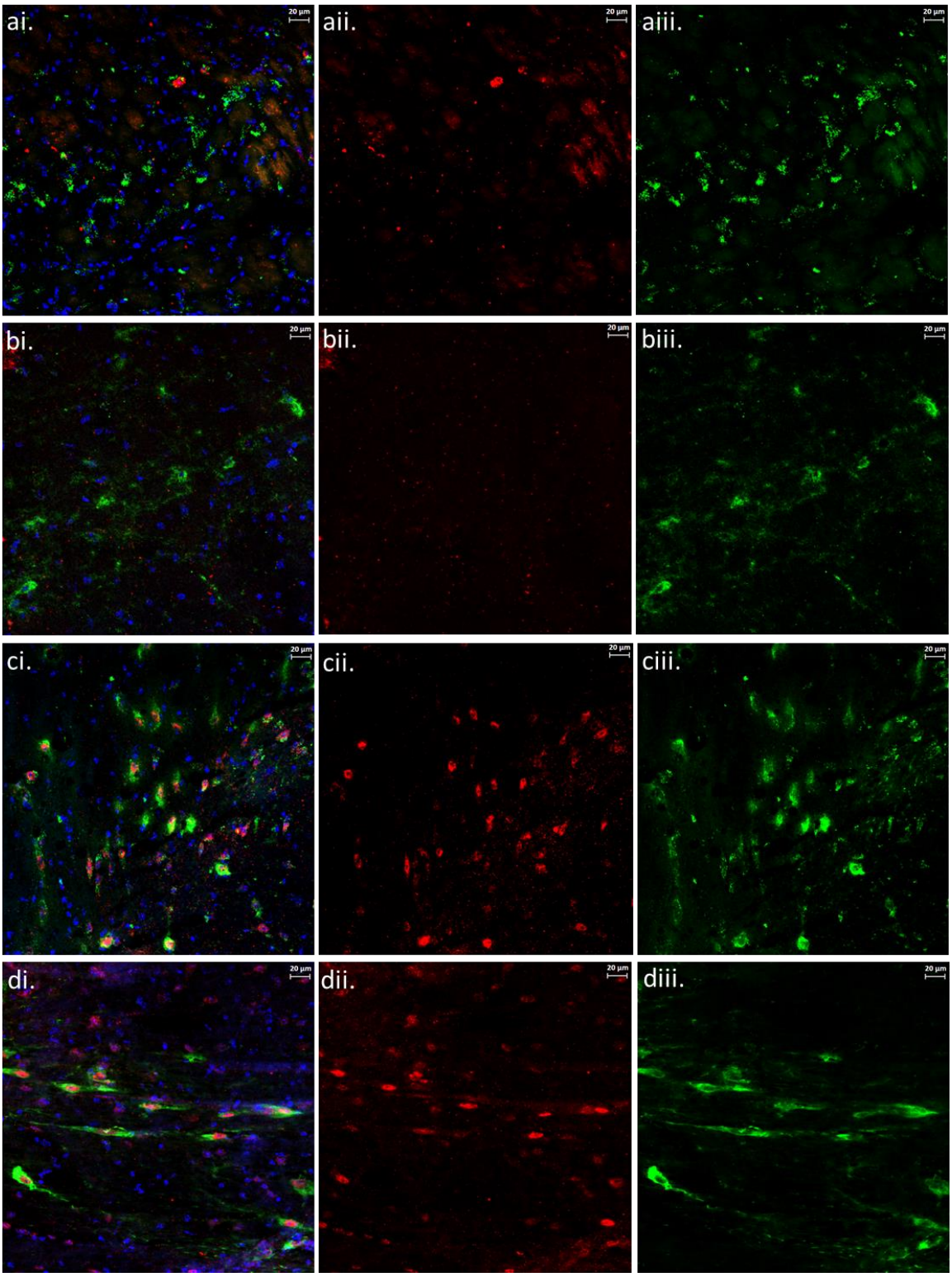

Figure 4.2.2. DAT-Cre; Zfhx3-Flox substantia nigra central showing *Zfhx3* expression in red, tyrosine hydroxylase in green, and DAPI nuclear stain in blue. (ai) female *Cre*$^{+}$ Flox-Hom; (bi) male *Cre*$^{+}$ Flox-Hom; (ci) female *Cre*$^{+}$ Flox-WT; (di) male *Cre*$^{+}$ Flox-WT; (ii) ZFHX3^{+} cells only (iii) TH^{+} cells only

4.3 Mouse Cohort Ages

Throughout the phenotyping pipeline analysis is separated by age of cohort. The categorisation of cohort ages was guided by data from the Jackson Laboratory (**Figure 4.3.1.**).

The design of this pipeline was centred on investigating dopamine dysfunction, with tests chosen to elicit endophenotype expression from dopamine-linked disorders. Many of these illnesses have age as a factor in disease onset, progression, and degeneration (*Introduction 1.2.2.*) – it is therefore essential that age is included as a factor in characterising the behavioural phenotype profile of the homozygous knockout mice.

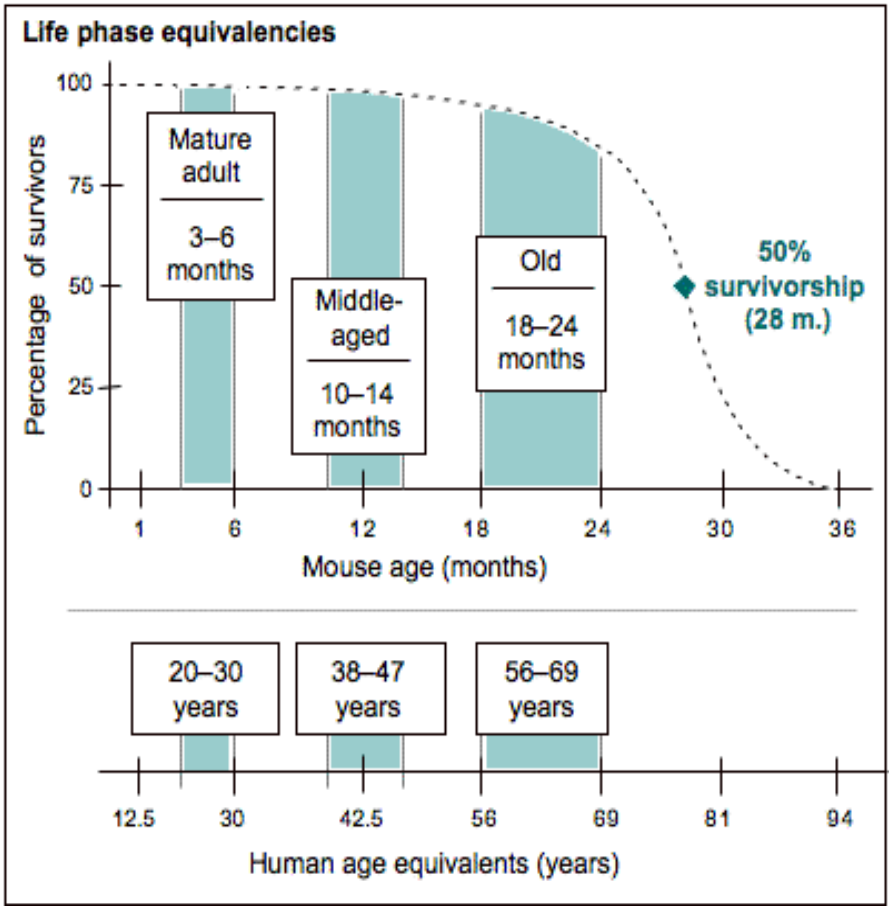

Figure 4.3.1. Mouse ageing infographic describing mouse-to-human age equivalencies. Modified from the Jackson Laboratory, using data from (Flurkey, M. Currer et al. 2007, Kanehisa, Furumichi et al. 2023).

In the analysis of this pipeline, using the guidance given by the Jackson laboratory, ages are defined at time of testing:

- ‘Young’ – 3-9 months
- ‘Old’ – 10-17 months

4.4 Aims

The intention of this arm of the project was to characterise the behavioural phenotype of homozygous knockout DAT-*Cre*; *Zfhx3*-Flox mice. This line was intended to be a schizophrenia-adjacent model, as well as a wider dopaminergic system dysfunction model, and the behavioural phenotyping pipeline reflects this.

While primarily single-sex analysis was carried out, n-numbers were low and some tests do not have high statistical power. Therefore combined-sex analysis was carried out wherever single-sex analysis produced a significant result, in order to assess if significance is maintained when the n-number is increased. However, it was found that some phenotypes were opposing between females and males, and this may interfere with results.

4.5 Results

Throughout pipeline analysis, statistical significance is represented by: * $p \leq 0.05$; ** $p \leq 0.01$.

4.5.1 Anxiety

4.5.1.1 Open Field

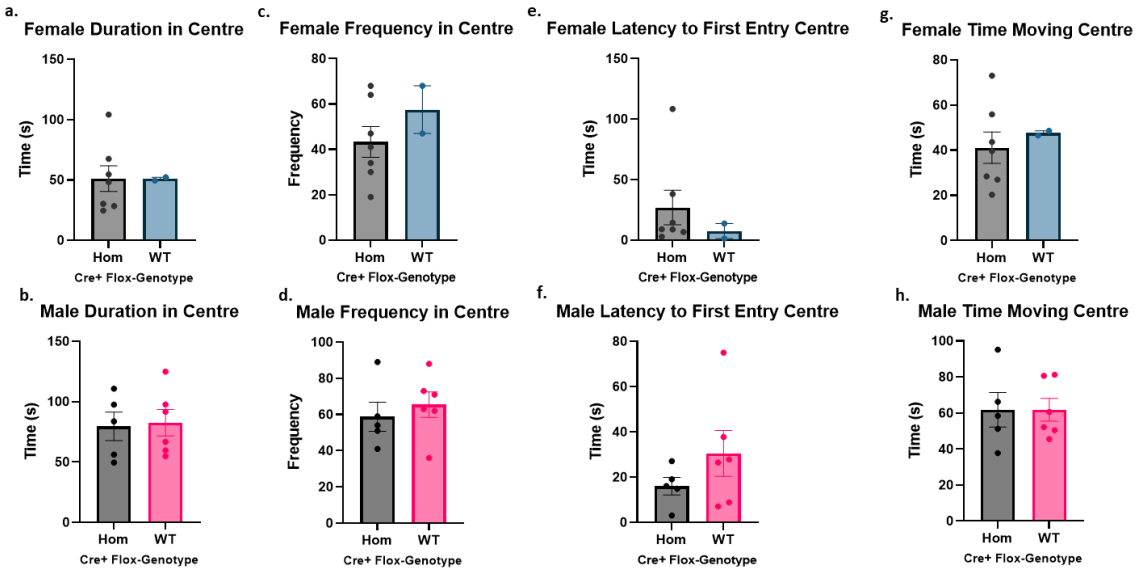

Figure 4.5.1.1.1 Open Field - centre zone parameters for young adult female and male mice analysis of the behaviour of mice within the centre zone only – duration in the centre (a)(b); frequency in the centre (c)(d); latency to first entry of the centre (e)(f); and time spent moving in the centre (g)(h). N numbers for homozygote and wildtype mice respectively: females (n=7; n=2), males (n=5; n=6).

Neither young female nor male homozygotes show a significant phenotype in the centre zone of the open field arena (**Figure 4.5.1.1.1**). Both young female and male homozygous mice show no significant difference in time spent (a; p=0.9924)(b; p=0.8554), frequency of entry (c; p=0.3435)(d; p=0.5456), latency to enter (e; p=0.5115)(f; p=0.2488), or time moving within (g; p=0.6506)(h; p=0.9985) the centre zone. Statistical analysis was performed using unpaired t-test. Data are shown as mean ± standard error of mean.

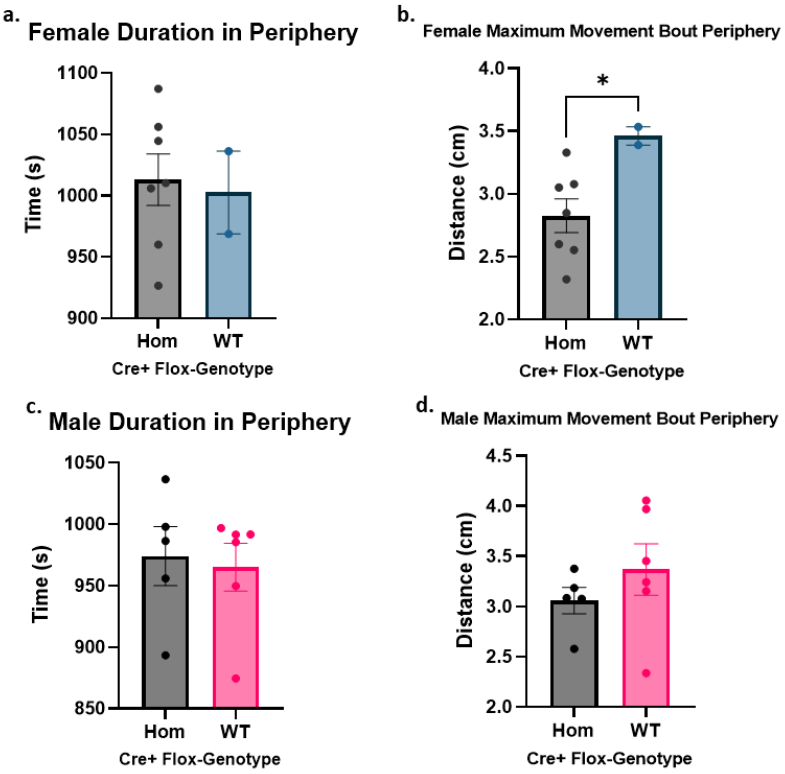

Figure 4.5.1.1.2. Open Field - periphery zone parameters for young adult male and female mice analysis of the behaviour of mice in the periphery zone only – duration in the periphery (a)(c); and maximum length of movement bouts in the periphery (b)(d). N numbers for homozygote and wildtype mice respectively: females (n=7; n=2), males (n=5; n=6).

While young female homozygotes spend the same amount of time in the periphery zone as their wildtype counterparts (**Figure 4.5.1.1.2**) (a; p=0.8191), they show significantly shorter movement bouts (b; p=0.0470). Young male homozygous mice also show no significant difference in time spent in the periphery zone (c; p=0.7723), however they do not reflect the female difference in movement bout distance (d; 0.3415). When carrying out combined-sex analysis of significant phenotypes, significance is maintained in 'Maximum Movement Bout Periphery' as seen in females alone (p=0.0265), with the wildtype score remaining higher than the homozygote's. Statistical analysis was performed using unpaired t-test. Data are shown as mean ± standard error of mean.

In summary - young homozygous mutant male mice do not show any change in anxiogenic behaviour compared to wildtype males in the open field area. However, young female homozygotes show a significantly shorter movement bouts. In addition, combined-sex analysis also show significantly shorter movement bouts in homozygotes.

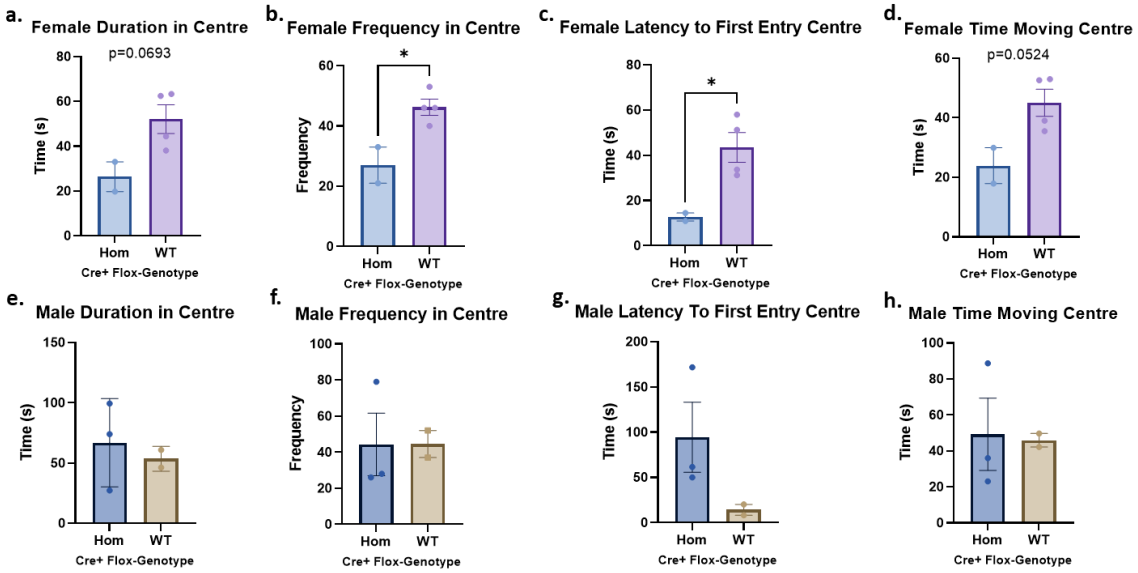

Figure 4.5.1.1.3. Open Field - centre zone parameters for old adult female and male mice analysis of the behaviour of mice in the centre zone only – duration in the centre (a)(e); frequency in the centre (b)(f); latency to first entry of the centre (c)(g); and time spent moving in the centre (d)(h). N numbers for homozygote and wildtype mice respectively: females (n=2; n=4), males (n=3; n=2).

Old female homozygotes show an abnormal anxiogenic phenotype regarding the centre zone (**Figure 4.5.1.1.3**). Homozygotes spend less time in the centre zone (a; p=0.0693), enter the centre zone significantly less (b; p=0.0238), and spend less time moving in the centre (d; p=0.0524). However, homozygotes also initially enter the centre zone significantly faster than wildtype mice (c; p=0.0360). Old male homozygotes do not show the same centre-based phenotype as females: time in the centre (e; p=0.6660); frequency in centre (f; p=0.9947); latency to centre (g; p=0.2085); and time moving in centre (h; p=0.9067) did not significantly

differ from their wildtype counterparts. When carrying out combined-sex analysis of significant phenotypes however, significance was not maintained in “Frequency in Centre” and “Latency to First Entry Centre) as seen in females alone (p=0.4283, p=0.3379). Statistical analysis was performed using unpaired t-test. Data are shown as mean ± standard error of mean.

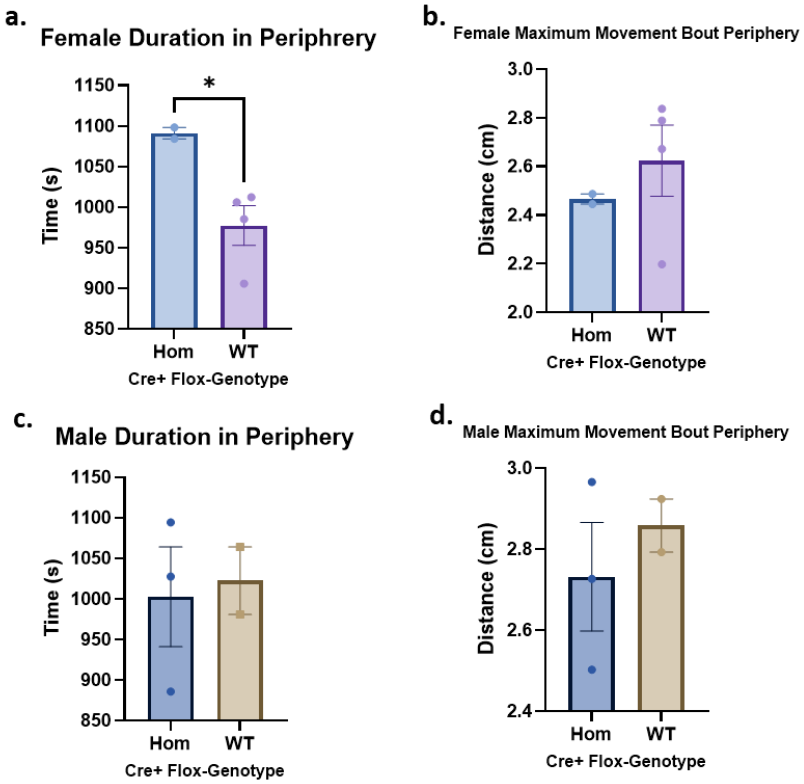

Figure 4.5.1.1.4. Open Field - periphery zone parameters for old adult male and female mice analysis of the behaviour of mice in the periphery zone only – duration in the periphery (a)(c); and maximum length of movement bouts in the periphery (b)(d). N numbers for homozygote and wildtype mice respectively: females (n=2; n=4), males (n=3; n=2).

Old female homozygotes show a significant preference to the periphery zone over wildtype mice (**Figure 4.5.1.1.4**) (a; p=0.0371). However contrary to young female homozygotes (**Figure 4.5.1.1.2**), old female homozygotes do not demonstrate significantly shorter movement bouts (b; p=0.5119). Old male homozygotes do not show significant differences in either parameter (c; p=0.8302)(d; p=0.5321). In

combined sex analysis of significant phenotypes, significance is not maintained in ‘Duration in Periphery’ as seen in females alone (p=0.3172). Statistical analysis was performed using unpaired t-test. Data are shown as mean ± standard error of mean.

In summary – young homozygous female mice display shorter maximum movement bouts in the periphery – with significance maintained with combined-sex analysis. Old homozygous mutant male mice do not show any difference in their anxiogenic behaviour to wildtype males in the open field arena. However, old homozygous females enter the centre significantly less frequently, spend significantly more time in the periphery zone, and enter the centre zone significantly sooner from the start of the test, neither of which maintained significance in sex-combined analysis.

4.5.1.2 Light-Dark Box

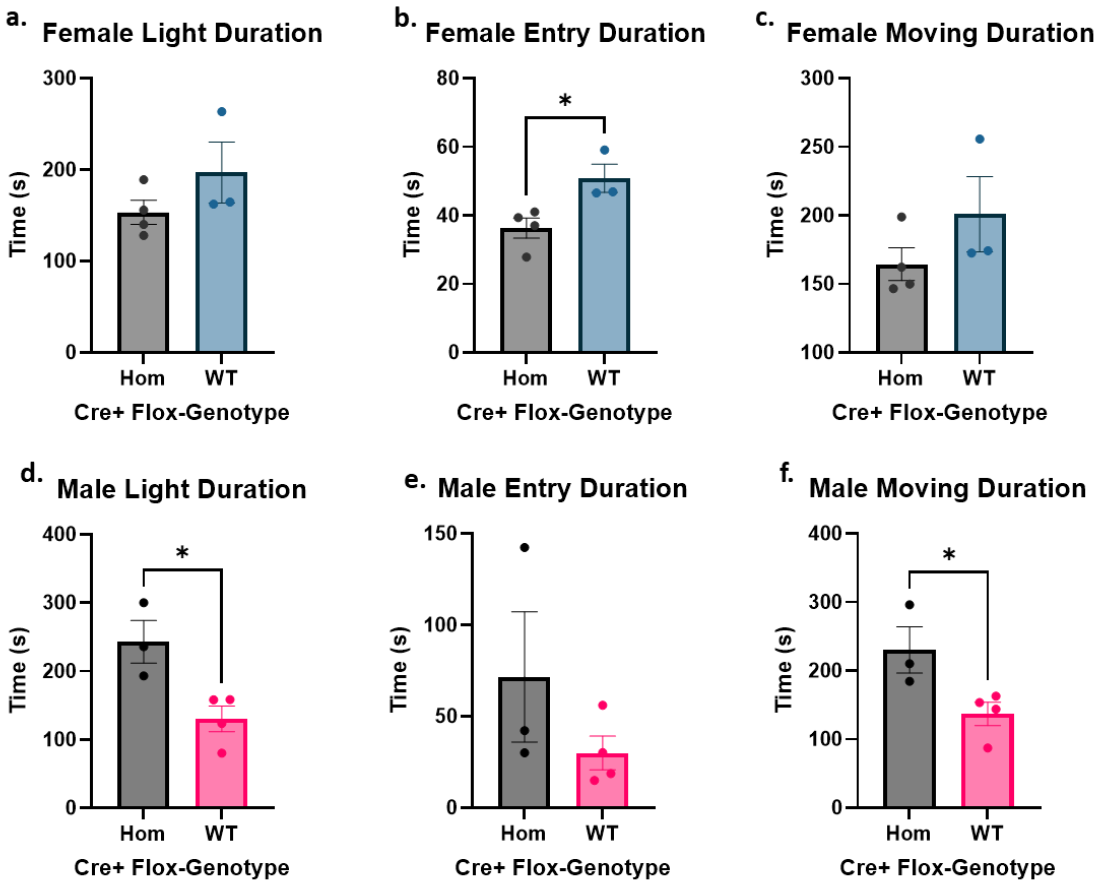

Figure 4.5.1.2.1. Light-Dark Box- timing measurements for young female and male mice measuring time spent in the light zone (a)(d), the entry zone (b)(e), and time spent moving while in those zones (c)(f). N numbers for homozygote and wildtype mice respectively: females (n=4; n=3), males (n=3; n=4).

Both female and male young homozygotes show a significant phenotype in the time spent in zones of the light-dark box, although from different parameters (**Figure 4.5.1.2.1**). Female homozygotes do not spend significantly more time in the light zone, while male homozygotes do (a; p=0.2311)(b; p=0.0210). Female homozygotes spend significantly less time in the entry zone, while male homozygotes do not (b; p=0.0315)(e; p=0.2469). Female homozygotes do not spend significantly more time moving, while male homozygotes do (c; p=0.8475)(f; p=0.0433). In combined-sex analysis of significant phenotypes, significance in not

maintained in any of the tests: female ‘Light Duration’, female ‘Entry Duration’, and male ‘Moving Duration’ (p=0.3172, p=0.3065, p=0.4682). Statistical analysis was performed using unpaired t-test. Data are shown as mean ± standard error of mean.

In summary - young female homozygotes spend less time in the non-hidden zones than wildtype mice, spending significantly less time in the entry zone. Males however spent significantly more time in the light zone, and significantly more time exploring there. In combined-sex analysis however, no single-sex phenotypes were maintained.

Data shown in old mice but not shown in young mice, as no significance was demonstrated: light frequency, entry frequency, hidden frequency, distance moved total, and moving frequency.

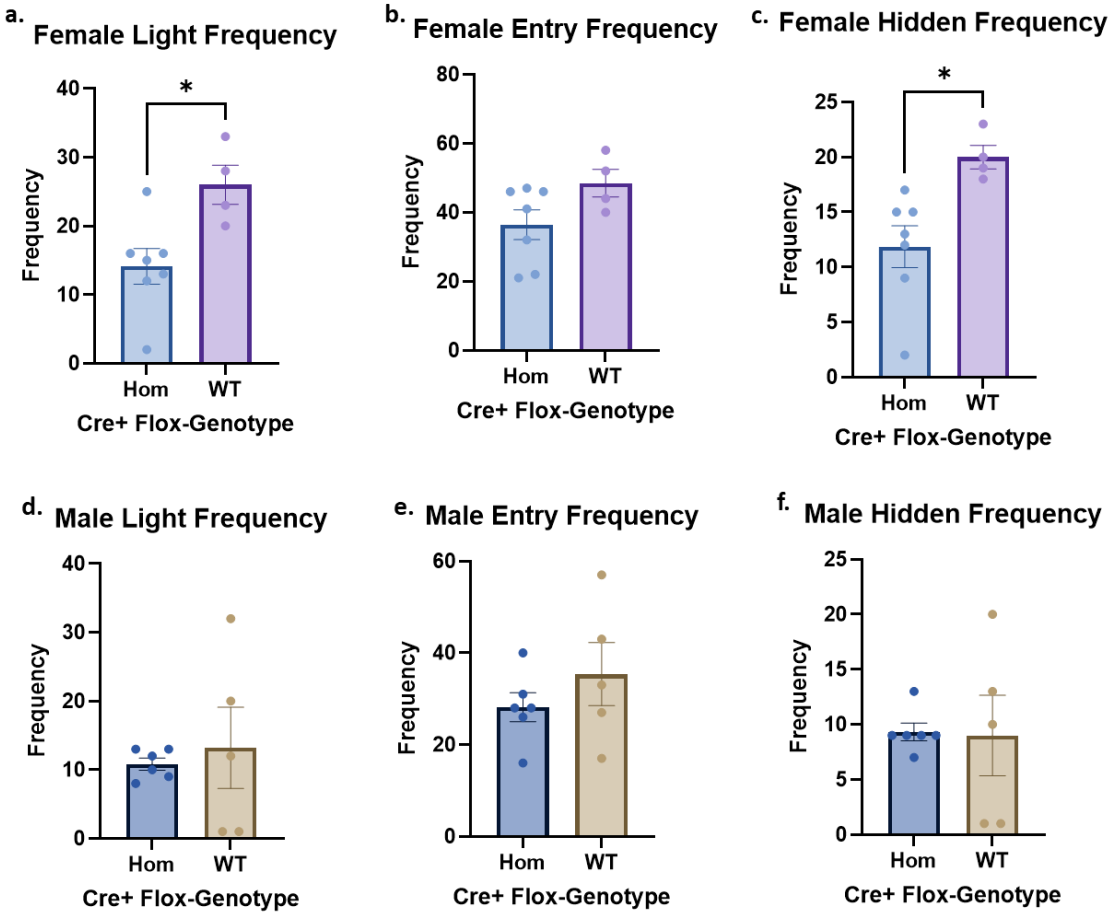

Figure 4.5.1.2.2. Light-Dark Box - zone entry frequency measurements for old female and male mice measuring frequency of entry into the light (a)(d), entry (b)(e), and hidden zones (c)(f). N numbers for homozygote and wildtype mice respectively: females (n=7; n=4), males (n=6; n=5).

(**Figure 4.5.1.2.2**) Old female homozygotes show significantly fewer entries into the light and hidden zones (a; p=0.0169)(c; p=0.0145) compared to wildtypes, although this difference is not shown regarding the entry zone (b; p=0.0975). Old male homozygotes however show no significant differences to wildtypes, under these same parameters (d; p=0.6728)(e; p=0.3345)(f; p=0.9243). In combined-sex analysis of significant phenotypes, significance is not maintained in 'Light Frequency' and 'Hidden Frequency' which are significant in females alone

(p=0.1102, p=0.2402). Statistical analysis was performed using unpaired t-test. Data are shown as mean ± standard error of mean.

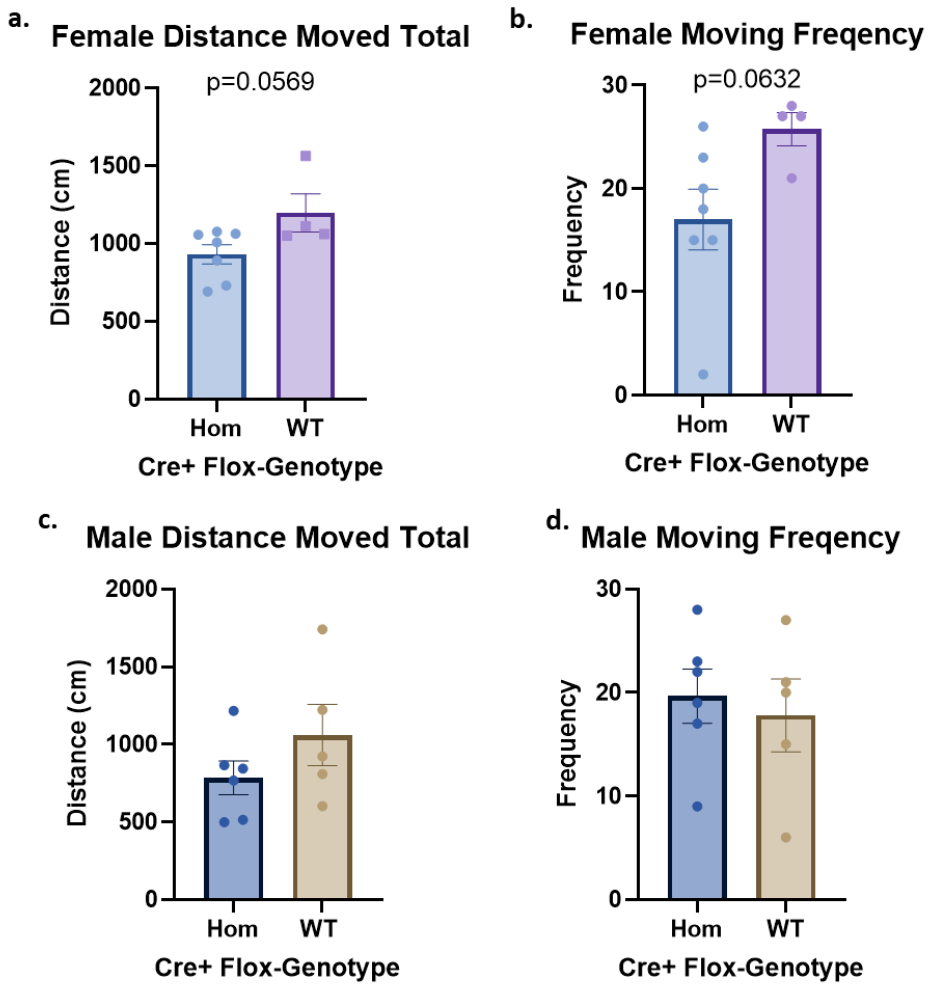

Figure 4.5.1.2.3. Light-Dark Box - zone movement measurements for old female and male adult mice measuring total distance moved,(a)(c) and frequency of movement bouts (b)(d). N numbers for homozygote and wildtype mice respectively: females (n=7; n=4), males (n=6; n=5).

Old female homozygotes show a trend (however no significant change is found) in their movement compared to wildtype (**Figure 4.5.1.2.3**). Homozygotes move less distance in total across the trial time (a; p=0.0569), and initiate movement less frequently (b; p=0.0632). Male homozygotes do not demonstrate the same trend in

either parameter (c; p=0.2320)(d; p=0.6745). Statistical analysis was performed using unpaired t-test. Data are shown as mean ± standard error of mean.

In summary – old male homozygotes show no difference in behaviour to wildtypes. However, old female homozygotes show differences in multiple parameters: they show significantly fewer transitions between light and dark zones, and possibly exhibit supressed locomotion compared to wildtypes – however this statement is not supported by significant findings. In addition, significant findings in females alone are not maintained in combined-sex analysis.

Data shown in young mice but not in old mice as no significance was demonstrated: light duration, entry duration, and moving duration.

4.5.1.3 Marble Burying

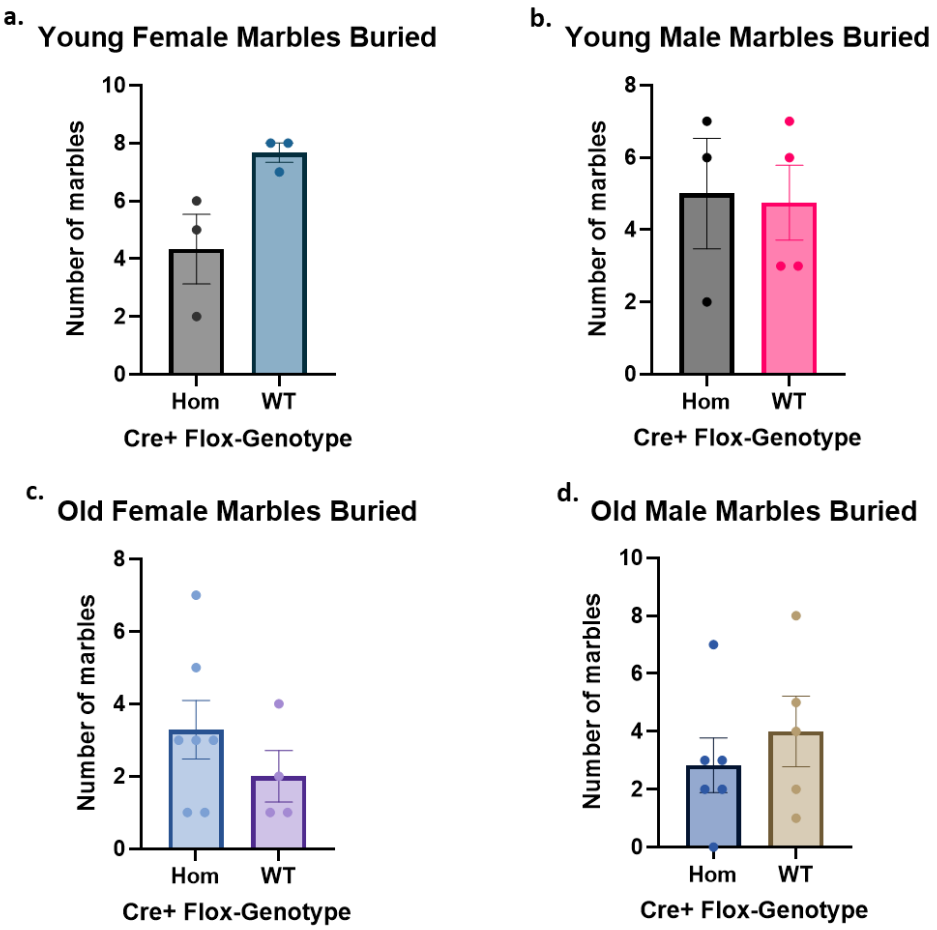

Figure 4.5.1.3.1. Marble Burying Test - number of marbles buried by young and old adult mice of both sexes measuring number of marbles that are ≥2/3 buried by young (a)(b) and old (c)(d) mice. N numbers for homozygote and wildtype mice respectively: young females (n=3; n=4); young males (n=3; n=4); old females (n=7; n=4); and old males (n=6; n=5).

(**Figure 4.5.1.3.1.**) Neither young (a, b) or old (c, d) homozygotes of either sex show any significance or trend in the number of marbles they bury (a; p=0.1000)(b; p=>0.9999)(c; p=0.3939)(d; p=0.4978) compared to wildtype mice. Statistical analysis was performed using Mann-Whitney test. Data are shown as mean ± standard error of mean.

In summary - no homozygotes of any group (sex or age) showed a behavioural phenotype in the marble burying test.

4.5.1.4 Elevated O Maze

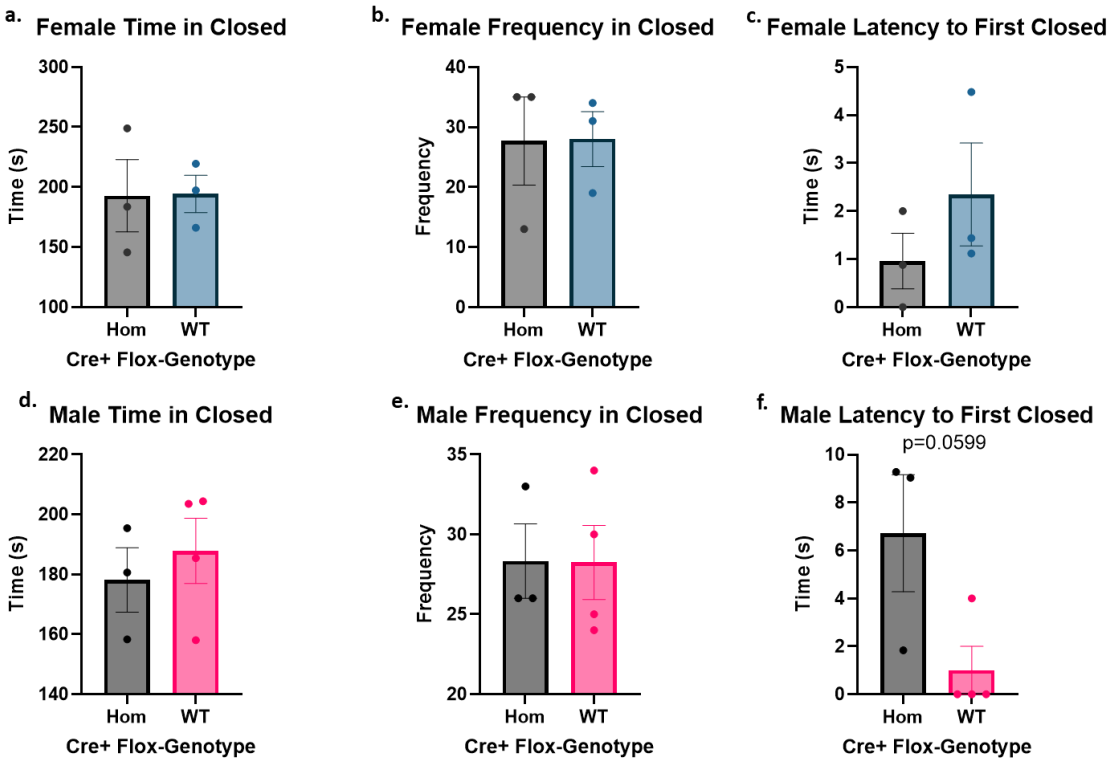

Figure 4.5.1.4.1. Elevated O-maze - closed zone parameters for young female and male adult mice measuring time in (a)(d), entry frequency (b)(e), and latency to first entry (c)(f) of the closed zone**.** N numbers for homozygote and wildtype mice respectively: females (n=3; n=3), males (n=3; n=4).

(**Figure 4.5.1.4.1.**) Young female homozygotes show no phenotype in their behaviour – time within, frequency of entry, or latency to first entry - around the closed zones of the arena (a; p=0.9658)(b; p=0.9711)(c; p=0.3182). Young male homozygotes also show no phenotype for time within and frequency of entry to closed zones (d; p=0.5631)(e; p=0.9812) however they do demonstrate a trend towards having a greater latency to first entry of the closed zones compared to wildtypes (f; p=0.9658) – although there is no statistical difference. Statistical analysis was performed using unpaired t-test. Data are shown as mean ± standard error of mean.

In summary - Neither young female nor male homozygotes show a significant phenotype in the elevated o maze, however males do show a possible trend towards spending longer in the open/light zone upon first introduction to the maze – however this statement is not supported by significant data.

4.5.2 Motor Function and Ability

4.5.2.1 Rotarod

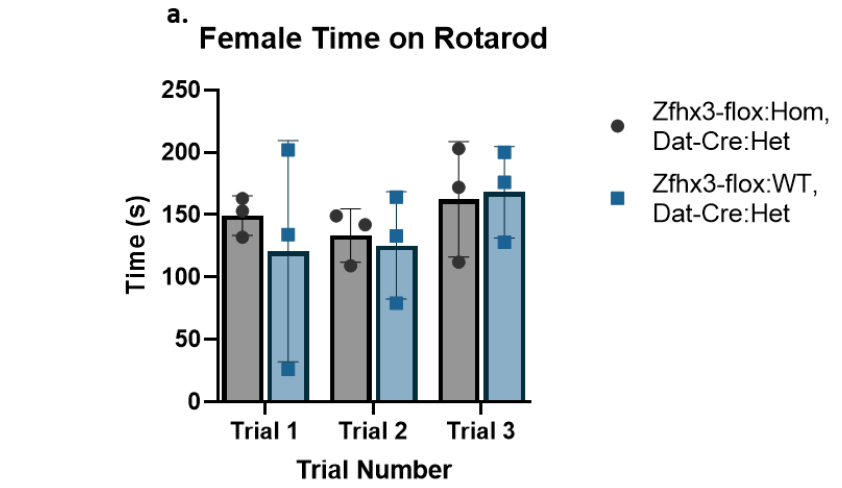
a.
Female Time on Rotarod
Time (s)
250
200
150
100
50
0
Trial 1
Trial 2
Trial 3
Trial Number
Zfhx3-flox:Hom, Dat-Cre:Het
Zfhx3-flox:WT, Dat-Cre:Het

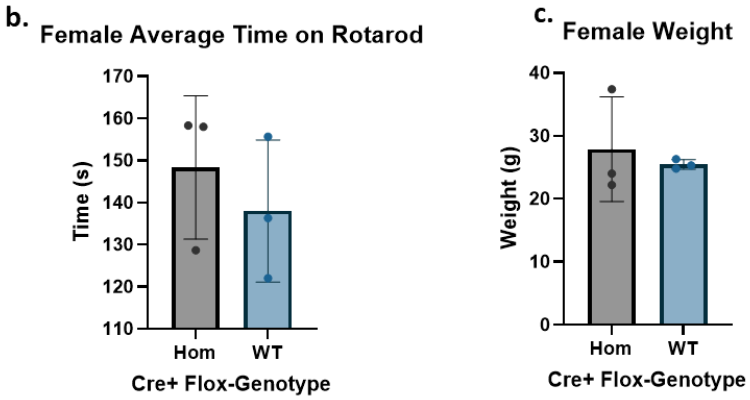
b.
Female Average Time on Rotarod
Time (s)
170
160
150
140
130
120
110
Hom
WT
Cre+ Flox-Genotype

c.
Female Weight
Weight (g)
40
30
20
10
0
Hom
WT
Cre+ Flox-Genotype

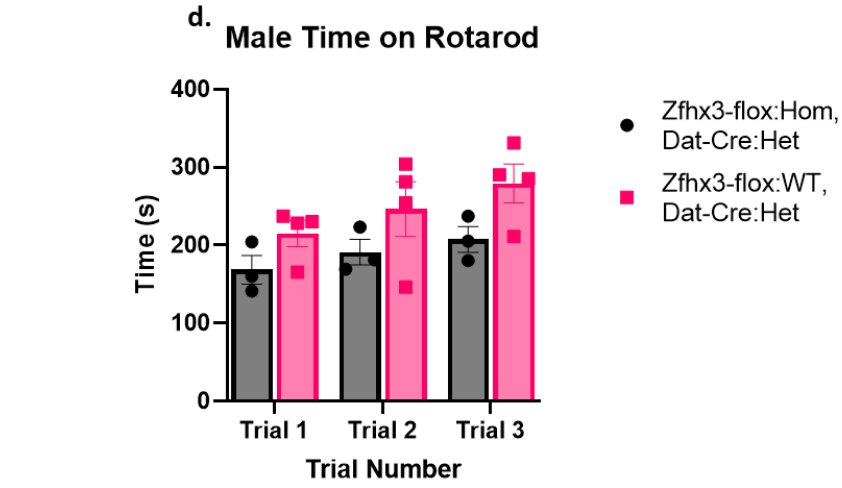
d.
Male Time on Rotarod
Time (s)
400
300
200
100
0
Trial 1
Trial 2
Trial 3
Trial Number
Zfhx3-flox:Hom, Dat-Cre:Het
Zfhx3-flox:WT, Dat-Cre:Het

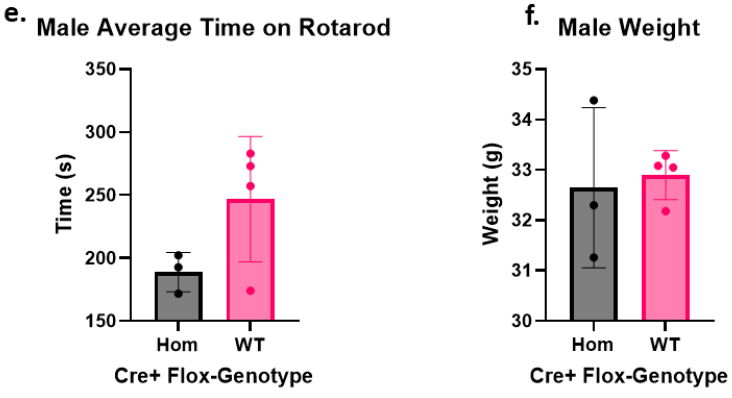
e.
Male Average Time on Rotarod
Time (s)
350
300
250
200
150
Hom
WT
Cre+ Flox-Genotype

f.
Male Weight
Weight (g)
35
34
33
32
31
30
Hom
WT
Cre+ Flox-Genotype

Figure 4.5.2.1.1. Rotarod Test – performance parameters for young female and male adult mice measuring time on rotarod across the 3 trials (a)(d), average time on rotarod overall (b)(e), and mouse weight (c)(f)**.** N numbers for homozygote and wildtype mice respectively: females (n=3; n=3), males (n=3; n=4).

(**Figure 4.5.2.1.1**) Young female homozygotes and wildtypes show no significant difference in time spent on the rotarod ($F_{1,4}$=0.5566, p=0.4971), or in the interaction between genotype and trial number ($F_{2,8}$=0.1470, p=0.8655). Comparing the average time on rotarod between female homozygotes and wildtypes shows no significant difference (b; p=0.4971). Female homozygotes show no significant difference in weight to wildtypes (c; p=0.6434). Similar can be found with the male homozygotes (d), who show no significant difference in performance to wildtypes ($F_{1,5}$=3.643, p=0.1143), and in the interaction between genotype and trial number ($F_{2,10}$=0.3954, p=0.6835). As with the females, male homozygotes show no significant difference in time on the rotarod when averaging the 3 trials (e; p=0.1146), and also show no significant difference in weight with their wildtype counterparts (f; p=0.7720). . Statistical analysis was performed using 2-way ANOVA with Šídák's multiple comparisons test (a, d), and unpaired t-test (b, c, e, f). Data are shown as mean ± standard error of mean.

In summary, neither young female nor male homozygotes show any difference in performance on the rotarod, or in body weight.

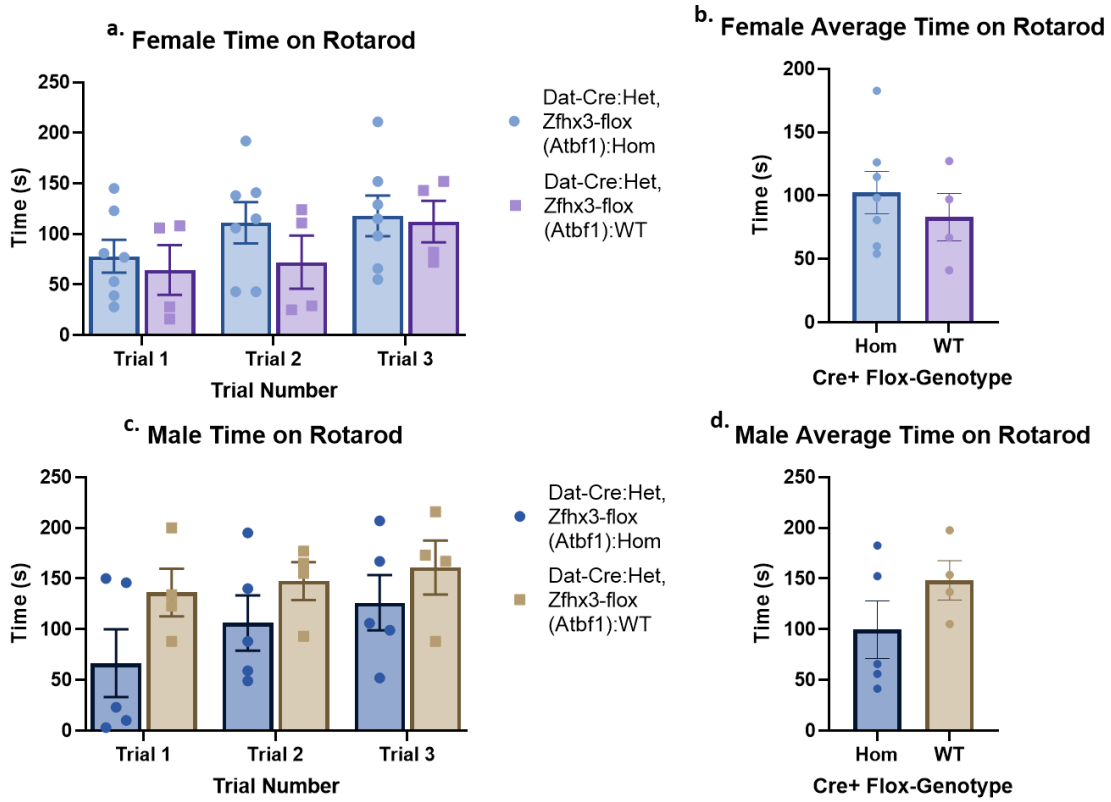

Figure 4.5.2.1.2. Rotarod Test – performance parameters for old female and male adult mice measuring time on rotarod across the 3 trials (a)(c), and average time on rotarod overall (b)(d) **.** N numbers for homozygote and wildtype mice respectively: females (n=7; n=4), males (n=5; n=4).

(**Figure 4.5.2.1.2.**) Similarly to young females (**Figure 4.5.2.1.1.**), the older female homozygotes show no significant phenotype from the time spent on the rotarod across 3 trials (a), comparing: between genotypes ($F_{1,9}$=0.5382, p=0.4818), and the interaction of genotype and trial number ($F_{2,18}$=0.7510, p=0.4861). When averaging time on rotarod between the 3 trials, female homozygotes and wildtypes show no significant difference in performance (b; p=0.4818). Male mice show no significant phenotype from time spent on the rotarod across 3 trials (c), comparing: between genotypes ($F_{1,7}$=0.1.787, p=0.2231), and the interaction of genotype and trial number ($F_{2,14}$=0.1.125, p=0.3522). When averaging time on rotarod between the 3 trials, male homozygotes and wildtypes show no significant difference in

performance (d; p=0.2231). Statistical analysis was performed using 2-way ANOVA with Šídák's multiple comparisons test (a,c), and unpaired t-test (b,d). Data are shown as mean ± standard error of mean.

Reflecting the results for the younger cohorts, neither female nor male homozygotes show differences in their rotarod performance, compared to their wildtype counterparts.

Data shown in young mice but not shown in old mice, as this data was not collected at the time: weight.

4.5.2.2 Locotronic

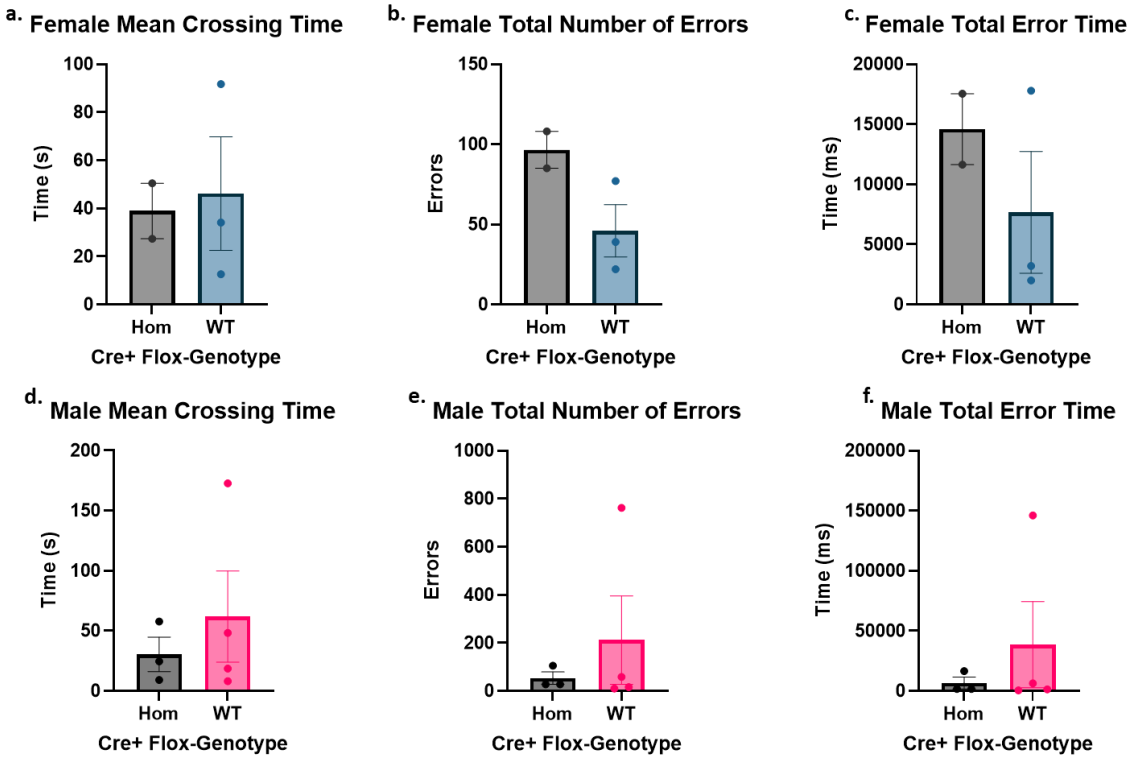

Figure 4.5.2.2.1. Locotronic Test – performance parameters for young female and mice adult mice measuring mean crossing time on the ladder (a)(d), total number of errors on the ladder rungs (b)(e), and total error time (c)(f)**.** N numbers for homozygote and wildtype mice respectively: females (n=2; n=3), males (n=3; n=4).

Neither young female nor male young homozygotes show any significant phenotype in the locotronic arena (**Figure 4.5.2.2.1.**). Female homozygotes show no significant difference in time crossing the locotronic (a; p=0.8336), in the total number of combined limb and tail errors (b; p=0.1123), and in the total time of limb and tail errors (c; p=0.3900). Male homozygotes also show no significant comparisons under the same parameters – in time crossing the locotronic (d; p=0.5281), in the total number of combined limb and tail errors (e; p=0.5017), and in the total time of limb and tail errors (f; p=0.4871). Statistical analysis was performed using unpaired t-test. Data are shown as mean ± standard error of mean.

In summary, in the locotronic test neither young female or male homozygotes show changes in their finer motor co-ordination compared to wildtype mice.

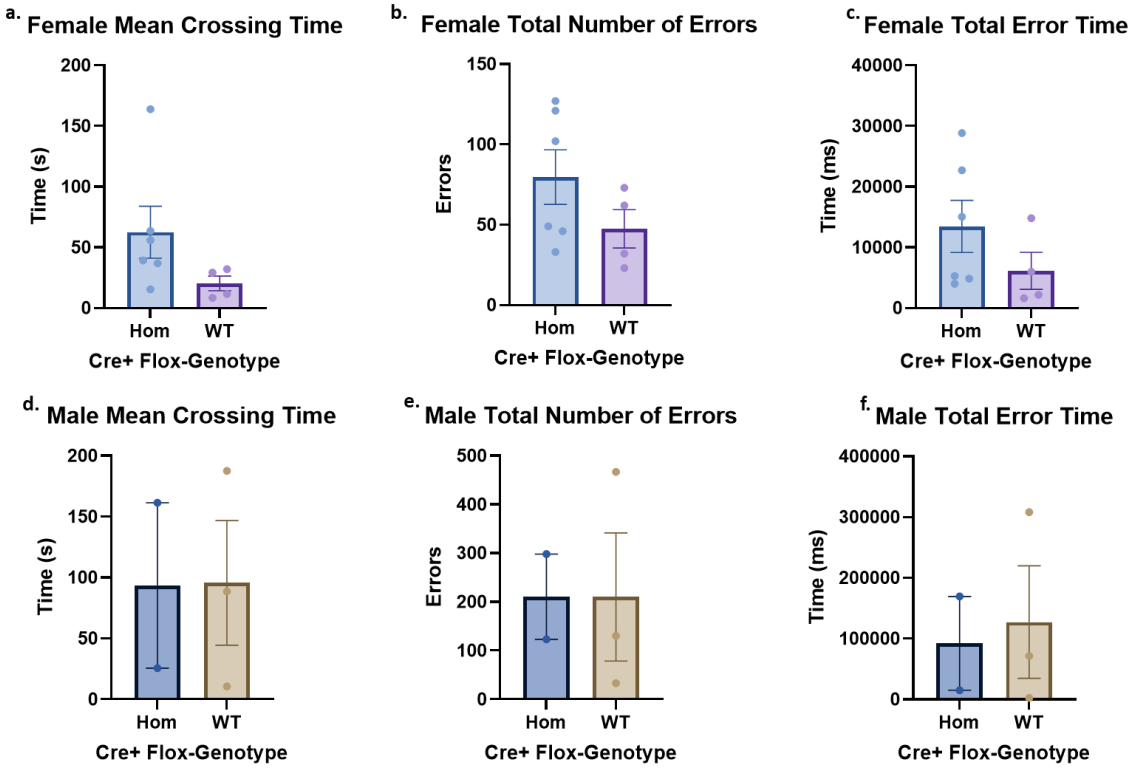

Figure 4.5.2.2.2. Locotronic Test – performance parameters for old female and mice adult mice measuring mean crossing time on the ladder (a)(d), total number of errors on the ladder rungs (b)(e), and total error time (c)(f)**.** N numbers for homozygote and wildtype mice respectively: females (n=6; n=6), males (n=2; n=3).

Neither old female nor male homozygotes show any significant phenotype in the locotronic arena (**Figure 4.5.2.2.2**). Female homozygotes show no significant phenotype in time crossing the locotronic (a; p=0.8336), in the total number of combined limb and tail errors (b; p=0.2043), and in the total time of limb and tail errors (c; p=0.0.2495). Male homozygotes also show no significant comparisons under the same parameters – in time crossing the locotronic (d; p=0.9817), in the total number of combined limb and tail errors (e; p=0.9980), and in the total time of limb and tail errors (f; p=0.8086). Statistical analysis was performed using unpaired t-test. Data are shown as mean ± standard error of mean.

As was found with young homozygotes, neither old female nor male homozygotes show any significant differences in their performance on the locotronic run.

4.5.2.3 Gait Analysis (MouseWalker)

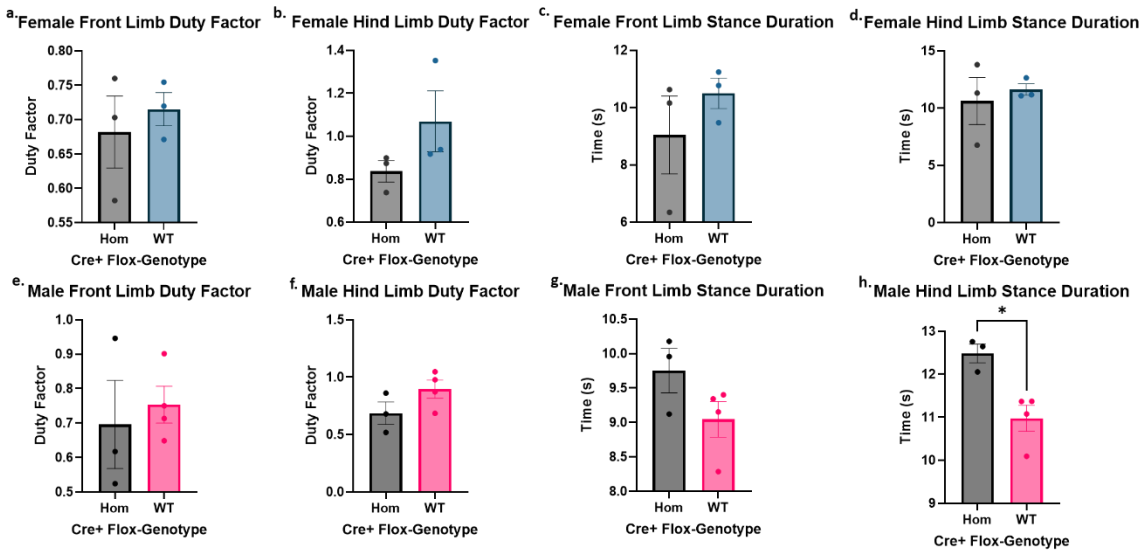

Figure 4.5.2.3.1. Gait Analysis - gait measurements for young female and male adult mice assessing the duty factor of both the front (a)(e) and hind (b)(f) limbs, and the stance duration of both the front (c)(g) and hind (d)(h) limbs. N numbers for homozygote and wildtype mice respectively: females (n=3; n=3), males (n=3; n=4).

(**Figure 4.5.2.3.1.**) Young female homozygotes do not show a significant gait phenotype under these parameters: front limb duty factor (a; p=0.5950), hind limb duty factor (b; p=0.1972), front limb stance duration (c; p=0.3748), and hind limb stance duration (d; p=0.6608). Male homozygotes similarly show a lack of phenotype in the front limb duty factor (e; p=0.06623), hind limb duty factor (f; p=0.1538), and front limb stance duration (g; p= 0.1436. However male homozygotes demonstrate a significant phenotype in hind limb stance duration (h; p=0.0133). In combined-sex analysis of significant phenotypes, significance is not maintained in ‘Hind Limb Stance Duration’ as seen in males alone (p=0.7656).

Statistical analysis was performed using unpaired t-test. Data are shown as mean ± standard error of mean.

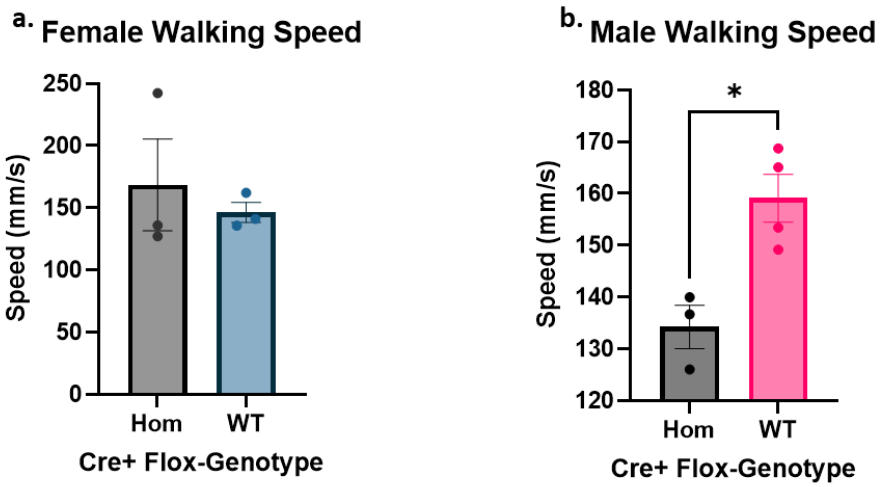

Figure 4.5.2.3.2. Gait Analysis - walking speed for young female and male adult mice measurement of walking speed (a)(b), taken from the gait analysis test. N numbers for homozygote and wildtype mice respectively: females (n=3; n=3), males (n=3; n=4).

(**Figure 4.5.2.3.2.**) Young female homozygotes do not show a significant difference in their walking speed compared to wildtype counterparts (a; p=0.5899). Male homozygotes walk significantly slower than wildtypes, while in the MouseWalker apparatus (b; p=0.0125). In combined-sex analysis of significant phenotypes, significance is not maintained in 'Walking Speed' as seen in males alone (p=0.9003). Statistical analysis was performed using unpaired t-test. Data are shown as mean ± standard error of mean.

In summary, while young female homozygotes show no phenotype under any gait analysis parameter, male homozygotes have a significantly increased limb stance duration and decreased walking speed. In combined-sex analysis, neither significant phenotype in males alone maintains significance.

Data shown in old mice but not shown in young mice, as no significance was demonstrated: front limb swing duration, front limb step length, and walking bout duration.

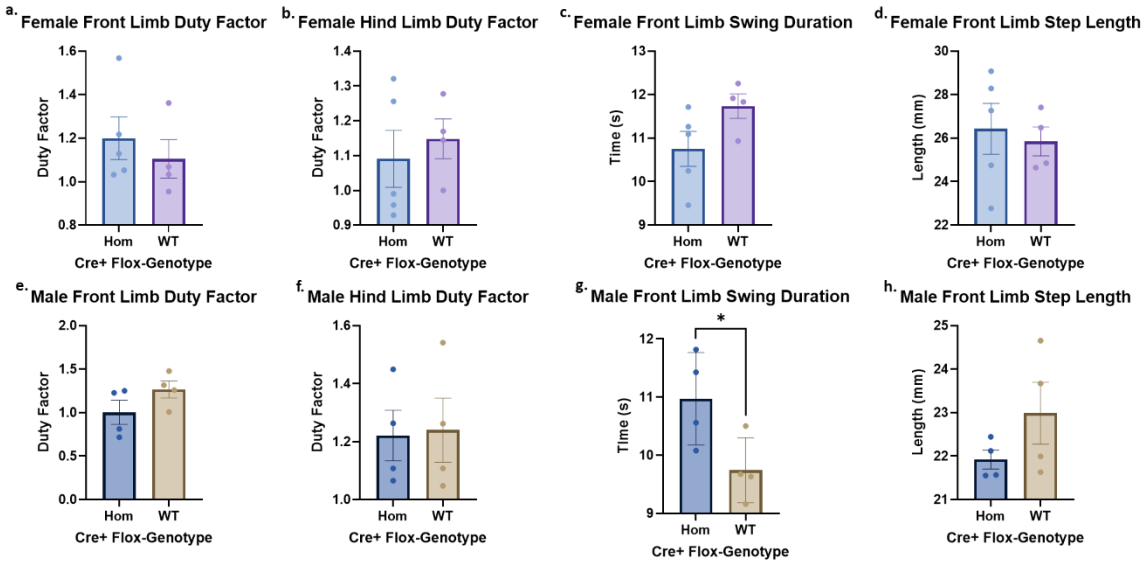

Figure 4.5.2.3.3. Gait Analysis – gait measurements for old female and male adult mice assessing the front (a)(e) and hind (b)(f) limb duty factor, front limb swing duration (c)(g), and front limb step length (d)(h). N numbers for homozygote and wildtype mice respectively: females (n=5; n=4), males (n=4; n=4).

(**Figure 4.5.2.3.3.**) Old female homozygotes show no significant phenotype in these parameters: front limb duty factor (a; p=0.5950), hind limb duty factor (b; p=0.6055), front limb swing duration (c; p=0.1015), and front limb swing length (d; p=0.7002). Male homozygotes also show no significant phenotype in front limb duty factor (e; p=0.1709) and hind limb duty factor (f; p=0.9005). However, male homozygotes have a significantly greater duration in front limb swing compared to wildtypes (g; p=0.0444), despite their step length having no significant difference to wildtypes (h; p=0.2027). In combined-sex analysis of significant data, significance is not maintained in ‘Front Limb Swing Duration’ as seen in male alone (p=0.8191).

Statistical analysis was performed using unpaired t-test. Data are shown as mean ± standard error of mean.

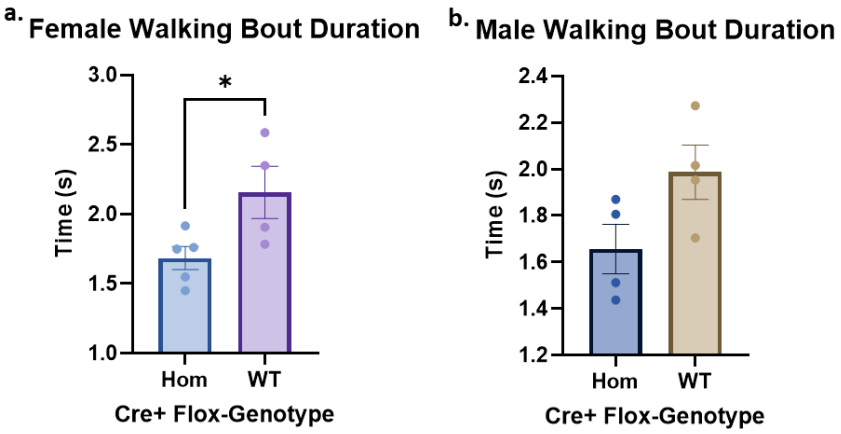

Figure 4.5.2.3.4. Gait Analysis - walking bout duration in old female and male adult mice measuring the duration of walking bouts (a)(b) taken while in the gait analysis test. N numbers for homozygote and wildtype mice respectively: females (n=5; n=4), males (n=4; n=4).

(**Figure 4.5.2.3.4.**) Old female homozygotes show significantly shorter duration of walking bouts compared to wildtypes (a; p=0.0418), while male homozygotes do not show this phenotype (b; p=0.0823). In combined-sex analysis of significant phenotypes, significance is maintained in 'Walking Bout Duration as seen in females alone (p=0.0047), with the wildtype score remaining higher than homozygous. Statistical analysis was performed using unpaired t-test. Data are shown as mean ± standard error of mean.

In summary, old female homozygotes walk in bouts that are significantly shorter in duration – significance of which is maintained in combined-sex analysis - and male homozygotes have significantly longer front limb swing duration, significance of which is not maintained in combined-sex analysis.

Data shown in young mice but not shown in old mice, as no significance was demonstrated: front stance duration, hind stance duration, and walking speed.

Data from hind limbs also not included (except for duty factor) due to lack of significance.

4.5.2.4 Motor Function Test (MO)

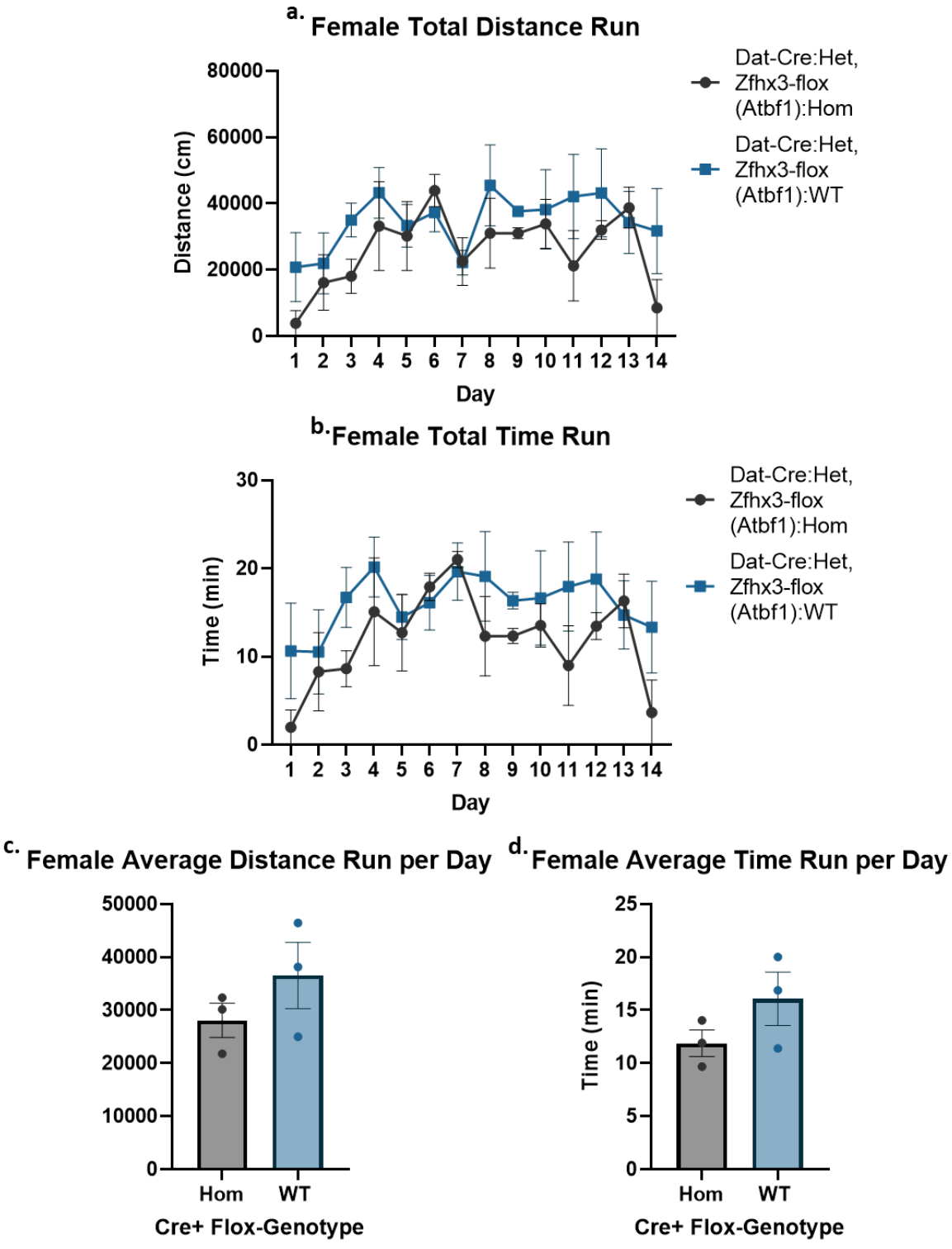

Figure 4.5.2.4.1. Motor Function Test – wheel running parameters for young female adult mice measuring daily distance run, and daily time run **–** presented as daily totals (a)(b), and as an overall average over the test course (c)(d). N numbers for homozygote and wildtype mice (n=3; n=3).

(**Figure 4.5.2.4.1.**) Young female homozygotes show no significant difference in total distance run in total over the 14 days of trial time (a), comparing: between genotypes ($F_{(1,4)}$=1.961, p=0.2340), and the interaction of genotype and trial day ($F_{(13,52)}$=0.6886, p=0.7551). Female mice also show no significant difference in the total time spent running over the 14 days of trial time (b), comparing: between genotypes ($F_{(1,4)}$=2.233, p=0.2094), and the interaction of genotype and trial day ($F_{(13,52)}$=0.0688, p=0.7651). Female homozygotes show no significant difference in average distance run per day to wildtypes, when comparing the average daily distance value of all subjects of each genotype (c; p=0.3823). Female homozygotes similarly show no significant difference to wildtypes when comparing the average daily running time of each subject (d; p=0.2094). Statistical analysis was performed using 2-way ANOVA with Šídák's multiple comparisons test (a,b), and unpaired t-test (c,d). Data are shown as mean ± standard error of mean.

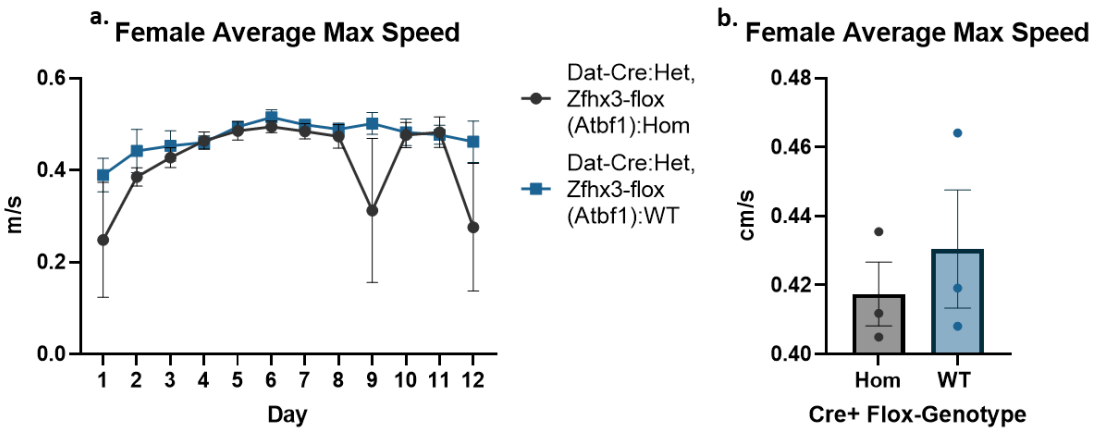

Figure 4.5.2.4.2. Motor Function Test – maximum speed run for young female adult mice measuring maximum speed each day (a), and average daily maximum speed over the test course (b). N numbers for homozygote and wildtype mice (n=3; n=3).

(**Figure 4.5.2.4.2.**) Young female homozygotes show no significant difference in maximum speed run on average per day, over the 12 days of trial time (a)

comparing: between genotypes ($F_{(1,4)}$=4.683, p=0.0964), and the interaction of genotype and trial day ($F_{(11,44)}$=0.9065, p=0.5421). Female homozygotes show no significant difference in average speed run per day to wildtypes, when comparing the average daily speed value of all subjects of each genotype (b; p=0.5401). Statistical analysis was performed using 2-way ANOVA with Šídák's multiple comparisons test (a), and unpaired t-test (b). Data are shown as mean ± standard error of mean.

In summary, young female homozygotes show no significant phenotype in their performance in the motor function test.

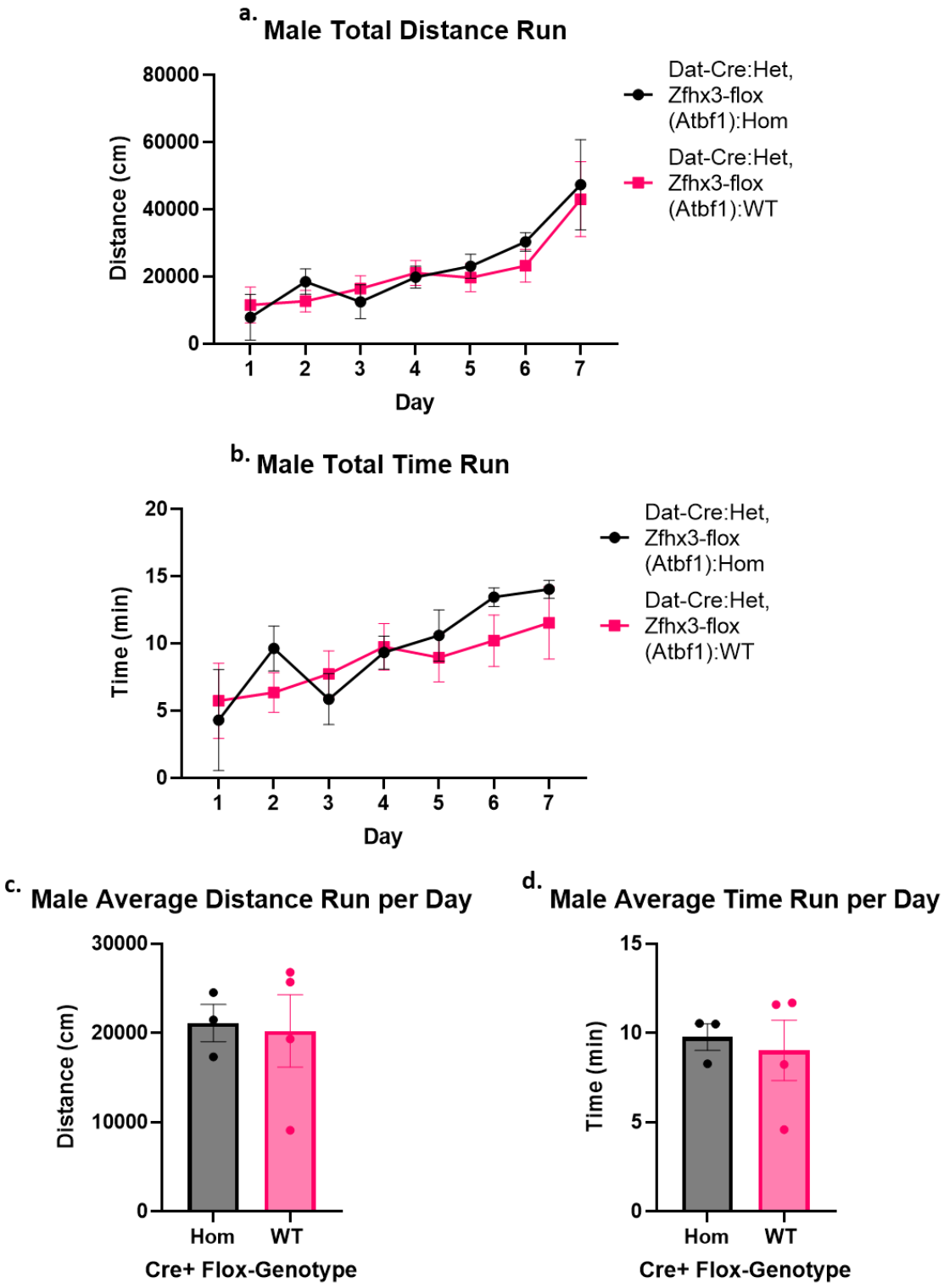

Figure 4.5.2.4.3. Motor Function Test – wheel running parameters for young male adult mice measuring daily distance run, and daily time run **–** presented as daily totals (a)(b), and as an overall average over the test course (c)(d). N numbers for homozygote and wildtype mice (n=3; n=4).

(**Figure 4.5.2.4.3**) Young male homozygotes show no significant difference in total distance run per day, over the 7 days of trial time (a) comparing: between genotypes ($F_{(1,5)}$=0.3383, p=0.5755), and the interaction of genotype and trial day ($F_{(6,30)}$=0.2607, p=0.0.9508). Male mice also show no significant difference in in the total time spent running over the 7 days of trial time (b), comparing: between genotypes ($F_{1,5}$=0.2623, p=0.6303), and the interaction of genotype and trial day ($F_{6,30}$=0.8356, p=0.5522). Male homozygotes show no significant difference in average distance run per day to wildtypes, when comparing the average daily distance value of all subjects of each genotype (c; p=0.8720). Male homozygotes similarly show no significant difference to wildtypes when comparing the average daily running time of each subject (d; p=0.7359). Statistical analysis was performed using 2-way ANOVA with Šídák's multiple comparisons test (a,b), and unpaired t-test (c,d). Data are shown as mean ± standard error of mean.

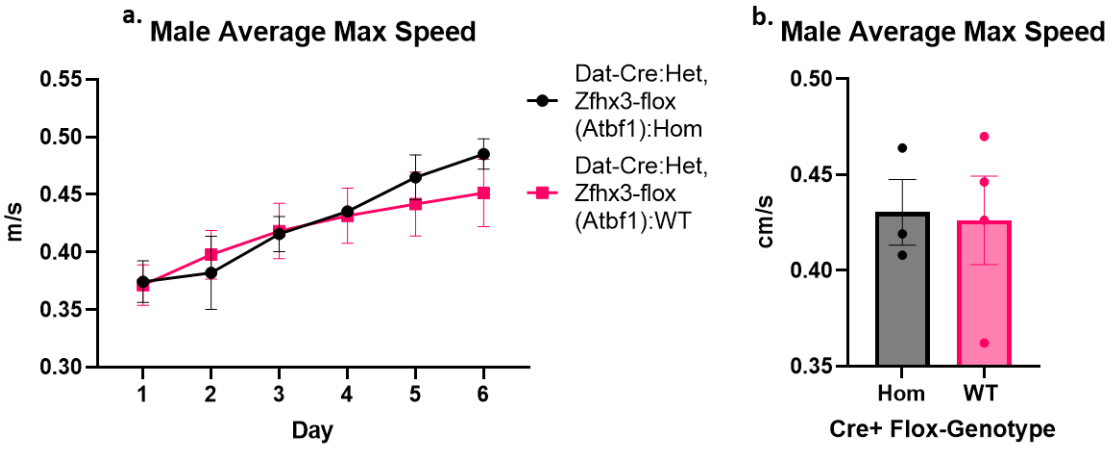

Figure 4.5.2.4.4. Motor Function Test – maximum speed run for young male adult mice measuring maximum speed each day (a), and average daily maximum speed over the test course (b). N numbers for homozygote and wildtype mice (n=3; n=4).

(**Figure 4.5.2.4.4.)** Young male homozygotes show no significant difference in maximum speed run on average per day, over the 6 days of trial time (a)

comparing: between genotypes ($F_{(1,5)}$=0.06965, p=0.8024), and the interaction of genotype and trial day ($F_{(5,25)}$=1.101, p=0.0.3848). Male homozygotes show no significant difference in average speed run per day to wildtypes, when comparing the average daily speed value of all subjects of each genotype (b; p=0.8965). Statistical analysis was performed using 2-way ANOVA with Šídák's multiple comparisons test (a), and unpaired t-test (b). Data are shown as mean ± standard error of mean.

In summary, much like young female homozygotes, males also show no phenotype in their performance in the motor function test.

4.5.2.5 Grip Strength

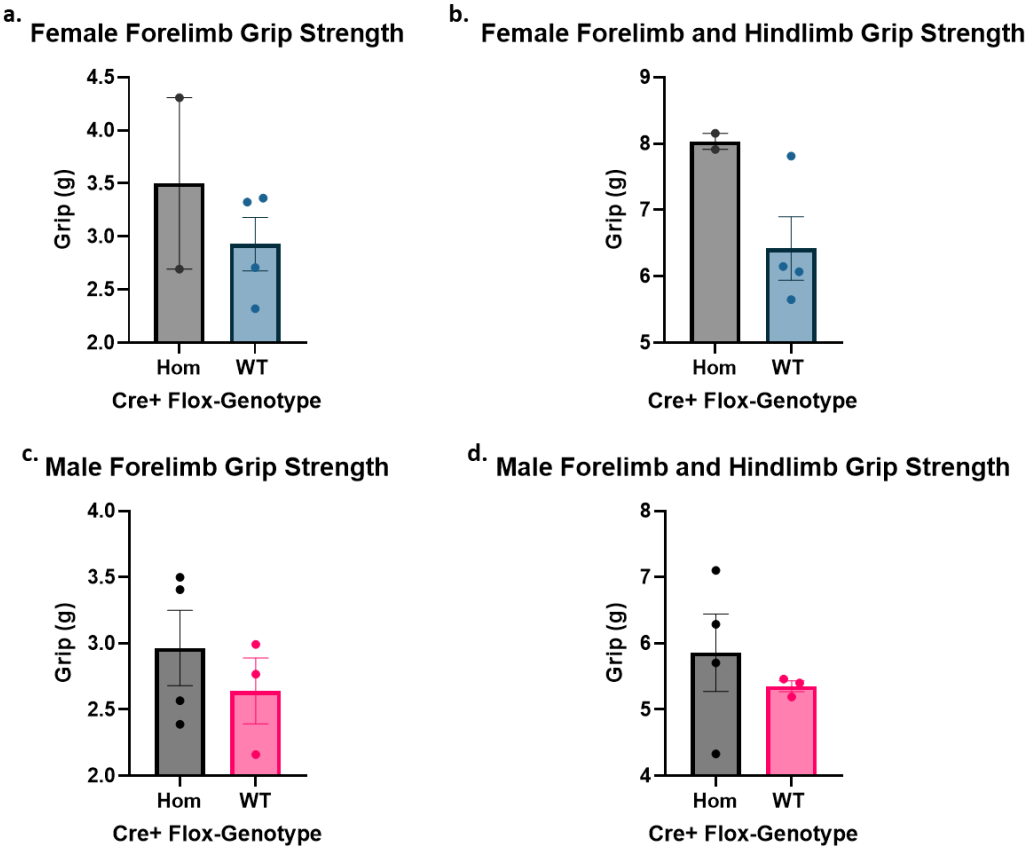

Figure 4.5.2.5.1. Grip Strength - measurement in young female and male adult mice measuring grip strength of forelimb alone (a)(b) , and forelimb and hind limb together (c)(d). N numbers for homozygote and wildtype mice respectively: females (n=2; n=4), males (n=4; n=3).

(**Figure 4.5.2.5.1.**) Young female homozygotes show no phenotype in forelimb grip strength when compared to wildtypes (a; p=0.4102), nor in combined fore- and hindlimb grip strength (b; p=0.0885). Male homozygotes similarly show no phenotype in forelimb grip strength when compared to wildtypes (c; p=0.4479), nor in combined for- and hindlimb grip strength (d; p=0.4987). Statistical analysis was performed using unpaired t-test. Data are shown as mean ± standard error of mean.

In summary, neither young females no males show a phenotype in their grip strength compared to wildtypes.

4.5.3 Memory

4.5.3.1 Forced Alternation (Y-maze)

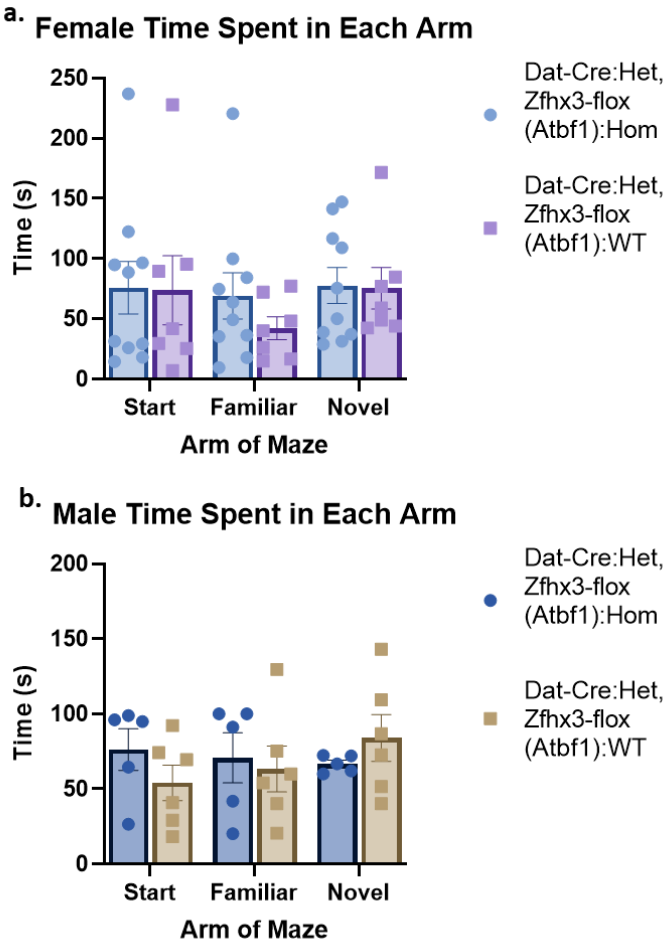

Figure 4.5.3.1.1. Forced Alternation (Y-maze) - time spent in arm for old female and male adult mice measuring time spent in each of the 3 arms of the Y-maze (a)(b). N numbers for homozygote and wildtype mice respectively: females (n=10; n=7), males (n=5; n=6).

Neither old female nor male homozygotes show a phenotype in time spent in each arm of the y-maze, compared to wildtypes (**Figure 4.5.3.1.1.**). Female mice show no significant difference in behaviour between homozygotes and wildtypes ($F_{1,15}$=0.6061, p=0.4484), and also the interaction of genotype and arm choice

($F_{2,30}$=0.2245, p=0.8002). Similarly male mice show no significant difference between homozygotes and wildtypes ($F_{1,9}$=0.07282, p=0.7934), nor in the interaction of genotype and arm choice ($F_{2,18}$=1.758, p=0.2007). Statistical analysis was performed using 2-way ANOVA with Šídák's multiple comparisons test. Data are shown as mean ± standard error of mean.

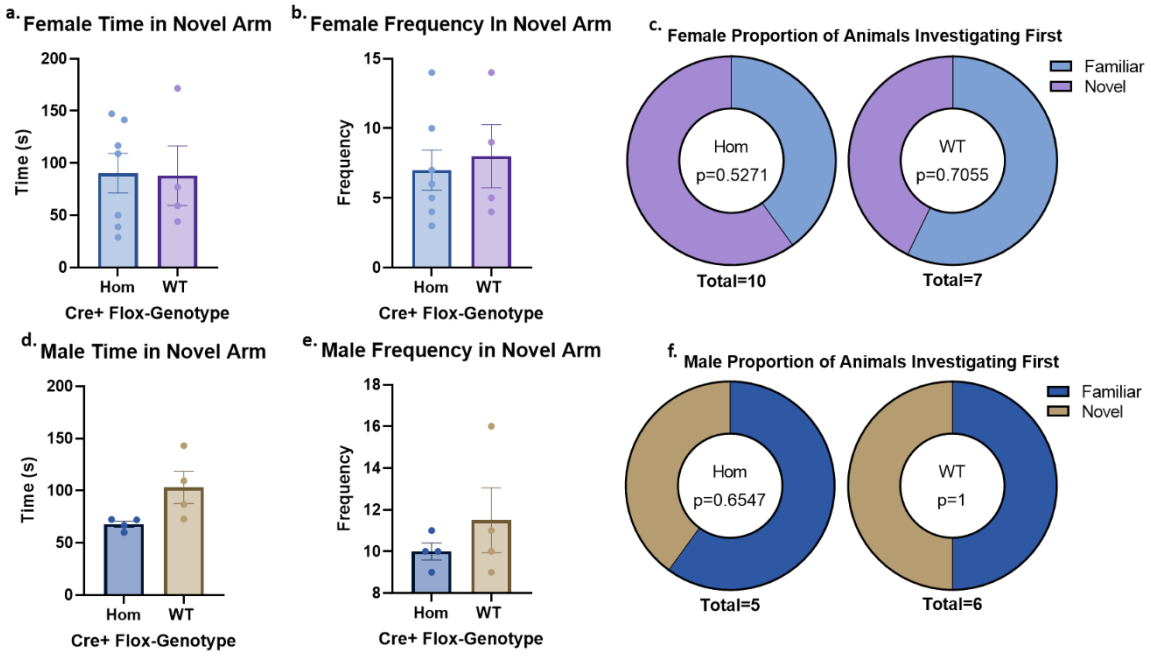

Figure 4.5.3.1.2. Forced Alternation (Y-maze) – novel arm behavioural parameters for old female and male adult mice measuring time in the novel arm (a)(d), frequency of entry into the novel arm (b)(e), and proportion of each genotype investigating either the novel or familiar arm first (c)(f). N numbers for homozygote and wildtype mice respectively: females (n=10; n=7), males (n=5; n=6).

Neither old male nor female homozygotes show a phenotype in their behaviour around the novel arm of the y-maze, compared to wildtypes (**Figure 4.5.3.1.2**). Female homozygotes show no significant phenotype in: time spent in novel arm (a; p=0.9228), and frequency of entry to the novel arm (b; p=0.2169). Analysing the choice to first investigate either the familiar and novel arm of the maze, both the female homozygotes (c; 'Hom' p=0.05271) and wildtype (c; 'WT' p=0.7055)

demonstrated no preference. Similarly, male homozygotes show no significant phenotype in: time spent in novel arm (d; p=0.3442), and frequency of entry to the novel arm (e; p=0.3020). Neither male homozygotes (f; 'Hom', p=0.06547) nor wildtypes (f; 'WT', p=1) show a significant preference to either the familiar or novel arm. Statistical analysis was performed using unpaired t-test (a, b, d, e) and chi^2 test (c, f). Data are shown as mean ± standard error of mean (a, b, d, e), or parts of whole (c, f).

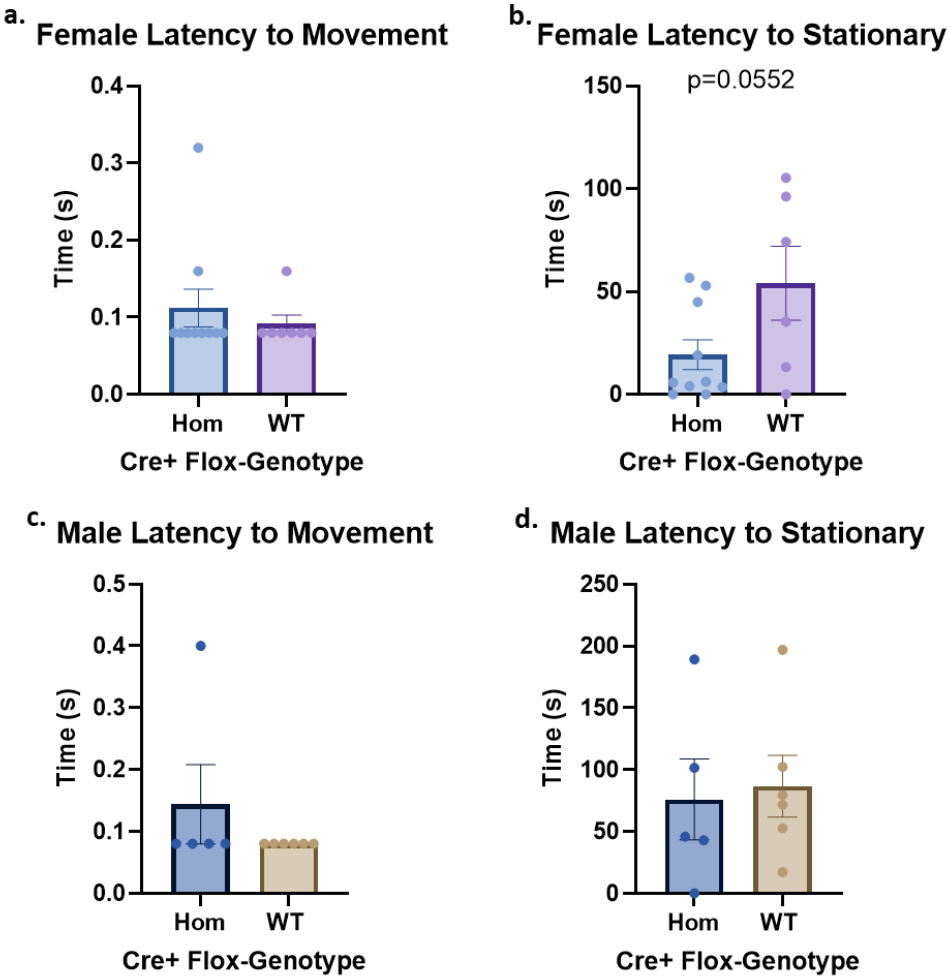

Figure 4.5.3.1.3. Forced Alternation (Y-maze) – movement parameters for old female and male adult mice measuring time latency to initiate movement (a)(c), and time latency to cease movement (b)(d), in the Y-maze. N numbers for homozygote and wildtype mice respectively: females (n=10; n=7), males (n=5; n=6).

(**Figure 4.5.3.1.3.**) Old female homozygotes do not show a significant phenotype in latency to initiating movement, from the beginning of the trial (a; p=0.5166). However female homozygotes do show a trend towards a lower latency to the first instance of being stationary (b; p=0.0552) – although this does not show a significant difference. Male homozygotes do not show a significant phenotype under either parameter: latency to initiating movement (c; p=2967), and latency to being stationary (d; p=0.7946). Statistical analysis was performed using unpaired t-test. Data are shown as mean ± standard error of mean.

In summary, while old males show no phenotype in the forced alternation test, female homozygotes showed a possible trend towards halting their initial exploration earlier than wildtypes – however this statement is not supported by significant data.

4.5.3.2 Novel Object Recognition

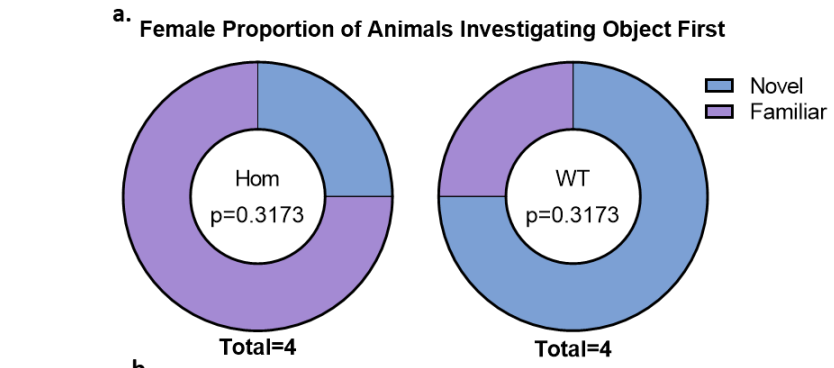
a.
Female Proportion of Animals Investigating Object First
Hom
p=0.3173
WT
p=0.3173
Novel
Familiar
Total=4
Total=4

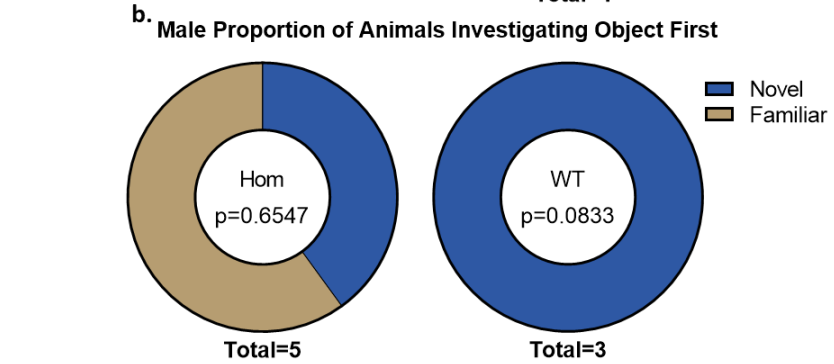
b.
Male Proportion of Animals Investigating Object First
Hom
p=0.6547
WT
p=0.0833
Novel
Familiar
Total=5
Total=3

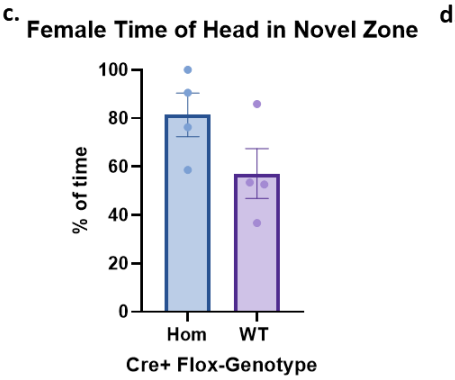
c.
Female Time of Head in Novel Zone
% of time
100
80
60
40
20
0
Hom
WT
Cre+ Flox-Genotype

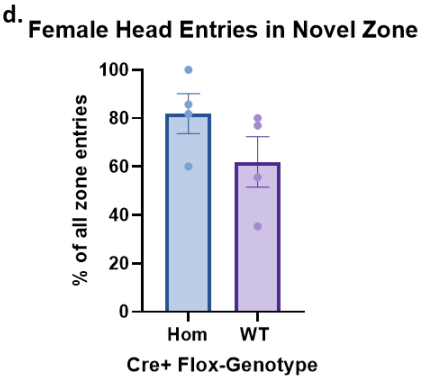
d.
Female Head Entries in Novel Zone
% of all zone entries
100
80
60
40
20
0
Hom
WT
Cre+ Flox-Genotype

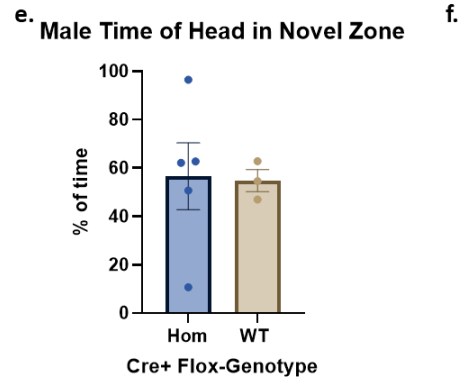
e.
Male Time of Head in Novel Zone
% of time
100
80
60
40
20
0
Hom
WT
Cre+ Flox-Genotype

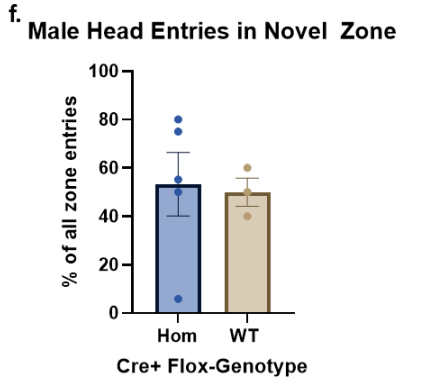
f.
Male Head Entries in Novel Zone
% of all zone entries
100
80
60
40
20
0
Hom
WT
Cre+ Flox-Genotype

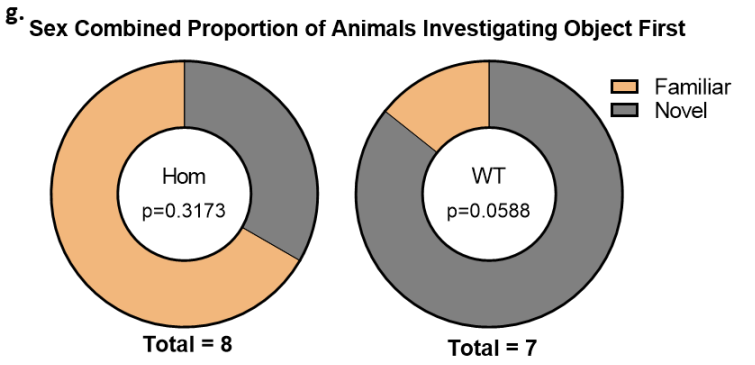
g.
Sex Combined Proportion of Animals Investigating Object First
Hom
p=0.3173
WT
p=0.0588
Familiar
Novel
Total = 8
Total = 7

Figure 4.5.3.2.1. Novel Object Recognition – parameters for old female and male adult mice analysing proportion of each genotype investigating the novel object first (a)(b)(g), time spent by the head in the novel zone (c)(e) and frequency of entry of the head into the novel zone (d)(f). N numbers for homozygote and wildtype mice respectively: females (n=4; n=4), males (n=5; n=3).

(**Figure 4.5.3.2.1.)** Neither the female homozygotes (a; 'Hom', p=0.3173) or wildtypes (a; 'WT', p=0.3173) show significant preference in investigating either the novel or familiar object first. Similarly, neither the male homozygotes (b; 'Hom' p=0.6547) nor wildtypes (b; 'WT', p=0.0833) show an object preference for initial investigation. Female homozygotes show no significant phenotype in the proportionate time spent in the novel object zone (c; p=0.1275), or proportionate number of head entries into the novel zone (d; p=0.1845). Male homozygotes also show no significant phenotype under the same parameters: in proportionate time spent in the novel object zone (e; p=0.9273), or proportionate number of head entries into the novel zone (f; p=0.8643). When sex is combined, and looking at the proportion of animals that investigate the novel object first, wildtypes show a trend towards investigating the novel object first (g; p=0.0588) (this is not supported by significant data) while homozygotes show preference over objects (g; p=0.3173). Statistical analysis was performed using unpaired t-test (c, d, e, f) and chi^2 test (a, b, g). Data are shown as mean ± standard error of mean (c, d, e, f), or parts of whole (c, f).

In summary, neither individual sex in old homozygotes showed any significant differences in behaviour. However when analysing combined sex, there is a trend for wildtype mice to investigate the novel object first – when the familiar and novel object are re-introduced to the cage – while this trend is lost on the homozygotes. However, this statement is not supported by significant data.

4.5.3.3 Fear Conditioning

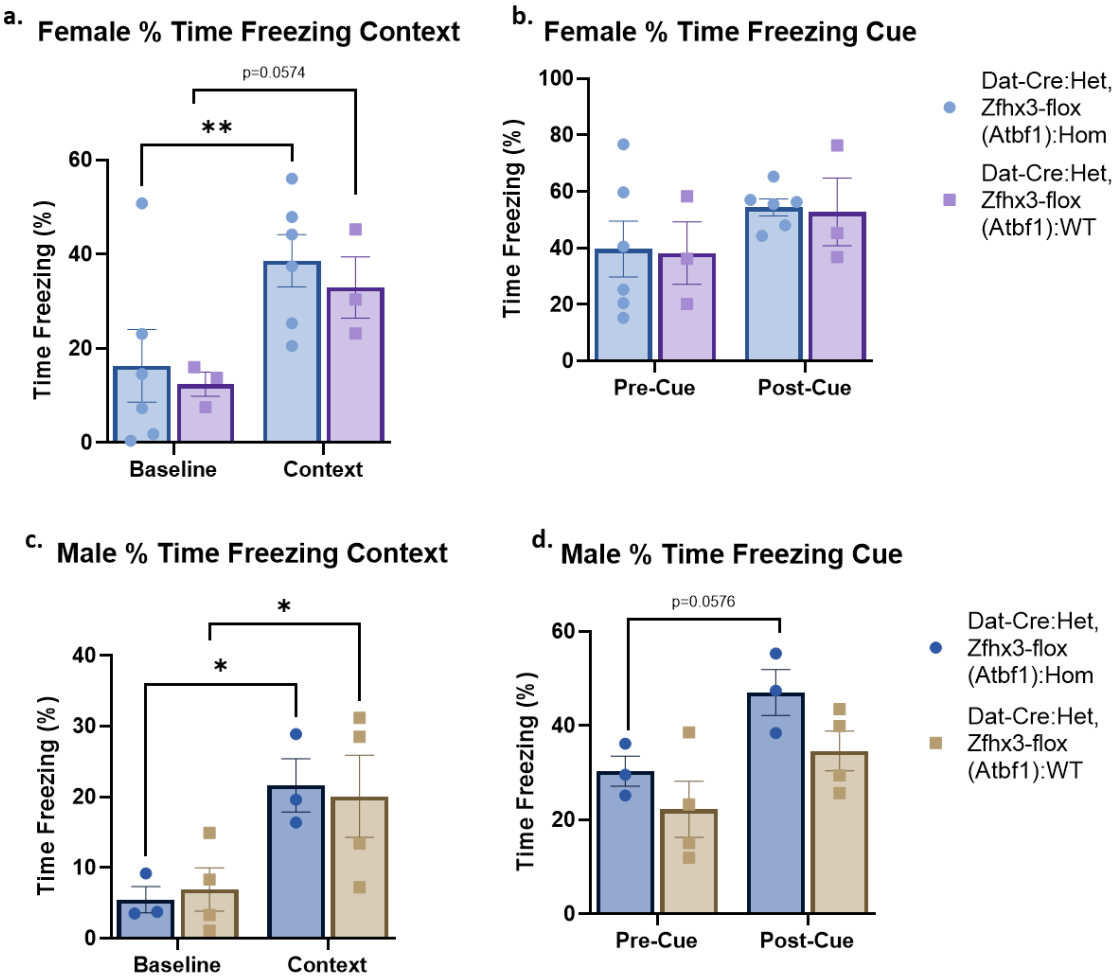

Figure 4.5.3.3.1. Fear Conditioning - parameters for old female and male adult mice analysing proportion of time spent freezing during the context trial (a)(c); and comparing proportion of time spent freezing before and after the shock-tone during the cue trial (b)(d). N numbers for homozygote and wildtype mice respectively: females (n=6; n=3), males (n=3; n=4).

(**Figure 4.5.3.3.1.**) Old female homozygotes show no significant phenotype in their time freezing during the context trial (a) when comparing: between genotypes ($F_{1,7}$=0.2656, p=0.6222), and the interaction of genotype and trial type ($F_{1,7}$= 0.03495, p=0.8570). Females do show a significant phenotype comparing

baseline and context freezing without accounting for genotype ($F_{1,7}$= 21.65, p=0.0023), with Šídák's multiple comparisons test showing a significant increase in freezing behaviour is expressed by homozygotes (p=0.0081) and wildtypes trending to increased freezing (p=0.0574) – although there is no significant data to support the final statement. During the cue trial (b), females show no significant phenotype when comparing: between genotypes ($F_{1,7}$=0.01737, p=0.8988), pre- and post-cue without accounting for genotype ($F_{1,7}$=5.412, p=0.0529), and in the interaction of genotypes and cue ($F_{1,7}$=0.0001216, p=0.9915). Males show no significant phenotype in their time freezing during the context trial (c) when comparing: between genotypes ($F_{1,5}$=9.599e-005, p=0.9926), and in the interaction of genotype and trial ($F_{1,5}$= 0.3108, p=0.6012). Males do show a significant phenotype comparing baseline and context freezing without accounting for genotype ($F_{1,5}$=29.81, p=0.0028), with Šídák's multiple comparisons test showing a significant increase in freezing behaviour is expressed both by homozygotes (p=0.0209) and wildtypes (p= 0.0266). During the cue trial (d), males show no significant phenotype when comparing: between genotypes ($F_{1,5}$=2.938, p=0.1472), and the interaction of genotype and cue ($F_{1,5}$=0.3501, p=0.5798). Males do show a significant phenotype of freezing time increasing post-cue without accounting for genotype ($F_{1,5}$=15.86, p=0.0105), with Šídák's multiple comparisons test demonstrating homozygotes trending towards an increase in freezing time post-cue (p=0.0576). Combined-sex analysis of significant phenotypes maintains significance, in regards to the ‘context’ trial: ‘combining baseline and context freezing without accounting for phenotype’ showing significance ($F_{1, 14}$= 46.12, p=<0.0001) with Šídák's multiple comparisons test showing a significant increase in freezing behaviour across trials in both

homozygotes (p=0.0001) and wildtypes (p=0.0024). Statistical analysis was performed using 2-way ANOVA with Šídák's multiple comparisons test. Data are shown as mean ± standard error of mean.

In summary, old female homozygotes spend more time freezing – giving a stronger reaction - during the context trial than their wildtype counterparts, in which significance is maintained during combined-sex analysis. During the cue trial, male homozygotes show a possible trend of increasing in freezing time post-cue (this statement is not supported by significant data) while wildtype mice do not.

4.5.4 Sleep

(**Figure 4.5.4.1.**) Looking at total time spent sleeping (a), there is no significant difference between old homozygote and wildtype mice in the total time slept ($F_{1,6}$=0.03426, p=0.8593), or in the interaction of genotype and Zeitgeber time (ZT) ($F_{23,138}$ = 0.8703, p=0.6372). There is a significant difference of time slept over the time of the test without considering genotype ($F_{23,138}$ = 8.133, p<0.0001). In total number of sleep bouts (b), there is no significant difference between homozygote and wildtype mice in the total number of bouts ($F_{1,6}$ = 1.667, p=0.2442), or in the interaction of genotype and ZT ($F_{23, 138}$=1.261, p=0.2060). There is a significant difference in number of bouts over the time of the test without considering genotype ($F_{4.998, 29.99}$= 2.776, p=0.0355), and when comparing between genotypes for individual hours of the test (ZT5 p=0.04846; ZT9 p=0.02132). For average sleep bout length (c), homozygotes and wildtypes show no significant difference ($F_{1, 6}$=3.085, p=0.1295), nor in the interaction of genotype and ZT ($F_{23, 136}$=1.252,

p=0.2131). Statistical analysis was performed using 2-way ANOVA with Šídák's multiple comparisons test (a, b) and mixed-effects analysis with multiple comparisons (c). Data are shown as mean ± standard error of mean.

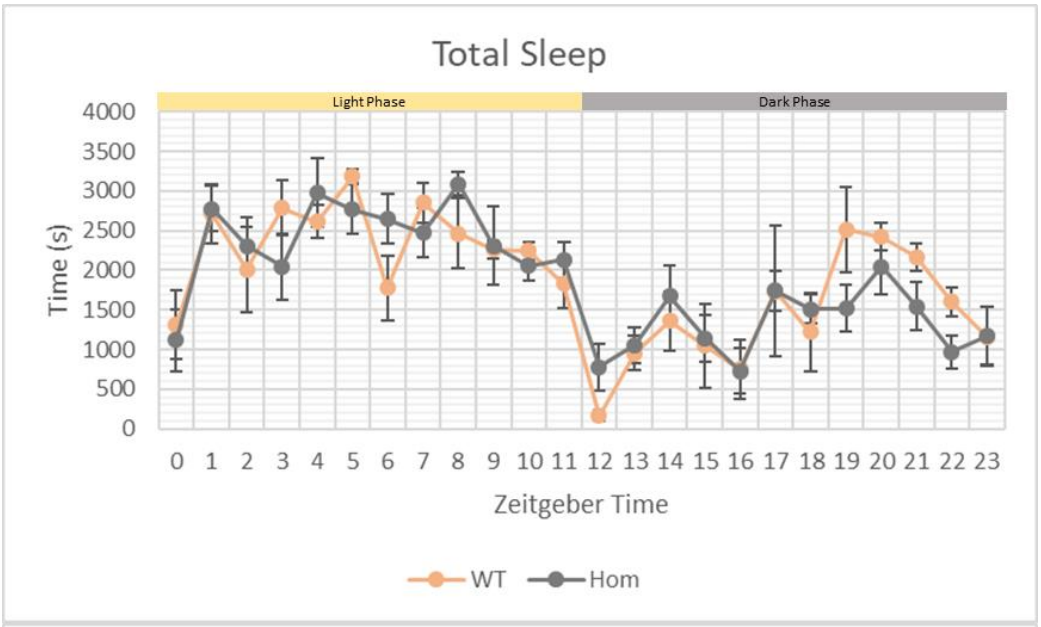
Total Sleep
Light Phase
Dark Phase
Time (s)
4000
3500
3000
2500
2000
1500
1000
500
0
0 1 2 3 4 5 6 7 8 9 10 11 12 13 14 15 16 17 18 19 20 21 22 23
Zeitgeber Time
WT
Hom

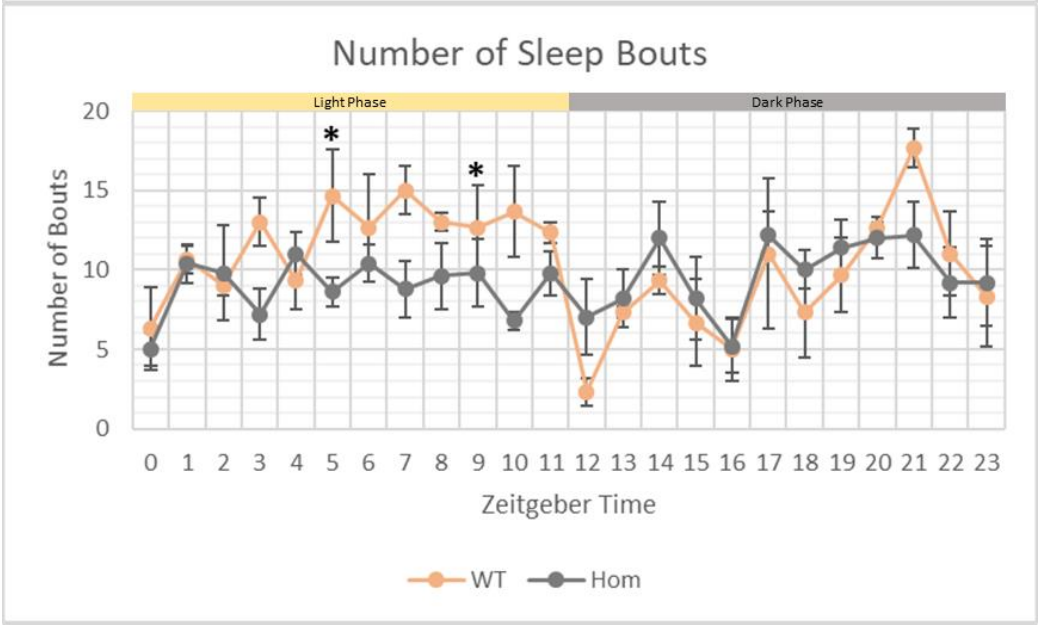
Number of Sleep Bouts
Light Phase
Dark Phase
Number of Bouts
20
15
10
5
0
*
*
0 1 2 3 4 5 6 7 8 9 10 11 12 13 14 15 16 17 18 19 20 21 22 23
Zeitgeber Time
WT
Hom

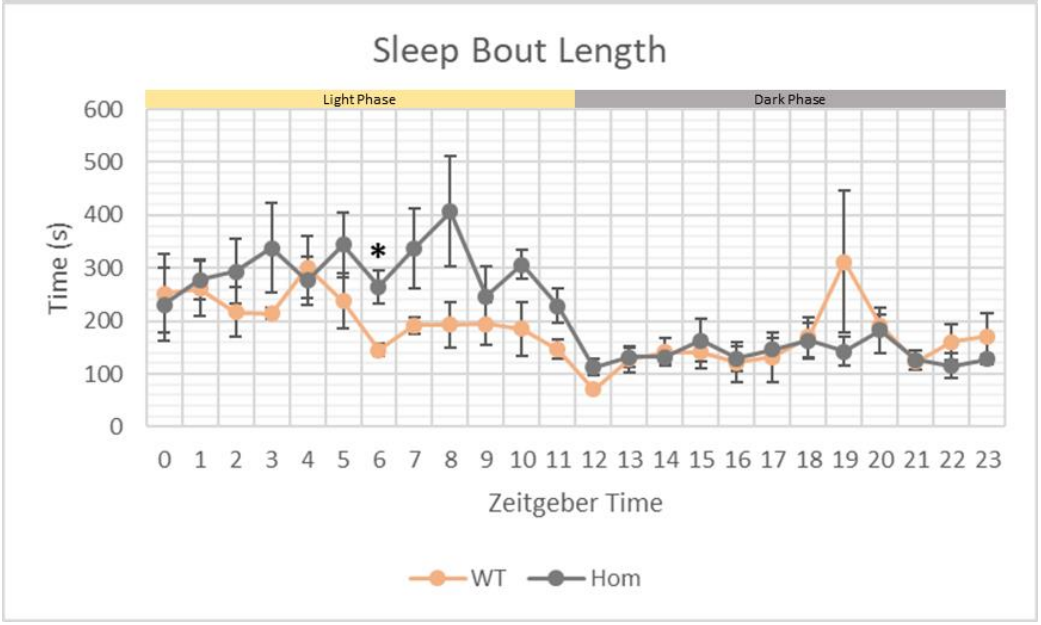
Sleep Bout Length
Light Phase
Dark Phase
Time (s)
600
500
400
300
200
100
0
*
0 1 2 3 4 5 6 7 8 9 10 11 12 13 14 15 16 17 18 19 20 21 22 23
Zeitgeber Time
WT
Hom

Figure 4.5.4.1. Sleep – parameters in each hour over 24 hours for old adult mice measuring total sleep per hour (a), number of sleep bouts per hour (b), and the average length of a sleep bout each hour (c). Results given with sex combined. N numbers for homozygote and wildtype mice respectively: (n=5)(n=3).

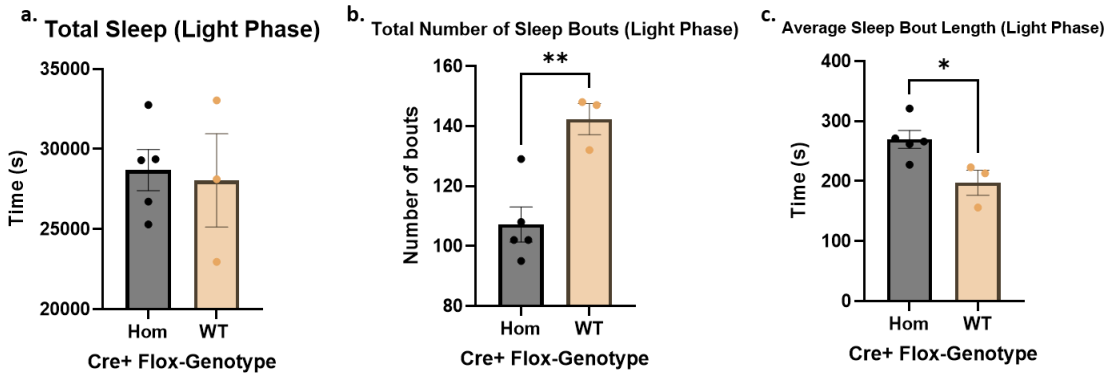

Figure 4.5.4.2. Sleep - parameters during the light phase (ZT12-23) for old adult mice measuring total sleep (a), number of sleep bouts (b), and the average length of a sleep bout each day (c). Results given with sex combined. N numbers for homozygote and wildtype mice respectively: (n=5)(n=3).

(**Figure 4.5.4.2.**) While there is no significant difference between homozygotes and wildtypes in the total sum of sleep during the light phase (a; p= 0.8195), homozygotes have significantly fewer sleep bouts (b; p= 0.0066) during this time, with sleep bouts being significantly longer (c; p= 0.0283). Statistical analysis was performed using unpaired t-test. Data are shown as mean ± standard error of mean.

In summary, old combined sex homozygotes spend the same amount of time sleeping during the light phase, however they sleep in significantly fewer but longer bouts.

4.5.5 Social Dominance

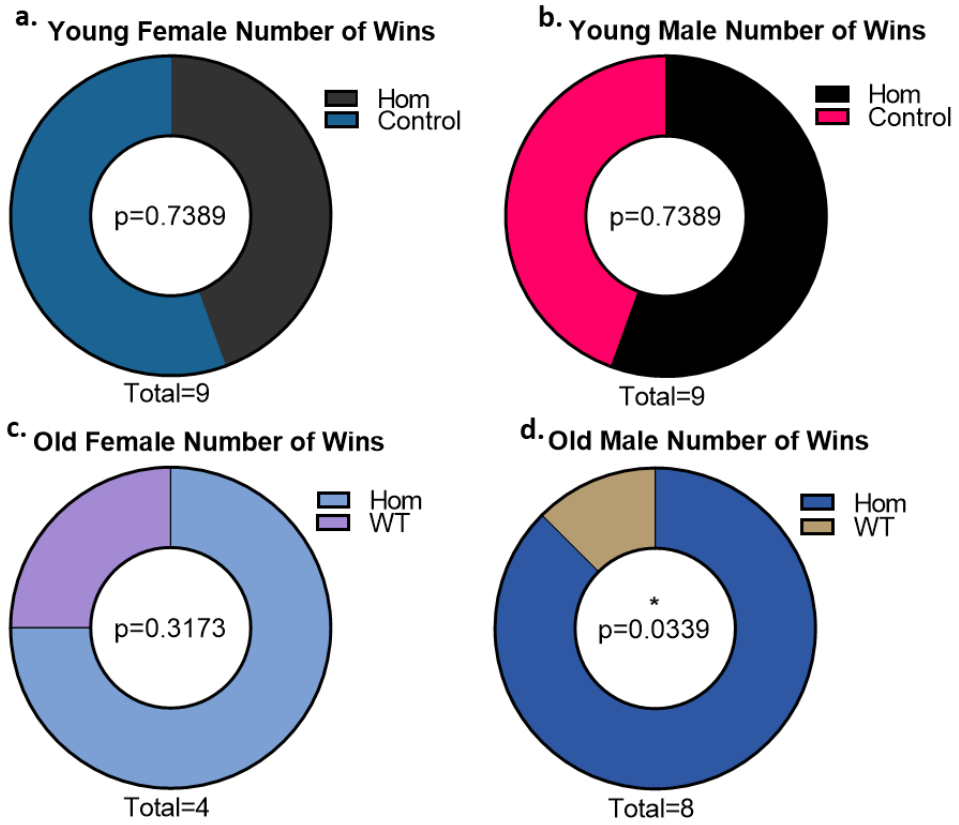

Figure 4.5.5.1. Social Dominance Test - young and old female and male adult mice showing the proportion of wins for homozygote or wildtype mice in a dominance contest**.** N numbers for homozygote and wildtype mice respectively: young females (n=3; n=5), young males (n=3; n=5), old females (n=2; n=2), old males (n=4; n=4). 'Total' number shown for each chart represents the total number of dominance contests for each sex.

(**Figure 4.5.5.1.**) In younger mice, there is no significant difference in the number of wins in the social dominance contest between homozygotes and wildtypes, in either females (a; p=0.7389) or males (b; p=0.7380). In older mice, female homozygotes and wildtypes show no significant difference in social dominance (c; p=0.3173), however older male homozygotes achieved significantly higher social dominance wins over their wildtype counterparts (d; p=0.0339). In combined-sex analysis of significant phenotypes, significance is maintained in 'Number of Wins'

as seen in old males alone (p=0.0209) with homozygote score remaining higher than wildtype. Statistical analysis was performed using chi^2 test. Data are shown as parts of whole.

In summary, old male homozygotes show dominance over their wildtype counterparts, including when a part of combined-sex analysis.

4.5.6 Pain: Von Frey Filament Test

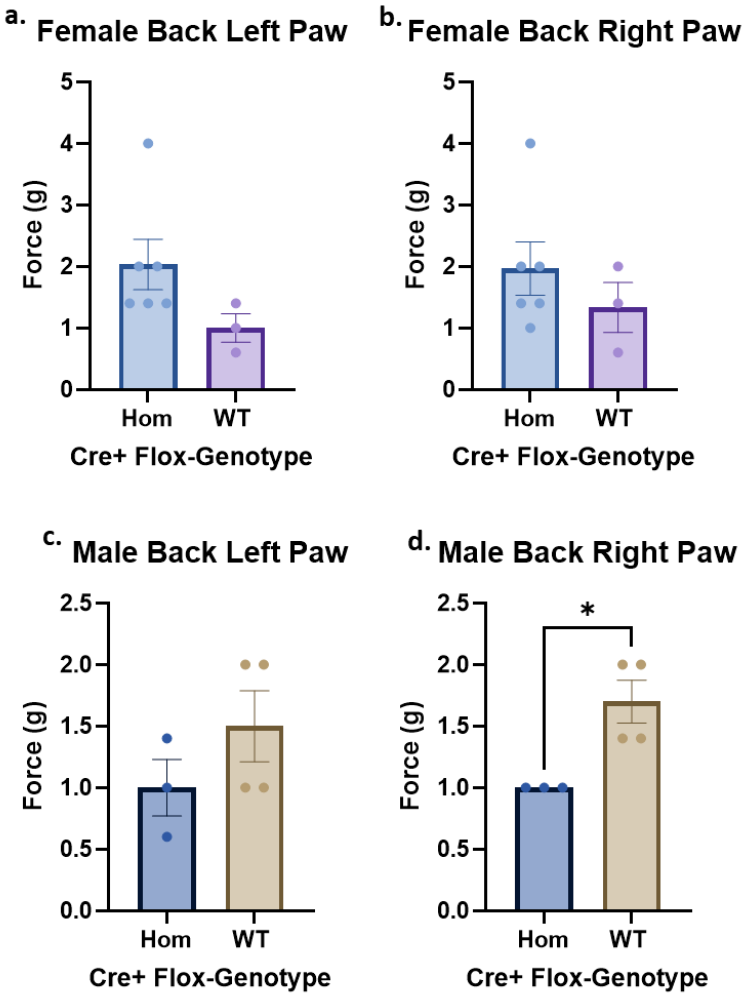

Figure 4.5.6.1. Von Frey Filament Test - for old female and male adult mice measuring reflexive pain threshold in back left (a)(c) and back right (b)(d) paws. N numbers for homozygote and wildtype mice respectively: females (n=6; n=3), males (n=3; n=4).

(**Figure 4.5.6.1.)** Old female homozygotes show no significant difference in their filament scores to wildtypes, in both their back left (a; p= 0.1399) and back right (b; p= 0.3904) paws. Male homozygotes show no significant phenotype in their back left paw (c; p= 0.2586), however they show a significant reduction in their filament score in their back right paw (d; p= 0.0189) compared to wildtypes. In combined sex analysis of significant phenotypes, significance is not maintained in 'Back Right Paw' as seen in males alone (p=0.8068). Statistical analysis was performed using unpaired t-test. Data are shown as mean ± standard error of mean.

In summary, old males showed a significantly reduced pain tolerance in their hind right paw – which does not maintain significance in combined-sex analysis.

4.5.7 Pre-Pulse Inhibition

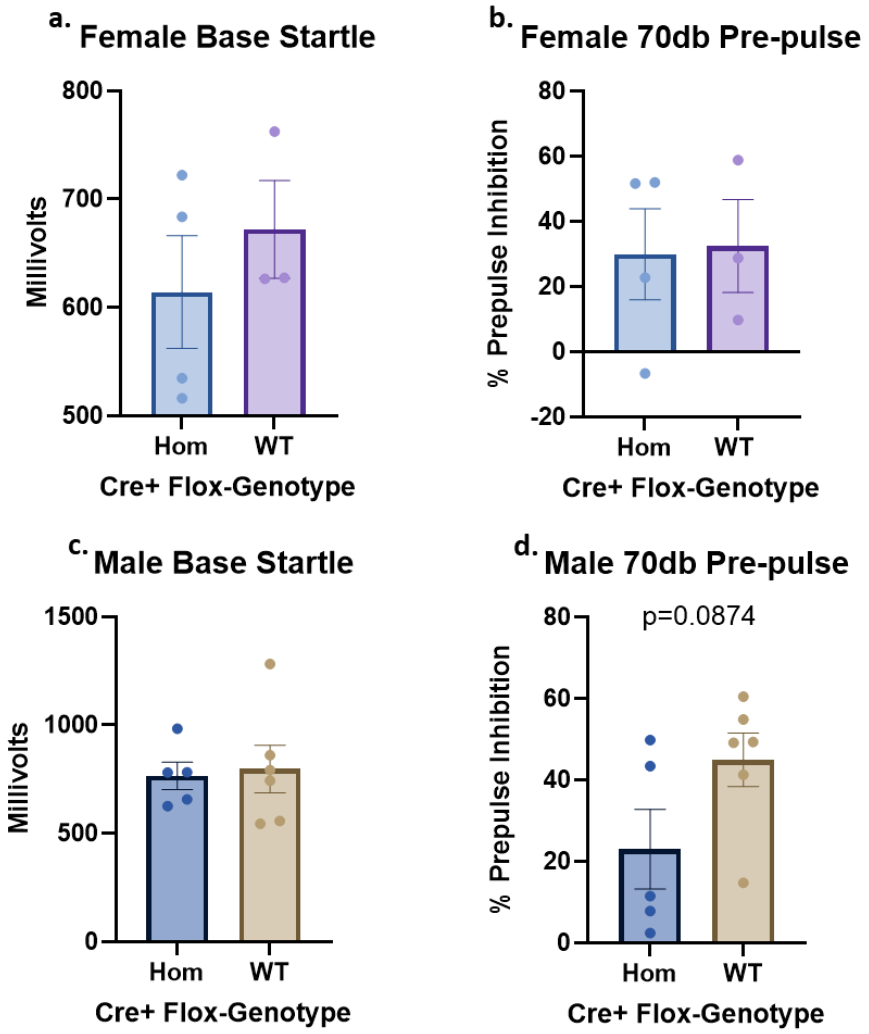

Figure 4.5.7.1. Startle and Pre-pulse Inhibition – for old female and male adult mice measuring startle response to an auditory stimulus (a)(c), and pre-pulse inhibition of base startle when given a 70db auditory pre-pulse. N numbers for homozygote and wildtype mice respectively: females (n=4; n=3), males (n=5; n=6).

(**Figure 4.5.7.1.**) In the base startle score, neither old females nor males show a significant difference between homozygotes and wildtypes (a; p= 0.4584)(b; p= 0.8228). In comparing pre-pulse inhibition using a 70db tone, female homozygotes show no significant difference to wildtypes (c; p= 0.9076). However, at a 70db pre-pulse, male homozygotes demonstrate a possible trend towards having an attenuated pre-pulse inhibition compared to wildtypes (d; p=0.0847) – although

there is no significant difference shown. Statistical analysis was performed using unpaired t-test. Data are shown as mean ± standard error of mean.

In summary, old male homozygotes show a possible trend to dysfunction in pre-pulse inhibition – however this is not supported by significant data.

4.6 LacZ investigation of DAT-*Cre* mice

The primary limitation of this study, and the following molecular analysis of this line, was the low n-number of homozygous knockout mice. Despite multiple rounds of breeding, genotype distribution in litters did not follow Mendelian inheritance ratio, with very few homozygous knockout mice of either sex being generated. DAT-*Cre* mice were crossed with B6-Gt(ROSA)26Sor^{tm1Sor}/J *Cre*-reporter mice. Dat-*Cre*:Het, *LacZ*:Het progeny express *lacZ* enzyme in tissues where *Cre* is expressed.

Tissue sections were taken between 50-56 days old, and stained with X-Gal to produce blue stain where *Cre* is expressed (**Figure 4.6.1.**). Both maternal and paternal-inherited DAT-*Cre* show expression in the intended midbrain dopaminergic regions (a,c), however male progeny show ectopic expression in the testes (b,d) indicating *Cre* expression in the male germline. *Zfhx3* plays a key role in development, with heterozygous deletion of *Zfhx3* in mice causing preweaning mortality, therefore in DAT-*Cre*; *Zfhx3*-Flox litters a germline introduction of *Cre* expression likely explains the relative lack of homozygous knockout mice, since male mice were used to introduce Cre to the experimental cohort cross (*Methods 2.1.4*.) (Sun, Fu et al. 2012).

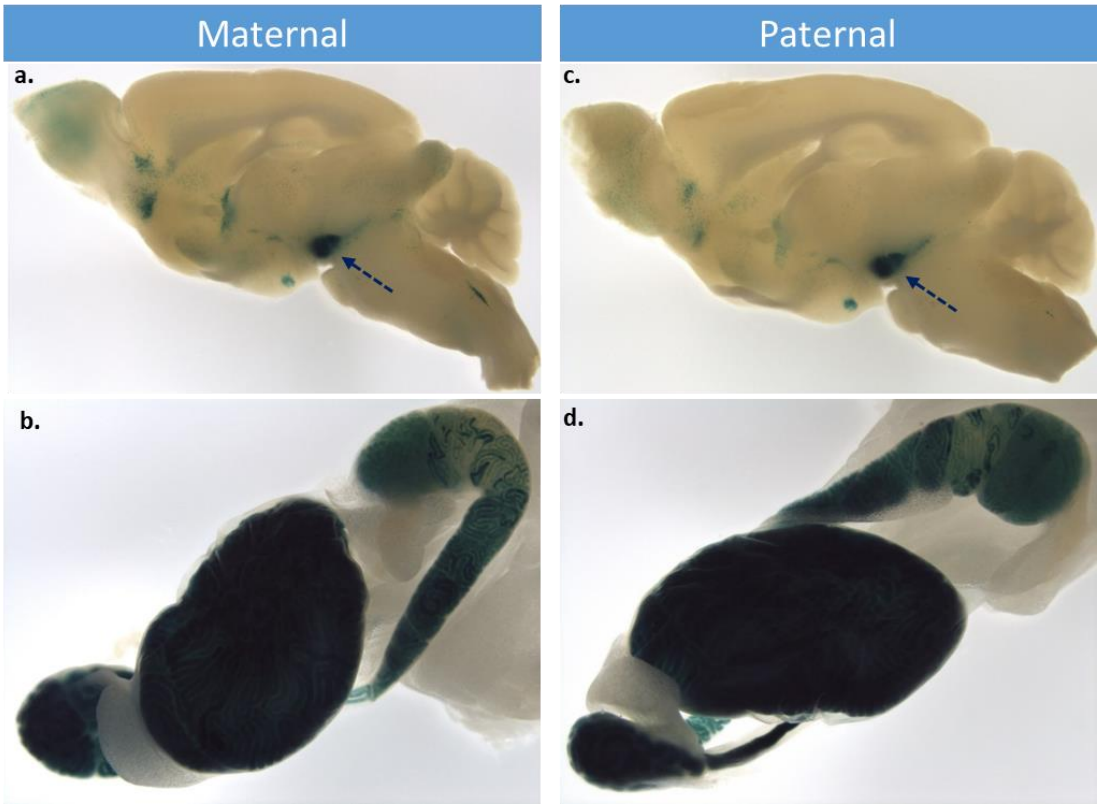

Figure 4.6.1. LacZ staining of Dat-Cre:Het, LacZ:Het sagittal brain section and testes, from maternal and paternal inherited DAT-*Cre* showing *Cre* expression in the midbrain (a,c) indicated with an arrow, and ectopic *Cre* expression in both maternal and paternal inherited DAT-*Cre*.

4.7 Discussion

DAT-*Cre*; *Zfhx3*-Flox homozygous mice do not display a primary behavioural phenotype, but instead demonstrate a mild and diffuse phenotype when comparing to their wildtype counterparts.

There is also measurable sexual dimorphism in the behavioural phenotype amongst the homozygotes.

The question of whether age plays a significant factor in behavioural phenotype is not as easily answered. To satisfactorily answer this question, greater n-numbers

would be required to fulfil the need for every behavioural test to have age-comparison cohorts, and further statistical analysis would have to be carried out for all the tests in this pipeline – for example, 3-way ANOVAs taking both sex and age into account. While further cohorts cannot be generated, we intend to carry out additional statistical analysis when moving forward with this dataset.

4.7.1 Anxiety

There are both sex and age differences in the behavioural profiles of homozygotes in anxiety tests.

In young female homozygotes, we see a significant phenotype in their anxiogenic behaviour compared to wildtypes. In the open field, homozygotes show a significantly lower maximum length of movement bout, specifically in the periphery zone. This suggests that female homozygotes were more anxious than wildtypes, despite being in the ‘safer’ periphery zone, with their exploratory drive being attenuated. In the light-dark box, they show less time in the entry zone, suggesting they are engaging in less risk-assessing – and more impulsive - behaviour.

In young male homozygotes, we also see a significant difference in their anxiogenic behaviour. In the light-dark box, homozygotes spend more time, and more time moving while in the light zone, exhibiting a clear attenuation of anxiogenic behaviours.

In old female homozygotes, significant differences in their anxiogenic behaviour are maintained, and possibly progress with age. In the open field, homozygotes show anxious behaviours in multiple parameters – lower frequency, and time

spent, in the centre zone compared to wildtypes. This logically includes more time spent in the periphery, however they no longer show lower maximum length of movement bout in the periphery, as seen in the younger females. Unexpectedly, female homozygotes enter the centre zone with a significantly lower latency time from start of test than wildtypes, suggesting an attenuated anxiety response as opposed to the heightened response suggested by other parameters. This could be exhibiting the same suppression of risk-assessing behaviour as seen in the young female homozygotes. In the light-dark box, they show differences in their ambulatory behaviour between zones. They exhibit fewer transitions between the light and dark zones, – suggesting an attenuation in their exploratory behaviour, and heightened anxiety.

In old males, we find that their anxiety phenotype is lost – with homozygotes showing no significant differences in behaviour to their wildtype counterparts.

In summary: combined-sex analysis show a mild anxiogenic phenotype in young homozygous mice, with no maintenance of significance in tests for old mice. Younger female homozygotes show a mild increase in anxiety behaviours compared to wildtypes. Older female homozygotes show a stronger phenotype, demonstrating a progressively heightened anxiety response - including supressed exploratory drive - in a greater number of parameters than younger homozygotes. Seemingly contrary to this, there are also multiple parameters that suggest that both young and old female homozygotes exhibit mild depression in risk-assessing behaviour, showing a more complex change in profile to their anxiogenic drives to wildtype mice.

Male homozygotes show a different profile. Younger males show an attenuated anxiety response over multiple parameters, indicating a suppression of avoidance behaviours and an increase in risk-taking behaviours. This phenotype however is entirely lost in older homozygotes, who show no anxiety difference to their wildtype counterparts. This ‘progressive normalisation’ could demonstrate that the suppression of anxiogenic behaviours linked to the knockout of *Zfhx3* in dopaminergic neurons of male mice during development can be ‘corrected’ over time.

In combined-sex analysis of sex-specific significant phenotypes, we find a mild anxiogenic phenotype in homozygous mice. In the open field test, young wildtype mice are shown to have significantly higher maximum movement bouts in the periphery. In the light-dark box, no significance is maintained from single-sex analysis when subject to combined-sex analysis, in both young and old mice. However when analysis is split into separate sexes, we find differences in their anxiety-related behaviour. These sex-dependent differences may be why we see less significant combined-sex analysis tests, as the sex-specific behaviours are ‘cancelling’ each other out.

4.7.2 Motor

There are both sex and age differences in the behavioural profiles of homozygotes in motor tests.

Young male homozygotes show a phenotype in their gait. They have a significantly increased duration in hind limb stance, and significantly decreased speed. This demonstrates that their hind paws spend longer on the walking

surface - and this foot drag is either the result of, or cause of, their decreased speed compared to wildtypes. This decrease in speed was not picked up in any of the other tests that also measure walking speed as a parameter, nor did their dragging back feet interfere with the other motor tests. It can be argued that gait analysis is the least anxiety-inducing motor test, since it is carried out in complete darkness except for red light. It is possible that the male's supressed anxiety response masks any motor deficit, when in brighter arenas.

Old female homozygotes show a difference from homozygotes in one parameter, that their walking bouts are significantly shorter in duration. As there is an absence of any other motor deficits, it is possible that this is a product of old female homozygotes' heightened anxiety response, supressing their exploratory drive – or this could be demonstrating supressed locomotion.

Old male homozygotes continue to show a phenotype in their gait, showing a significantly longer front limb swing duration. This could show another angle to the male homozygote's gait deficits, with a longer front limb swing duration possibly showing learned compensation for the younger cohort's deficit in their hind limbs – especially since the younger male's hind limb dysfunction is not observed in the older males.

In combined-sex gait analysis, we find a mild motor phenotype, suggesting a deficiency in homozygous mice. Significance is maintained from single-sex analysis for old mice duration of walking bouts, showing a higher time for wildtypes. No other tests maintained significance in both young and old mice.

4.7.3 Memory

Only older mouse cohorts were available for the memory tests, so age comparisons cannot be made.

Old female homozygotes reacted more strongly in the fear conditioning context trial than wildtype mice – freezing for a greater proportion of time. Given that old female homozygotes show a strong anxiety phenotype, that is consistent across multiple parameters, it's not possible to definitively say that the differences shown in the memory tests are not linked to their anxiety phenotype.

In combined-sex analysis, we find a possible memory phenotype. In the context trial, all significant tests were maintained from single-sex analysis - homozygous mice freeze for a greater proportion of time.

4.7.4 Sleep

Only older mouse cohorts were available for the sleep test, so age comparisons cannot be made. N-numbers for each sex were too low for informative analysis, so analysis is done with sex combined.

It can be seen that during the light phase (the 'sleep' phase for mice) homozygotes demonstrate a phenotype in their sleep fragmentation. While homozygote and wildtype mice sleep for the same length of time during this phase, they sleep in significantly fewer bouts, and these sleep bouts are significantly longer.

4.7.5 Social Dominance

Homozygotes from none of the cohort demographics showed social dominance over the wildtype counterparts, except for old male homozygotes who were significantly dominant. This could be a progressive phenotype in male homozygotes, as young male homozygotes who do not show this phenotype.

In combined-sex analysis, a clear social dominance phenotype emerges, with homozygous mice being dominant over wildtype.

4.7.6 Pain

Only older mouse cohorts were available for the Von Frey test, so age comparisons cannot be made.

Old female homozygotes do not show a pain phenotype, however old male mice show a significant decrease in pain tolerance in their right hind paw.

In combined-sex analysis, no pain phenotype was found as no single-sex significance was maintained.

4.7.7 Startle and Pre-Pulse Inhibition

Only older mouse cohorts were available for startle and pre-pulse inhibition, so age comparisons cannot be made.

C57BL/6 mice experience age-related hearing loss (Johnson, Tian et al. 2017), and since the startle test tests auditory processing, any mouse that exhibited a

base startle response of less than 500 mV was excluded from the pre-pulse inhibition analysis.

While female homozygotes showed no phenotype, male homozygotes showed a mild trend towards dysfunction of their pre-pulse inhibition. Since this could be seen in older mice, it is possible that a stronger trend could be seen in a younger cohort without hearing loss, or in a non-BL/6 line. Due to the relatively high p-value in this difference, it will not be discussed further.

4.7.8 Concluding Observations

Females show a heightened anxiety phenotype that appears to progress with age, showing over several parameters, over multiple arenas. Female homozygotes show a possible suppression in locomotion, however it can also be argued that other significant differences shown in parameters in other tests could also be due to heightened anxiety.

Males show an attenuated anxiety phenotype, which appears to normalise with age. They show a dysfunctional gait, with no apparent progression with age. Old males show lower pain threshold in the hind paws, and social dominance.

When combining sex for analysis, young homozygotes show a mild anxiety phenotype, old homozygotes show a motor deficit, and old homozygotes show a possible increase in pain-based memory (however since there is an anxiety phenotype it is not possible to separate the two), have a significant change in sleep fragmentation, and are socially dominant over wildtypes.

There is evidence to suggest that some phenotypes exhibited by homozygotes of both sexes change during ageing. However not all tests could be carried out with a young and old cohort, so age comparisons cannot be made for every behavioural test.

There is a clear sexual dimorphism in the behavioural phenotypes exhibited by homozygotes: male homozygotes show significant phenotypes and trends throughout the pipeline, while females exhibit a progressive anxiety phenotype that may have interfered with measurements in other tests.

Due to low n-numbers, it is also worth combined-sex analysis to increase the statistical power of the tests. In this thesis combined-sex analysis was carried out on tests that showed statistical significance in single-sex analysis, in order to analyse what significance was maintained when power was increased. Analysis showed an anxiogenic phenotype like young females, supressed locomotion like old females, sleep fragmentation differences, and social dominance like old males.

The molecular basis of the behavioural phenotype exhibited by homozygous mice was then investigated post-mortem, to determine if knockout of *Zhfx3* in dopaminergic neurons leads to changes in gene expression in the dopaminergic centres and dopamine circuit-target regions.

5

Results III: Molecular characterisation of brain regions affected by conditional knockout of *Zfhx3*

5

Results III: Molecular characterisation of brain regions affected by conditional knockout of *Zfhx3*

5.1 Introduction

DAT-*Cre; Zfhx3*-Flox homozygous knockout mice have *Zfhx3* knockout exclusively in dopaminergic neurons.

Zfhx3 is a transcription factor that has been reported to regulate the expression of genes in the brain, including neuropeptides responsible for intercellular signalling in the SCN (*Introduction 1.1.4.1.*). *Zfhx3* could therefore regulate gene expression in other areas of the adult mouse brain, that exhibit *Zfhx3* activity - such as dopaminergic centres (*Chapter 3*).

In Chapter 4, we see a significant behavioural phenotype in homozygous knockout mice compared to their wildtype counterparts. Investigating differential gene expression between homozygous knockout and wildtype mice could reveal the biological mechanism behind the behavioural changes, and link these changes to human disease pathology.

There is also measurable sexual dimorphism in the behavioural phenotype of the homozygous knockout mice. One possible cause of this dimorphism could be sex

differences in the differential gene expression between homozygous knockout mice and their wildtype counterparts.

5.2 Aims

The intention of this study is to characterise changes in gene expression in the brains of homozygous knockout DAT-*Cre*; *Zfhx3*-Flox mice, compared to their wildtype counterparts. The brain is sub-dissected to allow for specific analysis of different brain regions: the midbrain, the striatum, and the cortex. The midbrain is the location of the dopaminergic centres, the VTA and SNc. The striatum and the cortex are both target regions of dopaminergic projections from the midbrain (*Introduction 1.2.1.1.*).

5.3 Quantitative PCR of the striatum

A pilot test was carried out, investigating changes in gene expression between DAT-*Cre*; *Zfhx3*-Flox homozygote and wildtype mice using qPCR. qPCR analysis was carried out on the striatum, to give preliminary results on the possibility of changes in gene expression across dopaminergic pathways, which could then be investigated using RNA-Seq.

The striatum is a dopaminergic signalling target region - post-synaptic dopamine receptors were assessed for changes in expression (**Figure 5.3.1.**). Dopamine receptors D_1, D_2, and D_3 were investigated, with housekeeping gene RNA-binding protein 39 (Rbm39) as a control.

Before assessing expression changes, standard curves (**5.3.1.a**) were generated in order to accurately quantitate changes in expression of these genes. Both dopamine receptors D_1 and D_2 showed significantly reduced expression in homozygous knockout mice (**5.3.1.b, c**), while receptor D_3 did not show an expression change (**d**). These findings imply a disruption in dopamine signalling in the nigrostriatal pathway, and gives precedent to the behavioural changes seen in homozygous knockout mice (*Chapter 4*). This will be expanded upon further in the *Discussion* chapter.

To further elucidate possible changes in gene expression throughout the dopaminergic system, RNA-Seq was carried out on circuit terminus regions (striatum and cortex) and dopaminergic centres (midbrain).

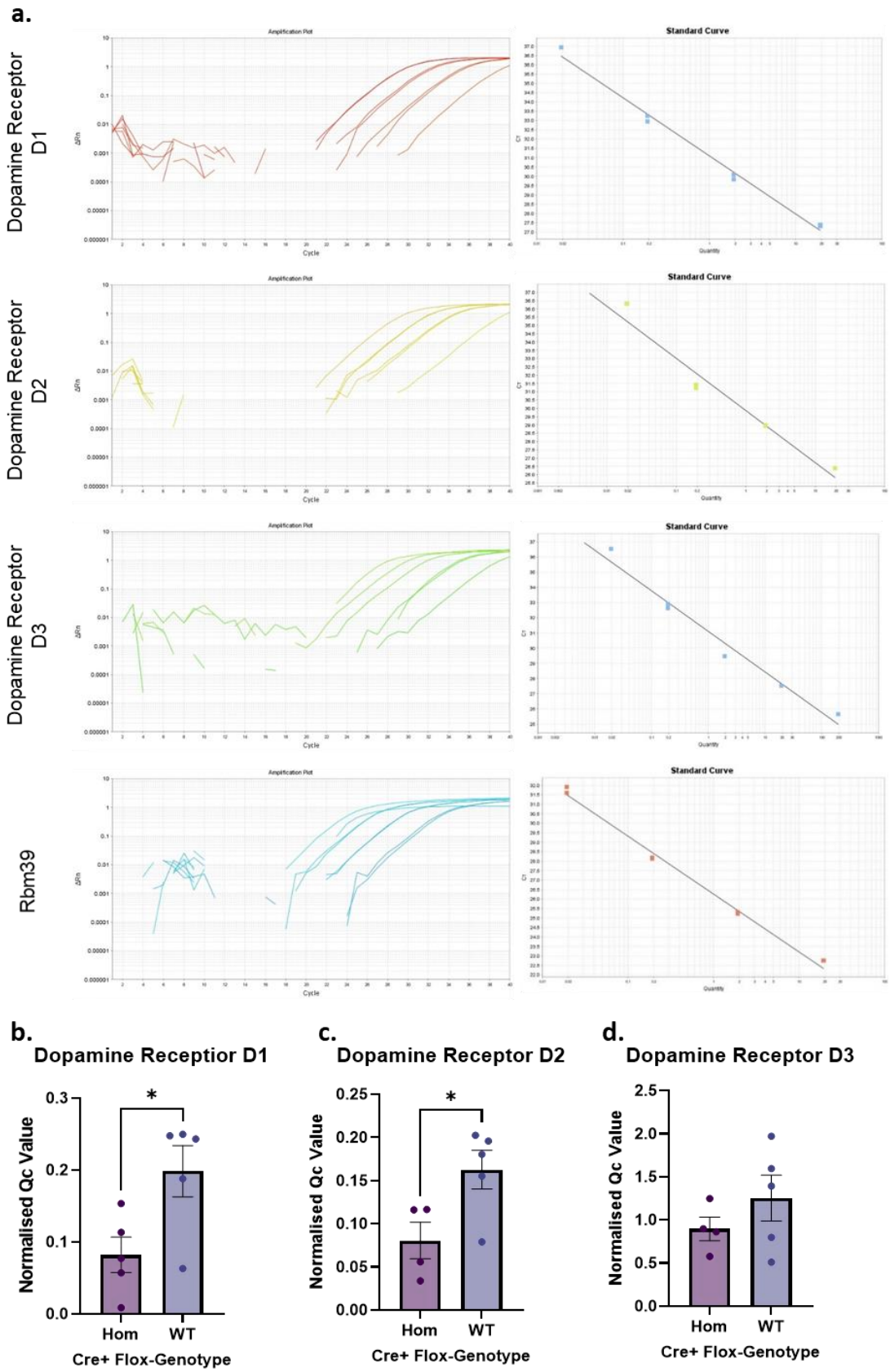

Figure 5.3.1. qPCR of striatum samples (a) amplification plots and standard curves of qPCR primer pairs; expression comparisons between genotypes in the striatum: (b) dopamine receptor D_1, (c) dopamine receptor D_2, (d) dopamine receptor D_3.

5.4 RNA sequencing

RNA was extracted from the midbrain, the striatum, and the cortex of both homozygous knockout mice and wildtype controls. Libraries were generated by The Oxford Genomics Centre using Poly(A) RNA-Seq (*Methods 2.5.3.*)

5.4.1 RNA extraction

Sample ID	Concentration (ng/ul)	Volume (ul)	Mass (ng)	260/280	260/230
36.2d Cortex	9.21	30	276.3	2.06	1.5
49.2c Cortex	3.71	30	111.3	2.1	1.69
47.3a Cortex	5.683333333	30	170.5	2.07	1.57
47.1d Cortex	4.676666667	30	140.3	2.15	1.49
46.3f Cortex	7.176666667	30	215.3	2.1	1.34
44.6c Cortex	3.563333333	30	106.9	2.15	1.47
45.1c Cortex	4.133333333	30	124	2.08	1.79
46.2c Cortex	6.086666667	30	182.6	2.12	1.53
36.2d Midbrain	3.64	30	109.2	2.03	0.72
50.1a Midbrain	3.748	30	112.44	2.03	0.44
47.3a Midbrain	5.194666667	30	155.84	2.06	1.26
47.1a Midbrain	6.83	30	204.9	2.13	0.63
46.3f Midbrain	3.98	30	119.4	2.07	0.82
44.6c Midbrain	4.575333333	30	137.26	2.06	0.74
45.1c Midbrain	4.048666667	30	121.46	2.06	0.79
46.2c Midbrain	3.982	30	119.46	2.06	0.9
36.2d Striatum	3.475	30	104.25	2.25	0.46
49.2c Striatum	4.11	30	123.3	2.07	0.77
47.1d Striatum	4.575	30	137.25	2.16	1.02
47.1a Striatum	4.4	30	132	2.3	0.56
46.3f Striatum	3.684	30	110.52	1.97	0.34
44.6c Striatum	4.168	30	125.04	2.07	0.91
48.2b Striatum	4.230333333	30	126.91	1.96	1.03
46.2c Striatum	4.453333333	30	133.6	1.97	0.34

Table 5.4.1.1. NanoDrop analysis of RNA extractions for RNA-Seq

RNA was extracted from the cortex, midbrain, and striatum. Samples underwent initial quality control using the NanoDrop (**Table 5.4.1.1.**)

5.4.2 Quality control

Once RNA-Seq reads were created, they were entered onto Galaxy Europe web platform for further analysis, which is detailed here. Initial steps were to carry out quality control of the reads:

1. FastQC (**Figure 5.4.2.1.a, b**) is used to quality control check high-throughput sequence data (Andrews 2010). Sequence length distribution (**a**) measures the length of reads generated by sequencing, and flags any outlying short reads or reads of zero base pairs. Mean quality scores (**b**) show the quality score (y-axis) of each nucleotide position across every read (x-axis).
2. RNA STAR or RNA Spliced Transcripts Alignment to a Reference (**Figure 5.4.2.1.c**) was first carried out to align the RNA read pairs to the reference genome, which in this case is *Mus musculus* (Dobin, Davis et al. 2013). Alignment scores are quantitative measurements of read alignment fidelity to the reference genome, with penalties given for mismatches and gaps.

Sequence reads were determined to be of high enough quality to progress onto differential expression comparison.

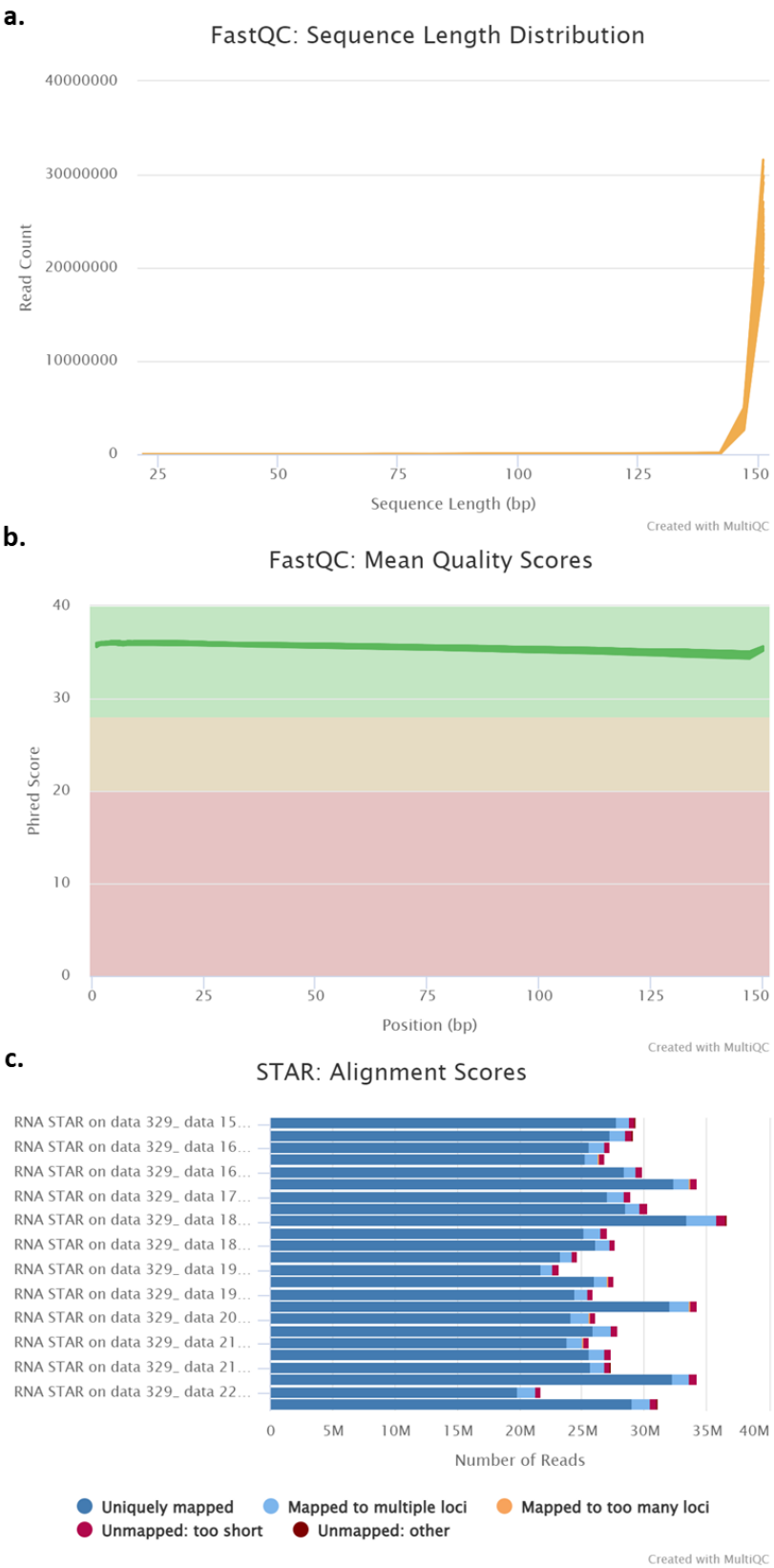

Figure 5.4.2.1. Quality control of RNA-Seq reads (a) RNA STAR alignment scores; (b) FastQC sequence length distribution; (c) FastQC mean quality scores. Image generated using Galaxy (data from (Afgan, Baker et al. 2018, Kanehisa 2019)).

5.5 RNA-Seq comparisons

5.5.1 Differential expression counts

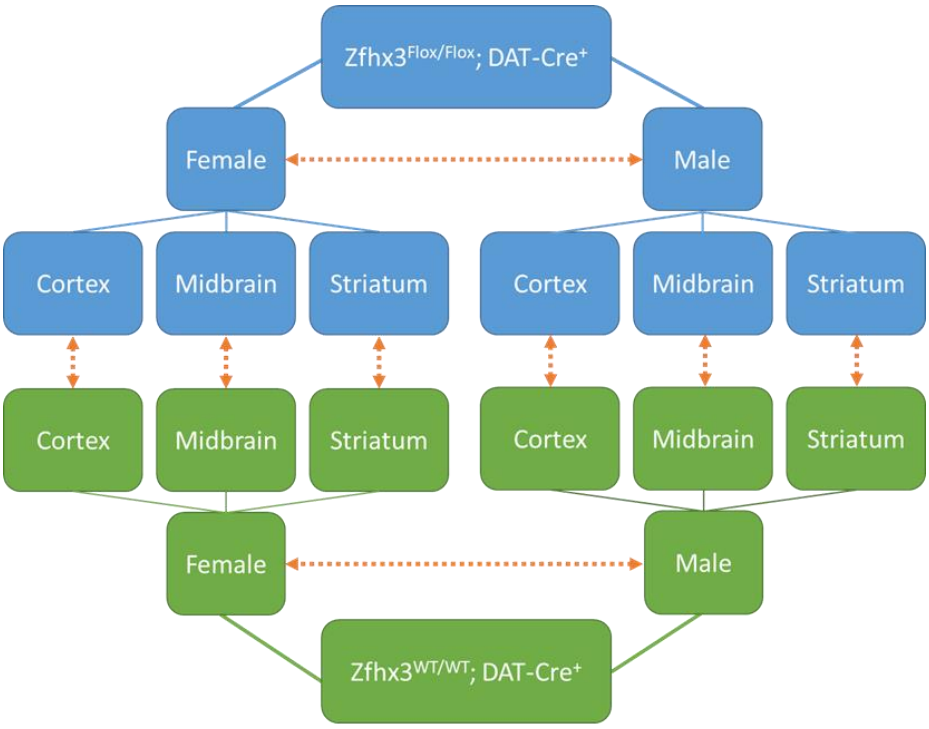

	Up	Flat	Down
CortexWTM-CortexWTF	4	15105	0
CortexMUTM-CortexMUTF	3	15105	1
CortexMUTM-CortexWTM	0	15109	0
CortexMUTF-CortexWTF	0	15109	0

	Up	Flat	Down
MidbrainWTM-MidbrainWTF	2	15339	1
MidbrainMUTM-MidbrainMUTF	61	15275	6
MidbrainMUTM-MidbrainWTM	0	15342	0
MidbrainMUTF-MidbrainWTF	651	13973	718

	Up	Flat	Down
StriatumWTM-StriatumWTF	4	15447	0
StriatumMUTM-StriatumMUTF	4	15447	0
StriatumMUTM-StriatumWTM	0	15451	0
StriatumMUTF-StriatumWTF	0	15451	0

Figure 5.5.1.1. Comparisons between genotype and sex a schematic showing RNA-Seq comparisons. Comparisons shown in yellow give the most differential genes. Differential genes are determined as having p≤0.1. Table generated using Galaxy (data from (Afgan, Baker et al. 2018, Kanehisa 2019)).

In this section, ‘mutant’ or ‘MUT’ refers to homozygous knockout DAT-*Cre*; *Zfhx3*-Flox mice.

Following quality control steps, differential expression comparison was carried out on sequence reads (**Figure 5.5.1.1.).** Dopaminergic regions were compared between mutant and wildtype samples of both females and males, and between females and males of the same genotype. In comparison tables, ‘up’ and ‘down’ signify the number of genes that are significantly (p≤1) either up or down regulated from the first sample compared to the sequential sample in each row. ‘Flat’ signifies the number of genes that do not significantly change expression levels.

Two comparisons showed a notable differential expression count: midbrain mutant males compared to females (MidbrainMUTM-MidbrainMUTF); and midbrain mutant females compared to wildtype females (MidbrainMUTF-MidbrainWTF).

5.5.2 Midbrain – Mutant Male vs. Mutant Female

Differential expression of genes in the midbrain between sexes in mutant mice is higher than in wildtype mice (**Figure 5.5.2.1. a, b**). Y-linked genes are upregulated in males of both mutant and wildtype genotype, and X-linked gene ‘Xist’ is downregulated in both.

Looking at the top three downregulated (**c, d, e**) and upregulated (**f, g, h**) genes from the MidbrainMUTM-MidbrainMUTF comparison, and generating strip charts including wildtype expression from both sexes, it is revealed that mutant female mice represent a distinct expression profile compared to both mutant males and wildtype mice of both sexes.

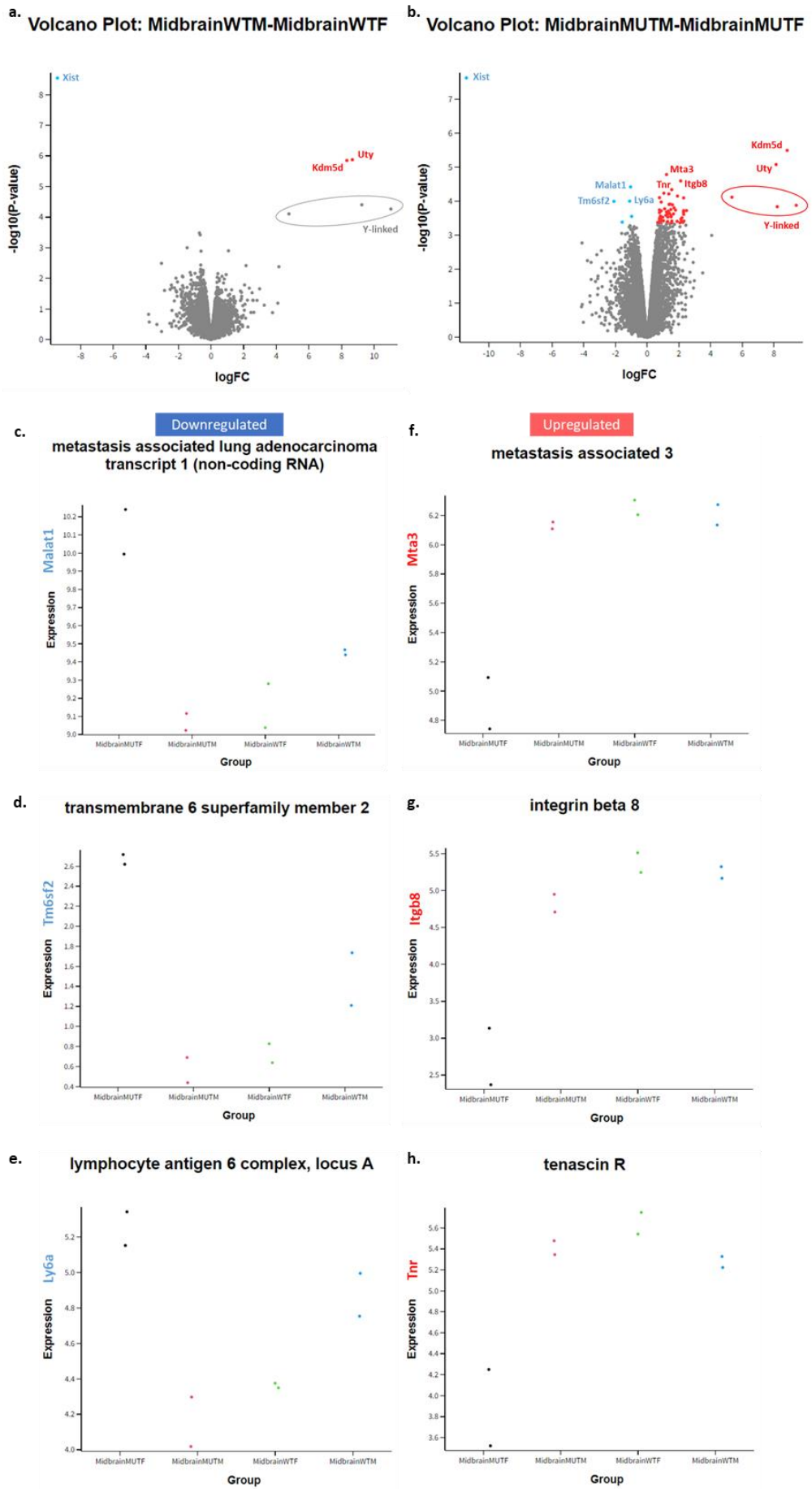
a.
Volcano Plot: MidbrainWTM-MidbrainWTF
Xist
Uty
Kdm5d
Y-linked
-log10(P-value)
logFC
b.
Volcano Plot: MidbrainMUTM-MidbrainMUTF
Xist
Kdm5d
Uty
Mta3
Malat1
Tnr
Itgb8
Tm6sf2
Ly6a
Y-linked
-log10(P-value)
logFC
Downregulated
Upregulated
c.
metastasis associated lung adenocarcinoma transcript 1 (non-coding RNA)
Malat1
Expression
MidbrainMUTF
MidbrainMUTM
MidbrainWTF
MidbrainWTM
Group
f.
metastasis associated 3
Mta3
Expression
Group
d.
transmembrane 6 superfamily member 2
Tm6sf2
Expression
Group
g.
integrin beta 8
Itgb8
Expression
Group
e.
lymphocyte antigen 6 complex, locus A
Ly6a
Expression
Group
h.
tenascin R
Tnr
Expression
Group

Figure 5.5.2.1. Volcano plots and strip charts of differential counts between male and female midbrain (a) wildtype comparison volcano plot; (b) homozygous comparison volcano plot; strip charts showing, in homozygous males compared to homozygous females: (c,d,e) top 3 downregulated genes; (f,g,h) top 3 upregulated genes. Image generated using Galaxy (data from (Afgan, Baker et al. 2018, Kanehisa 2019)).

5.5.3 Midbrain – Mutant Female vs. Wildtype Female

To investigate how the conditional mutation affects mutant female midbrain function, significant differentially expressed genes were analysed using the STRING database and SynGO (*Methods 2.5.3.3.*).

5.5.3.1 Mutant Female – upregulated genes

	KEGG Pathway	Observed gene count	Strength	False discovery rate
Upregulated	Ribosome	85	1.37	8.02E-74
	Oxidative phosphorylation	54	1.17	6.21E-38
	Parkinson disease	**60**	**0.95**	**3.41E-32**
	Huntington disease	**64**	**0.88**	**2.78E-31**
	Thermogenesis	57	0.95	6.45E-31
	Prion disease	**58**	**0.89**	**1E-28**
	Amyotrophic lateral sclerosis	**62**	**0.78**	**1.75E-25**
	Non-alcoholic fatty liver disease	41	0.99	1.84E-23
	Alzheimer disease	**57**	**0.75**	**3.98E-22**
	Spliceosome	30	0.91	3.26E-15
	Retrograde endocannabinoid signaling	28	0.84	9.75E-13
	Metabolic pathways	84	0.28	0.00000044
	Proteasome	11	0.93	0.00000968
	Protein export	8	1.07	0.0000448
	Cardiac muscle contraction	12	0.7	0.00029
	RNA polymerase	7	0.94	0.00084
	Protein processing in endoplasmic reticulum	13	0.44	0.0315

Figure 5.5.3.1.1. KEGG pathways of upregulated genes in the homozygous female midbrain, compared to wildtype brain-specific KEGG pathways highlighted for further analysis. Table generated using https://string-db.org/ (data from (Kanehisa and Goto 2000, Kanehisa 2019, Kanehisa, Furumichi et al. 2023)).

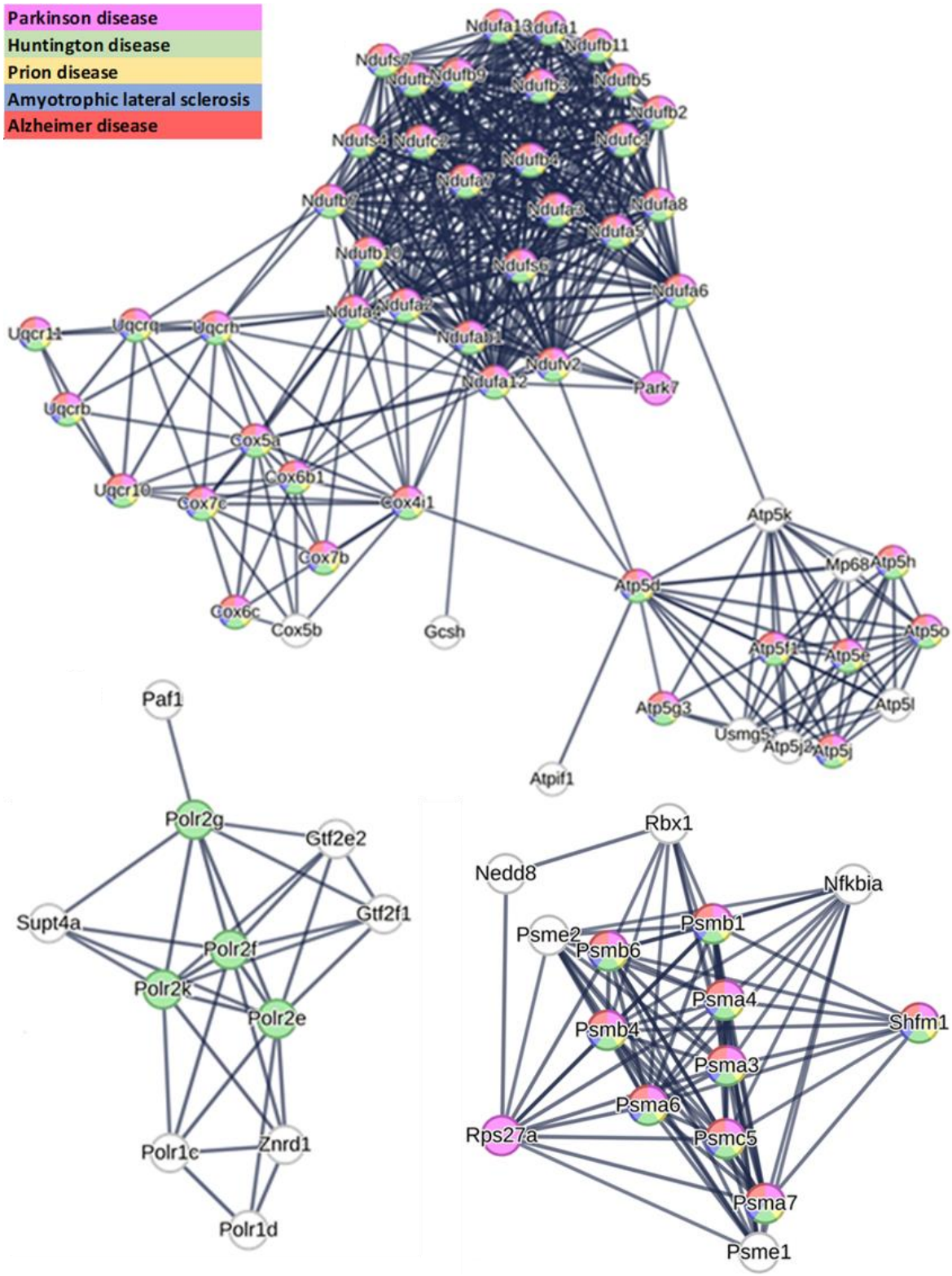

Figure 5.5.3.1.2. Protein-protein interaction networks from upregulated genes isolating networks involved in brain-specific KEGG pathways. Image generated using https://string-db.org/ (data from (Kanehisa and Goto 2000, Kanehisa 2019, Kanehisa, Furumichi et al. 2023))

Parkinsons	Huntingtons	ALS	Alzheimers	Prion Disease
Ndufa1	Ndufa1	Ndufa1	Ndufa1	Ndufa1
Ndufa2	Ndufa2	Ndufa2	Ndufa2	Ndufa2
Ndufa6	Ndufa6	Ndufa6	Ndufa6	Ndufa6
Ndufs6	Ndufs6	Ndufs6	Ndufs6	Ndufs6
Uqcrh	Uqcrh	Uqcrh	Uqcrh	Uqcrh
-	Polr2k	-	-	-

Table 5.5.3.1.1. Upregulated genes from brain-specific KEGG pathways genes upregulated in homozygous females, taken from the top 50-scoring differential genes (data from (Kanehisa and Goto 2000, Kanehisa 2019, Kanehisa, Furumichi et al. 2023).

Post-differential analysis of genes that are upregulated in the mutant female midbrain compared to the wildtype, implicates multiple brain-specific KEGG pathways ((Kyoto Encyclopaedia of Genes and Genomes)(Kanehisa and Goto 2000, Kanehisa 2019, Kanehisa, Furumichi et al. 2023): Parkinson's disease, Huntington's disease, prion diseases, Amyotrophic lateral sclerosis (ALS), and Alzheimer's disease (**Figure 5.5.3.1.1.**). Multiple protein-protein interaction networks generated from the differential gene list show networks of upregulated genes involved in these KEGG pathways (**Figure 5.5.3.1.2.**).

Specific genes of interest were isolated via cross-referencing the top 50 differentially upregulated genes (sorted by lowest p-value and highest expression change score), and genes involved in these brain-specific KEGG pathways (**Table 5.5.3.1.1.**)

NDUFA1, *2*, *6*, and *NDUFS6* are genes encoding proteins: NADH dehydrogenase [ubiquinone] 1 alpha subcomplex subunit 1; 2; 6; and NADH dehydrogenase [ubiquinone] iron-sulphur protein 6, mitochondrial. All of these genes are subunits of NADH:ubiquinone oxidoreductase, also known as complex I of the electron transport chain.

UQCRH gene encodes protein Cytochrome b-c1 complex subunit 6, mitochondrial. This is a subunit of protein Coenzyme Q – cytochrome c reductase, also known as complex III of the electron transport chain

POLR2K gene encodes the protein DNA-directed RNA polymerases I, II, and III subunit RPABC4. That is, *POLR2K* encodes for the RPABC4 subunit which is utilised by multiple protein complexes (RNA polymerases).

These genes are upregulated in mutant female midbrain samples when compared to wildtype female midbrain samples, but also when compared to both mutant and wildtype male midbrain (**Figure 5.5.3.1.3.**).

a.

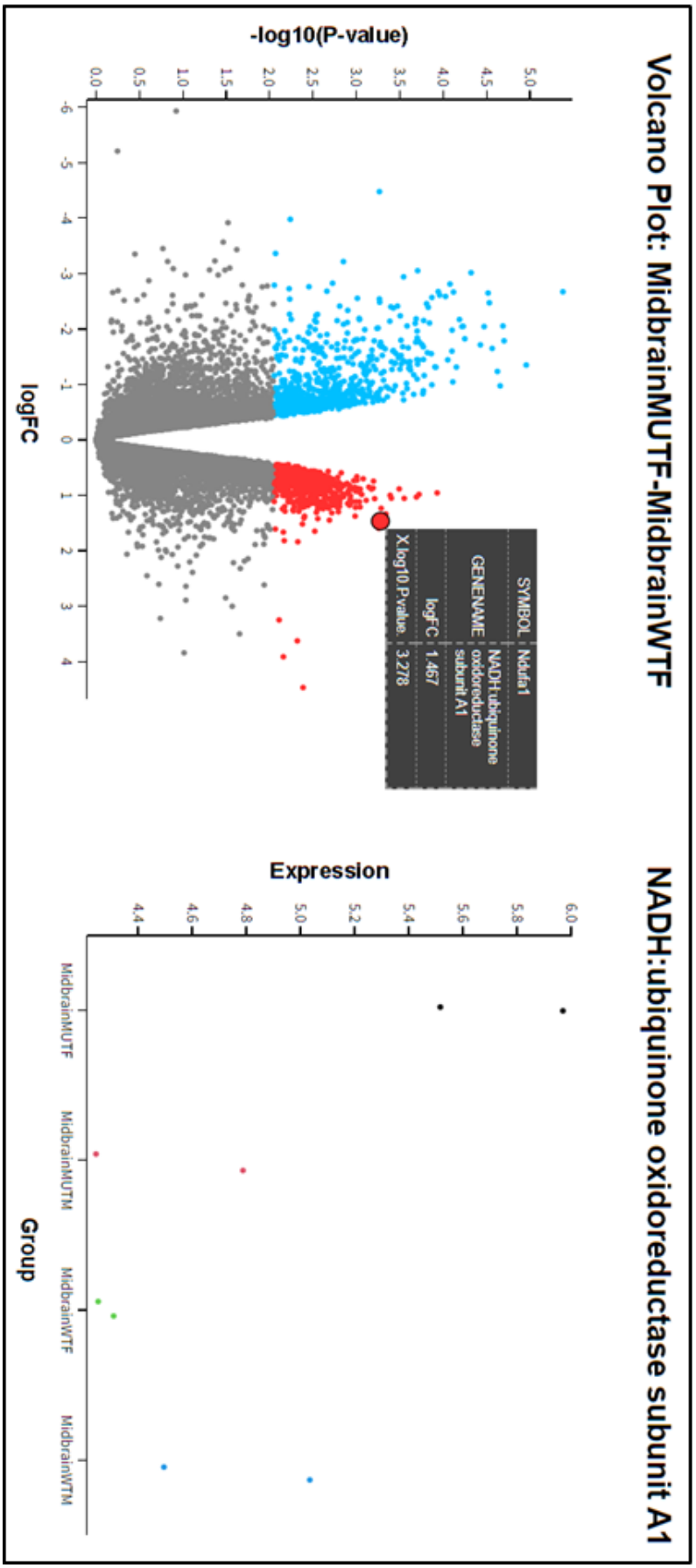
Volcano Plot: MidbrainMUTF-MidbrainWTF
-log10(P-value)
logFC
SYMBOL Ndufa1
GENENAME NADH:ubiquinone oxidoreductase subunit A1
logFC 1.467
X.log10.P.value. 3.278
NADH:ubiquinone oxidoreductase subunit A1
Expression
Group
MidbrainMUTF
MidbrainMUTM
MidbrainWTF
MidbrainWTM

b.

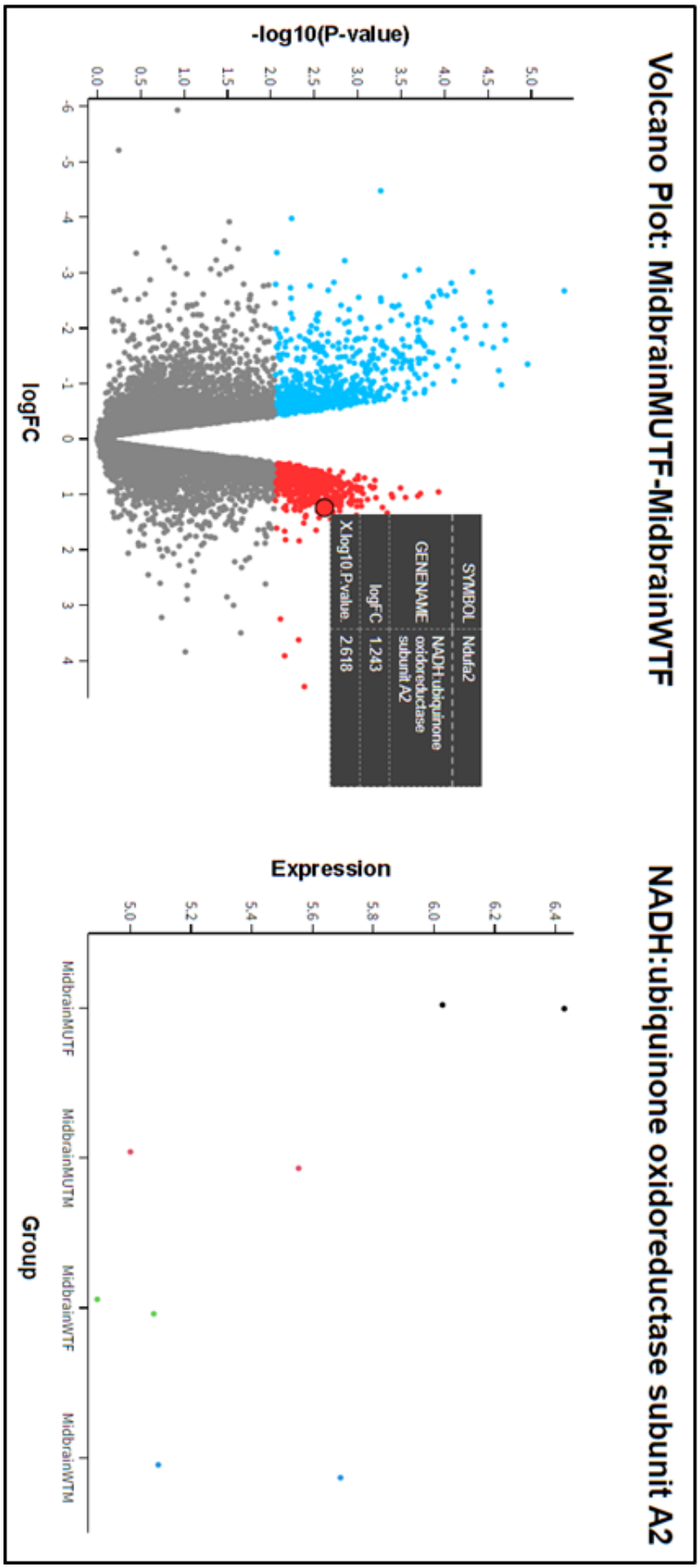
Volcano Plot: MidbrainMUTF-MidbrainWTF
-log10(P-value)
logFC
SYMBOL Ndufa2
GENENAME NADH:ubiquinone oxidoreductase subunit A2
logFC 1.243
X.log10.P.value. 2.618
NADH:ubiquinone oxidoreductase subunit A2
Expression
Group
MidbrainMUTF
MidbrainMUTM
MidbrainWTF
MidbrainWTM

C.

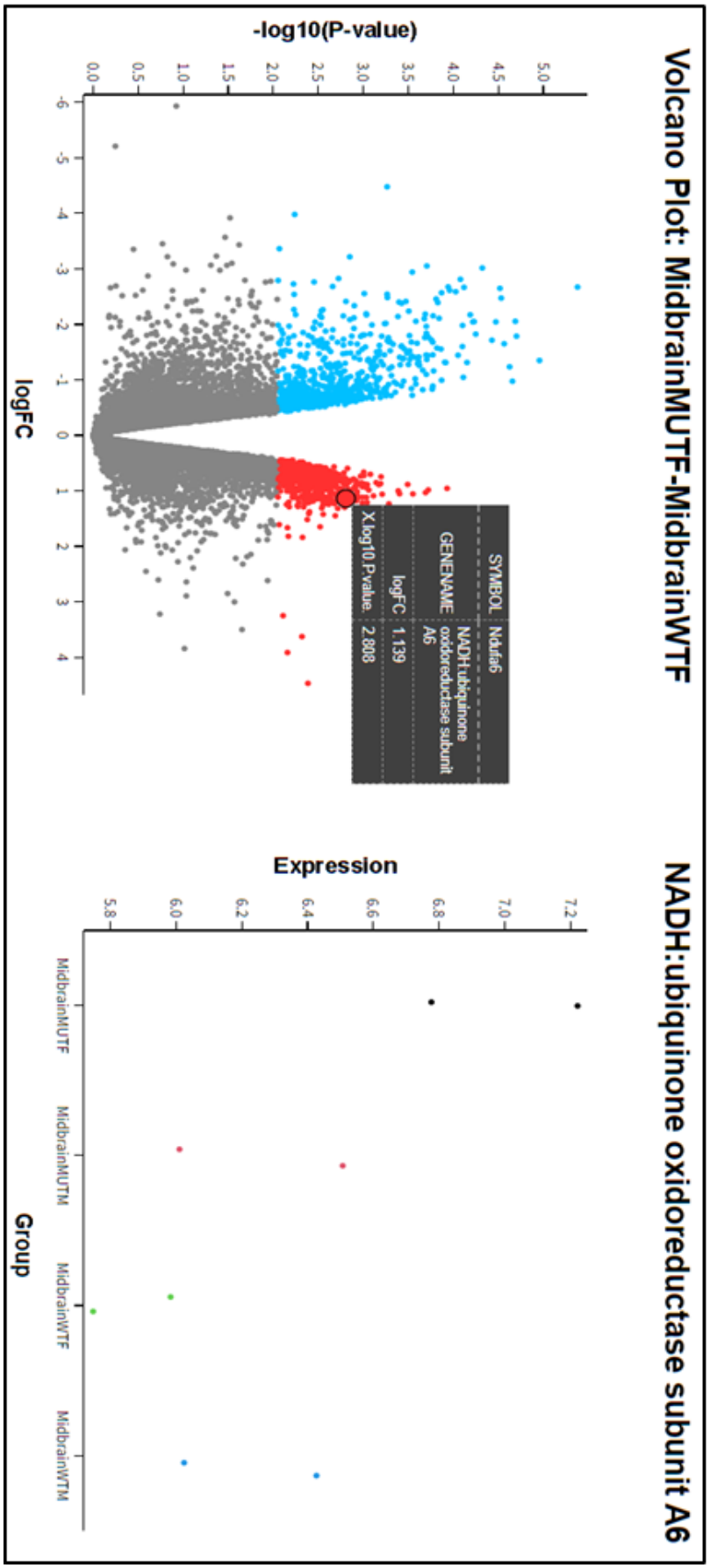
Volcano Plot: MidbrainMUTF-MidbrainWTF
-log10(P-value)
logFC
SYMBOL Ndufa6
GENENAME NADH:ubiquinone oxidoreductase subunit A6
logFC 1.139
X.log10.P.value. 2.803
NADH:ubiquinone oxidoreductase subunit A6
Expression
Group
MidbrainMUTF
MidbrainMUTM
MidbrainWTF
MidbrainWTM

d.

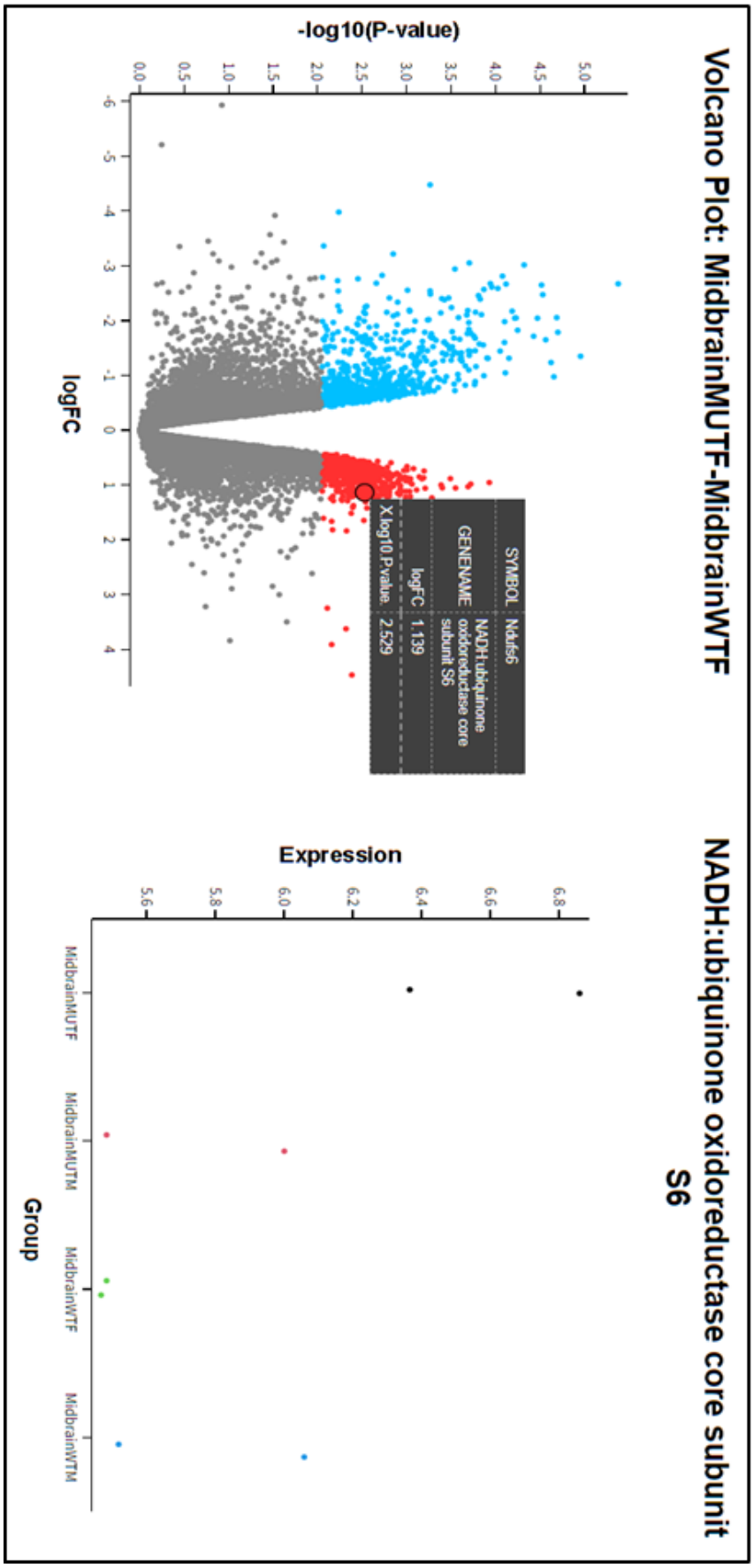
Volcano Plot: MidbrainMUTF-MidbrainWTF
-log10(P-value)
logFC
SYMBOL Ndufs6
GENENAME NADH:ubiquinone oxidoreductase core subunit S6
logFC 1.139
X.log10.Pvalue. 2.529
NADH:ubiquinone oxidoreductase core subunit S6
Expression
Group
MidbrainMUTF
MidbrainMUTM
MidbrainWTF
MidbrainWTM

e.

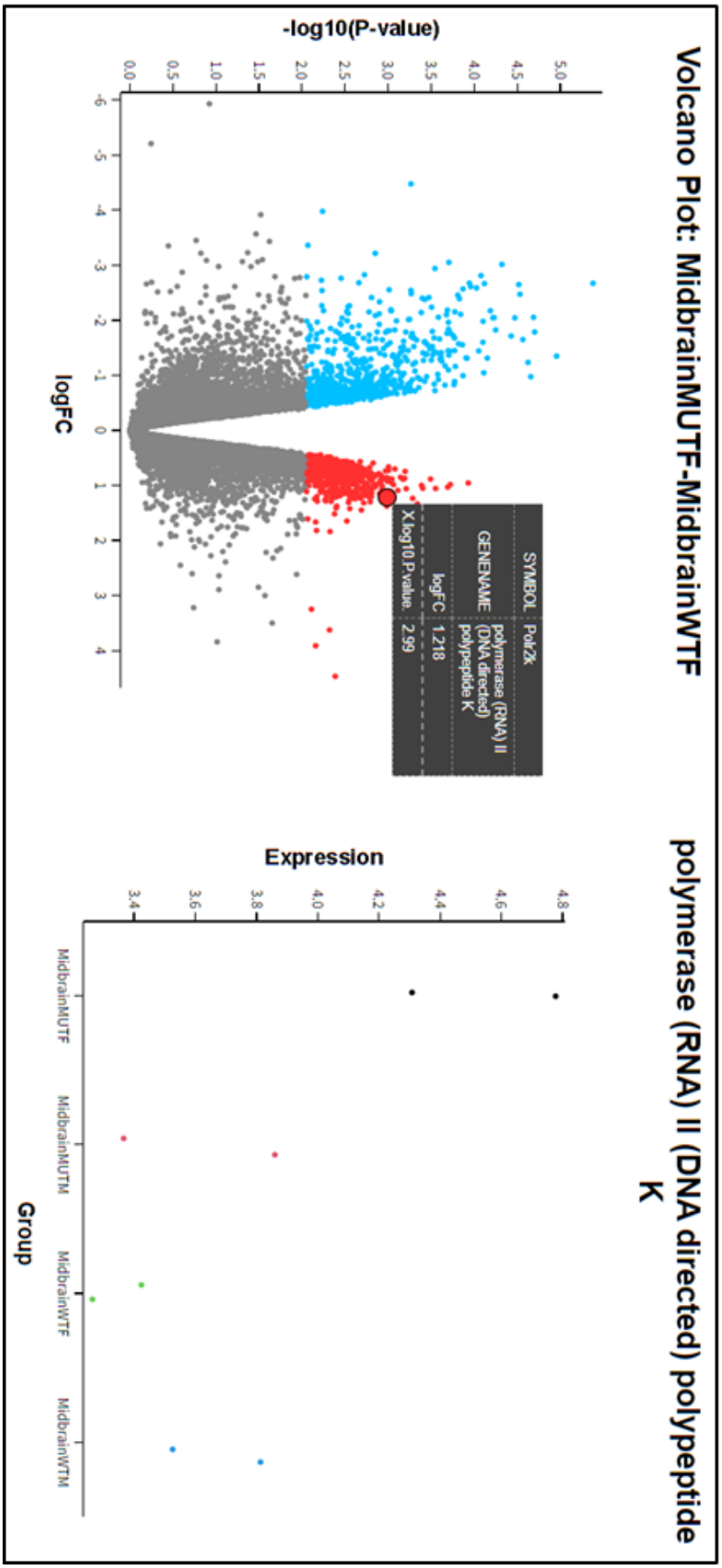
Volcano Plot: MidbrainMUTF-MidbrainWTF
-log10(P-value)
logFC
SYMBOL Polr2k
GENENAME polymerase (RNA) II (DNA directed) polypeptide K
logFC 1.218
X.log10.Pvalue. 2.99
polymerase (RNA) II (DNA directed) polypeptide K
Expression
Group
MidbrainMUTF
MidbrainMUTM
MidbrainWTF
MidbrainWTM

f.

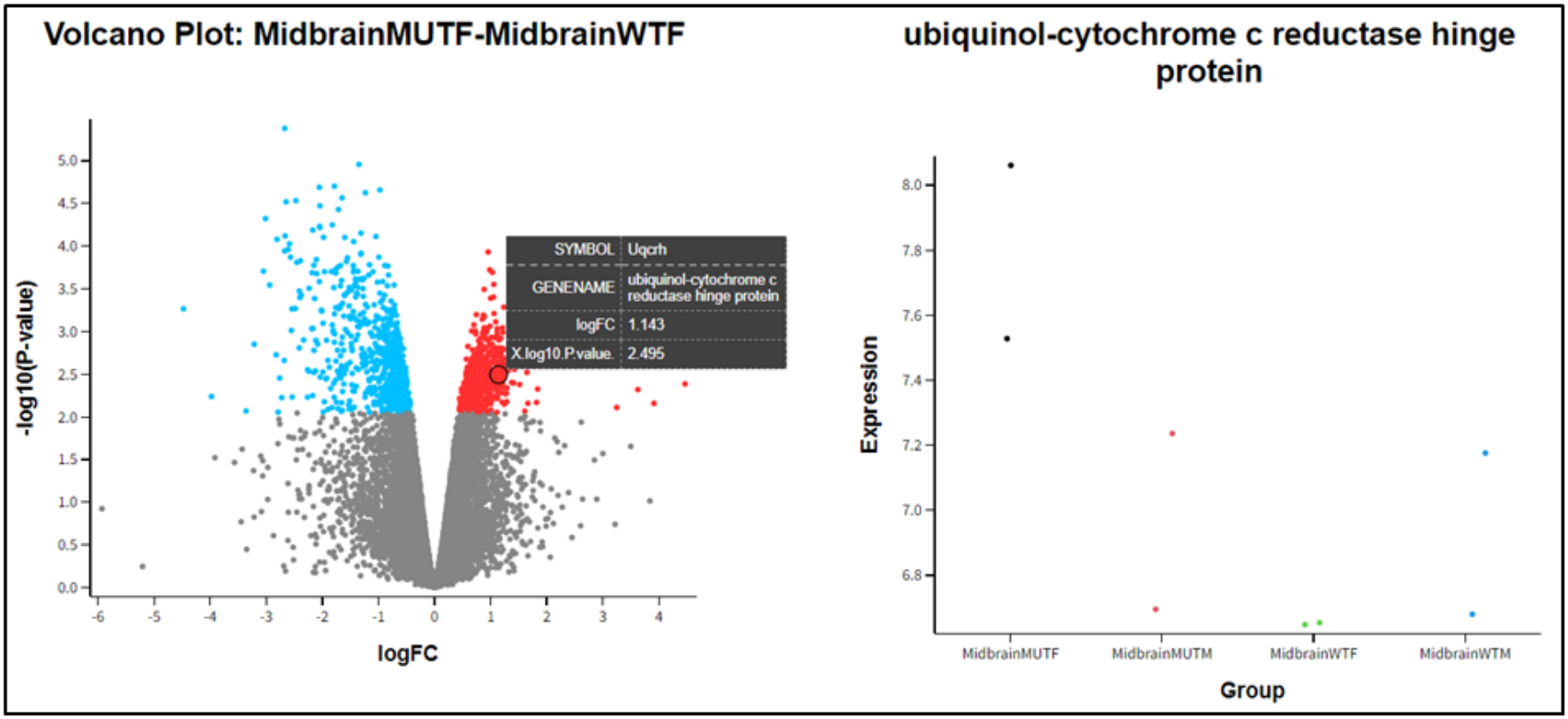
Volcano Plot: MidbrainMUTF-MidbrainWTF
-log10(P-value)
logFC
SYMBOL Uqcrh
GENENAME ubiquinol-cytochrome c reductase hinge protein
logFC 1.143
X.log10.P.value. 2.495
ubiquinol-cytochrome c reductase hinge protein
Expression
MidbrainMUTF
MidbrainMUTM
MidbrainWTF
MidbrainWTM
Group

Figure 5.5.3.1.3. Upregulated genes from brain-specific KEGG pathways – Volcano Plots and strip charts genes upregulated in homozygous females, taken from the top 50-scoring differential genes. Images generated using Galaxy (data from (Afgan, Baker et al. 2018, Kanehisa 2019)).

Biological Process	Strength	False Discovery Rate
Mitochondrial atp synthesis coupled proton transport	1.34	1.41E-07
Protein insertion into mitochondrial inner membrane	1.34	0.0018
ATP synthesis coupled proton transport	1.27	8.41E-08
Mitochondrial respiratory chain complex i assembly	1.26	9.53E-18
Ribosomal small subunit assembly	1.2	7.88E-06
Mitochondrial electron transport, nadh to ubiquinone	1.16	0.00033
Protein insertion into mitochondrial membrane	1.16	0.00033
Ribosomal large subunit assembly	1.12	6.38E-06
Mitochondrial respiratory chain complex assembly	1.1	1.11E-18
Mitochondrial atp synthesis coupled electron transport	1.09	7.43E-11
Ribosomal small subunit biogenesis	1.06	8.50E-13
Inner mitochondrial membrane organization	1.05	7.37E-05
Ribosome assembly	1.04	9.99E-11

Table 5.5.3.1.2. Upregulated genes involved in biological processes (Gene Ontology) biological processes with a strength ≥1 selected (data from (Kanehisa and Goto 2000, Kanehisa 2019, Kanehisa, Furumichi et al. 2023))

Gene Ontology enrichment analysis was carried out on the biological function of upregulated genes (**Table 5.5.3.1.2.**). Out of 13 processes, 9 are related to the mitochondria or ATP synthesis, and 4 are centred on the ribosome.

Searching the Synaptic Gene Ontology (SynGO) database using the upregulated differential gene list (**Figure 5.5.3.1.4.**), significant enrichment is found in genes associated in translation both pre- and post-synaptically.

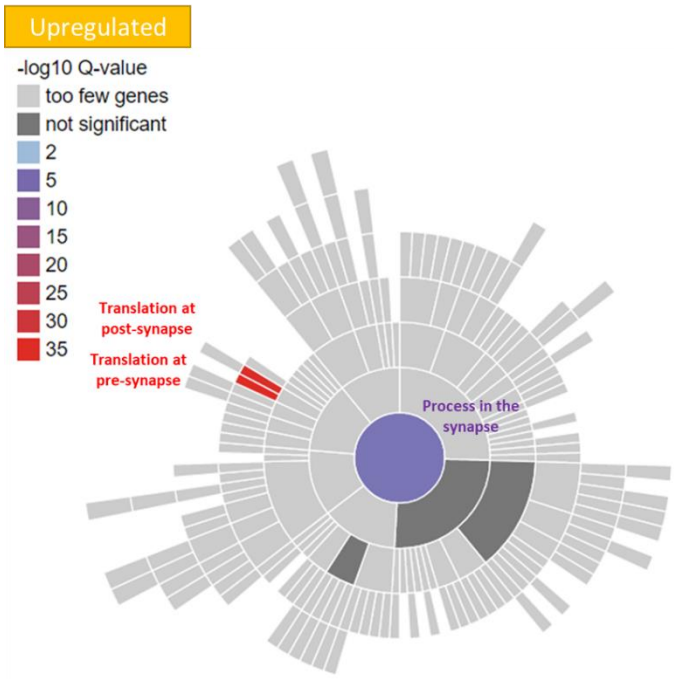

Figure 5.5.3.1.4. Sunburst figure of upregulated gene synapse function (SynGO) upregulated gene function across the synapse, Q-value showing gene enrichment. Image generated using https://www.syngoportal.org/ (data from (Koopmans, van Nierop et al. 2019).

5.5.3.2 Mutant Female – downregulated genes

Similarly to upregulated genes, post-differential analysis of genes that are downregulated in the mutant female midbrain compared to the wildtype reveals multiple brain-specific KEGG pathways: cholinergic synapse, spinocerebellar ataxia, dopaminergic synapse, and circadian entrainment. In addition, genes in the estrogen signalling pathway are downregulated in the mutant females compared to the wildtypes (**Figure 5.5.3.2.1.**). Multiple protein-protein interaction networks generated from the differential gene list show networks of downregulated genes involved in these KEGG pathways (**Figure 5.5.3.2.2.**).

Specific genes of interest were isolated via cross-referencing the top 50 differentially downregulated genes (sorted by lowest p-value and highest expression fold-change score), and genes involved in these brain-specific KEGG pathways (**Table 5.5.3.2.1.)**

Downregulated

KEGG Pathway	Observed gene count	Strength	False discovery rate
Phospholipase D signaling pathway	19	0.62	0.00025
Regulation of actin cytoskeleton	23	0.54	0.00025
cAMP signaling pathway	22	0.52	0.00029
cGMP-PKG signaling pathway	18	0.54	0.0011
Longevity regulating pathway	13	0.67	0.0011
Endocytosis	22	0.45	0.0016
Adrenergic signaling in cardiomyocytes	16	0.55	0.0016
Calcium signaling pathway	18	0.47	0.0035
Choline metabolism in cancer	12	0.6	0.0044
Gap junction	11	0.62	0.0048
Insulin signaling pathway	14	0.53	0.0049
Longevity regulating pathway - multiple species	9	0.67	0.0072
MicroRNAs in cancer	15	0.48	0.0072
EGFR tyrosine kinase inhibitor resistance	10	0.61	0.008
Salivary secretion	10	0.61	0.0082
Vascular smooth muscle contraction	13	0.5	0.0086
Estrogen signaling pathway	**13**	**0.5**	**0.0086**
Aldosterone synthesis and secretion	11	0.56	0.0086
Growth hormone synthesis, secretion and action	12	0.53	0.0086
Rap1 signaling pathway	17	0.42	0.0091
Axon guidance	15	0.43	0.0122
Endocrine and other factor-regulated calcium reabsorption	8	0.64	0.0128
Endocrine resistance	10	0.54	0.0145
Pathways in cancer	31	0.27	0.0145
Ras signaling pathway	17	0.38	0.0155
Phosphatidylinositol signaling system	10	0.54	0.0155
Cholinergic synapse	**11**	**0.5**	**0.0155**
ErbB signaling pathway	9	0.55	0.0191
Apelin signaling pathway	12	0.46	0.0191
Neurotrophin signaling pathway	11	0.48	0.0191
Focal adhesion	15	0.39	0.0223
Thyroid hormone signaling pathway	11	0.47	0.0223
Spinocerebellar ataxia	**12**	**0.44**	**0.0241**
Glioma	8	0.56	0.0246
AMPK signaling pathway	11	0.46	0.0251
Dopaminergic synapse	**11**	**0.44**	**0.0298**
Pancreatic secretion	10	0.47	0.0298
Circadian entrainment	**9**	**0.49**	**0.0341**

Figure 5.5.3.2.1. KEGG pathways of downregulated genes in the homozygous female midbrain, compared to wildtype brain-specific KEGG pathways highlighted for further analysis. Image generated using https://string-db.org/ (data from (Kanehisa and Goto 2000, Kanehisa 2019, Kanehisa, Furumichi et al. 2023)).

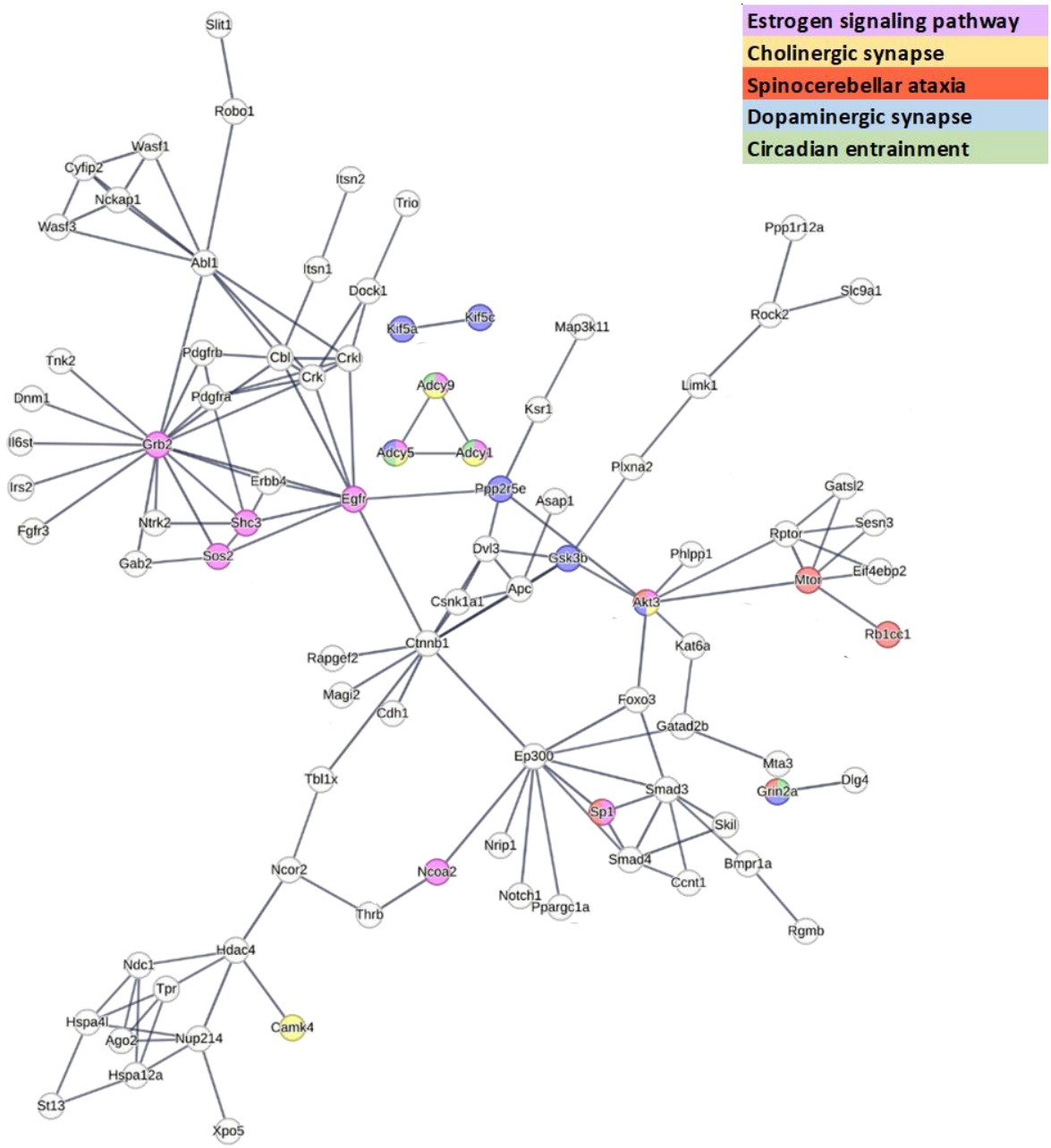

Figure 5.5.3.2.2. Protein-protein interaction networks from downregulated genes with genes involved in KEGG pathways of interest labelled. Image generated using https://string-db.org/ (data from (Kanehisa and Goto 2000, Kanehisa 2019, Kanehisa, Furumichi et al. 2023))

Estrogen signaling pathway	Cholinergic synapse	Spinocerebellar ataxia	Dopaminergic synapse	Circadian entrainment
-	-	Grin2a	Grin2a	Grin2a
-	Kcnq3	-	-	-
Gabbr2	-	-	-	-

Table 5.5.3.2.1. Downregulated genes from brain-specific KEGG pathways genes downregulated in homozygous females, taken from the top 50-scoring differential genes (data from (Kanehisa and Goto 2000, Kanehisa 2019, Kanehisa, Furumichi et al. 2023))

GRIN2A gene encodes protein Glutamate Ionotropic Receptor NMDA Type Subunit 2A, which is an N-methyl-D-aspartate (NMDA) receptor subunit.

KCNQ3 gene encodes protein Potassium Voltage-Gated Channel Subfamily Q Member 3, which forms an M-channel when associated with other members of the *KCNQ* gene family.

GABBR2 gene encodes Gamma-Aminobutyric Acid (GABA) Type B Receptor Subunit 2, which is a multi-pass membrane protein which when associated with subunit 1 forms a G protein-coupled receptor.

These genes are downregulated in mutant female midbrain samples when compared to wildtype female midbrain samples, but also when compared to both mutant and wildtype male midbrain (**Figure 5.5.3.2.3.**).

Gene Ontology enrichment analysis on the biological function of downregulated genes (**Table 5.5.3.2.2.**) revealed 8 processes - 2 are involved in receptor signalling pathways, 2 in synaptic vesicle function, 3 to neuronal development (including neuron neo/morphogenesis), and 1 is linked directly to locomotor behaviour.

Searching the SynGO database using the downregulated differential gene list (**Figure 5.5.3.2.4.**), the function of downregulated genes have a far broader scope across the synapse than upregulated genes. Significant enrichment is found in genes involved in: organisation of synaptic constituents, chemical trans-synaptic signalling, and the pre-synapse vesicle cycle.

a.

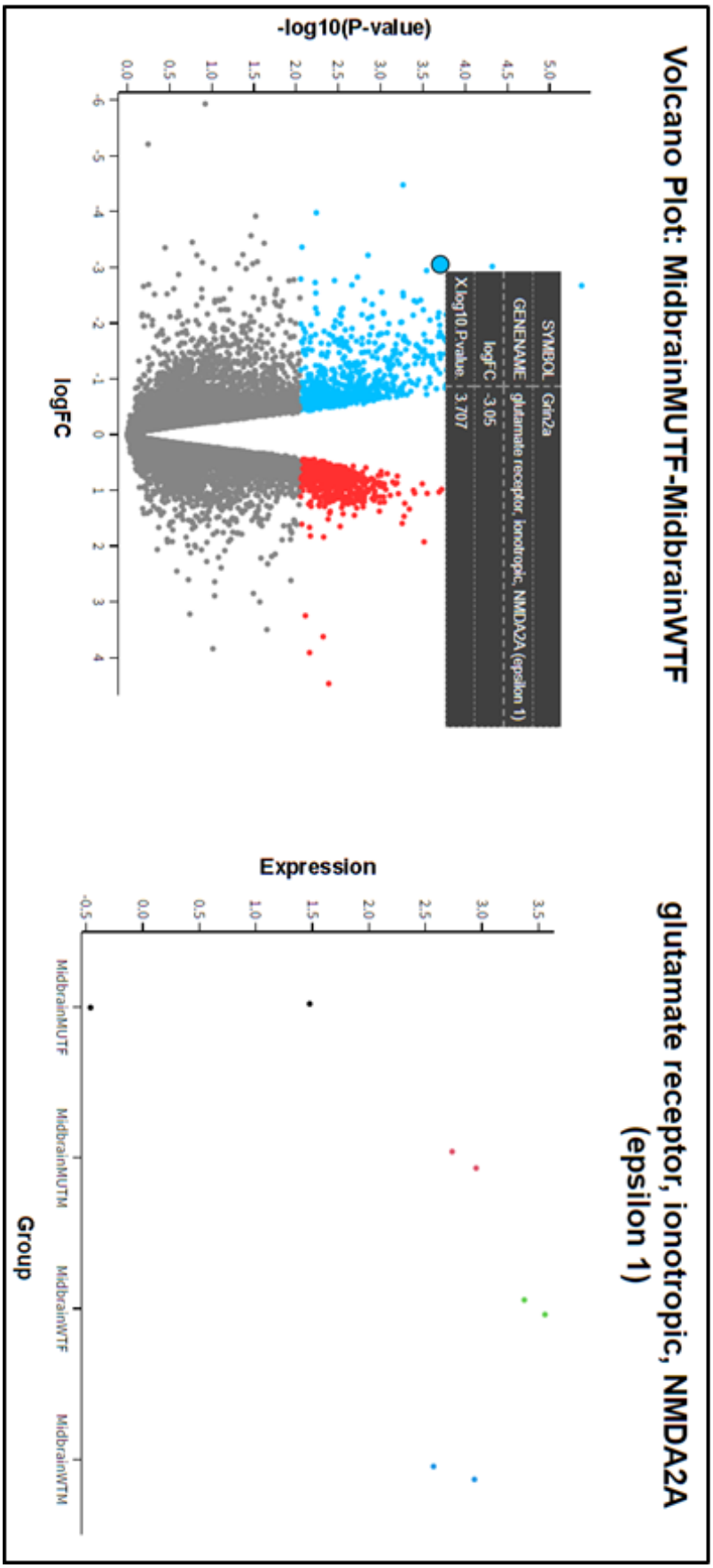
Volcano Plot: MidbrainMUTF-MidbrainWTF
-log10(P-value)
logFC
SYMBOL Grin2a
GENENAME glutamate receptor, ionotropic, NMDA2A (epsilon 1)
logFC -3.05
X.log10.Pvalue. 3.707
glutamate receptor, ionotropic, NMDA2A (epsilon 1)
Expression
Group
MidbrainMUTF
MidbrainMUTM
MidbrainWTF
MidbrainWTM

b.

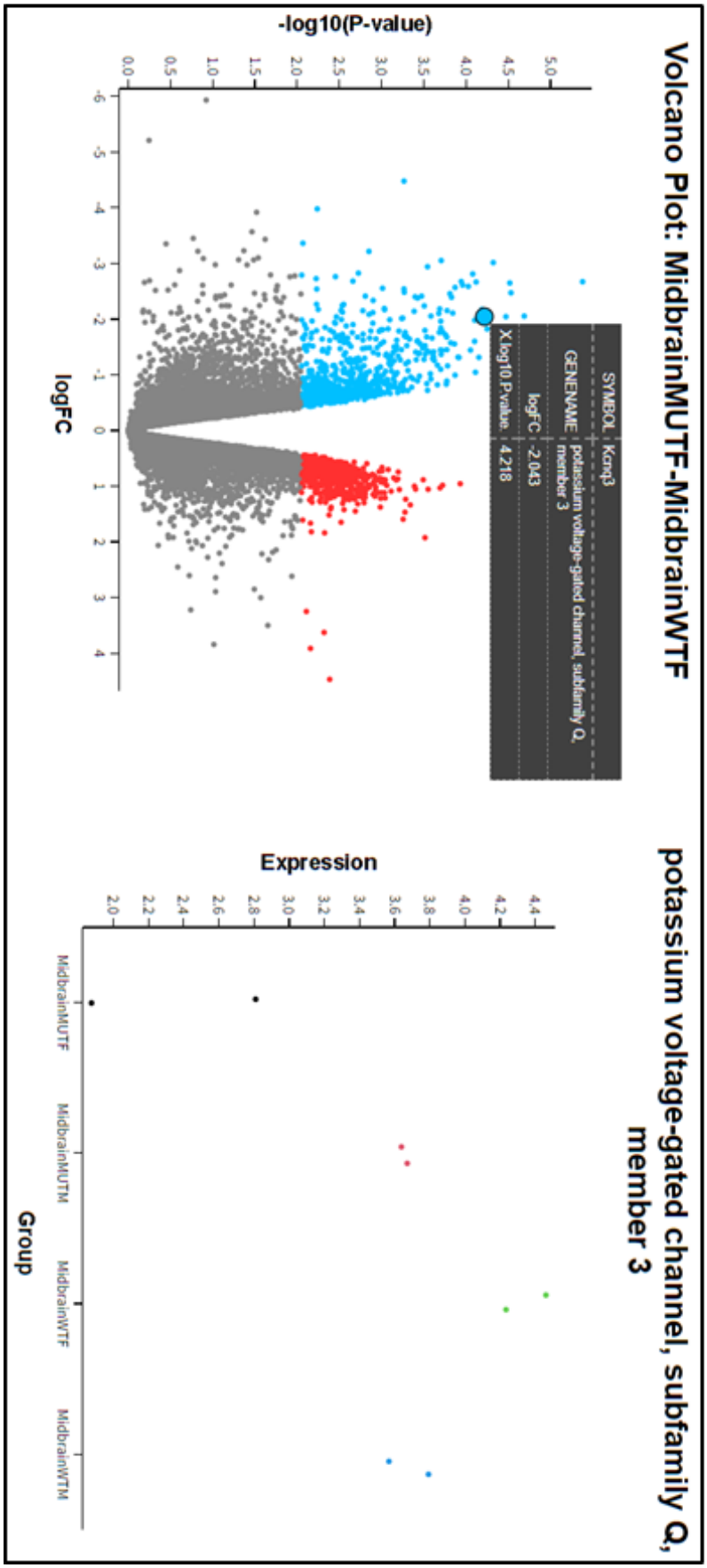
Volcano Plot: MidbrainMUTF-MidbrainWTF
-log10(P-value)
logFC
SYMBOL Kcnq3
GENENAME potassium voltage-gated channel, subfamily Q, member 3
logFC -2.043
X.log10.Pvalue. 4.218
potassium voltage-gated channel, subfamily Q, member 3
Expression
Group
MidbrainMUTF
MidbrainMUTM
MidbrainWTF
MidbrainWTM

C.

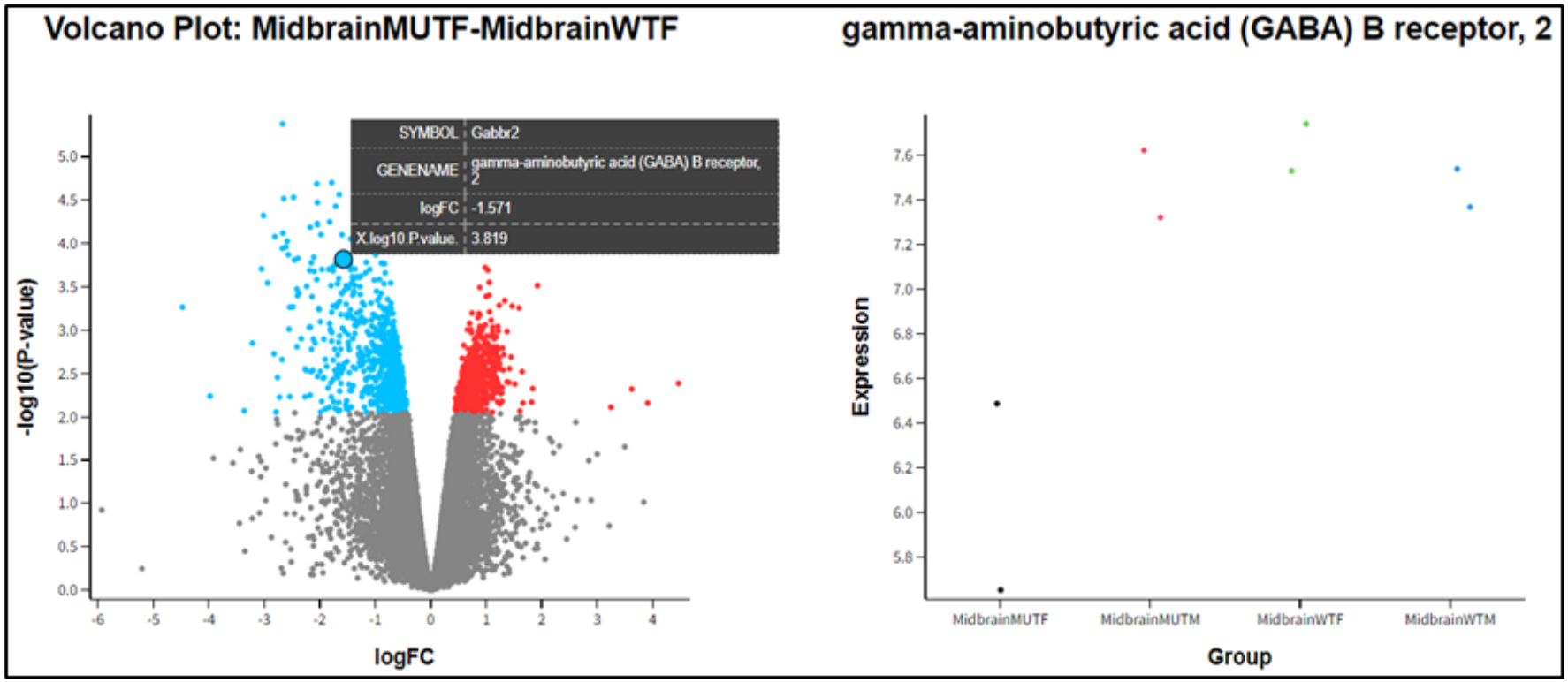
Volcano Plot: MidbrainMUTF-MidbrainWTF
SYMBOL Gabbr2
GENENAME gamma-aminobutyric acid (GABA) B receptor, 2
logFC -1.571
X.log10.P.value. 3.819
-log10(P-value)
logFC
gamma-aminobutyric acid (GABA) B receptor, 2
Expression
MidbrainMUTF
MidbrainMUTM
MidbrainWTF
MidbrainWTM
Group

Figure 5.5.3.2.3. Downregulated genes from brain-specific KEGG pathways – Volcano Plots and strip charts genes downregulated in homozygous females, taken from the top 50-scoring differential genes, Image generated using Galaxy (data from (Kanehisa and Goto 2000, Kanehisa 2019, Kanehisa, Furumichi et al. 2023))

Biological Process	Strength	False Discovery Rate
Positive regulation of ampa glutamate receptor clustering	1.37	0.0234
Brain-derived neurotrophic factor receptor signaling pathway	1.37	0.0234
Neural plate pattern specification	1.32	0.0054
Retrograde neuronal dense core vesicle transport	1.28	0.0326
Positive regulation of neuron projection arborisation	1.2	0.0105
Locomotion involved in locomotary behaviour	1.2	0.0105
Positive regulation of neuron maturation	1.2	0.0446
Regulation of synaptic vesicle priming	1.16	0.0033

Table 5.5.3.2.2. Downregulated genes involved in biological processes (Gene Ontology) biological processes with a strength ≥1 selected (data from (Kanehisa and Goto 2000, Kanehisa 2019, Kanehisa, Furumichi et al. 2023)).

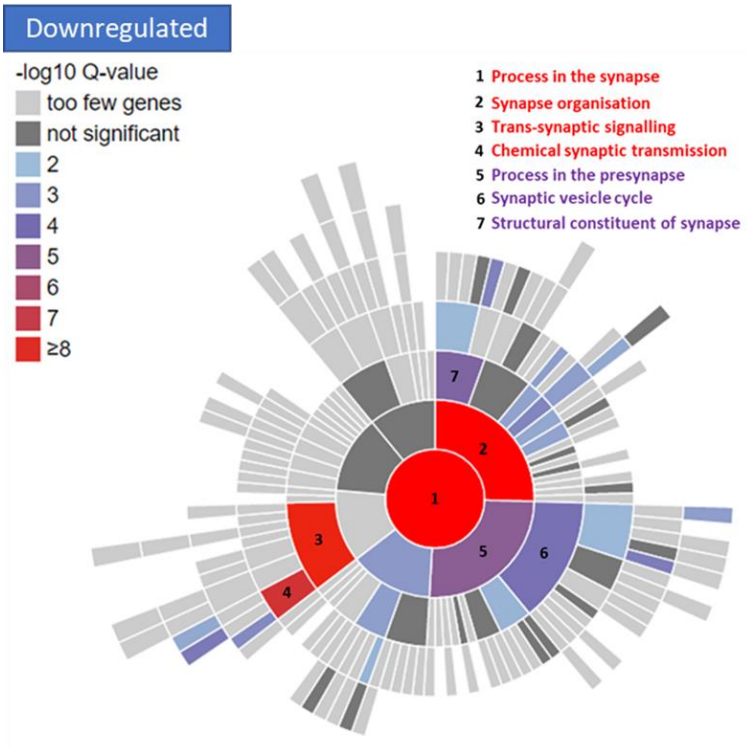

Figure 5.5.3.2.4. Sunburst figure of downregulated genes synapse function (SynGO) downregulated gene function across the synapse, Q-value showing gene enrichment. Image generated using https://www.syngoportal.org/ (data from (Koopmans, van Nierop et al. 2019)).

5.5.3.3 Mutant Female – up and downregulated genes

Post-differential analysis of genes that are both up and downregulated in the mutant female midbrain compared to the wildtype does not reveal any unique KEGG pathways that are not seen from looking at the two gene lists independently – with the exception of the neurotrophin signalling pathway (**Figure 5.5.3.3.1.**), for which multiple related genes can be seen in a protein-protein interaction network of the gene list (**Figure 5.5.3.3.2.**). However, no genes involved in the neurotrophin signalling pathway could be found in the top 50 genes (lowest p-value and highest fold-change in expression) in the differential comparison gene list.

Gene Ontology enrichment analysis on the biological function of up and downregulated genes reveals 2 biological processes – both of which are in the mitochondria, as is also seen in GO enrichment analysis of upregulated genes only (**Table 5.5.3.3.1.**).

Searching the SynGO database using the up and downregulated differential gene list (**Figure 5.5.3.3.3.**) gives a combination of synaptic gene function seen in the independent analysis of the up and down gene lists: metabolism, synaptic organisation, chemical trans-synaptic transmission, and both pre- and post-synapse translation.

KEGG Pathway	Observed gene count	Strength	False discovery rate
Ribosome	85	1.05	9.95E-48
Oxidative phosphorylation	55	0.85	4.66E-23
Huntington disease	77	0.64	1.45E-21
Thermogenesis	65	0.68	2.93E-20
Parkinson disease	67	0.67	2.93E-20
Prion disease	66	0.62	6.80E-18
Amyotrophic lateral sclerosis	75	0.54	2.52E-16
Alzheimer disease	74	0.54	3.62E-16
Non-alcoholic fatty liver disease	47	0.73	3.90E-16
Retrograde endocannabinoid signaling	34	0.6	9.15E-09
Spliceosome	32	0.61	1.56E-08
Metabolic pathways	134	0.16	0.00051
Spinocerebellar ataxia	22	0.42	0.003
Cardiac muscle contraction	16	0.5	0.0034
Endocytosis	31	0.32	0.0059
Proteasome	11	0.6	0.0061
Protein export	8	0.75	0.0061
RNA polymerase	8	0.68	0.0133
Longevity regulating pathway	15	0.45	0.0133
Regulation of actin cytoskeleton	26	0.31	0.0162
Phospholipase D signaling pathway	20	0.36	0.0188
Neurotrophin signaling pathway	17	0.39	0.02
EGFR tyrosine kinase inhibitor resistance	13	0.45	0.025
Longevity regulating pathway - multiple species	11	0.48	0.0308
Protein processing in endoplasmic reticulum	21	0.32	0.031
Choline metabolism in cancer	14	0.38	0.0491

Figure 5.5.3.3.1. KEGG pathways of up and downregulated genes in the homozygous female midbrain, compared to wildtype brain-specific KEGG pathways highlighted for further analysis. Image generated using https://string-db.org/ (data from (Kanehisa and Goto 2000, Kanehisa 2019, Kanehisa, Furumichi et al. 2023)).

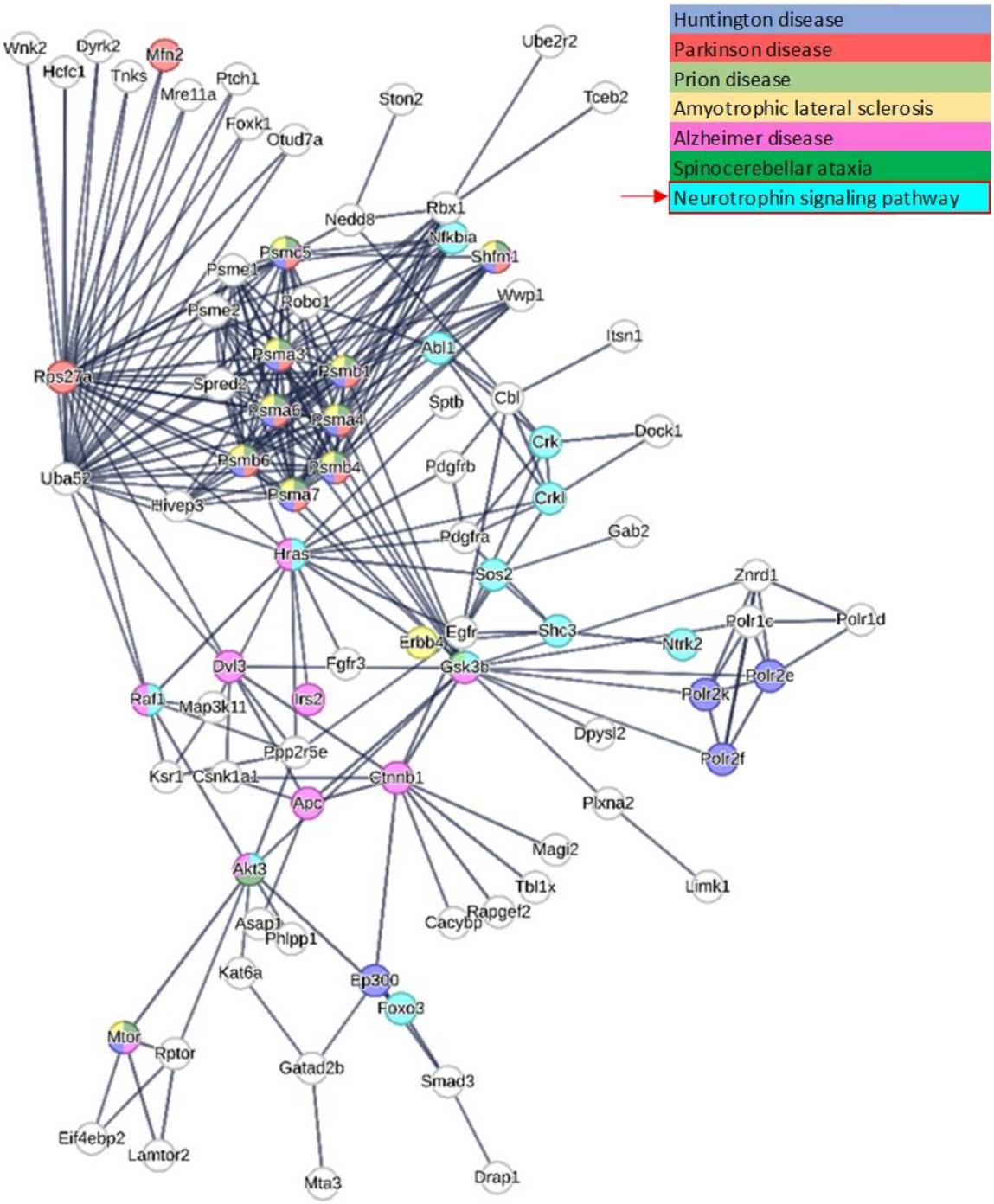

Figure 5.5.3.3.2. Protein-protein interaction networks from up and downregulated genes isolating networks involved in brain-specific KEGG pathways. The neurotrophin signalling pathway is unique to up and downregulation analysis. Image generated using https://string-db.org/ (data from (Kanehisa and Goto 2000, Kanehisa 2019, Kanehisa, Furumichi et al. 2023)).

Biological Process	Strength	False Discovery Rate
Mitochondrial ATP Synthesis Coupled Proton Transport	1.02	8.52E-05
Protein insertion into mitochondrial inner membrane	1.02	0.0224

Table 5.5.3.3.1. Up and Downregulated genes involved in biological processes (Gene Ontology) biological processes with a strength ≥1 selected (data from (Kanehisa and Goto 2000, Kanehisa 2019, Kanehisa, Furumichi et al. 2023)

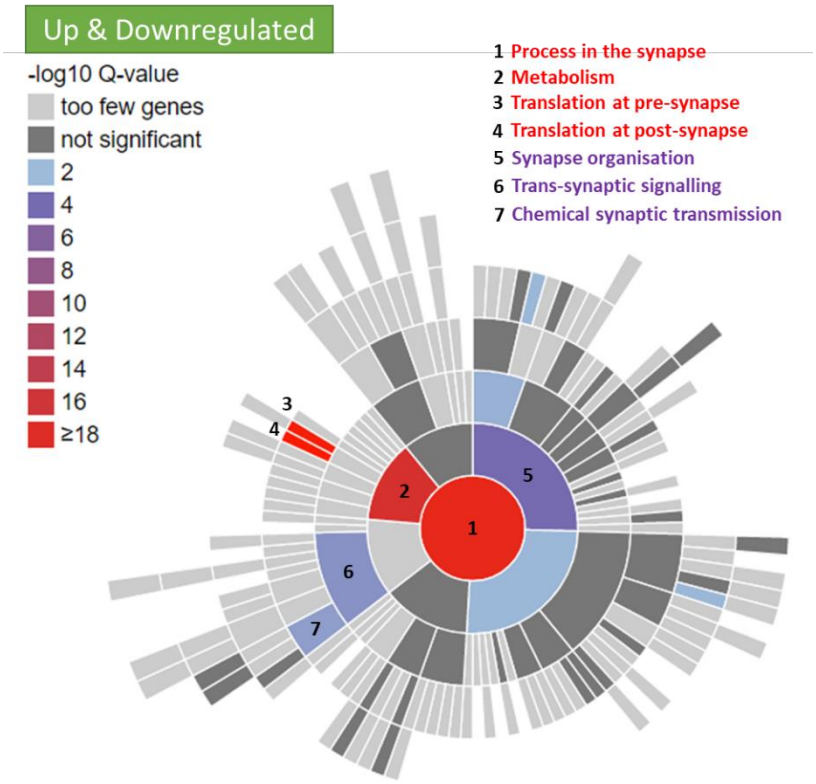

Figure 5.5.3.3.3. Sunburst figure of up and downregulated genes synapse function (SynGO) up and downregulated gene function across the synapse, Q-value showing gene enrichment. Image generated by https://www.syngoportal.org/ (data from (Koopmans, van Nierop et al. 2019)).

5.6 Discussion

5.6.1 Overview

From RNA-Seq analysis, differential gene expression in homozygous knockout DAT-*Cre*; *Zfhx3*-Flox mice is focused in the female midbrain. Homozygous males and other regions in the dopaminergic system of either sex do not generate notable differential expression lists. All discussion is therefore reserved for the homozygous female midbrain.

It should be noted that this RNASeq study is underpowered, having n=2 for each genotype, which will influence the results. This study will gain validity with an

increase in n-number – and thus an increase in statistical power - and should be taken as a pilot study, and an example of how an RNASeq analysis can be run if a larger sample size was analysed as outlined in this chapter.

It is noteworthy that *Zfhx3* was not found to be downregulated in the homozygous knockout mice. This could be due to the study being underpowered and therefore unable to discern downregulation of *Zfhx3*. It could also be that *Zfhx3* is expressed in other cell types in the midbrain in addition to dopaminergic neurons (*Chapter 3*), for example other neuron subtypes (GABA and glutamate), and expression in these cells masks the downregulation of *Zfhx3* in dopaminergic neurons.

This lack of power may also be the cause of the lack of significant difference in expression of Y-linked genes between the wildtype male and wildtype female midbrain analysis (*Figure 5.5.2.1.*).

When investigating which KEGG pathways contain genes from the upregulated gene list, multiple neurological disease pathways are revealed. This includes: Parkinson's disease, Huntington's disease, Prion disease, ALS, and Alzheimer's disease.

When investigating which KEGG pathways contain genes from the downregulated gene list, multiple signalling pathways are revealed, including: estrogen signalling, the cholinergic synapse, and the dopaminergic synapse. Another downregulated KEGG pathway is circadian entrainment, which is noteworthy given that *Zfhx3* is a circadian gene, and that it regulates the expression of neuropeptides responsible for intercellular signalling in the SCN (*Introduction 1.1.4.1.*). Investigating KEGG pathways using both the up and downregulated gene expression lists reveals an additional affected signalling pathway – neurotrophin signalling.

Entering the upregulated gene list into gene ontology databases for biological processes and synapse function, upregulated genes were highly associated with metabolism and the mitochondria, and with translation and the ribosome. Downregulated genes however are focused around synaptic structure, signalling, and neuronal development/maturation. Analysis of both the up and downregulated list together did not reveal any associations or functions that were not seen in analysis of the individual lists.

5.6.2 Selected gene breakdown

The upregulated and downregulated differential gene lists were sorted by p-value (lowest to highest) and then by expression fold-change (highest to lowest) to give the most significant genes with the highest fold-change in the mutant female. The top 50-scoring genes were then cross-referenced to highlighted relevant KEGG pathways to generate a gene-of-interest list for further discussion.

5.6.2.1 Upregulated genes

5.6.2.1.1 Complex I – electron transport chain

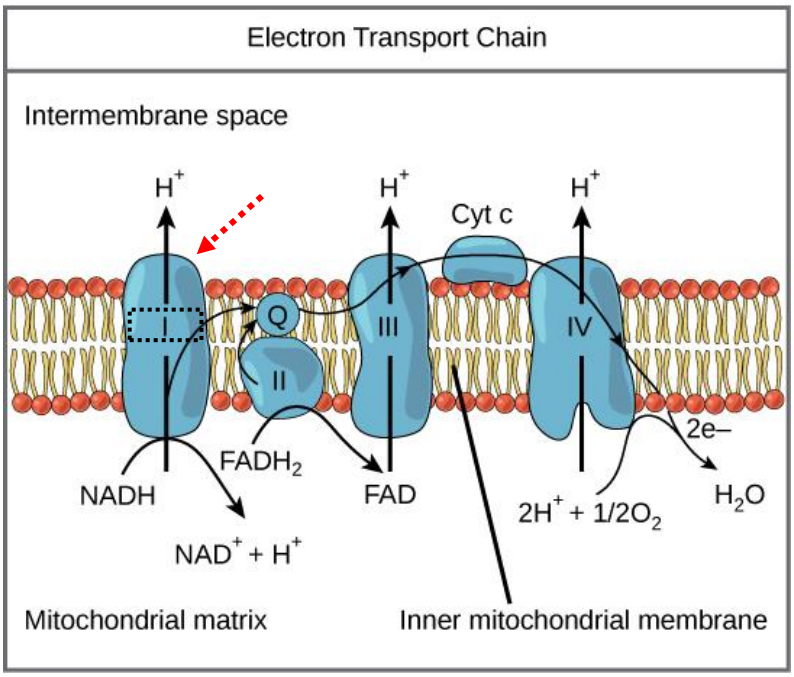

Figure 5.6.2.1.1.1. Complex I of the electron transport chain (*modified from OpenStax "Biology" (OpenStax)).*

NDUFA1, *2*, *6*, and *NDUFS6* are genes that encode subunits of NADH:ubiquinone oxidoreductase, also known as complex I of the electron transport chain (**Figure 5.6.2.1.1.1**.) (Vinothkumar, Zhu et al. 2014).

Mammalian complex I contains 45 subunits in total – 14 conserved subunits, and 31 mammalian-specific subunits (Hirst, Carroll et al. 2003, Hirst 2013). *NDUFA1*, *2*, *6*, and *NDUFS6* are all members of the nuclear-encoded mammalian-specific subunits.

The constituent proteins of the electron transport chain reside in the inner mitochondrial membrane, and generate ATP (adenosine triphosphate) through a series of redox reactions. Complex I is the first complex in the chain, and reduces NADH (nicotinamide adenine dinucleotide) as the first step of the electron transport chain reaction. In addition to its role in the electron transport chain,

complex I plays a key role in the production of reactive oxygen species (ROS) in the mitochondria (Murphy 2008).

5.6.2.1.2 Complex III – electron transport chain

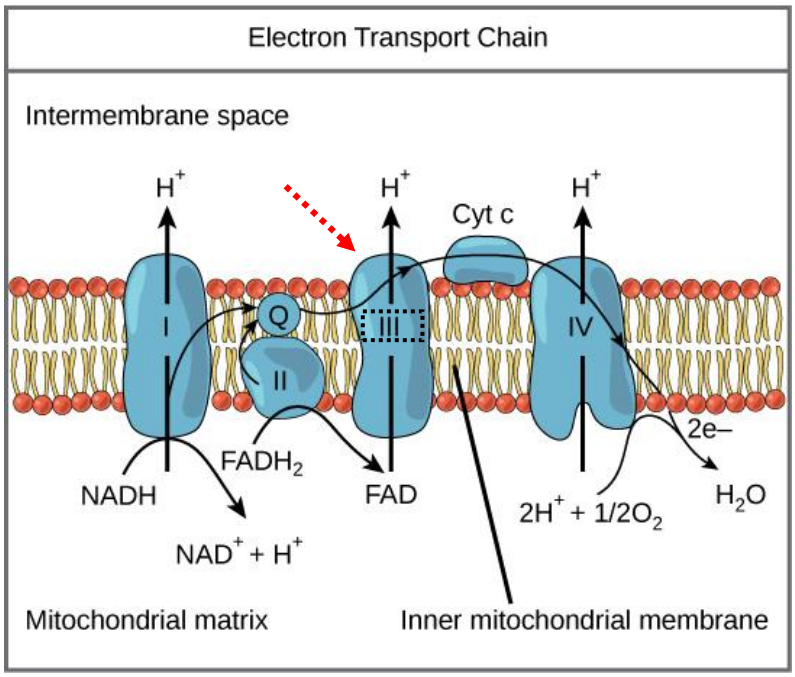

Figure 5.6.2.1.2.1. Complex III of the electron transport chain *(modified from OpenStax "Biology" (OpenStax))*

UQCRH gene encodes a subunit of Coenzyme Q – cytochrome c reductase, also known as complex III of the electron transport chain (**Figure 5.6.2.1.2.1.**) (Ohta, Goto et al. 1987).

Complex III is the location of the Q-cycle, where a sequential redox reaction of Coenzyme Q functions as part of the electron transport chain (Mitchell 1975).

Coenzyme Q has a wider role outside of the electron transport chain, and is also involved in: modulation of gene expression, regulation of physicochemical properties of cell membranes, wider mitochondrial function, and in addition serves as an antioxidant in the cell as a whole (Crane 2002, Turunen, Olsson et al. 2004).

5.6.2.1.3 RNA Polymerases I, II, III

POLR2K gene encodes subunit RPABC4, which is a subunit utilised by RNA polymerases I, II, and III. Each polymerase synthesises a different type of RNA: polymerase I is involved in rRNA synthesis (ribosomal RNA); II synthesises mRNA (messenger RNA); and III synthesises tRNA (transfer RNA), in addition to being involved in rRNA synthesis ((Seifart and Sekeris 1969, Kedinger, Gniazdowski et al. 1970, Lindell, Weinberg et al. 1970, Zylber and Penman 1971, Weinmann and Roeder 1974) *as cited by* (Vannini and Cramer 2012)).

5.6.2.2 Downregulated Genes

5.6.2.2.1 NMDA receptors

GRIN2A gene encodes protein Glutamate Ionotropic Receptor NMDA Type Subunit 2A, a subunit of NMDA receptors, which are a subset of glutamate receptors (Traynelis, Wollmuth et al. 2010).

NMDA receptors have a wide scope of function in the central nervous system. They are involved in: spatial learning, working memory, and neuronal plasticity. (Morris, Anderson et al. 1986, Collingridge 1987, Lisman, Fellous et al. 1998).

5.6.2.2.2 M-channels

KCNQ3 is a member of the *KCNQ* gene family, which encode proteins that form M-channels when associated with other members of the same gene family.

M-channels facilitate M-current, which is a voltage-sensitive potassium current that modulates the excitability of a neuron by regulating the action potential threshold – both facilitating, or conversely preventing, repeated action potentials that result from neurotransmitter release (Brown and Adams 1980, Cooper and Jan 2003, Brown and Passmore 2009).

5.6.2.2.3 GABA receptor – type B

GABBR2 gene encodes a multi-pass protein that is a component of the G protein-coupled second-messenger receptor system with the $GABA_B$ receptor (Schwenk, Metz et al. 2010)

GABA is the primary inhibitory neurotransmitter, and plays a role in modulating neuronal activity by altering the excitability of neurons. $GABA_B$ receptors execute their function via secondary messaging using G protein-coupled receptors, including but not limited to: inhibit presynaptic calcium ion channels, activate postsynaptic potassium ion channels, and modulate adenylyl cyclase activity (Bettler, Kaupmann et al. 2004).

5.6.2.2.4 qPCR results – Dopamine Receptors

Data from qPCR analysis of dopamine receptor expression in mixed-sex samples of the striatum show significant downregulation of dopamine receptors D_1 and D_2.

Dopamine receptors D_1 and D_2 are G protein-coupled receptors, much like $GABA_B$ receptors (*5.6.2.2.3.*). D_1 receptors function by activating adenylyl cyclase and phospholipase C, and D_2 receptors function by inhibiting adenylyl cyclase and activating potassium channels. Both of these receptors are involved in memory, impulse control, attention, locomotion, and sleep. (Mishra, Singh et al. 2018, Bhatia A 2022).

The downregulation of dopamine receptor expression seen in the striatum with qPCR is contrary to the RNA-Seq data, which did not show significant differential expression of dopamine receptors between homozygous knockout or wildtype mice, in any region, or either sex. This could be due to the RNA-Seq data having insufficient power - with each genotype of each sex having n=2 – and therefore unable to elucidate a significant difference in expression.

5.6.3 Concluding remarks

In RNA-Seq analysis, significant differential gene expression was seen only in homozygous knockout female – when compared both to homozygous knockout males, and wildtype females. Strip charts of the top-scoring genes (lowest p-value and greatest fold-change in expression) suggest that homozygous knockout females have a distinct expression profile compared to both homozygous knockout and wildtype mice of either sex.

Upregulated genes in homozygous female mice are associated with multiple neurological diseases, including Parkinson’s and Huntington’s disease. Functionality of differentially expressed genes is focused around the mitochondria and ribosome, and therefore around metabolism and gene translation. Genes of

interest in the top 50-scoring differential genes encode protein complexes in the electron transport chain, and a subunit of RNA polymerase proteins.

Downregulated genes in homozygous female mice are associated with synaptic signalling and signalling pathways, with the addition of circadian entrainment. Functionality of differentially expressed genes is focused around synaptic structure, signalling, and neuronal development/maturation. Genes of interest in the top 50-scoring differential genes encode neurotransmitter receptors, and a potassium channel regulating neuron firing. Data from qPCR experiments (on homozygous knockout mice of both sexes) also show a downregulation of dopamine receptors.

Analysis of both up and downregulated gene lists together agrees with the associations seen in both the up and downregulated gene lists separately, and also reveals an additional affected signalling pathway – neurotrophin signalling.

The significance of these findings, and their association with human disease will be covered in the *Discussion* chapter.

6

Results IV: Characterisation of *Zfhx3*-Flox knockout mice generated via intracranial injection of adeno-associated virus

6

Results IV: Characterisation of *Zfhx3-Flox* knockout mice generated via intracranial injection of adeno-associated virus

6.1 Introduction

Creating a knockout mouse line by crossing a *Cre*-expressing line and a loxP-flanked gene line has limitations, especially when studying the adult-only function a gene which is embryonic lethal or plays a key role in development – such as *Zfhx3* (*Chapter 1, Introduction*). Using instead a *Cre*-expressing viral vector, introduced into neurons of floxed mice via transduction from AAV, we can circumvent this limitation (Ahmed, Chakravarthy et al. 2004).

Stereotaxic intracranial injection of adeno-associated virus (AAV) is an increasingly common method used to transduce transgenes into cells for extended expression in both cells and whole animals, with different viral serotypes used for targeting specific tissue types (McCown, Xiao et al. 1996, Asokan, Schaffer et al. 2012). Using a stereotaxic frame to keep the skull orientated and stable, co-ordinates taken from a brain atlas allow for targeting of a specific region within the brain – done by measuring along the x, y, and z-axis from the bregma point on the dorsal of the skull. Measurements are made using micromanipulators on the stereotaxic frame to precisely position a needle or micropipette for injection (Keiser, Chen et al. 2018). The accuracy of the injection co-ordinates can be determined by post-mortem analysis of brain sections, either by using antibodies for the introduced transgene, or by detecting expression of a transduced fluorescent reporter gene.

6.2 AAV Serotypes

Selecting the correct AAV serotype for the experimental aim is essential, as different AAV capsid proteins: target specific tissues, have different transduction efficacy, and have varying spread from injection site. Common AAV serotypes for targeting neurons are natural-capsid AAV1, AAV2, AAV5, AAV8, and AAV9, including engineered-capsid AAV-DJ (Haery, Deverman et al. 2019).

Initially for this study AAV2 was selected, as transduction is preferably tropic to neurons, and less commonly in astrocytes and microglia. Importantly, spread of viral transduction of AAV2 is minimal – suited for targeting a discrete area such as the dopaminergic centres (Kaplitt, Leone et al. 1994, Bartlett, Samulski et al. 1998).

During troubleshooting, the classical AAV2 serotype was replaced with the more contemporary AAV5 serotype. AAV5 also has preference for transduction into neurons, while delivering greater vector gene expression in the central nervous system, and spreading further from the injection site - but without trans-synaptic spread to other brain regions along dopamine pathways (Haggerty, Grecco et al. 2020).

Zfhx3 is expressed in non-neuronal cells within the brain (Karlsson, Zhang et al. 2021) however as the surgical *Zfhx3* knockout cohort is intended to be a comparison to the DAT-*Cre*; *Zfhx3*-Flox line, we wish to study the effect of neuronal knockout only. As both AAV2 and AAV5 transfect non-neuronal cells, all viral vectors used in this study use the hSyn (human synapsin 1) promotor, which

has a broadly neuronal expression in mammals (Kügler, Kilic et al. 2003, Nathanson, Jappelli et al. 2009, Yaguchi, Ohashi et al. 2013).

Details on AAV serotypes and viral vectors used in this study can be found in the *Methods* section.

6.3 Aims

The purpose was to create an adult-only knockout of *Zfhx3* within targeted midbrain dopaminergic neurons, as comparison to the DAT-*Cre; Zfhx3*-Flox line which has *Zfhx3* knocked out from development (E13) onwards in the entire dopaminergic system.

This was to study contrast between developmental and adult-only function of *Zfhx3*; and targeted knockout of *Zfhx3* in neurons of the midbrain dopaminergic centres, and the entire dopaminergic system.

Both female and male *Zfhx3*$^{Flox/Flox}$ mice were injected with either *Cre*$^{+}$ or *Cre*$^{-}$ adeno-associated virus into the VTA to create a knockout cohort with a surgical control. These mice were then to undergo a behavioural phenotype pipeline mirroring the DAT-*Cre; Zfhx3*-Flox pipeline (*Methods 2.3.)*. Post-mortem coronal brain sections were imaged to determine the accuracy of injection and efficacy of *Cre*-expression using the viral vector fluorescent reporter protein.

6.4 Overview of intracranial injection of adeno-associated virus

*Full updated protocol and details on original protocol can be found in the Methods chapter***.**

This method of intracranial injection uses a stereotaxic frame to position the skull of the mouse - using a combination of a mouth-piece, ear bars, and micromanipulators on the frame. Correct orientation of the skull is essential for accurate insertion of the surgical needle/pipette into the brain, and firm positioning of the head it needed for safe injection as any movement could cause damage to brain tissue.

After a medial incision down the top of the skull, co-ordinates to the targeted brain region are measured against the bregma marker on the dorsal of the skull, using a reference atlas for guidance (Paxinos and Franklin 2012) (**Figure 6.4.1.**).

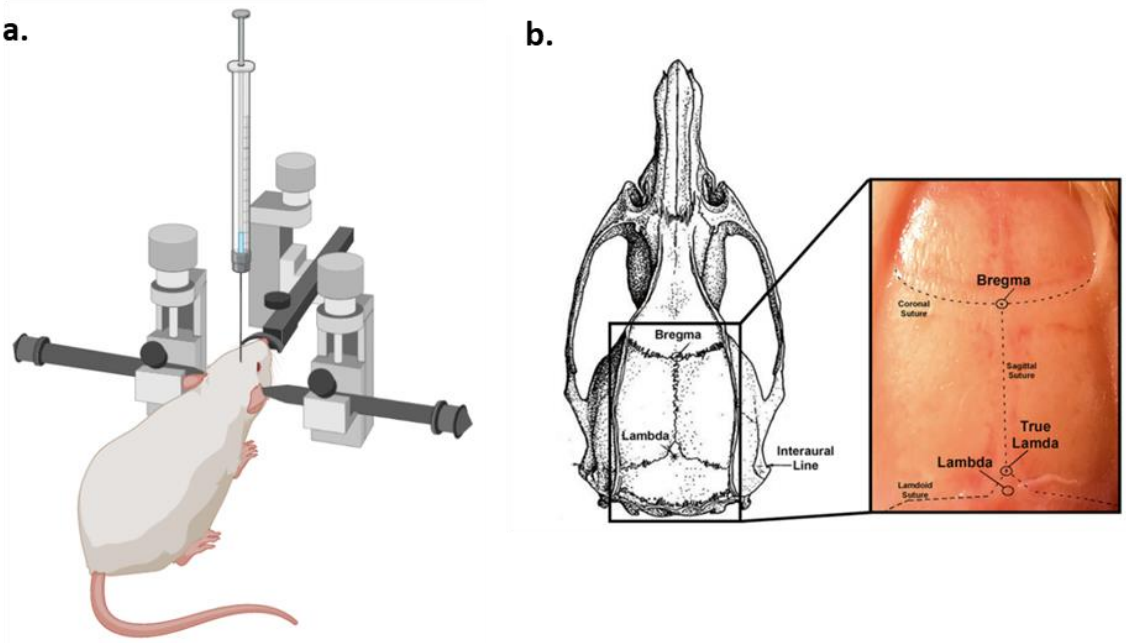

Figure 6.4.1. Details on the intracranial injection surgical procedure (a) A schematic of the stereotaxic frame used to position the head, and how the Hamilton syringe and needle are situated (b) Markers bregma and lambda labelled on the mouse skull, used to determine co-ordinates for viral injection. (a) image from BioRender.com; (b) image modified from (Benskey and Manfredsson 2016)

Using the scales on the frame micromanipulator to measure, bi-lateral holes are drilled through which the needle can pass to inject the virus into the targeted region, in this case the VTA (**Figure 6.4.2**).

Once injected, an interval of 7-14 days is needed for the virus to transduce neurons in the targeted region, and for the viral vector to express (Kaspar, Vissel et al. 2002, Ayturk 2016).

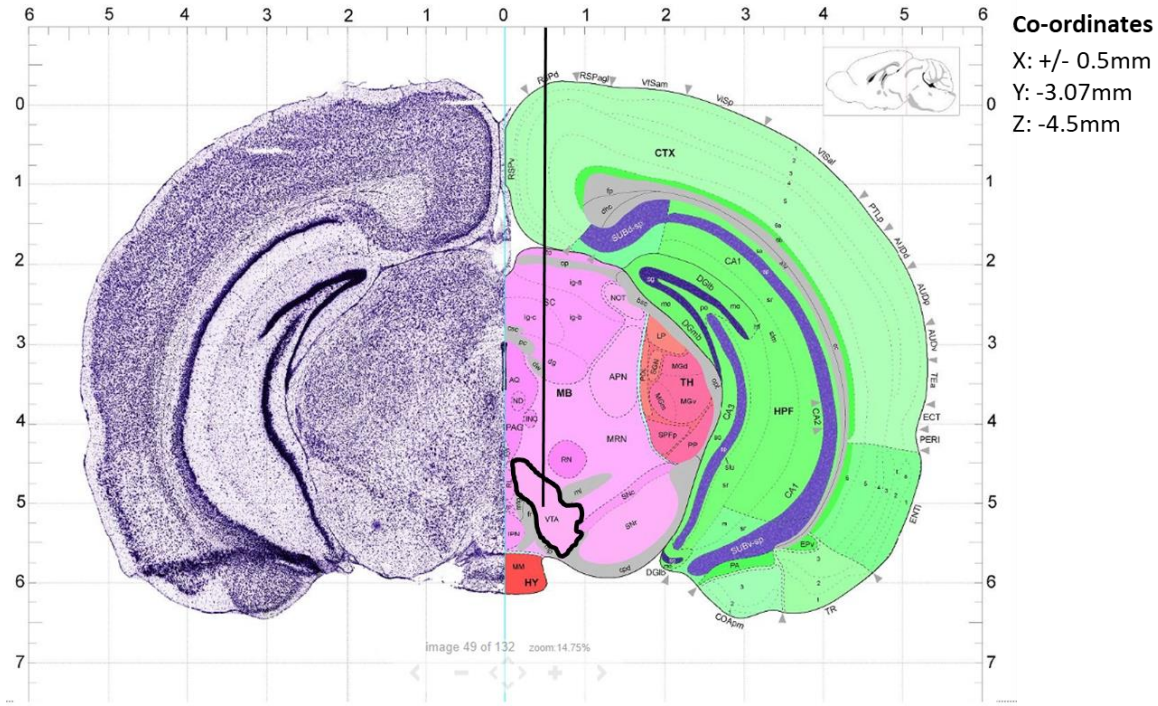

Figure 6.4.2. Map of a coronal section of the mouse brain with the ventral tegmental area outlined in black, and a black line showing the path of the needle during the injection. On the right are the co-ordinates followed to reach the VTA (modified from the Allen Brain Atlas (Lein, Hawrylycz et al. 2007)).

The original protocol used by the Mary Lyon Centre did not give reliable results during preliminary surgeries, and a new protocol was developed after multiple steps of troubleshooting, which are detailed in this chapter.

The original surgical protocol uses AAV2 viruses, expressing green Venus fluorescent protein as a marker for vector expression, with mice being allowed at least 14 days post-surgery before any post-mortem analysis.

6.5 Troubleshooting Phase I: Virus Validation

When the study initiated, the institute protocol used for intracranial injection did not give useable, reproducible results. Frequently no Venus reporter protein could be found, or if it could be found expression was sporadic - showing that very few neurons had been transduced (**Figure 6.5.1.**).

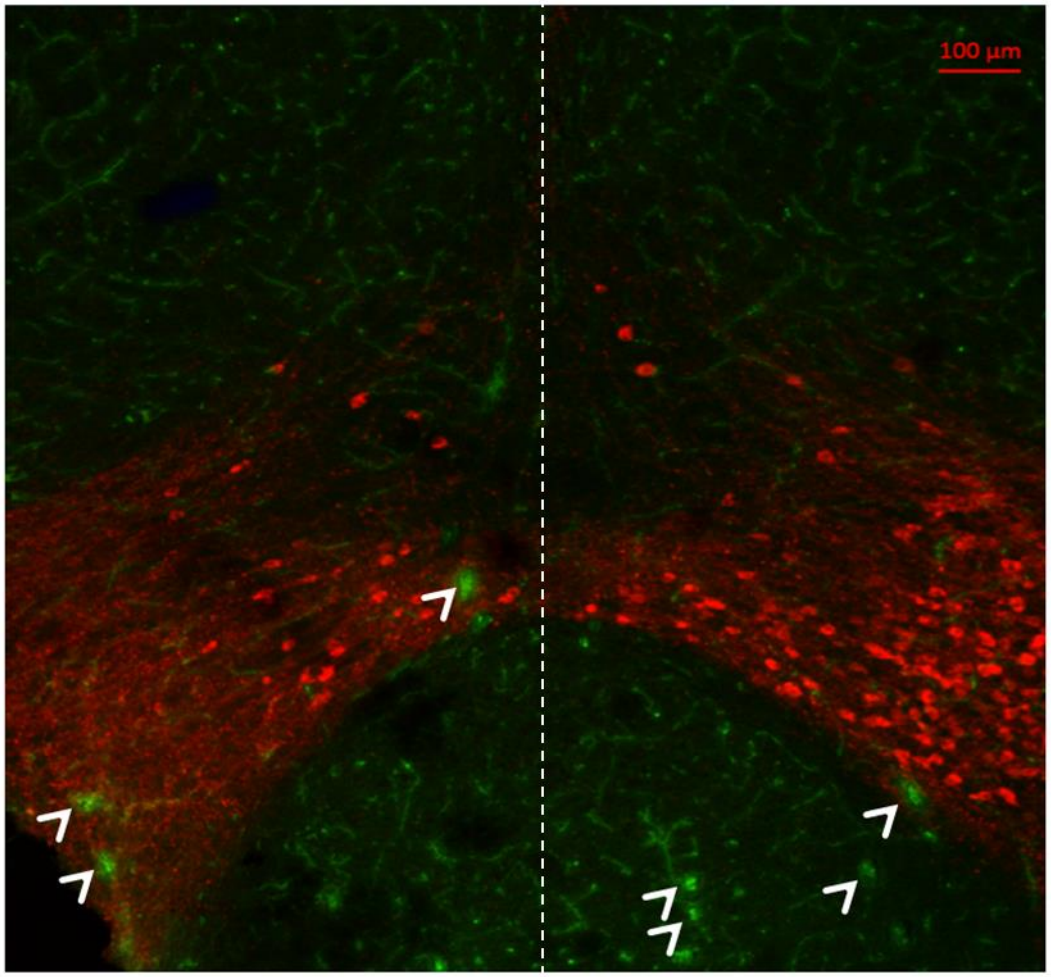

Figure 6.5.1. Composite image of a coronal section of a *Zfhx3*$^{Flox/Flox}$ brain that had undergone intracranial injection the VTA stained red (tyrosine hydroxylase used as a dopamine neuronal marker), and green showing neurons expressing Venus fluorescent reporter protein. The dotted line shows the midline of the brain. Injected virus was at 10^{11} vg/ml concentration. Images taken at x10 magnification.

Dopamine-expressing cells are stained red using anti-tyrosine hydroxylase (a dopamine neuronal marker), with green fluorescence indicating transduction of Venus fluorescent protein-expressing virus.

For the study to proceed multiple rounds of troubleshooting were needed to determine the issues, starting with investigating the efficacy of the AAV2 viruses used. Primary cortical and hippocampal neuronal cultures from P0 B6N mice *(Methods 2.1.1.)* were inoculated with either *Cre*$^{+}$ or *Cre*$^{-}$ AAV2 virus, with both 10^{12} vg/ml (the titre used at the time) and 10^{13} vg/ml titres tested (**Figure 6.5.2.**).

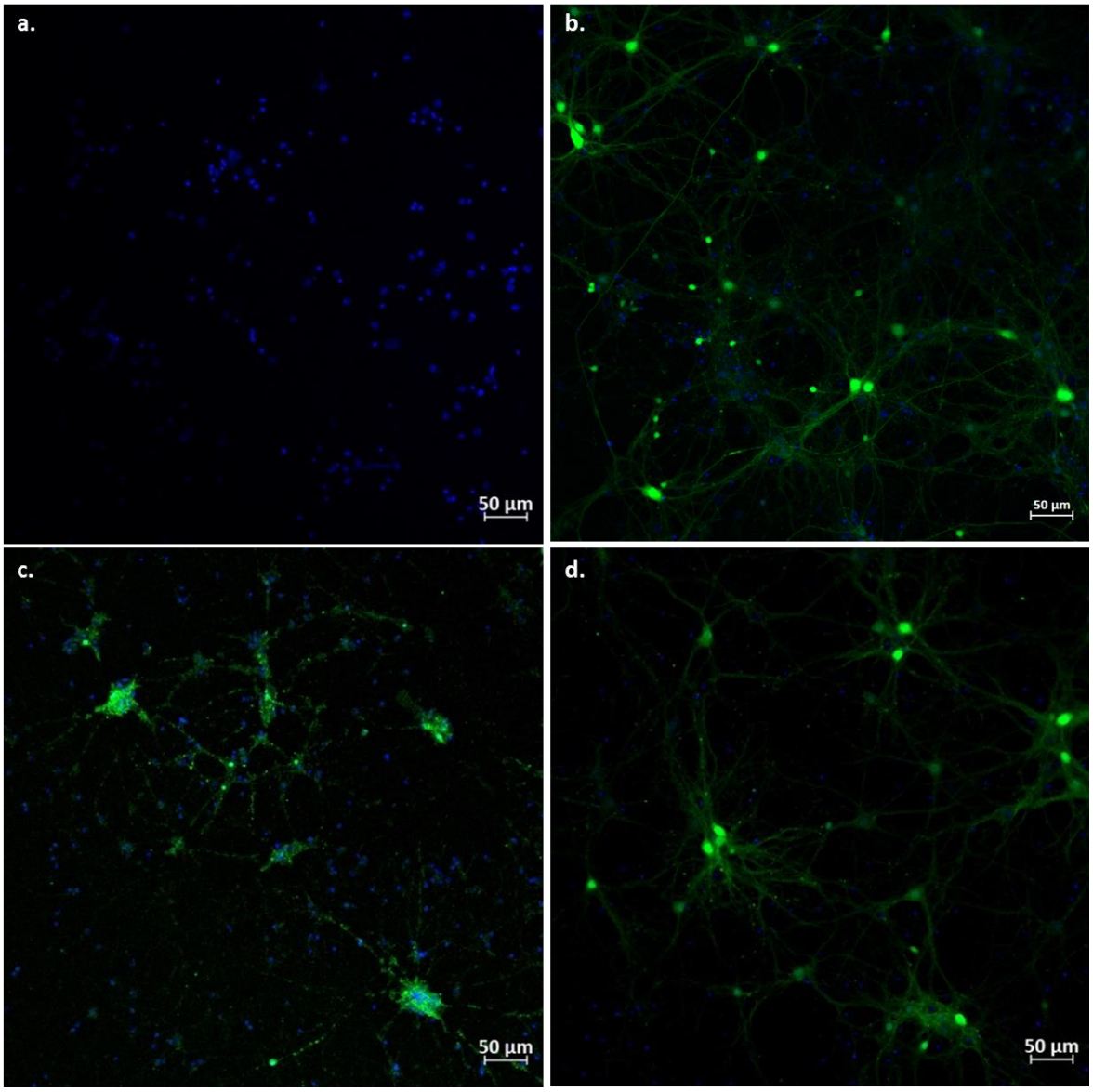

Figure 6.5.2. Primary neuron cell culture each inoculated with AAV2, green showing Venus immunofluorescent protein and blue showing DAPI expression. **(a)** Control culture with no AAV2 added **(b)** Inoculated with *Cre*$^{-}$ virus at 10^{12} vg/ml concentration **(c)** Inoculated with *Cre*$^{-}$ virus at 10^{12} vg/m concentration **(d)** Inoculated with *Cre*$^{+}$ virus at 10^{13} vg/ml concentration. Images taken at x10 magnification.

The expression of green fluorescent Venus reporter protein demonstrates that both the *Cre*$^{+}$ and *Cre*$^{-}$ viral vectors successfully transfected neurons, and that both vectors were expressed, at the concentration used in the intracranial injection. This demonstrated that neither the efficacy nor the titre of the virus were

the causative factor in the minimal of viral reporter expression seen in the post-surgery brains using the established protocols.

6.6 Troubleshooting Phase II: Needle to micropipette

Given that viral reporter genes were expressed *in vitro*, another round of troubleshooting was carried out with careful observation of each individual step of the surgical protocol.

When first priming the syringe and needle with distilled water, it was protocol to introduce an air bubble into the solution to allow for tracking withdrawal and injection of viral solution. It was theorised that this could be detrimental to the pressure gradient in the syringe when withdrawing and injecting into the brain due to compression of the bubble. Therefore the bubble was eliminated from the protocol.

With this change, subsequent surgeries showed Venus expression in each hemisphere, following the line of the needle path from the dorsal of the skull to the injection co-ordinates in the VTA (**Figure 6.6.1**).

It has been reported that a needle with more than 9 μm inner diameter produces too-low ejection pressure for effective viral suffusion, and viral solution passes back up along the outer surface of the needle – which would cause the line of Venus expression observed in these injections (Cetin, Komai et al. 2006). We therefore determined at least one issue with the protocol was the diameter of the needle.

The outcome of this troubleshooting round was to replace the 25g Hamilton needle (260µm I.D.) with a finer glass micropipette, to be used with the same Hamilton syringe (*Methods 2.4.1.*).

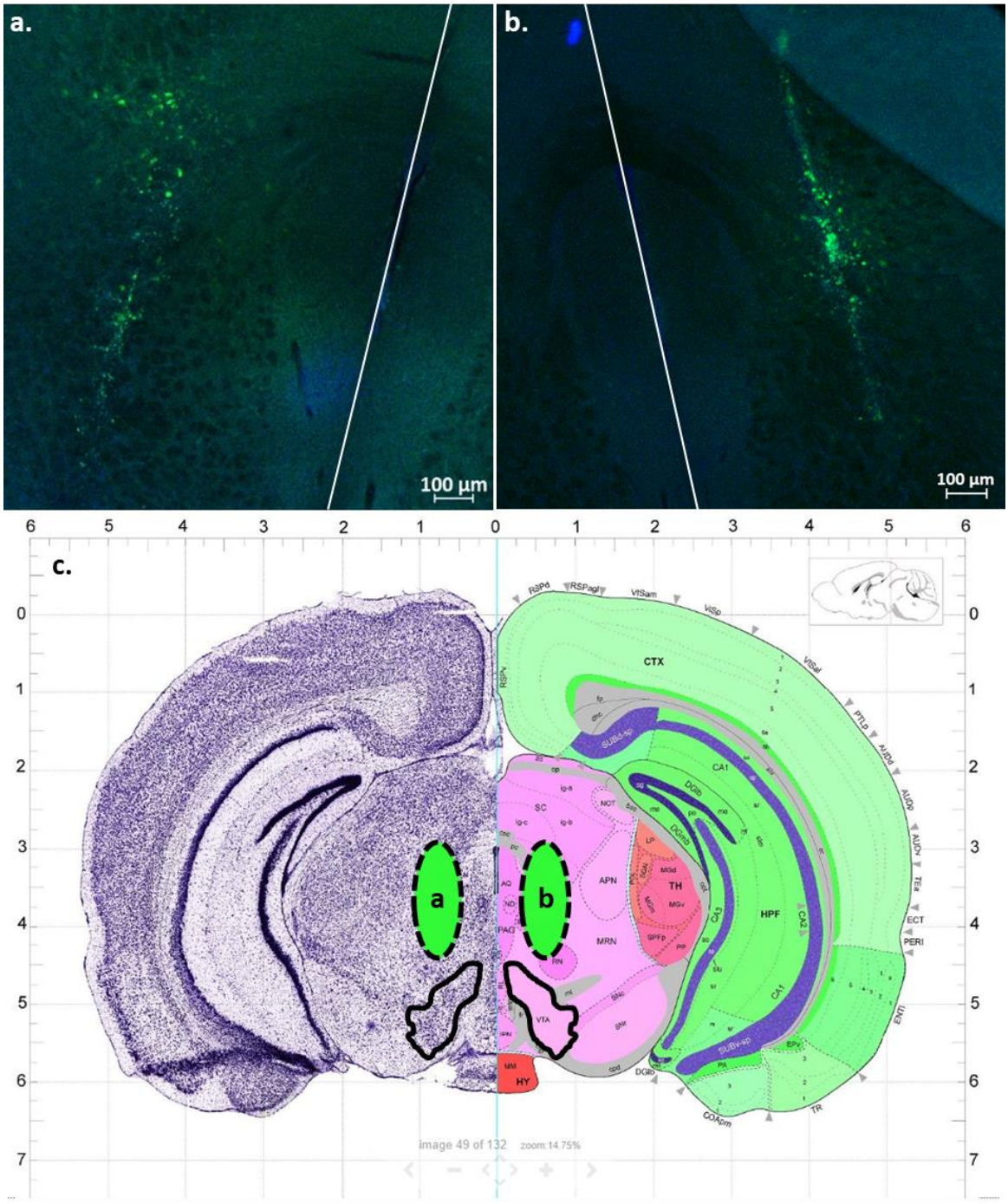

Figure 6.6.1. '**Streaks' of Venus fluorescence found in an injected brain (a)(b)** transfected neurons showing Venus fluorescent protein, in the right and left hemispheres respectively, with white lines showing the midline **(c)** a coronal map of the mouse brain, with shapes 'a' and 'b' showing the locations of fluorescence seen in images a and b, respectively, (modified from the Allen Brain Atlas (Lein, Hawrylycz et al. 2007)). The VTA is outlined in both hemispheres. Images taken at x5 magnification.

6.7 Troubleshooting Phase III: Co-ordinates and volume

Two adaptations to the original protocol had been made: exclusion of an air bubble in the priming solution, and exchange of 25g Hamilton needles to custom glass micropipettes.

Following visualisation of coronal sections of brains injected using the corrected procedure, Venus fluorescence can be seen in an oval-like shaped cluster of cells close to the desired injection co-ordinate, demonstrating the effectiveness of the new glass micropipettes (**Figure 6.7.1.**).

However two more problems needed troubleshooting before conducting the experiment proper – firstly, the reporter is expressed at sites that are too ventral in

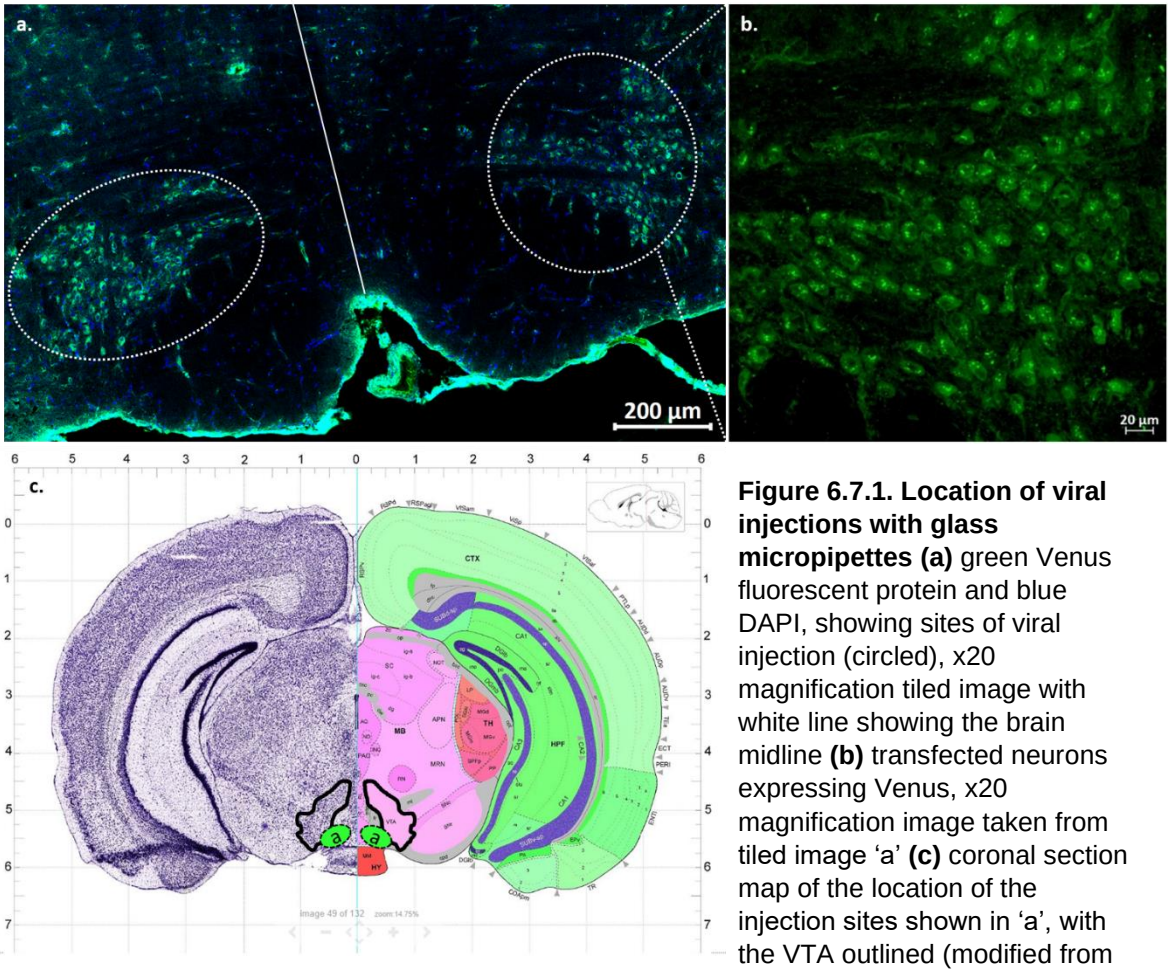

Figure 6.7.1. Location of viral injections with glass micropipettes (a) green Venus fluorescent protein and blue DAPI, showing sites of viral injection (circled), x20 magnification tiled image with white line showing the brain midline **(b)** transfected neurons expressing Venus, x20 magnification image taken from tiled image 'a' **(c)** coronal section map of the location of the injection sites shown in 'a', with the VTA outlined (modified from the Allen Brain Atlas (Lein, Hawrylycz et al. 2007))

to target the VTA; and secondly, the level of fluorescence seen at the injection sites is less than would be expected considering the injection volume (800 nl per hemisphere).

Firstly, it was theorised that the misplaced injection sites may be related to craniofacial defects previously observed in the *Zfhx3*-Flox line of mice (**Figure 6.7.2.**). These defects cause "short-face" in *Zfhx3*$^{Flox/Flox}$ mice, and the differences in skull shape could lead to co-ordinates from the Allen Brain Atlas being inapplicable. The "short-face" deformity includes malocclusion, which could also cause differences in head orientation on the stereotaxic frame for *Zfhx3*$^{Flox/Flox}$ mice, and lead to inaccurate skull measurements and micropipette insertion misalignment. While any observed "short-face" mice were excluded from the surgery cohort, it is possible that mice with a more subtle deformity were missed by qualitative checks.

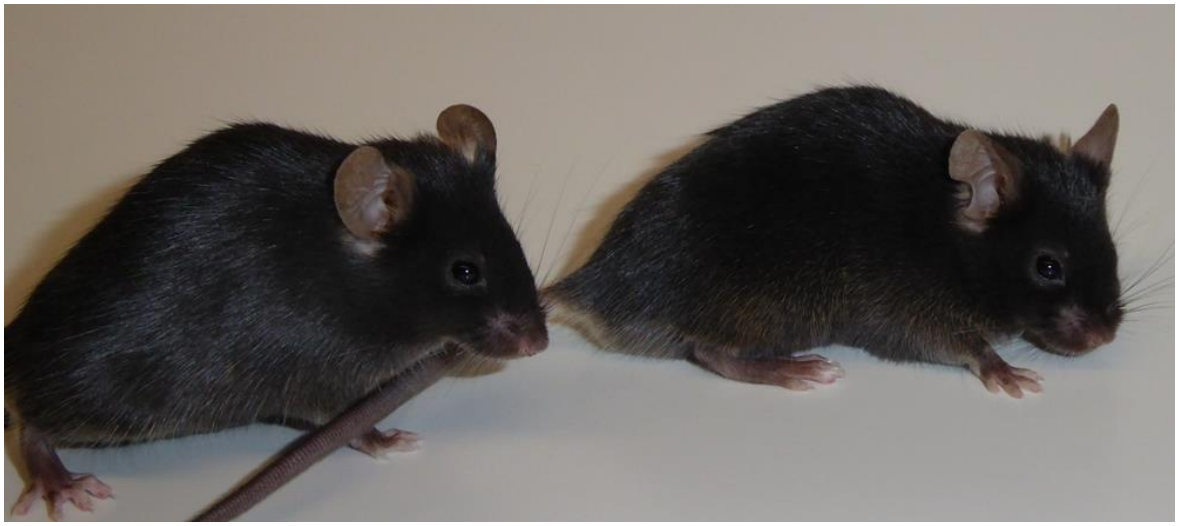

Figure 6.7.2. "Short-face" mouse from *Zfhx3*-Flox line left: *Zfhx3*$^{-/-}$ mouse; right: *Zfhx3*$^{Flox/Flox}$ "short-face" mouse. Short-face mice have a compressed facial structure, including malocclusion.

Secondly, while it was evident that the injection method was effective, the number of cells expressing viral Venus fluorescent protein was less than expected, which suggested an issue in the injection volume of AAV2. Research suggested that this could be due to distilled water being used as the priming solution for the syringe and micropipette. This can cause issues for two reasons: one, that water is compressible, and therefore does not effectively transfer injection pressure from the syringe plunger to the viral solution in the micropipette tip (Bielefeld, Sierra et al. 2017); and two, because when viral solution is withdrawn into the micropipette tip it could mix with the priming water and become diluted, which would lower the viral titre in the injected solution (Hamilton 2019). To solve this, the priming solution was changed to mineral oil, as it is both non-compressible and cannot mix with the viral solution.

In addition to changing both injection co-ordinates and the priming solution, the AAV2 were replaced with the new AAV5. This was another attempt to increase viral spread and reporter protein expression (*Chapter 6, AAV Serotypes*). These new viruses express either dTomato (AAV-*Cre*$^{+}$) or mCherry (AAV-*Cre*$^{-}$) red reporter proteins.

6.8 Troubleshooting Phase IV: Priming Solution

With the following changes to the original protocol: switching from a 25g needle to a glass micropipette, changing the syringe priming solution to mineral oil, using a new AAV serotype (AAV5), and adjusting injection co-ordinates – the surgery injection finally showed expression of vector reporter protein in the VTA (**Figure 6.8.1.).**

With proof that the surgery injection protocol will transfect neurons in the VTA with AAV5, an experimental cohort for phenotyping was generated.

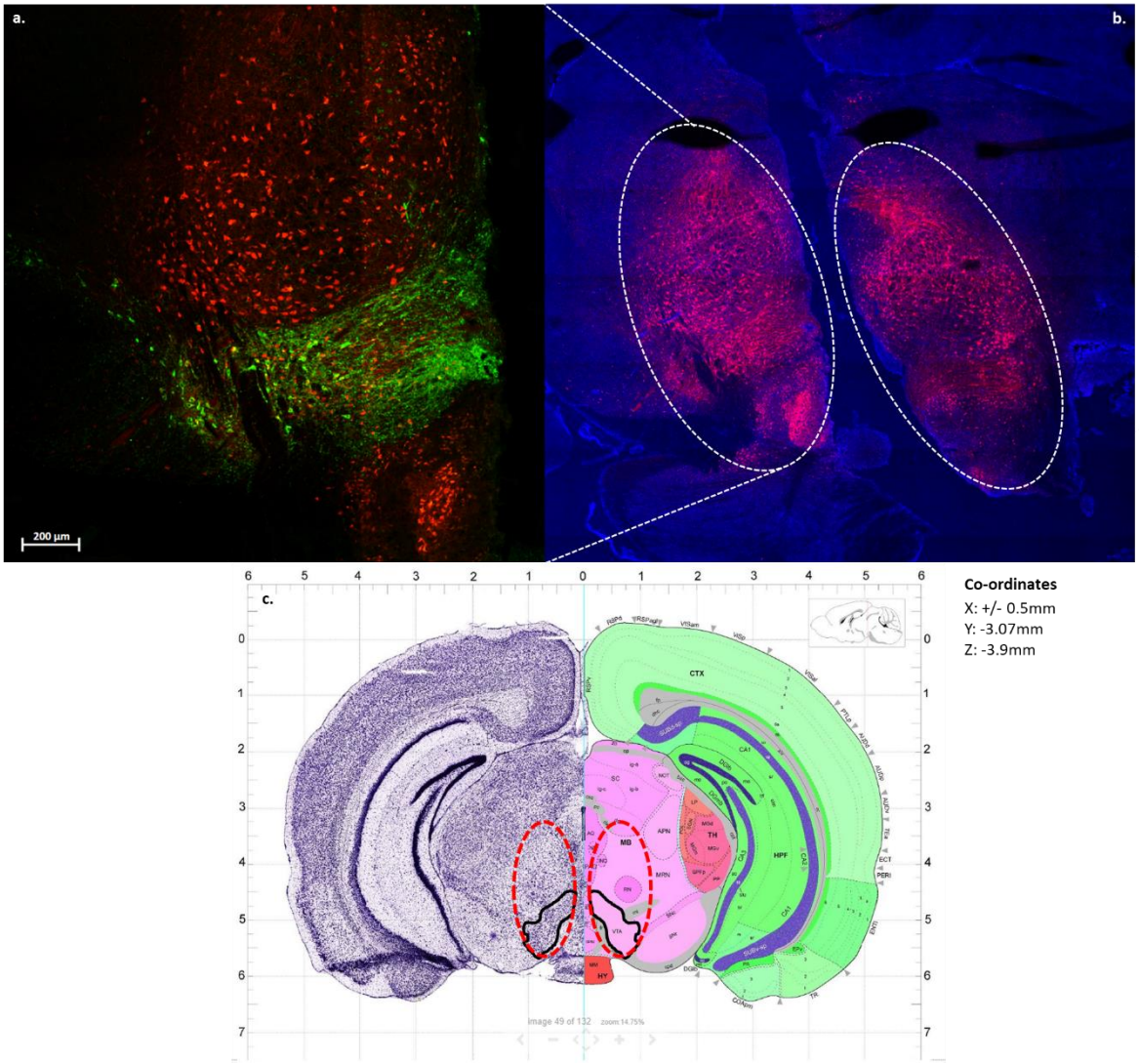

Figure 6.8.1. Images showing injection sites after multiple troubleshooting steps (a) transfected neurons expressing red mCherry reporter protein, and dopaminergic neurons of the VTA stained green, x20 magnification tiled image **(b)** Red mCherry and blue DAPI x10 tiled image of viral transduction from the injection **(c)** coronal section map showing the location of viral transduction in a red dotted outline, encompassing the VTA which is outlined in solid black (image modified from the Allen Brain Atlas (Lein, Hawrylycz et al. 2007)). New co-ordinates now used for viral injection included.

6.9 Immunofluorescent proof of injection site in experimental cohort

Post-mortem immunofluoresent staining and imaging was carried out on surgical cohort mice that survived at least 14 days post-surgery to prove accurate viral solution injection and effective transduction of viral vector (**Figure 6.9.1.**). Sections were stained with tyrosine hydroxylase antibody – a marker for dopaminergic centres – to investigate co-expression of tyrosine hydroxylase and viral fluorecent reporter proteins: either dTomato (AAV-*Cre*$^{+}$) or mCherry (AAV-*Cre*$^{-}$).

In the final surgical cohort, co-expression of viral vector reporter proteins and tyrosine hydroxylase was found, demonstrating that viral vectors were effectively transduced and expressed in dopaminergic neurons in the VTA and SNc, and therefore expression of *Cre* in AAV-*Cre*$^{+}$ injected mice.

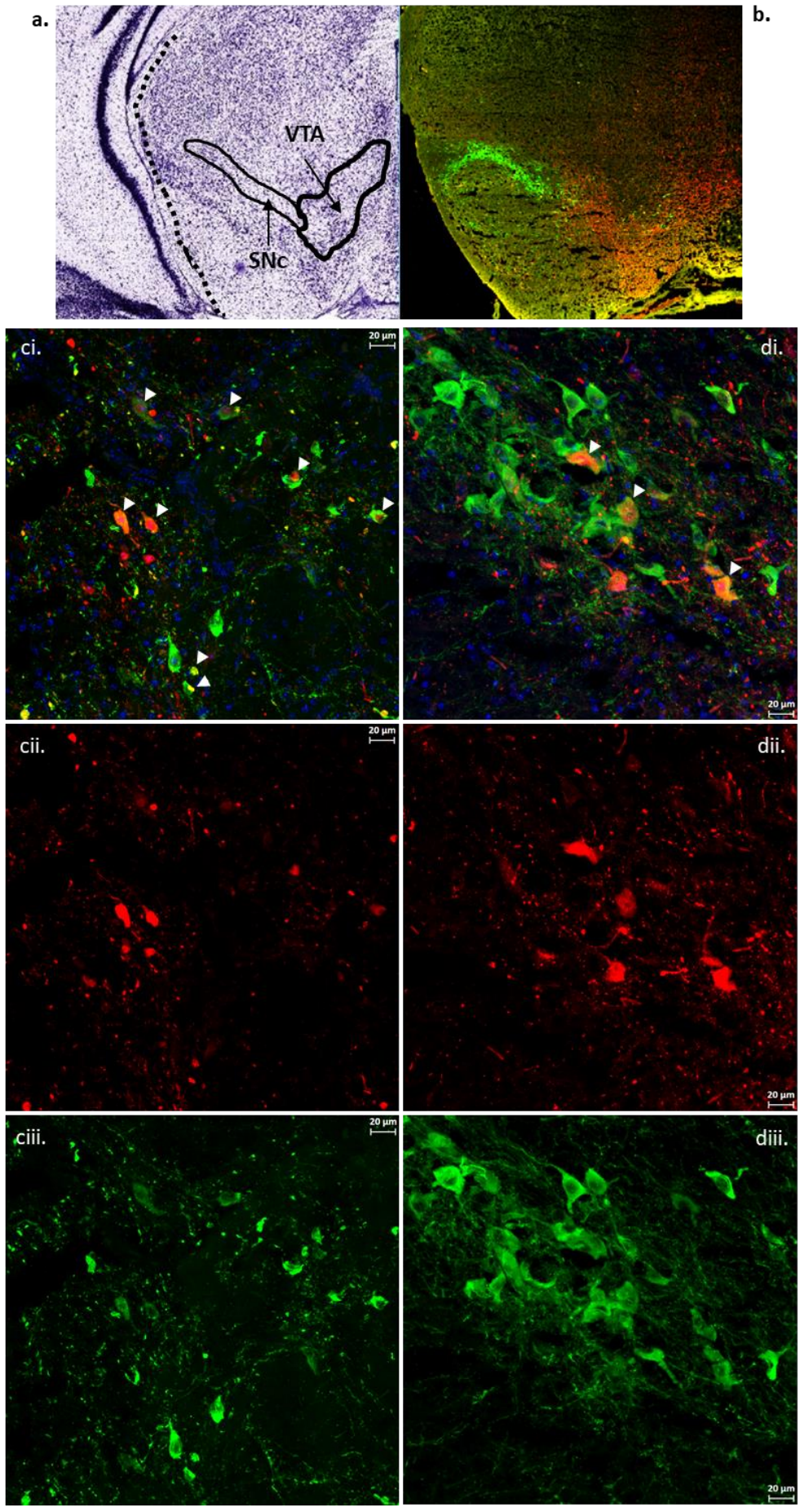
a.
b.
VTA
SNc
ci.
di.
cii.
dii.
ciii.
diii.
20 µm

Figure 6.9.1. Proof of injection accuracy and viral vector expression representative immunofluorescent confocal images of stained AAV-*Cre*$^{+}$-injected brain sections. Green fluorescence showing tyrosine hydroxylase – marker for dopaminergic centres (VTA and SNc), red fluorescence showing activity of injected virus via expression of dTomato fluorescent reporter protein. (a) modified image from the Allen Brain Atlas (Lein, Hawrylycz et al. 2007) labelling morphology and location of dopaminergic centre targets VTA and SNc; (b) x20 magnification tiling image of AAV-*Cre*$^{+}$ brain section; (ci) x20 magnification image of florescence in the VTA, showing co-expression of tyrosine hydroxylase (green) and dTomato reporter protein (red); (cii) VTA dTomato expression only; (ciii) VTA tyrosine hydroxylase staining only; (di) x20 magnification image of fluorescence in the SNc, showing co-expression of tyrosine hydroxylase (green) and dTomato reporter protein (red); (dii) SNc dTomato expression only; (diii) SNc tyrosine hydroxylase staining only.

6.10 Surgical Cohort Phenotype

Unfortunately it was not possible to carry out the planned behavioural phenotyping pipeline (*Methods 2.3.)* as mice injected with AAV-*Cre*$^{+}$ exhibited multiple phenotypes that would not allow for regular behavioural tests (**Table 6.10.1.**) with stereotypic circling being the most confounding behaviour. Many behavioural tests measure ambulation and orientation as parameters for demonstration of other behaviours, and circling would interfere with those measurements.

All mice injected with AAV-*Cre*$^{+}$ virus were noted to display one or more of the following, before recording: adverse reaction/aggression to handling, head tilt, and/or stereotypic circling. The frequent sequential nature of head tilt and circling onset suggests that head tilt and circling behaviour are related, with the latter phenotype being more severe.

In addition to the confounding effect these adverse phenotypes had upon potential behavioural phenotyping, progression of these phenotypes led to several mice to be culled due to welfare concerns. Five female and two male AAV-*Cre*$^{+}$ injected mice were culled early. Onset of head tilt initially warranted cull due to Home Office licencing and welfare standards, as head tilt was classified as a welfare

Intracranial injection cohort post-surgery phenotype					
		Time Post-Surgery (Days)			
AAV-Cre	Sex	Biting/Reactive to handling	Head Tilt	Circling	Cull Point
-	F	-	-	-	-
-	F	-	-	-	-
-	F	-	-	-	-
-	M	-	-	-	4
-	M	-	-	-	-
-	M	-	-	-	-
-	M	-	-	-	-
-	M	-	-	-	-
-	M	-	-	-	-
+	F	7	-	-	7
+	F	-	15	-	15
+	F	15	-	14	18
+	F	-	20	20	20
+	F	16	-	15	23
+	F	17	-	14	-
+	M	-	19	20	21
+	M	66	58	58	66
+	M	-	20	21	-
+	M	17	12	23	-
+	M	62	-	55	-

Table 6.10.1. **Surgical cohort of injected *Zfhx3*$^{Flox/Flox}$ mice**, showing development of phenotype in days post-surgery, including early cull points due to welfare concerns. This includes cull points due to foot injuries.

concern. As increasing numbers of AAV-*Cre*$^{+}$ mice began exhibiting the same behaviour, the Home Office issued a temporary licence amendment to allow these mice to be kept, as head tilt was determined to likely be an experimental outcome.

However, despite the licence amendment many AAV-*Cre*$^{+}$ injected mice had to be welfare-culled due to severity of circling, or circling behaviour causing weight loss to below licence standards.

Since these mice were not suitable to be tested via same pipeline as the DAT-*Cre; Zfhx3*-Flox mice, they instead were recorded with ANY-maze software to

investigate activity and circling behaviour over 24 hours. Since peak viral vector expression is expected 7-14 days post-surgery, any phenotyping test would need to be carried out at least 14 days post-surgery. Most AAV-*Cre*$^{+}$ injected mice did not survive for ANY-maze recording, as they had to be culled for welfare concerns.

A non-neurological post-surgery effect was swollen or necrotic hind toes, with occasional digit loss (**Table 6.10.2.**). The cause of this effect was determined to be most likely due to the temperature of the heat mat being too high and causing burns. Placing a square of blue roll under the back feet of the mouse prevented further issues with hind toes. This led to one premature welfare cull, which was a *Cre*$^{-}$ male with both hind feet having been burned – the singular *Cre*$^{-}$ mouse with a premature cull point marked in the table (**Table 6.10.1.**).

Intracranial injection cohort post-surgery adverse effects				
AAV-Cre	Sex	Surgery Comments	Adverse effect	Time Post-Surgery (Days)
-	F	none	necrotic/swollen toes (left hind)	1
-	F	none	necrotic/swollen toes (left hind)	2
-	F	none	-	-
-	M	none	necrotic/swollen toes (both hind)	1
-	M	none	necrotic/swollen toes (left hind)	3
-	M	none	-	-
-	M	foot protection	-	-
-	M	foot protection	-	-
-	M	foot protection	-	-
+	F	none	-	-
+	F	none	-	-
+	F	none	-	-
+	F	foot protection	-	-
+	F	foot protection	-	-
+	F	foot protection	-	-
+	M	none	-	-
+	M	none	-	-
+	M	none	-	-
+	M	foot protection	-	-
+	M	foot protection	-	-

Table 6.10.2. **Surgical cohort of injected *Zfhx3* Flox mice**, showing development of foot and toe injuries post-surgery, including early cull points due to welfare concerns.

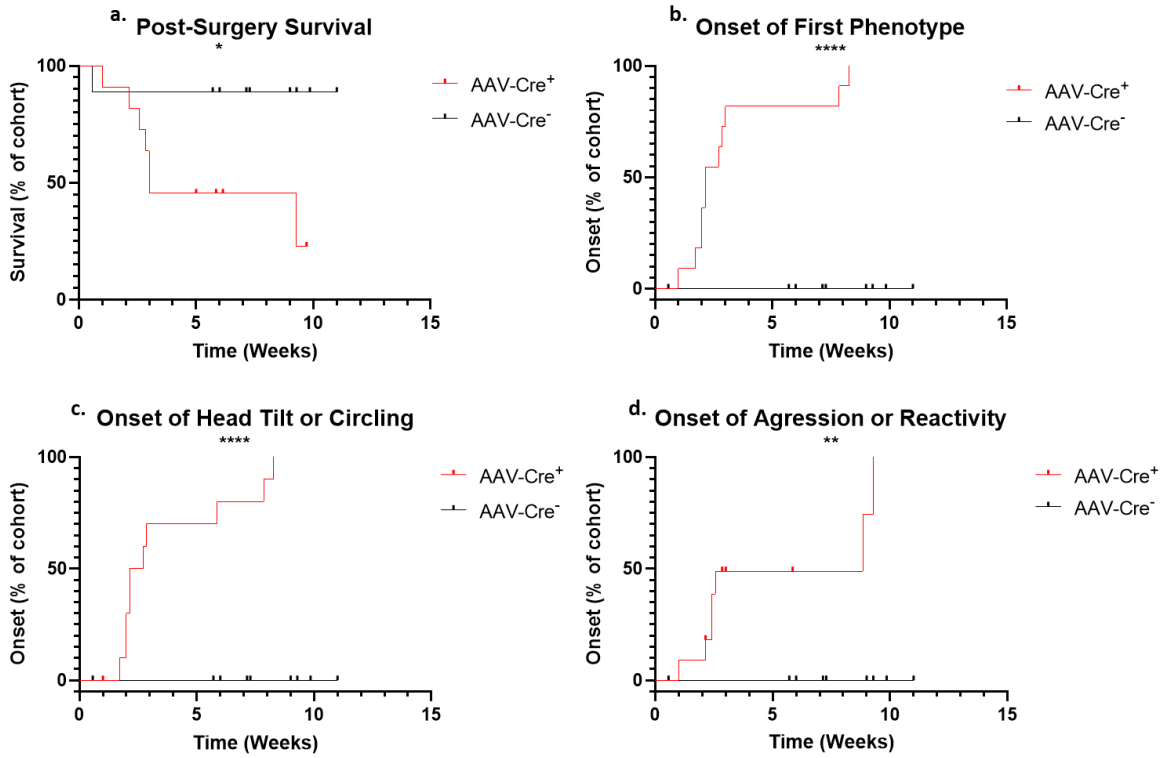

Figure 6.10.1. Survival curves of early welfare culls, and phenotype onset in the surgical cohort Significance is represented by: * $p \leq 0.05$; ** $p \leq 0.01$; and **** $p \leq 0.0001$.

Analysis of post-surgery phenotypes was performed, excluding the incidence of necrotic toes as it is unlikely that this was caused by viral vector expression.

Analysis was carried out of the latency following injection at which these occurred: reactivity to handling, head tilt, circling, and premature welfare cull point. In all cases, mice injected with *Cre*$^{+}$ virus showed a significant and progressive phenotype in these parameters (**Figure 6.10.1.**).

In post-surgery "early" culls (culls before ANY-maze recording) *Cre*$^{+}$ injected mice were culled at a significantly higher rate (a; p=0.0340) due to welfare concerns. Combining all observed phenotypes (excluding necrotic toes), *Cre*$^{+}$ mice expressed significantly more post-surgery behavioural phenotypes than *Cre*$^{-}$ injected mice (b; p<0.0001). As it is likely that head tilt is a precursor to circling,

and both phenotypes were on occasion observed as initiating on the same day, they are combined here – with significantly more *Cre*$^{+}$ mice developing head tilt/circling post-surgery (c; p <0.0001). When handled during welfare checks and cage changing, *Cre*$^{+}$ mice were observed to show significant rates of aggression or excessive reactivity to the handler, compared to *Cre*$^{-}$ mice (d; p= 0.0024). Survival curves analysed using Mantel-Cox test.

6.11 ANY-maze recording and analysis

Due to the distinct sexual dimorphism seen in the behavioural phenotype of the DAT-*Cre; Zfhx3*-Flox mice, analysis of activity and circling was sex differentiated to allow for comparison. However, analysis of female mice was excluded as only one *Cre*$^{+}$ female mouse survived to recording. All results shown are from male mice only. Recording took place over 24 hours, and behaviour was analysed using ANY-maze video tracking software.

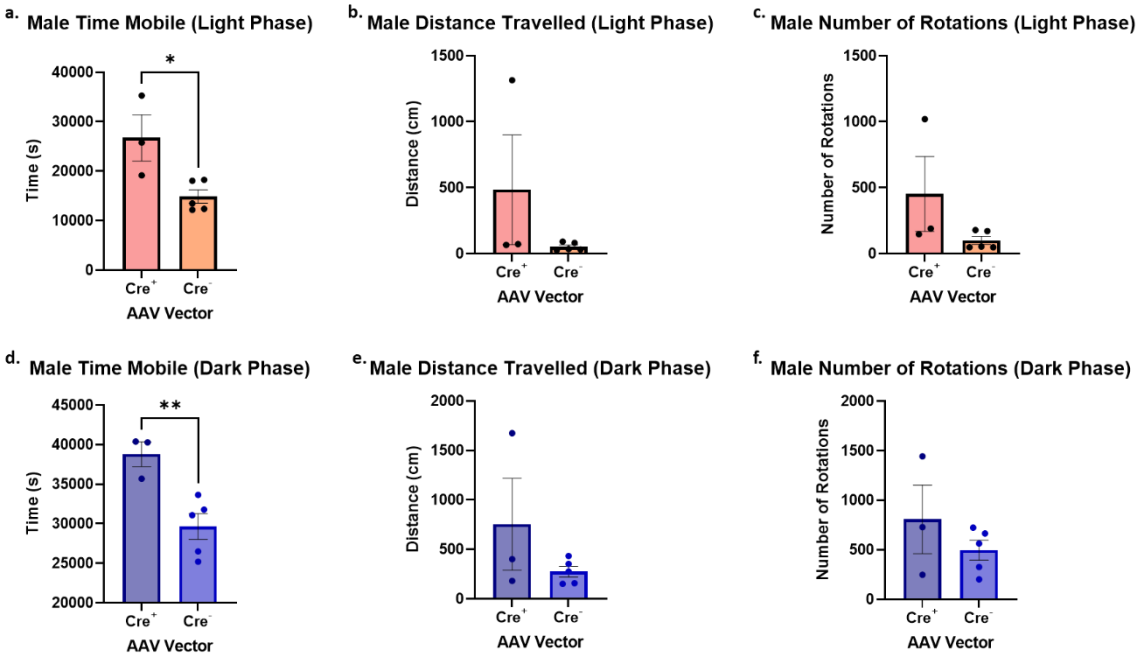

Figure 6.11.1. Male parameters of circling behaviour during light and dark phase showing time spent mobile during (a) light and (d) dark phases; distance travelled during (b) light and (e) dark phases; and number of rotations made while circling, during (c) light and (f) dark phases. Significance is represented by: * $p \leq 0.05$; ** $p \leq 0.01$.

(**Figure 6.11.1.**) AAV-*Cre*$^{+}$ injected males were mobile for significantly more time during both the light phase (ZT0-12) (a; p=0.0219) and the dark phase (ZT13-24) (d; p=0.0095) than AAV-*Cre*$^{-}$ control males. However, AAV-*Cre*$^{+}$ males did not show a significant difference in distance travelled (b; p= 0.2052)(e; p= 0.2181) nor in number of rotations in their circling (c; p= 0.1468)(f; p= 0.3199) in either the light or dark phases. Statistical analysis was performed using unpaired t-test. Data are shown as mean ± standard error of mean.

From qualitative observation, the primary activity of AAV-*Cre*$^{+}$ mice was stereotypic circling behaviour. There was no significant difference in number of rotations between AAV-*Cre*$^{+}$ and AAV-*Cre*$^{-}$ males, however when investigating

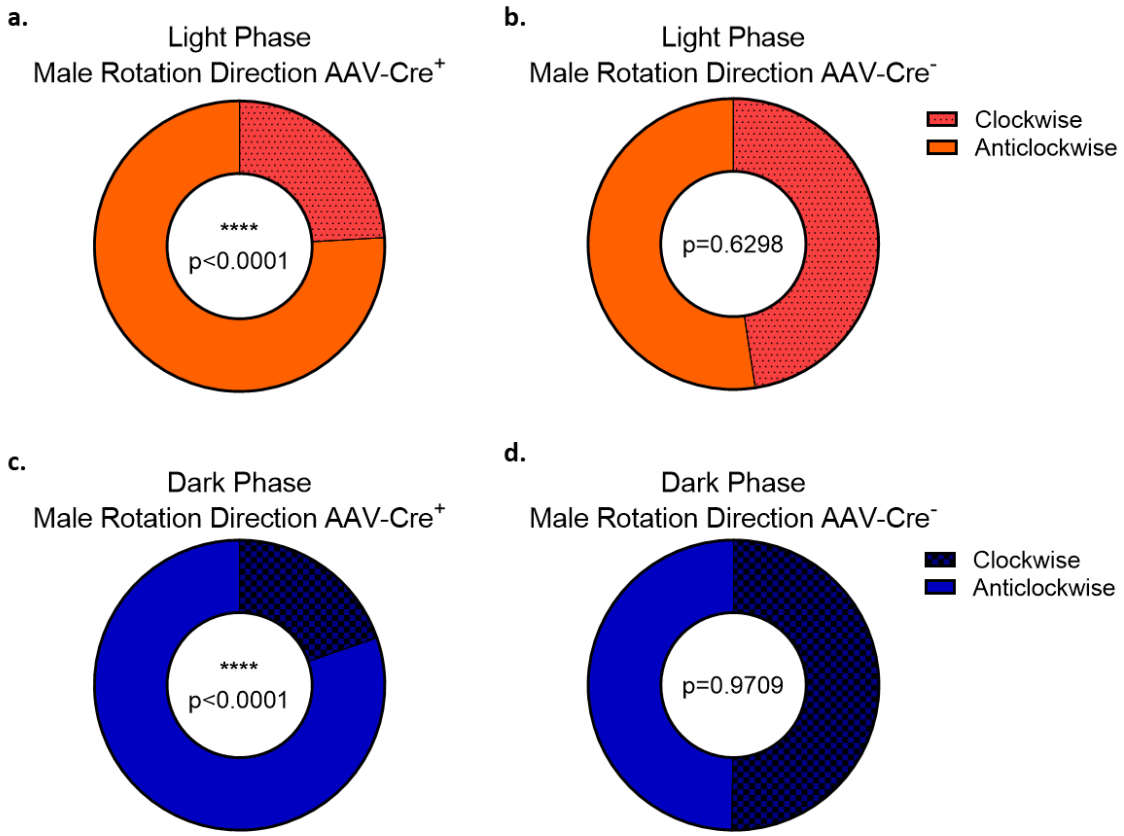

Figure 6.11.2. Male preference in circling rotation during light and dark phases showing preference in direction of rotations when circling, during the light phase: (a) AAV-*Cre*$^{+}$, (b) AAV-*Cre*$^{-}$; and during the dark phase: (c) AAV-*Cre*$^{+}$, (d) AAV-*Cre*$^{-}$. Significance is represented by: **** $p \leq 0.0001$.

circling behaviours – specifically rotation directionality – it can be seen that AAV-*Cre*$^{+}$ mice overwhelmingly prefer to circle in an anticlockwise direction (**Figure 6.11.2.**) during both light and dark phases. In the light phase, AAV-*Cre*$^{+}$ males circle anticlockwise in 75.94% of their rotations (a; $p<0.0001$) while AAV-*Cre*$^{-}$ males circle anticlockwise 52.41% of rotations (b; $p= 0.6298$). This is mirrored in the dark phase, with AAV-*Cre*$^{+}$ males circling anticlockwise for 80.26% of their rotations (c; $p<0.0001$) and AAV-*Cre*$^{-}$ circling anticlockwise for 49.82% of their rotations (d; $p= 0.9709$). Statistical analysis was performed using chi^{2} test, and data presented as parts of whole.

Post-analysis consideration of the data reveals a consistent AAV-*Cre*$^{+}$ outlier in many ANY-maze measured parameters (**Figure 6.11.1.**). This mouse was the longest-surviving post-surgery AAV-*Cre*$^{+}$ male – ZFHX3-FLOX-B6-IC/90.1a - and expressed a more severe phenotype than either the control or the other AAV-*Cre*$^{+}$ males (**Table 6.11.1**.).

Light								
Animal ID	Sex	AAV	Weeks Post-Surgery	Time Mobile (s)	Distance (cm)	Rotations	Clockwise	Anticlockwise
ZFHX3-FLOX-B6-IC/90.1i	M	CRE^{+}	9.43	35288.3	1314.904	1019	214	805
ZFHX3-FLOX-B6-IC/91.2e	M	CRE^{+}	5.86	25769.6	65.111	189	63	126
ZFHX3-FLOX-B6-IC/88.3f	M	CRE^{+}	5.57	19164.2	72.279	147	49	98
Dark								
Animal ID	Sex	AAV	Weeks Post-Surgery	Time Mobile (s)	Distance (cm)	Rotations	Clockwise	Anticlockwise
ZFHX3-FLOX-B6-IC/90.1i	M	CRE^{+}	9.428571429	40394.4	1673.805	1442	223	1219
ZFHX3-FLOX-B6-IC/91.2e	M	CRE^{+}	5.857142857	35671.5	180.975	247	75	172
ZFHX3-FLOX-B6-IC/88.3f	M	CRE^{+}	5.571428571	40275.6	401.238	728	179	549

Table 6.11.1. Male measurements of activity and circling behaviour during light and dark phase highlighting the outlying parameters of the longest surviving AAV-*Cre*$^{+}$ post-surgery mouse - ZFHX3-FLOX-B6-IC/90.1a.

To elucidate the outlying behaviour of mouse 90.1a, sleep (inactivity) and distance travelled were plotted over the 24 hours of recording, with each AAV-*Cre*$^{+}$ plotted individually against the AAV-*Cre*$^{-}$ group (**Figure 6.11.3.**). This longest-surviving AAV-*Cre*$^{+}$ mouse sleeps less and travels more than AAV-*Cre*$^{-}$ and other AAV-*Cre*$^{+}$ mice – in both the light and dark phases.

a.

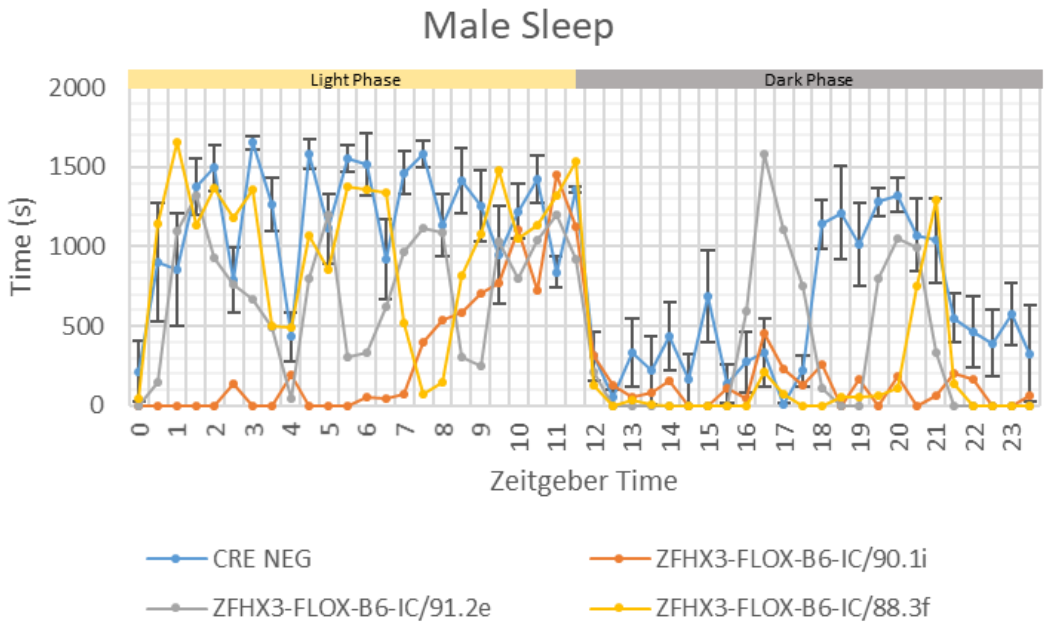

b.

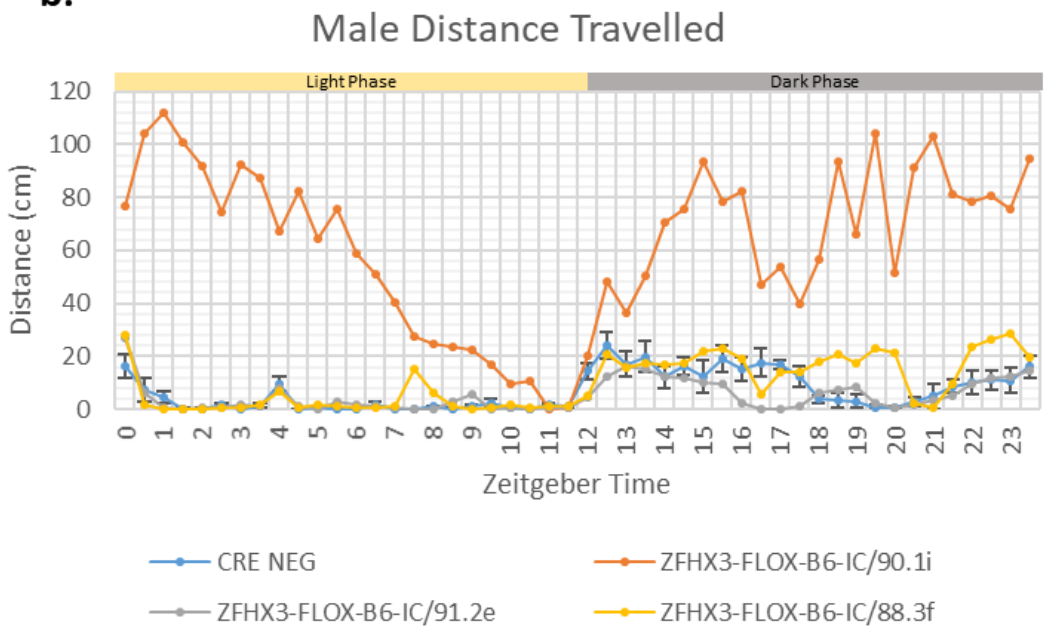

Figure 6.11.3. Sleep and distance travelled parameters with AAV-*Cre*$^{+}$ mice individually plotted
measurements of (a) sleep and (b) distance travelled over 24 hours of recording, with AAV-*Cre*$^{-}$ mice grouped and each AAV-*Cre*$^{+}$ mouse plotted individually for each behavioural parameter. (c) Table displaying time post-surgery that recording occurred for AAV-*Cre*$^{-}$ mice

c.

AAV-Cre^{+} Males	
Animal ID	Weeks Post-Surgery
ZFHX3-FLOX-B6-IC/90.1i	9.43
ZFHX3-FLOX-B6-IC/91.2e	5.86
ZFHX3-FLOX-B6-IC/88.3f	5.57

6.12 Discussion

The aim of this study was to generate a surgical cohort of *Zfhx3* knockout mice to compare to the DAT-*Cre; Zfhx3*-Flox behavioural cohort - where adult-only non-specific neuronal knockout of *Zfhx3* in dopaminergic centres in the midbrain, could be compared to dopamine-circuit specific *Zfhx3* knockout from E13.

Qualitative observation of AAV-*Cre*$^{+}$-injected mice revealed that these knockout mice displayed a severe phenotype of heightened locomotor activity in the form of stereotypic circling, and aggression when handled. Whether AAV-*Cre*$^{+}$ mice are aggressive to other mice is unknown, as mice that undergo intracranial injection are single-housed post-surgery.

Due to the nature of the circling exhibited by the AAV-*Cre*$^{+}$ mice, behavioural assessment could not be completed according to the original experimental plan - where surgical cohorts were to undergo the same phenotyping pipeline as the DAT-*Cre; Zfhx3*-Flox mice, to allow for direct comparison. Behavioural phenotyping tests used for DAT-*Cre; Zfhx3*-Flox characterisation often rely on measurements of ambulatory behaviour as parameters of other behaviours. The severity of the circling behaviour dictated that these measurements would be confounded, therefore non-comparable to behavioural phenotypes exhibited by DAT-*Cre; Zfhx3*-Flox mice.

In addition, the severity of behavioural phenotypes exhibited by AAV-*Cre*$^{+}$ mice meant many mice had to be culled for welfare reasons, and consequently only male mice could be studied in ANY-maze recording. This further limits the effectiveness of the AAV-injected mice as a comparison to the DAT-*Cre; Zfhx3*-

Flox cohort, as there is prominent sexual dimorphism in the behavioural phenotype of the latter.

Through characterisation of activity and circling behaviour via ANY-maze software analysis of recordings, it was found that AAV-*Cre*$^{+}$ mice exhibited significantly more time engaging in locomotor activity (non-specific to circling) during both the light and dark phases, although distance travelled and number of rotations in circling behaviour showed no significant difference to AAV-*Cre*$^{-}$-injected mice. The lack of significance in differences in circling-specific parameters between AAV-*Cre*$^{+}$ and AAV-*Cre*$^{-}$ mice could be due to the fact that circling mice often lost weight to below licence standards shortly after initiating circling behaviour and had to be welfare-culled – *ipso facto* not surviving for ANY-maze recording. Therefore, the AAV-*Cre*$^{+}$ mice in recording were possibly yet to exhibit the severe circling phenotype that was eventually observed in all AAV-*Cre*$^{+}$ mice post-surgery.

However, the significant difference seen in time engaging in locomotor activity implies that AAV-*Cre*$^{+}$ mice exhibit non-specific hyperactivity before onset of stereotypic circling, and circling may be an end-stage expression of post-surgery deleterious behavioural phenotypes.

When differentiating direction of any circling behaviour, AAV-*Cre*$^{+}$ mice displayed a strong preference for circling anticlockwise (leftprone) while AAV-*Cre*$^{-}$ mice displayed no preference when they circled in their cage.

Individual consideration of AAV-*Cre*$^{+}$ mice led to the discovery of an outlier (90.1i), with a more severe phenotype than the other AAV-*Cre*$^{+}$ mice. 90.1a was the longest-surviving post-surgery AAV-*Cre*$^{+}$ male, being recorded at approximately 9 weeks post-surgery while the other two AAV-*Cre*$^{+}$ mice were approximately 6

weeks post-surgery at time of recording. An implication of this result is that severity of behavioural phenotypes are progressive post-knockout of *Zfhx3* in the midbrain of adult mice. This mouse exhibited a far greater number of rotations, and travelled further, than either AAV-*Cre*$^{-}$ or other AAV-*Cre*$^{+}$ mice in recording, lending credence to the theory that stereotypic circling behaviour is an end-stage to non-specific hyperactivity in AAV-*Cre*$^{+}$ mice.

Despite the inability of the AAV-injected mice to proceed with the common phenotyping pipeline with the DAT-*Cre; Zfhx3*-Flox experimental cohort, some comparisons can be made between the two cohorts.

The behavioural phenotypes expressed by AAV-*Cre*$^{+}$-injected mice – hyperactivity, head tilt, stereotypic circling, and aggression – are stronger, and are more detrimental to welfare, than the phenotypes expressed by DAT-*Cre; Zfhx3*-Flox mice.

Both mouse cohorts express aggression-like behaviours, with AAV-*Cre*$^{+}$ mice attempting to bite handlers, and old male DAT-*Cre; Zfhx3*-Flox mice displaying significant social dominance over their wildtype counterparts.

It is possible that both methods of knockout cause progressive phenotypes, with one AAV-*Cre*$^{+}$ male's hyperactivity and stereotypic circling behaviour increasing in severity in proportion to time since surgery, and the changes seen in behavioural phenotypes in both males and females in DAT-*Cre; Zfhx3*-Flox mice between the young and old cohorts.

The contrast in behavioural phenotype profile could be due to two factors, as previously stated: that *Zfhx3* knockout in AAV-*Cre*$^{+}$-injected mice is in adulthood-only with no developmental effect, and knockout was non-specific and targeted all

neurons around the injection sites in the midbrain. This is opposed to DAT-*Cre; Zfhx3*-Flox mice where *Zfhx3* is knocked out from E13, and only in dopaminergic neurons. It is not possible to definitively conclude which factors could be contributing to the contrast seen in phenotype profile, however this will be explored in the *Discussion* chapter.

While this study assumes any significant differences in behaviour are due to the knockout of *Zfhx3* using *Cre*-expressing AAV, there are other possibilities as to what causes these differences. AAVs are known to be cytotoxic and immunogenic, where injection of AAV can lead to death of transduced cells and tissue damage (Ertl 2022). Differences in cytotoxicity and immunogenicity between Cre^- and Cre^+ viral solutions could lead to cell death in the midbrain and the significant differences in behaviour seen here. *Cre* itself has also been shown to be cytotoxic, causing apoptosis through genetic instability caused by its function as a recombinase enzyme (Silver and Livingston 2001). For example, instability can be caused by cleavage at 'pseudo-*lox*' sites found naturally occurring in the chromosome, causing multiple breaks in the DNA. Therefore the expression of *Cre* in one mouse cohort could be causing the observed behavioural phenotype through damage in the cells in the midbrain, as opposed to *Zfhx3* knockout. The absence of images demonstrating both the reduced expression of ZFHX3, and the integrity of the cells, means it is impossible to make the distinction at this time.

7
Discussion

7

Discussion

Throughout this chapter, there are multiple technical limitations that need to be addressed when interpreting this data. Throughout the study, n-numbers were low – therefore analysis lacked statistical power, when claiming statistical significance. This was due to multiple reasons. In the DAT-*Cre* lines of inquiry (*Chapters 4 and 5*) numbers were low due to: breeding (homozygous knockouts did not follow Mendelian principles and were born less frequently); COVID caused large cohorts of mice to be culled due to welfare concerns; and personal illness led to cohorts aging and splitting the study into older and younger mice (although this added another parameter for analysis). In the surgery mice (*Chapter 6*) the n-number was low for ANY-Maze recording due to the fatal phenotype exhibited by Cre^{+} virus-injected mice, meaning only a few mice made it through to testing – including only one female mouse, so sexual dimorphism in behaviour was impossible to study. It is worth noting this when reading the interpretation of results in this chapter.

7.1 Dopaminergic Region ZFHX3 Expression

ZFHX3 is highly expressed in the developing brain. It is essential to the process of neuronal cell differentiation, and brain region-specific developmental deletion causes loss of specialised neuron identity in those regions (Jung, Kim et al. 2005, Wilcox, Bains et al. 2021). Postnatal expression however is sparse, and highly localised to specific regions. One of those regions is the SCN, and another is in

the midbrain, specifically the VTA and SNc (Ishii, Kawaguchi et al. 2003, Lein, Hawrylycz et al. 2007). In *Results I*, we sought to characterise the levels and pattern of expression of ZFHX3 in the VTA and SNc of the wildtype mouse brain – i.e. what proportion of dopaminergic cells in these regions express ZFHX3, and how much of ZFHX3 expression is localised to dopaminergic cells in the mouse brain. In this study, the number of cells in each region expressing ZFHX3, and the pattern of expression among cells, showed no significant sexual dimorphism – a retroactive analysis carried out due to the sexual dimorphism shown in the behaviour of conditional knockout mice DAT-*Cre*; *Zfhx3*-Flox. We found that ZFHX3 is highly expressed in the dopaminergic neuron population in these regions – with approximately 91-95% of dopaminergic neurons in the VTA and 88-91% in the SNc expressing ZFHX3. ZFHX3 was also expressed in additional cell types in these regions – with approximately 56-59% of non-dopaminergic cells in the VTA and 63-71% in the SNc expressing ZFHX3. The high percentage of $ZFHX3^{+}$ dopaminergic neurons indicates that it may play an important role in these neurons, and possibly in the dopaminergic system as a whole. ZFHX3 is also expressed in other cell types in these regions, and attempts were made to identify other neuron identities – however difficulties with antibody staining meant that only dopaminergic neurons could be reliably identified. There is also evidence to suggest that ZFHX3 is expressed in non-neuronal cells in these regions, as the SNc has only dopaminergic neurons, yet non-dopaminergic $ZFHX3^{+}$ cells are still observed. This is supported by evidence from the Human Protein Atlas, which reports expression of *Zfhx3* mRNA in glial cells, most prominently in astrocytes and microglial cells (Karlsson, Zhang et al. 2021).

While no sexual dimorphism was observed in the proportions of cell types in each region expressing ZFHX3, sexual dimorphism was observed in comparisons between the VTA and SNc in each sex. In female mice, there is a significantly greater proportion of ZFHX3^{+} cells in the VTA than in the SNc, which is not seen in males. Conversely, in males there is a trend towards a greater proportion of ZFHX3^{+} cells having a dopaminergic identity in the VTA compared to the SNc, which is not seen in females. This data suggests: that ZFHX3 plays a greater role in the VTA of females compared to the SNc, in all cell types in the region; and that ZFHX3 plays a greater role in dopaminergic neurons over other cell-types in the VTA of males over the SNc. These results could give some precedence to the sexual dimorphism seen in both the behavioural phenotype and molecular changes seen in the DAT-*Cre*; *Zfhx3*-Flox mice.

Attempts were made to more thoroughly define the distribution of expression of ZFHX3 using antibodies for GABA-ergic and glutamatergic neuron identity markers, however these attempts are yet to give consistent, reliable results. More time is needed to develop a method for each of these antibodies, and to add antibodies for glia cell identity markers, in order to generate a more thorough picture of ZFHX3 expression. Knowledge of the expression pattern of *Zfhx3* over the different neuronal sub-populations in these regions could open new inquiries into the gene's role in different neuronal circuits.

7.1.1 Auditory Cortex Expression

Contrary to ISH data from the Allen Brain Atlas, immunofluorescent staining of coronal brain sections with ZFHX3 antibody revealed expression in 54-58% of all

cells in the auditory complex, with no significant difference between females and males. *Zfhx3* mRNA upregulation was seen in the superior temporal gyrus (homologous region to the murine auditory complex) of schizophrenic patients, suggesting that *Zfhx3* may play a role in the dysfunction of auditory sensory processing seen in schizophrenic patients. This is currently being further investigated using a cortex-specific conditional knockout mouse line of *Zfhx3*: CAMKII-*Cre*; *Zfhx3*-Flox.

7.2 DAT-*Cre*; *Zfhx3*-Flox

In order to examine the developmental and adult function of *Zfhx3* in the dopaminergic system, a Cre-Lox mouse line was generated - where dopamine-specific DAT promotor drives the expression of *Cre* in dopaminergic neurons from E13 onwards, causing deletion of *Zfhx3* via recombination of LoxP sites flanking exons 7 and 8 of the *Zfhx3* gene (Zhuang, Masson et al. 2005, Sun, Fu et al. 2012). These mice were characterised through a dopamine function-specific behavioural phenotyping pipeline, followed by molecular analysis using immunofluorescence and RNA-Seq.

7.2.1 Behavioural Phenotyping

The behavioural phenotyping pipeline for the DAT-*Cre*; *Zfhx3*-Flox line focused on assessing behaviours associated with dopamine function and disease, as discussed in *Introduction*. Both males and females were assessed, as well as two

different age cohorts – to account for both the sexual dimorphism and age-related progression of dopamine-based diseases.

It is unfortunately uncommon for animal model studies to separate analysis by sex. Therefore in this discussion, many animal model comparisons have been made without taking sex into account despite the sexual dimorphism in behaviour seen in the DAT-*Cre*; *Zfhx3*-Flox mice.

7.2.1.1 Anxiety

Anxiety is a complex emotional state found in both humans and animals, which in summary is the psychological and physiological state achieved when under the perceived threat of harm or death (Steimer 2002). There is ample scientific basis to using animals to model anxiety. The phylogenetic argument of anxiety proposes that anxiety has evolutionary importance, and is thus conserved across species (Stein and Bouwer 1997), and it is the “misfiring” of these primitive anxiety-like responses that are the basis of anxiety and panic symptoms/disorders . Population validity also argues that an animal model is valid if the occurrence of specific phenotype within an (epi)genetically heterogeneous population of the animal matches that of the observed occurrence in humans (Schmidt 2011). This has been observed in mouse models of anxiety, for example in mouse models of post-traumatic stress disorder (Cohen, Zohar et al. 2004).

Ethologically relevant assays are used in animal models to induce an anxiety-like response by submitting the subject to a species-relevant threat (e.g. predators) or stress (e.g. novel objects) (Lezak, Missig et al. 2017). Two classical models of

anxiety modelling in mice are the assessment of ‘approach versus avoidant’, and defensive behaviours.

Approach-avoidant paradigms include tests such as open field and light-dark box. They exploit the two drives of mice to both explore through their environment, while also wanting to avoid open and bright areas to evade predation (La-Vu, Tobias et al. 2020). These behaviours can be measured by assessing ambulation within arenas that exploit these two drives simultaneously.

Defensive behaviour paradigms use a cue – conditioned or unconditioned – to project the presence of a predator, eliciting an anxious response. Rodents can be conditioned to anticipate an electric shock after a long-duration tone, which has been shown to be an anxiety-specific test and excludes the fear response (Waddell, Morris et al. 2006). Defensive tests can also exploit the innate fear of predators - for example by using cat odour (Zangrossi and File 1992). These behaviours can be measured using freezing or startle responses. In this study, the anxiety-specific section of the pipeline utilises the lower-stress ‘approach versus avoidance’ classical paradigm. The behavioural phenotyping pipeline for this mouse line is comprised of multiple test types, which increase along a stress gradient from the first (open field) to last (fear conditioning) test. Defensive behaviour tests such as a foot-shock test would be high-stress, and would be inappropriate to have early in the pipeline as it could confound later tests, especially other assessments of anxiety. However, this information is relevant later when considering the response of homozygous males to the Fear Conditioning foot-shock test.

- *Open Field*: The open field test was first devised as a measurement of emotionality in rodents through measuring their levels of defecation and urination in an open field maze (Hall 1934, as cited by (Seibenhener and Wooten 2015)). It has since been shown that open field data – from observing ambulation, rearing, stretching, sniffing, and defecation - provide a complex representation of anxiogenic behaviour in mouse models (Carola, D'Olimpio et al. 2002). In this study, ambulation between and within the periphery and centre zone were used as measurements of anxiogenic behaviour.

- *Light-Dark Box*: The Light-Dark chamber box test was originally developed to study the effect of anxiolytics on rodents. The test assesses anxiety by measuring the conflict of the exploratory drive and the aversion to brightly lit arenas exhibited by rodents (Crawley 1985). It consists of a dark chamber and an aversive brightly-illuminated chamber conjoined together. Its effectiveness was demonstrated by the findings of Costall et al, that administering anxiolytic drugs increased exploratory behaviour in the light zone, while anxiogenic agents decreased this behaviour (Costall, Jones et al. 1989). In this test, transitions between and ambulation within the light and dark chambers are measured, including the small ‘entry zone’ defined around the opening between the chambers.

Both female and male homozygous knockout mice, of both younger and older age cohorts, demonstrated significant differences in anxiety-like behaviours compared to their wildtype counterparts. The anxiety tests in this pipeline assessed the ‘approach-avoid’ instinct, specifically assessing the conflict in the natural curiosity to explore versus the instinct to avoid bright/open spaces and remain covered.

Both young combined-sex and young female homozygotes show an attenuation of their exploratory drive, walking in shorter bouts while in the open field. Young female homozygotes also demonstrate impulsive behaviour in the light dark box, where they spend less time in the risk-assessing entry zone between the light and dark zones. Older female homozygotes show progression of these behaviours, exhibiting them across a greater number of parameters in the same tests. They generally avoid the centre zone in the open field, and show fewer transitions between zones in the light dark box, both of which demonstrate an attenuation in their overall exploratory behaviour. However, the older females also exhibit impulsive behaviours, similar to their younger counterparts, having a shorter latency to enter the centre zone in the open field. Overall, combined-sex and female homozygous knockouts show possible anxiety-like behaviour, with female homozygotes displaying apparent age progression of this phenotype, plus the inclusion of impulsive behaviours. Anxiety is seen in both Parkinson's and Huntington's disease, with symptoms becoming more severe as the disease progresses, and presents more prevalently in female patients (Broen, Leentjens et al. 2018, Hentosh, Zhu et al. 2021). Non-progressive anxiety is also a feature of schizophrenia, and is more pronounced in female patients (Goldstein, Seidman et al. 1998). Impulsive behaviour is also a symptom of Parkinson's and ADHD in patients of both genders (Austerman 2015, Ruitenberg, Wu et al. 2018). The attenuation of the exploratory drive seen in homozygous mice could also be linked to apathy seen in schizophrenic patients (American Psychiatric Association 2013).

Younger male homozygotes show the opposite anxiety phenotype to females, showing a possible attenuated anxiety response and a stronger exploratory drive to their wildtype counterparts. They spend more time exploring the centre zone of

the open field. Older male homozygotes however do not exhibit this same behaviour. Impulsive behaviours are seen more prevalently in males with both Parkinson's and ADHD, however the observed normalisation of these behaviours with age seen in this mouse model is unexplained (Bhattacharjee 2018, Slobodin and Davidovitch 2019).

Mouse models for Parkinson's disease exhibit anxiogenic behaviour. Both 6-hydroxydopamine (6-OHDA) and paraquat (PQ) Parkinsonsian models - where intracranial injection of either toxin 6-OHDA or herbicide PQ causes dopaminergic neuronal loss in the midbrain - exhibited an increase in anxiogenic behaviours compared to sham controls (Campos, Carvalho et al. 2013). In knock-in Hdh(Q111) mice, a Huntington's disease mouse model, male mice exhibit progressive anxiety-like behaviours, however female mice do not (Orvoen, Pla et al. 2012).

7.2.1.2 Motor

Motor performance and co-ordination tests are of paramount importance in a phenotyping pipeline such as the one in this project, as many other behavioural tests rely on ambulation, orientation, and strength to demonstrate non-motor phenotypes in other tests (Deacon 2013). When testing motor function, the following parameters need to be considered: strength, locomotion, co-ordination, balance, and endurance (Justice, Carter et al. 2014) with tests ideally being able to challenge more than one of these parameters at once.

- *Gait Analysis (Mousewalker)*: The gait analysis test measures specific parameters that are unique to discussing gait, using unique terms that are

shared between both mice and humans. “Stance duration” refers to duration between heel strike (start of the step) and toe off (end of the step) of the same foot – measuring the time that the foot is on the walking surface. “Swing duration” is the counterpart to stance, measuring the time that the foot in question is in the air, off the walking surface (Silva and Stergiou 2020). In humans, stance duration accounts for 60% of the gait cycle duration, while swing comprises the remaining 40% (Blanc, Balmer et al. 1999). “Duty factor” usually only applies for bipedal locomotion (Fihl and Moeslund 2007), which is why for the mouse the duty factor has been divided into the front and the back two limbs for separate measurement. Duty factor describes the fraction of time in the gait cycle that each foot is on the walking surface (McNeill Alexander 2002).

Both old combined-sex and old female homozygotes display a possible suppression of locomotion with shorter walking bout durations in gait analysis. It can however also be argued that this is a further demonstration of their anxiety phenotype, therefore it is impossible to state with certainty that old combined-sex and old female mice have a true motor phenotype.

Male homozygous mice may be exhibiting more defined motor deficits, seen in both younger an older males, with no apparent progression in severity. In gait analysis, younger males show decreased walking speed, and increased hind limb stance time. A longer-duration hind limb stance means the duration between heel strike (start of the step) and toe off (end of the step) of the same foot – measuring the time that the foot is on the walking surface – is longer in the hind feet of the mouse. This could be the factor reducing the walking speed, with the mouse essentially ‘dragging’ its hind feet. Older males also show possible defects in their

gait, displaying a longer front limb swing duration, which is the counterpart to stance, measuring the time that the foot in question is in the air.

Motor function is heavily tied to the dopaminergic system, with typical motor function mediated by the nigrostriatal pathway – which involves the SNc innervating the striatum. Progressive motor deficits are seen in both Parkinson's and Huntington's disease, involving both movement co-ordination (including gait) and movement initiation (Roos 2010, Postuma, Berg et al. 2015). Notably, male Parkinson's patients are reported to have earlier onset of motor symptoms than female patients (Haaxma, Bloem et al. 2007).

Mouse models for both Parkinson's and Huntington's disease show motor deficits. Many rodent Parkinson's models induce the aggregation of α-synuclein - for example, multiple α-synuclein gene point mutations, and viral transduction of α-synuclein using adeno-associated/lentivirus. These models exhibit mild to moderate motor deficits, although not all show dopamine neuron degeneration (Konnova 2018). An extensively used Huntington's mouse model is the R6/2 line, which is transgenic for one copy of a human genomic fragment, containing: *HTT* promoter sequences, exon 1 of *HTT* and 200 bp of intron 1. This line develops motor deficits from as early as 5 weeks old, as huntingtin protein inclusion bodies form in the brain (Farshim and Bates 2018).

7.2.1.3 Memory

Memory testing covers an array of different types of memory loss and cognitive impairment, including: learning memory, working memory, object discrimination, spatial memory, long-term memory, recognition memory, and episodic-like

memory. It must also be considered that since these tests rely on the performance of other secondary behaviours e.g. ambulation, phenotypes in other behaviours such as in motor and anxiety parameters may confound memory test results (Wolf, Bauer et al. 2016).

- *Fear Conditioning*: The protocol used in this study can also be described as 'Context and Cued Fear Conditioning', which assesses associative learning and memory. Associative learning is a form of adaptation that allows an organism to learn to anticipate events. In this test a mouse is placed into a novel environment, and an aversive unconditioned stimulus (in this case, a foot shock) is applied in relation to a cue, in this case a tone. The mouse's response to the unconditioned stimulus is then compared to the mouse's response (after a time interval) to both the context (novel environment) and cue (tone) associated with the stimulus (Buccafusco 2009). As previously mentioned, a foot-shock protocol can also be used as a measure of anxiety, which is a confounding factor that needs to be considered in protocol design.

In the memory tests for this study, only older mouse cohorts were available, so age comparisons could not be made. Combined-sex and female homozygous mice showed a stronger freeze response to the context trial of the fear conditioning test than their wildtype counterparts. However, since both young combined-sex homozygotes and older female homozygotes demonstrate an apparent anxiety phenotype, it is not possible to separate the behavioural differences shown in these memory test parameters from an anxious response.

Typical memory (working) is mediated by the mesocortical pathway, involving primarily D_1 receptors (Lidow, Goldman-Rakic et al. 1991). Deficits in memory and

progressive cognitive decline are seen in both Parkinson's and Huntington's disease, with the possible addition of a cognitive impairment seen in schizophrenic patients (American Psychiatric Association 2013, Bates, Dorsey et al. 2015, Schapira, Chaudhuri et al. 2017).

Mouse models of these diseases are consistent with these observations. The Parkinsonian mouse model Thy1-aSyn mice, which over-express human α-synuclein, showed fewer spontaneous alternations in the Y-maze and spent less time exploring novel objects in the novel object recognition test than wildtype controls (Magen, Fleming et al. 2012). The previously mentioned Huntington's mouse model R6/2 show an increase in freezing response to the cue trial of foot-shock fear conditioning tests, but not in context trials – mirroring the behaviour of male homozygotes in this study. This varied response to cue and context trials is hypothesised to be due to impaired plasticity in the hippocampus of R6/2 mice (Murphy, Carter et al. 2000, Bolivar, Manley et al. 2003). Mice carrying a heterozygous loss-of-function mutation of *SETD1A* – a schizophrenia susceptibility gene – show deficits in working memory due to impaired cortical synaptic plasticity (Mukai, Cannavò et al. 2019).

7.2.1.4 Sleep

Sleep assessment over 24 hours in this study was carried out on only older mice, with sex combined analysis due to low n-numbers. Homozygous knockout mice showed differences in sleep fragmentation, but not length, compared to wildtype mice - sleeping in fewer but longer bouts. Sleep is, in part, mediated by dopaminergic signalling from the VTA, which modulates sleep-wake behaviour via

D_1 and D_2 receptors (Eban-Rothschild, Rothschild et al. 2016). All of the dopaminergic disorders discussed in this study present with disordered sleeping: Parkinson's patients suffer with excessive daytime sleepiness; Huntington's patients also experience excessive daytime sleepiness, in addition insomnia and frequent nocturnal awakening; people with ADHD often experience restless leg syndrome and circadian disturbances; and schizophrenic patients often present with insomnia, circadian disturbances, and restless leg syndrome (Knie, Mitra et al. 2011, Kaskie, Graziano et al. 2017, Wajszilber, Santiseban et al. 2018, Herzog-Krzywoszanska and Krzywoszanski 2019).

Mouse studies of dopamine function in sleep have uncovered a complex relationship between dopamine and REM (rapid-eye-movement) sleep. Hyperdopaminergic mice – DAT-knockout or amphetamine-treated – model schizophrenia, and are reported to show electrophysiological hippocampal readings that resemble those seen in REM-sleep, while in an awake state. Conversely, wildtype mice with depleted dopamine via D_2 antagonist treatment model Parkinson's, and show reduced REM-sleep. These findings suggest that dopamine plays a central role in mediating sleep and wake states (Dzirasa, Ribeiro et al. 2006). Our immobility-based sleep monitoring apparatus cannot distinguish between REM and non-REM states, but considering the changes in sleep fragmentation seen in the homozygous knockout mice, this mouse line is a candidate for more detailed electrophysiology sleep recordings.

7.2.1.5 Social Dominance

Social dominance assesses the social hierarchy between two animals, in this case a homozygous knockout mouse and a same-sex wildtype counterpart. Social dominance can be measured using a range of tests, for example having groups of animals compete over restrictive food and water resources, or for a small warm spot in a cold cage (Merlot, Moze et al. 2004, Zhou, Zhu et al. 2017, Ujita, Kohyama-Koganeya et al. 2018). The 'tube test' used in this study was developed specifically for testing transgenic mouse lines. The homozygous and wildtype mice face off against each other in a narrow tube, and the mouse that backs out the tube is the 'loser', with the other mouse declared the 'winner'. Measuring social hierarchy/dominance with the tube test has been used to investigate social behaviours in multiple mouse models of psychiatric disease (Crawley 1999, Fan, Zhu et al. 2019).

In the social dominance test, old combined-sex and old male homozygous knockout mice were shown to likely be dominant over their wildtype counterparts, winning confrontations in the tube test and forcing wildtype mice to back away. In schizophrenia, social submission and withdrawal is seen in patients, classed as a 'negative' symptom (American Psychiatric Association 2013). The social dominance tube test is distinct from other social tests in that it excludes aggressive behaviours (Fan, Zhu et al. 2019), however it is likely that older male homozygotes had an aggression phenotype. Qualitative observations noted that group-housed males would often have to be transferred to single-housed conditions due to fights and barbering (data not shown), and a facet of this phenotype may have been demonstrated in the tube test. Considering aggression, patients with Huntington's disease exhibit irritation and aggressive behaviours at all stages of the disease (van Duijn, Kingma et al. 2007).

Both D_1 and D_2 receptors have been implicated in the study of social hierarchy in mice. Administration of a D_1 antagonist facilitates social dominance in a group-housed setting with non-drug cage-mates, while administration of a D_2 antagonist attenuates dominance in 'high rank' mice in group-housing (Yamaguchi, Lee et al. 2017, Yamaguchi, Lee et al. 2017). Conversely to what is seen in this study, a range of schizophrenia mouse models have shown social withdrawal behaviours, particularly in males (Leger and Neill 2016).

7.2.1.6 Pain

Nociception in this study is measured using the Von Frey filament test. Specifically, punctate mechanical allodynia and hyperalgesia – i.e. assessing touch-triggered hypersensitivity to pain using filaments of varying thickness to determine the mechanical pain threshold of the hind paws (Deuis, Dvorakova et al. 2017).

Assessment with the Von Frey filament test revealed that older male mice exhibited apparent hyperalgesia in their hind paws, giving a reflexive pain reaction to lower-force filaments. Pain is mediated primarily through the nigrostriatal pathway, involving D_2 receptors, and increased sensitivity to nociception is a key feature of Parkinson's disease (Michael-Titus, Bousselmame et al. 1990, Schapira, Chaudhuri et al. 2017).

1-methyl-4-phenyl-1,2,3,6-tetrahydropyridine (MPTP)-induced Parkinson's mouse model exhibits increased sensitivity to nociception. MPTP neurotoxin administration induces neurodegeneration in the SNc and striatum, and these mice have reduced latency of response to mechanical and thermal pain stimuli,

demonstrating increased sensitivity (Park, Lim et al. 2015). Another neurotoxin-induced Parkinsonian mouse model – injection of 6-OHDA in the medial forebrain bundle – demonstrates sensitivity to painful stimuli, which can then be relieved with the administration of a D_2 agonist (Tang, Luan et al. 2021).

7.2.2 Molecular Analysis

Zfhx3 is a large transcription factor, binding to gene promotors and enhancers. Loss-of-function mutations such as *Sci* have been shown to have an effect on expression levels of circadian neuropeptides in the SCN (Parsons, Brancaccio et al. 2015). To investigate whether *Zfhx3* exacts a similar function in the dopaminergic system, molecular analysis on differential gene expression was carried between age-matched homozygous knockout mice of both sexes and their wildtype counterparts, using both qPCR and RNA-Seq.

7.2.2.1 qPCR - Differential Gene Expression

Through qPCR dopamine receptors D_1 and D_2 were identified to be possibly downregulated in the striatum (mixed sex, age-matched) in homozygous knockout mice. The striatum is involved in the nigrostriatal pathway, receiving dopaminergic projections from the SN. The nigrostriatal pathway is involved in motor function, and pain modulation (Michael-Titus, Bousselmame et al. 1990, Matsumoto, Hanakawa et al. 1999). Both D_1 and D_2 receptors are involved in locomotion – D_1 being post-synaptic and having an excitatory effect, and D_2 being pre-synaptic and having a modulatory effect (Missale, Nash et al. 1998, Sibley 1999). These results

alone do not give a clear picture on what knockdown of both receptors could have on locomotive behaviour as they functionally oppose each other. It is also worth noting that the downregulation of these genes was not seen in this region (or any other) in the RNA-Seq results. It is only possible to speculate as to why, with the most likely reason being the low n-number of samples in the RNA-Seq analysis not providing enough power to show significance in the differential expression of these receptors.

7.2.2.2 RNA-Seq – Differential Gene Expression

RNA-Seq analysis of three brain regions – the midbrain, the striatum, and the cortex – revealed that the midbrain in homozygous knockout females was the only experimental group to give notable differential gene lists. Unexpectedly, homozygous knockout males did not show significant gene differentiation from wildtypes, and more analysis would be needed to uncover why this may be. However, the low n-number of samples in the RNA-Seq analysis could also be contributing to this unexpected result , since male homozygous mice show a significant behavioural phenotype. Therefore as in *Chapter 4*, all discussion is reserved for differentiation between knockout and wildtype female midbrain. It is again worth noting that the n-number is low (n=2 for each genotype) and therefore results lack statistical power to give conclusive results.

7.2.2.3 RNA-Seq KEGG Pathways

STRING (Search Tool for the Retrieval of Interacting Genes/Proteins) database analysis on relevant KEGG pathways related to the upregulated and downregulated gene lists identified multiple brain-relevant pathways in the differentially expressed gene lists. Here discussion will be focused on dopamine and *Zfhx3*-relevant pathways.

Analysis of upregulated genes highlighted differential genes were involved in Parkinson's disease and Huntington's disease, which as previously discussed are both diseases based on dopamine dysfunction – these are large topics, and will be referred to throughout this chapter.

Downregulated genes were involved in estrogen signalling, the dopamine synapse, and circadian entrainment. The differentiation in estrogen signalling seen in the female homozygotes may influence the sexual dimorphism observed in the behavioural phenotype of knockout mice, something that can be explored with further analysis of the DAT-*Cre*; *Zfhx3*-Flox phenotyping data with 3-way ANOVA to elucidate the role of sex in behaviour. The downregulation of genes involved in the dopamine synapse relates back to qPCR analysis of the striatum, suggesting that there could be a loss of function in signalling across the dopamine synapse. Parkinson's disease pathophysiology incorporates the degeneration of dopaminergic neurons leading to reduction in dopamine signalling, causing a range of motor and non-motor symptoms, and Huntington's motor symptoms are caused by a similar loss of dopaminergic neurons (Bédard, Wallman et al. 2011, Beitz 2014). Downregulation of genes in circadian entrainment supports data found by Parsons et al. who found that a loss-of-function mutation in *Zfhx3* led to downregulation of circadian neuropeptides, receptors, and signalling molecules in the SCN (Parsons, Brancaccio et al. 2015). Searching for related KEGG pathways

to the combined up and downregulated differential gene list also uncovered the neurotrophin signalling pathway – regulating neuronal development, survival, function, and plasticity (Huang and Reichardt 2001). It has previously been reported that conditional regional *Zfhx3* knockout causes loss of neuron identity (Wilcox, Bains et al. 2021) - it is therefore possible that the disruption in neuron identity development seen by Wilcox et al was caused by dysregulation in neurotrophin signalling pathways as observed here, despite the dopaminergic regions retaining neuronal identity in this mouse line.

7.2.2.4 RNA-Seq - Biological Process and Synapse Gene Ontology

STRING database analysis was carried out on biological processes related to the upregulated and downregulated gene lists, then reduced to processes with a strength score of 1 or more (less likely to be a coincidental correlation), to identify biological processes associated with the differential gene lists.

Analysis of upregulated genes revealed multiple biological processes that fall into two functional categories – ATP synthesis, and ribosome assembly and subunit genesis. Upregulation in ATP synthesis indicates an increase in ROS in the cell, and dysfunction in mitochondrial respiration. *Zfhx3* has been implicated in mitochondrial function, as knockdown of *Zfhx3* leads to an increase in ROS in the cell (*Introduction 1.1.3.4.*). An increase in ROS has been linked to every dopaminergic disorder outlined in this study: Parkinson's disease, Huntington's disease, ADHD, and schizophrenia. In Parkinson's disease, ROS produced by multiple processes – including dopamine metabolism - has been linked to

dopamine neuronal loss in the midbrain (Jenner and Olanow 2006). In mouse models of Huntington's disease, accumulation of oxidative DNA damage has been closely correlated to CAG expansion in the mutant huntingtin gene, the key pathophysiological mechanism behind the disease (Kumar and Ratan 2016). ADHD has been linked to metabolic disorder – evidence showing an increase in ROS production and overall mitochondrial dysfunction, including the possibility of impairment of ATP production (Kul, Unal et al. 2015, Sezen, Kandemir et al. 2016, Verma, Singh et al. 2016). Increase in ROS and a decrease in antioxidant defense pathways have been linked to both the pathogenesis and symptomology of schizophrenia – specifically negative and cognitive symptoms (Murray, Rogers et al. 2021). An upregulation in ribosome assembly and subunit genesis indicates an increase in protein synthesis in the cell. Both Parkinson's and Huntington's disease pathophysiology are associated with an accumulation of inclusion bodies that lead to neuron degeneration – α-synuclein and ubiquitin in Parkinson's, and huntingtin in Huntington's disease (Beitz 2014, Farshim and Bates 2018) . Both diseases have demonstrated dysfunction in protein synthesis, showing upregulation in both overall protein synthesis and ribosomal subunit synthesis (Garcia-Esparcia, Hernández-Ortega et al. 2015, Creus-Muncunill, Badillos-Rodríguez et al. 2019).

Analysis of downregulated genes revealed multiple biological processes, involved in: receptor signalling pathways, synaptic vesicle function, neuronal development (including neuron neo/morphogenesis), and locomotor behaviour. This includes regulation of glutamate receptor clustering – as previously outlined, the contemporary hypothesis of schizophrenia is that patients have hypoactive glutamatergic signalling, leading to a hyperresponsive dopaminergic system

(Grace and Gomes 2019). These findings are in line with the expanded dopamine hypothesis of schizophrenia – the NMDA-R hypofunction hypothesis - where hypoactive glutamate signalling leads to an increase in dopamine signalling (Olney and Farber 1995)

Downregulated synapse vesicle processes suggests that contrary to what is seen in schizophrenia homozygous knockout mice - who experience hyperactive dopaminergic system - dopamine centres are in fact hypoactive – which mirrors Parkinson's and Huntington's pathophysiology. Downregulated neuronal development processes relate to the identified neurotrophin signalling pathway, further hinting to dysfunction in neuronal differentiation, development, and maintenance. For example, downregulation of genes associated with neuronal structure and function has been reported in mouse models of Huntington's disease (Creus-Muncunill, Badillos-Rodríguez et al. 2019). Locomotor behaviour as a downregulated process has no strong link to the behaviour phenotype seen in the homozygous knockout females. However, any behavioural testing has a limited scope, and additional testing may have uncovered a subtle motor phenotype.

Analysis of the combined up and downregulated gene lists confirmed mitochondrial function as a possible associated biological function of the differential gene list, however without generating any novel hits.

Searching the SynGO database gave additional detail on biological function of differential genes at the synapse level, corroborating with STRING analysis.

Upregulated genes were possibly associated with protein translation both pre- and post- synapse, which mirrors data from KEGG and biological function analysis linking upregulation in protein translation to Parkinson's and Huntington's disease.

Downregulated genes were possibly associated with synapse organisation and construction, signalling, and vesicle cycling. As with upregulated genes, these results link to the synaptic and receptor signalling and organisation gene functions seen in other database analysis.

Analysis of the combined up and down-regulated gene lists gave the same results as the separated lists, with the addition of metabolism – which links to Parkinson's and Huntington's disease as previously discussed.

7.2.2.5 RNA-Seq Gene Discussion

Upregulated and downregulated differential gene lists were sorted by p-value and expression fold-change, producing a gene list of both highest significance then greatest fold-change in expression. The top 50-scoring genes were then cross-referenced to CNS-relevant KEGG pathways to shortlist genes of interest. Discussed here are functions associated with genes listed in *Chapter 5.*

Proteins synthesised from upregulated genes include: Complexes I and III of the electron transport chain, and RNA Polymerases I, II, and III. The electron transport chain generates ATP in the mitochondria, and is a primary source of ROS – as a proportion of electrons leak from the mitochondria and react with oxygen (Turrens 2003). Complexes I and III are both considered the greatest generators of ROS in the mitochondria – generated through leaky internal redox reactions (Zhao, Jiang

et al. 2019). Upregulation of these genes associates with mitochondrial dysfunction previously discussed, directly linking to Parkinson's and Huntington's diseases as outlined in KEGG pathways. RNA Polymerases I, II, and III generate rRNA, tRNA, and mRNA respectively (*Chapter 5, 5.6.2.1.3.*), and upregulation of subunits of these proteins corroborates with increase in protein synthesis machinery uncovered in the STRING database – which links once more to Parkinson's and Huntington's disease.

Proteins synthesised from downregulated genes include: NDMA receptors, M-channels, and $GABA_B$ receptors. NDMA receptors are a class of glutamate receptors, downregulation of which links to downregulation of glutamate receptor clustering seen in biological function analysis, and both hypoglutamatergic and hyperdopaminergic signalling as previously discussed. M-channels are voltage-gated potassium channels that facilitate potassium current in central and periphery neurons, modulating neuron excitability (Brown and Passmore 2009). Dysfunction and downregulation of potassium channels of the same family as M-channels (KCNQ3), are associated with Parkinson's and Huntington's disease (Chen, Xue et al. 2018, Zhang, Wan et al. 2018). However, discussing specifically M-channels, downregulation or blockade of KCNQ3 has been linked to hyperalgesia in rats – with hyperalgesia being a female-associated Parkinson's symptom, and which was also observed in (male) homozygous knockout mice (Passmore, Reilly et al. 2012, Silverdale, Kobylecki et al. 2018, Kang, Li et al. 2019). Activation of $GABA_B$ receptors is involved in both pre- and post-synaptic inhibition, with localisation to glutamate synapses and crosstalk with NDMA receptors to modulate signalling (Gassmann and Bettler 2012). $GABA_B$ receptor activation in the substantia nigra (SN) has also been shown to affect dopaminergic signalling, with activation of

$GABA_B$ receptors associated to a reduction in dopamine neuron firing rate (Engberg, Kling-Petersen et al. 1993). In addition, $GABA_B$ receptor expression downregulation has been implicated in multiple psychiatric conditions, including major depression, bipolar disorder, and schizophrenia (Fatemi, Folsom et al. 2011).

7.3 Intracranial Injection of AAV-Cre

This mouse cohort was generated alongside the DAT-*Cre*; *Zfhx3*-Flox line. Adult *Zfhx3*-Floxed mice underwent intracranial injection of AAV5, transducing either control or *Cre*-expressing viral vectors. Injections targeted the midbrain, specifically the VTA and SNc in order to knock out *Zfhx3* from these regions. This line contrasted DAT-*Cre*; *Zfhx3*-Flox mice – injected mice had *Zfhx3* knockout from adulthood only - excluding any developmental effect – and had *Zfhx3* knockout out in all cell types in the VTA and SNc, not only dopaminergic neurons.

AAV-Cre^+ injected mice began exhibiting a severe phenotype between 7-14 days post-injection. These mice would develop a head-tilt, which developed into stereotypic circling that progressed in severity. It was also observed that these mice became aggressive to handlers in this same timeframe. Unfortunately many of these mice progressed to welfare cull boundaries, and only three male AAV-Cre^+ mice could be behaviourally assessed. Due to the severity of the circling behaviour observed in AAV-Cre^+ mice, they were unable to undergo the same phenotyping pipeline as DAT-*Cre*; *Zfhx3*-Flox mice, so instead activity was recorded in home-cage.

AAV-Cre$^+$ mice moved more during both the light and dark phases than control mice, although this was non-specific hyperactivity, and AAV-Cre$^+$ mice were not measured to circle more than control mice. This could be due to the apparent progressive nature of the circling phenotype, as AAV-Cre$^+$ mice who were observed to demonstrate severe deleterious circling were often culled due to related weight loss, and were therefore unable to be recorded. One outlier male AAV-Cre$^+$ demonstrated more severe behaviour than the other AAV-Cre$^+$ mice, being around 9 weeks post-surgery as opposed to around 6 weeks. This mouse was recorded as sleeping less, travelling more, and engaging in stereotypic leftprone circling behaviour. While sexual dimorphism could not be assessed, the data suggests that deleterious hyperactive and circling behaviours were possibly progressive post-injection.

Stereotypic circling is a well-documented behaviour in animals, and has been reported as a dopamine-mediated behaviour. Stereotypic behaviour is defined as repetitive and purposeless behaviours (Low 2003), and studies have reported an association between the nigrostriatal dopamine pathway and stereotypic behaviours in mice. Introduction of indirect dopamine agonists such as cocaine, amphetamine, and methylphenidate cause stereotypic behaviours such as head-bobbing and rearing, while D_1 antagonists can attenuate similar stereotypic behaviours (Karler, Calder et al. 1995, Roffman and Raskin 1997, Presti, Mikes et al. 2003, Krolewski, Bishop et al. 2005). An example of stereotypic behaviour in both rodents and humans is circling. In rodents, circling has been reported to be associated with a significant increase in dopamine release in the striatum, and that asymmetrical circling occurs when there is an imbalance in dopaminergic activity in the nigrostriatal pathway between the two brain hemispheres – turning away

from the hermisphere for higher activity (Glick, Jerussi et al. 1976). An example of dopamine-mediated circling is in homozygous $Tshr^{hyt}$ mice (*hyt*/*hyt*), which are genetically hypothyroid due to a loss-of-function mutation in the thyroid-stimulating hormone receptor (*Tshr*) gene. Around 25% of the homozygotes exhibited unilateral circling behaviour, either left or rightprone, with an absolute directional preference. Circling mice were found to have a 40% reduction in dopaminergic neuron number in the midbrain, however the asymmetrical nature of the circling behaviour did not correlate to any asymmetry in midbrain neuron loss. These results suggests that while circling behaviour is dopamine-mediated, directional preference may be mediated in part by additional neuronal sub-populations (Kincaid 2001).

Stereotypic behaviour is associated with multiple neuropsychiatric disorders, including autism, degenerative dementias, Tourette's syndrome, and - most pertinent to this study – Parkinson's disease, and schizophrenia (Luchins, Goldman et al. 1992, Lewis and Bodfish 1998, Evans, Katzenschlager et al. 2004, Prioni, Fetoni et al. 2012, Ubhi, Achinivu et al. 2020). A small subset of Parkinson's patients experience 'punding' – defined as repeated handling and examining of everyday objects, aimless driving or walking, compulsive grooming, hoarding, and talking with no content. It has primarily been reported in patients prescribed with L-dopa, which acts as a D_1 and D_2 receptor agonist (Evans, Katzenschlager et al. 2004). Studies on schizophrenia report that stereotypic behaviours are distinct from cognitive symptoms, and are progressive with age - as patients' ability to produce random spontaneous movements declines, and become more repetitive (Morrens, Hulstijn et al. 2006). Stereotypic leftprone circling specifically has also been reported in under and never-medicated

schizophrenia patients, which was theorised to be due to right anterior subcortical or cortical regions exhibiting dopamine over-activity compared to the left hemisphere (Bracha 1987).

7.4 Final Summary

Zfhx3 is a large transcription factor that binds AT-rich core sequences in gene enhancer and promotor regions. It has been reported to play a role in a large range of functions both in development and adulthood, and is implicated in multiple diseases.

It has been theorised that *Zfhx3* plays a role in the dopaminergic system. *Zfhx3* has been reported to have enriched expression in the midbrain, specifically dopamine centres VTA and SNc, implying a possible role in dopamine function. Multiple human studies have also linked *Zfhx3* to schizophrenia, which is a dopaminergic disorder. The aim of this study was to investigate both the developmental and adult role of *Zfhx3* within the dopaminergic system, through the behavioural and molecular characterisation of two conditional *Zfhx3* knockout mouse lines, and investigation of wildtype *Zfhx3* expression in the mouse brain.

Investigation of dopaminergic regions via immunofluorescent antibody labelling has found ZFHX3 expression in dopaminergic neurons in these regions, in addition to other yet to be identified neuronal sub-populations and non-neuronal cells.

Conditional knockout line DAT-*Cre*; *Zfhx3*-Flox – where *Zfhx3* is knocked out in dopaminergic neurons from E13 – demonstrated multiple possible behavioural

and molecular phenotypes. Early qualitative assessment of the VTA and SNc of homozygous knockout mice show a possible reduction of *Zfhx3* expression in dopaminergic neurons. Adult homozygous knockout mice display an apparent sexually dimorphic and age-differential behavioural phenotype – with females showing a possible progressive heightened anxiety and paradoxically impulsive behaviour, and males showing a possibly more complex phenotype profile of: attenuated anxiety that partially corrects with age, abnormal gait, improved associative memory, hyperalgesia, and social dominance. Tests using combined-sex analysis show homozygous knockouts have possible increase in anxiety, locomotor suppression, (possibly) improved associative memory, social dominance, and changes in sleep fragmentation. Molecular analysis of differences in gene expression in dopaminergic brain regions shows a downregulation of dopaminergic receptors in the striatum in a mixed sex cohort sample, and differential gene expression in homozygous knockout female midbrain compared to their wildtype counterparts. Female homozygous midbrain samples demonstrated an upregulation of genes associated with Parkinson's and Huntington's disease, mitochondrial function, ribosome production, and RNA synthesis. They demonstrated a downregulation of genes associated with dopaminergic, glutamatergic, and GABA-ergic signalling; in addition to neuronal development and action potential sensitivity. Through the behavioural and molecular phenotype of homozygous knockout mice, continual suggestive links to dopaminergic diseases Parkinson's, Huntington's, ADHD, and schizophrenia were made. Only female homozygous knockout mice demonstrated a notable gene expression differential in any brain region compared to wildtypes, however this

could be due to low n-number and could be explored further with a larger sample size.

The complimentary conditional *Zfhx3* knockout cohort was generated via adult *Zfhx3*-Floxed mice undergoing intracranial injection of AAV5 into the midbrain, transducing either control or *Cre*-expressing viral vectors. This line contrasted DAT-*Cre*; *Zfhx3*-Flox mice, as injected mice had *Zfhx3* knockout from adulthood only - excluding any developmental effect – and had *Zfhx3* knockout out in all cell types in the VTA and SNc, not only dopaminergic neurons. AAV-*Cre* injected mice showed a severe and progressive deleterious circling phenotype, including qualitative observations of aggression towards handlers. Stereotypic and progressive behaviours can be linked to both Parkinson's disease and schizophrenia in humans, with strong links between circling and dopaminergic dysfunction in rodents.

In conclusion, *Zfhx3* is highly expressed in adult dopaminergic regions, and has been shown with two conditional knockout lines to likely play differing roles during development and adulthood. Knockout/knockdown of *Zfhx3* in dopaminergic neurons, either from development or adulthood only, causes possible dopamine-related behavioural phenotypes in mice - including behaviours and molecular changes related to a range of dopaminergic diseases.

Considering the entirety of the data produced in this study, the effect of *Zfhx3* knockout/knockdown in the dopaminergic system is most consistent with: loss of dopamine function when knocked out from development onwards, and increase in dopamine signalling when knocked out in adulthood only. The vast majority of DAT-*Cre*; *Zfhx3*-Flox behavioural phenotypes and molecular changes link to

Parkinson's and Huntington's disease endophenotypes and pathophysiology (as seen in both humans and animal models) - which both involve loss of dopamine function. However, the stereotypic circling and hyperactivity phenotypes seen in AAV5-*Cre* injected mice contradicts this, as studies suggest that these behaviours are caused by an increase in dopamine release and dopamine receptor activation. This difference could be due to the role *Zfhx3* plays in development, causing DAT-*Cre*; *Zfhx3*-Flox mice to have the additional influence of any developmental changes caused by knockout of *Zfhx3* - in addition to the adult effect. Alternatively, this contrast could be due to the knockout/knockdown of *Zfhx3* in additional neuron sub-populations in the VTA and SNc of AAV5-Cre injected mice - for example glutamatergic neurons, which themselves influence dopaminergic signalling. This would also suggest that *Zfhx3* plays a role in the function of additional neuron types.

It is impossible to say whether knockout/knockdown of *Zfhx3* in dopaminergic neurons or the midbrain is the cause of the observed behavioural and molecular phenotypes, or whether these phenotypes are caused by a different process induced by *Zfhx3* knockout/knockdown – for example changes in other neuronal populations.

Without establishing a causal link, the possibility of other processes being involved cannot be excluded. In addition, it is not possible to see if changes in expression of *Zfhx3* in human disease (e.g. schizophrenia – *Chapter 1*) are the cause of symptoms, or are the consequence of other processes causing disease. In the case of this study, we can assume the cause of expression change of *Zfhx3* (DAT-*Cre* or AAV-*Cre*$^{+}$) however it is not possible to say whether this had a direct effect

on phenotypes or whether there was an off-target effect causing the observed phenotypes.

7.5 Future Directions

Most prominently, to further the hypothesis set out by this study the n-number must be increased. Many of the tests in this study lack statistical power in order to draw any conclusions, especially as it is possible that there is sexual dimorphism in the behavioural phenotype of these mice, and each sex needs to be separated for analysis.

For brain region-specific study of expression of *Zfhx3,* there are multiple areas of development to explore. Changing imaging and counting method from manual to stereological method would increase the accuracy of cell counting - developing a method of defining the SNc region is also vital, in order to correctly identify *Zfhx3* expression within the brain region e.g. using co-ordinates to standardise positioning. It is also imperative to find antibodies for additional neuronal subpopulations – i.e. glutamatergic and GABAergic, in order to better understand the pattern of *Zfhx3* expression in the midbrain, and uncover possible future lines of inquiry.

For the DAT-*Cre*; *Zfhx3*-Flox line, greater n-numbers are needed in order to have significant results with statistical power in both behavioural and molecular testing. These mice could also undergo further behavioural testing to elucidate more facets of their demonstrated behavioural phenotypes, for example the beam walking assay to further assess motor deficits. In addition to further behavioural testing, statistical tests could be carried out on the already available data (in

addition to any further data) with 3-way ANOVA, testing both age and sex in each behavioural test. With increased n-numbers, it is hopeful that RNASeq would give more comprehensive and accurate results, allowing for matching behavioural phenotype to molecular changes.

To further our understanding, the use of additional conditional knockout models to uncover the role of *Zfhx3* in more neuronal subpopulations in addition to dopaminergic – for example glutamatergic and GABAergic neurons - would give a more extensive outlook on the role of *Zfhx3* in additional brain regions, circuits, and neuropsychiatric disorders, in addition to neuron identity development.

In AAV-*Cre*$^{+}$ injected mice brain sections need to be stained with a *Zfhx3* label to ensure the virus is causing knockout/knockdown of *Zfhx3*, and the integrity of midbrain cells needs to be assessed, in order to elucidate the cause of the behavioural phenotype seen in these mice. To uncover whether knockout/knockdown of *Zfhx3* in the midbrain is causing the behavioural phenotype observed via dopaminergic neurons, viral vectors that are specific to dopaminergic neurons e.g. with a tyrosine hydroxylase promoter, should be used for injection of virus into the midbrain.

Finally, this study should be considered a pilot study, due to the low n-number throughout each chapter. With an increased n-number, the tests outlined in this project could be carried out statistical power, and these further tests can be carried out, expanding our understanding on the topic.

8
References

References

Afgan, E., D. Baker, B. Batut, M. van den Beek, D. Bouvier, M. Čech, J. Chilton, D. Clements, N. Coraor, B. A. Grüning, A. Guerler, J. Hillman-Jackson, S. Hiltemann, V. Jalili, H. Rasche, N. Soranzo, J. Goecks, J. Taylor, A. Nekrutenko and D. Blankenberg (2018). "The Galaxy platform for accessible, reproducible and collaborative biomedical analyses: 2018 update." Nucleic Acids Research **46**(W1): W537-W544.

Ahmed, B. Y., S. Chakravarthy, R. Eggers, W. T. Hermens, J. Y. Zhang, S. P. Niclou, C. Levelt, F. Sablitzky, P. N. Anderson, A. R. Lieberman and J. Verhaagen (2004). "Efficient delivery of Cre-recombinase to neurons in vivo and stable transduction of neurons using adeno-associated and lentiviral vectors." BMC Neuroscience **5**(1): 4.

Alcaro, A., R. Huber and J. Panksepp (2007). "Behavioral functions of the mesolimbic dopaminergic system: an affective neuroethological perspective." Brain Res Rev **56**(2): 283-321.

Alexander, A., S.-L. Cai, J. Kim, A. Nanez, M. Sahin, K. H. MacLean, K. Inoki, K.-L. Guan, J. Shen and M. D. Person (2010). "ATM signals to TSC2 in the cytoplasm to regulate mTORC1 in response to ROS." Proceedings of the National Academy of Sciences **107**(9): 4153-4158.

Alkan, E., G. Davies and S. L. Evans (2021). "Cognitive impairment in schizophrenia: relationships with cortical thickness in fronto-temporal regions, and dissociability from symptom severity." npj Schizophrenia **7**(1): 20.

Andreasen, N. C., J. C. Ehrhardt, V. W. Swayze, R. J. Alliger, W. T. Yuh, G. Cohen and S. Ziebell (1990). "Magnetic resonance imaging of the brain in schizophrenia: The pathophysiologic significance of structural abnormalities." Archives of General Psychiatry **47**(1): 35-44.

Andreasen, N. C., P. Nopoulos, V. Magnotta, R. Pierson, S. Ziebell and B.-C. Ho (2011). "Progressive Brain Change in Schizophrenia: A Prospective Longitudinal Study of First-Episode Schizophrenia." Biological Psychiatry **70**(7): 672-679.

Andrews, S. (2010). "FastQC: A Quality Control Tool for High Throughput Sequence Data [Online]." from http://www.bioinformatics.babraham.ac.uk/projects/fastqc/.

Asokan, A., D. V. Schaffer and R. J. Samulski (2012). "The AAV vector toolkit: poised at the clinical crossroads." Mol Ther **20**(4): 699-708.

Association, A. P. (2013). "Diagnostic and statistical manual of mental disorders." Am Psychiatric Assoc **21**(21): 591-643.

Austerman, J. (2015). "ADHD and behavioral disorders: Assessment, management, and an update from DSM-5." Cleveland Clinic Journal of Medicine **82**(11 suppl 1): S2-S7.

Ayturk, D. G. (2016). "AAV: A Versatile Viral Tool for Gene Expression in Mammals."

Baik, J. H. (2013). "Dopamine signaling in reward-related behaviors." Front Neural Circuits **7**: 152.

Balu, D. T., Y. Li, M. D. Puhl, M. A. Benneyworth, A. C. Basu, S. Takagi, V. Y. Bolshakov and J. T. Coyle (2013). "Multiple risk pathways for schizophrenia converge in serine racemase knockout mice, a mouse model of NMDA receptor hypofunction." Proc Natl Acad Sci U S A **110**(26): E2400-2409.

Bartlett, J. S., R. J. Samulski and T. J. McCown (1998). "Selective and rapid uptake of adeno-associated virus type 2 in brain." Hum Gene Ther **9**(8): 1181-1186.

Bates, G. P., R. Dorsey, J. F. Gusella, M. R. Hayden, C. Kay, B. R. Leavitt, M. Nance, C. A. Ross, R. I. Scahill and R. Wetzel (2015). "Huntington disease." Nature reviews Disease primers **1**(1): 1-21.

Bédard, C., M.-J. Wallman, E. Pourcher, P. V. Gould, A. Parent and M. Parent (2011). "Serotonin and dopamine striatal innervation in Parkinson's disease and Huntington's chorea." Parkinsonism & related disorders **17**(8): 593-598.

Beitz, J. M. (2014). "Parkinson's disease: a review." FBS **6**(1): 65-74.

Benjamin, E. J., K. M. Rice, D. E. Arking, A. Pfeufer, C. van Noord, A. V. Smith, R. B. Schnabel, J. C. Bis, E. Boerwinkle, M. F. Sinner, A. Dehghan, S. A. Lubitz, R. B. D'Agostino, Sr., T. Lumley, G. B. Ehret, J. Heeringa, T. Aspelund, C. Newton-Cheh, M. G. Larson, K. D. Marciante, E. Z. Soliman, F.

Rivadeneira, T. J. Wang, G. Eiriksdottir, D. Levy, B. M. Psaty, M. Li, A. M. Chamberlain, A. Hofman, R. S. Vasan, T. B. Harris, J. I. Rotter, W. H. Kao, S. K. Agarwal, B. H. Stricker, K. Wang, L. J. Launer, N. L. Smith, A. Chakravarti, A. G. Uitterlinden, P. A. Wolf, N. Sotoodehnia, A. Kottgen, C. M. van Duijn, T. Meitinger, M. Mueller, S. Perz, G. Steinbeck, H. E. Wichmann, K. L. Lunetta, S. R. Heckbert, V. Gudnason, A. Alonso, S. Kaab, P. T. Ellinor and J. C. Witteman (2009). "Variants in ZFHX3 are associated with atrial fibrillation in individuals of European ancestry." Nat Genet **41**(8): 879-881.
Benskey, M. and F. Manfredsson (2016). Intraparenchymal Stereotaxic Delivery of rAAV and Special Considerations in Vector Handling. **1382:** 199-215.
Berry, F. B., Y. Miura, K. Mihara, P. Kaspar, N. Sakata, T. Hashimoto-Tamaoki and T. Tamaoki (2001). "Positive and negative regulation of myogenic differentiation of C2C12 cells by isoforms of the multiple homeodomain zinc finger transcription factor ATBF1." J Biol Chem **276**(27): 25057-25065.
Bettler, B., K. Kaupmann, J. Mosbacher and M. Gassmann (2004). "Molecular structure and physiological functions of GABA(B) receptors." Physiol Rev **84**(3): 835-867.
Bevan, S., M. Traylor, P. Adib-Samii, R. Malik, N. L. Paul, C. Jackson, M. Farrall, P. M. Rothwell, C. Sudlow, M. Dichgans and H. S. Markus (2012). "Genetic heritability of ischemic stroke and the contribution of previously reported candidate gene and genomewide associations." Stroke **43**(12): 3161-3167.
Bhatia A, L. J., Saadabadi A. (2022). Biochemistry, Dopamine Receptors, StatPearls Publishing.
Bhattacharjee, S. (2018). "Impulse control disorders in Parkinson's disease: Review of pathophysiology, epidemiology, clinical features, management, and future challenges." Neurol India **66**(4): 967-975.
Bielefeld, P., A. Sierra, J. M. Encinas, M. Maletic-Savatic, A. Anderson and C. P. Fitzsimons (2017). "A Standardized Protocol for Stereotaxic Intrahippocampal Administration of Kainic Acid Combined with Electroencephalographic Seizure Monitoring in Mice." Front Neurosci **11**: 160.
Bjerke, I. E., S. C. Yates, H. Carey, J. G. Bjaalie and T. B. Leergaard (2023). "Scaling up cell-counting efforts in neuroscience through semi-automated methods." iScience **26**(9): 107562.
Blanc, Y., C. Balmer, T. Landis and F. Vingerhoets (1999). "Temporal parameters and patterns of the foot roll over during walking: normative data for healthy adults." Gait & Posture **10**(2): 97-108.
Bolivar, V. J., K. Manley and A. Messer (2003). "Exploratory activity and fear conditioning abnormalities develop early in R6/2 Huntington's disease transgenic mice." Behavioral neuroscience **117**(6): 1233.
Bowden, N. A., R. J. Scott and P. A. Tooney (2008). "Altered gene expression in the superior temporal gyrus in schizophrenia." BMC Genomics **9**: 199.
Bracha, H. S. (1987). "Asymmetric rotational (circling) behavior, a dopamine-related asymmetry: Preliminary findings in unmedicated and never-medicated schizophrenic patients." Biological Psychiatry **22**(8): 995-1003.
Broen, M. P. G., A. F. G. Leentjens, J. T. Hinkle, A. J. H. Moonen, M. L. Kuijf, N. M. Fischer, K. Perepezko, A. Bakker and G. M. Pontone (2018). "Clinical Markers of Anxiety Subtypes in Parkinson Disease." J Geriatr Psychiatry Neurol **31**(2): 55-62.
Brown, D. A. and P. R. Adams (1980). "Muscarinic suppression of a novel voltage-sensitive K+ current in a vertebrate neurone." Nature **283**(5748): 673-676.
Brown, D. A. and G. M. Passmore (2009). "Neural KCNQ (Kv7) channels." Br J Pharmacol **156**(8): 1185-1195.
Bryant, N. L., R. W. Buchanan, K. Vladar, A. Breier and M. Rothman (1999). "Gender differences in temporal lobe structures of patients with schizophrenia: a volumetric MRI study." American Journal of Psychiatry **156**(4): 603-609.
Buccafusco, J. J. (2009). Frontiers in Neuroscience. Methods of Behavior Analysis in Neuroscience. J. J. Buccafusco. Boca Raton (FL), CRC Press/Taylor & Francis

Burgner, D., S. Davila, W. B. Breunis, S. B. Ng, Y. Li, C. Bonnard, L. Ling, V. J. Wright, A. Thalamuthu, M. Odam, C. Shimizu, J. C. Burns, M. Levin, T. W. Kuijpers and M. L. Hibberd (2009). "A genome-wide association study identifies novel and functionally related susceptibility Loci for Kawasaki disease." PLoS Genet **5**(1): e1000319.
Campos, F., M. Carvalho, A. Cristovão, G. Je, G. Baltazar, A. Salgado, Y.-S. Kim and N. Sousa (2013). "Rodent models of Parkinson's disease: beyond the motor symptomatology." Frontiers in Behavioral Neuroscience **7**.
Cantuti-Castelvetri, I., C. Keller-McGandy, B. Bouzou, G. Asteris, T. W. Clark, M. P. Frosch and D. G. Standaert (2007). "Effects of gender on nigral gene expression and parkinson disease." Neurobiol Dis **26**(3): 606-614.
Carli, M., J. L. Evenden and T. W. Robbins (1985). "Depletion of unilateral striatal dopamine impairs initiation of contralateral actions and not sensory attention." Nature **313**(6004): 679-682.
Carola, V., F. D'Olimpio, E. Brunamonti, F. Mangia and P. Renzi (2002). "Evaluation of the elevated plus-maze and open-field tests for the assessment of anxiety-related behaviour in inbred mice." Behavioural Brain Research **134**(1): 49-57.
Castellanos, F. X., J. N. Giedd, W. L. Marsh, S. D. Hamburger, A. C. Vaituzis, D. P. Dickstein, S. E. Sarfatti, Y. C. Vauss, J. W. Snell, N. Lange, D. Kaysen, A. L. Krain, G. F. Ritchie, J. C. Rajapakse and J. L. Rapoport (1996). "Quantitative brain magnetic resonance imaging in attention-deficit hyperactivity disorder." Arch Gen Psychiatry **53**(7): 607-616.
Castner, S. A., G. V. Williams and P. S. Goldman-Rakic (2000). "Reversal of antipsychotic-induced working memory deficits by short-term dopamine D1 receptor stimulation." Science **287**(5460): 2020-2022.
Caye, A., J. M. Swanson, D. Coghill and L. A. Rohde (2019). "Treatment strategies for ADHD: an evidence-based guide to select optimal treatment." Molecular Psychiatry **24**(3): 390-408.
Cetin, A., S. Komai, M. Eliava, P. H. Seeburg and P. Osten (2006). "Stereotaxic gene delivery in the rodent brain." Nat Protoc **1**(6): 3166-3173.
Chen, X., B. Xue, J. Wang, H. Liu, L. Shi and J. Xie (2018). "Potassium Channels: A Potential Therapeutic Target for Parkinson's Disease." Neurosci Bull **34**(2): 341-348.
Cholerton, B., C. O. Johnson, B. Fish, J. F. Quinn, K. A. Chung, A. L. Peterson-Hiller, L. S. Rosenthal, T. M. Dawson, M. S. Albert, S. C. Hu, I. F. Mata, J. B. Leverenz, K. L. Poston, T. J. Montine, C. P. Zabetian and K. L. Edwards (2018). "Sex differences in progression to mild cognitive impairment and dementia in Parkinson's disease." Parkinsonism Relat Disord **50**: 29-36.
Chou, S. Y., J. M. Shulman, B. T. Keenan, E. A. Secor, A. S. Buchman, J. Schneider, D. A. Bennett and P. L. De Jager (2013). "Genetic susceptibility for ischemic infarction and arteriolosclerosis based on neuropathologic evaluations." Cerebrovasc Dis **36**(3): 181-188.
Cohen, H., J. Zohar, M. A. Matar, K. Zeev, U. Loewenthal and G. Richter-Levin (2004). "Setting apart the affected: the use of behavioral criteria in animal models of post traumatic stress disorder." Neuropsychopharmacology **29**(11): 1962-1970.
Cohen, J. (1988). Statistical Power Analysis for the Behavioral Sciences. New York.
Collingridge, G. (1987). "The role of NMDA receptors in learning and memory." Nature **330**(6149): 604-605.
Colombo, D., G. Abbruzzese, A. Antonini, P. Barone, G. Bellia, F. Franconi, L. Simoni, M. Attar, E. Zagni, S. Haggiag and F. Stocchi (2015). "The "gender factor" in wearing-off among patients with Parkinson's disease: a post hoc analysis of DEEP study." ScientificWorldJournal **2015**: 787451.
Cooper, E. C. and L. Y. Jan (2003). "M-Channels: Neurological Diseases, Neuromodulation, and Drug Development." Archives of Neurology **60**(4): 496-500.
Costall, B., B. J. Jones, M. E. Kelly, R. J. Naylor and D. M. Tomkins (1989). "Exploration of mice in a black and white test box: Validation as a model of anxiety." Pharmacology Biochemistry and Behavior **32**(3): 777-785.

Coyle, J. T. and P. Puttfarcken (1993). "Oxidative stress, glutamate, and neurodegenerative disorders." Science **262**(5134): 689-695.
Crane, F. (2002). "Biochemical Functions of Coenzyme Q10." Journal of the American College of Nutrition **20**: 591-598.
Crawley, J. N. (1985). "Exploratory behavior models of anxiety in mice." Neuroscience & Biobehavioral Reviews **9**(1): 37-44.
Crawley, J. N. (1999). "Behavioral phenotyping of transgenic and knockout mice: experimental design and evaluation of general health, sensory functions, motor abilities, and specific behavioral tests." Brain research **835**(1): 18-26.
Creus-Muncunill, J., R. Badillos-Rodríguez, M. Garcia-Forn, M. Masana, G. Garcia-Díaz Barriga, A. Guisado-Corcoll, J. Alberch, C. Malagelada, J. M. Delgado-García, A. Gruart and E. Pérez-Navarro (2019). "Increased translation as a novel pathogenic mechanism in Huntington's disease." Brain **142**(10): 3158-3175.
Cullity, E. R., H. B. Madsen, C. J. Perry and J. H. Kim (2019). "Postnatal developmental trajectory of dopamine receptor 1 and 2 expression in cortical and striatal brain regions." J Comp Neurol **527**(6): 1039-1055.
Deacon, R. M. (2013). "Measuring motor coordination in mice." J Vis Exp(75): e2609.
Deuis, J. R., L. S. Dvorakova and I. Vetter (2017). "Methods Used to Evaluate Pain Behaviors in Rodents." Front Mol Neurosci **10**: 284.
Dobin, A., C. A. Davis, F. Schlesinger, J. Drenkow, C. Zaleski, S. Jha, P. Batut, M. Chaisson and T. R. Gingeras (2013). "STAR: ultrafast universal RNA-seq aligner." Bioinformatics **29**(1): 15-21.
Dunlap, J. C. (1999). "Molecular Bases for Circadian Clocks." Cell **96**(2): 271-290.
Dzirasa, K., S. Ribeiro, R. Costa, L. M. Santos, S. C. Lin, A. Grosmark, T. D. Sotnikova, R. R. Gainetdinov, M. G. Caron and M. A. Nicolelis (2006). "Dopaminergic control of sleep-wake states." J Neurosci **26**(41): 10577-10589.
Eban-Rothschild, A., G. Rothschild, W. J. Giardino, J. R. Jones and L. de Lecea (2016). "VTA dopaminergic neurons regulate ethologically relevant sleep-wake behaviors." Nat Neurosci **19**(10): 1356-1366.
Engberg, G., T. Kling-Petersen and H. Nissbrandt (1993). "GABAB-receptor activation alters the firing pattern of dopamine neurons in the rat substantia nigra." Synapse **15**(3): 229-238.
Enjalbert, A. and J. Bockaert (1983). "Pharmacological characterization of the D2 dopamine receptor negatively coupled with adenylate cyclase in rat anterior pituitary." Molecular Pharmacology **23**(3): 576-584.
Ertl, H. C. J. (2022). "Immunogenicity and toxicity of AAV gene therapy." Frontiers in Immunology **13**.
Evans, A. H., R. Katzenschlager, D. Paviour, J. D. O'Sullivan, S. Appel, A. D. Lawrence and A. J. Lees (2004). "Punding in Parkinson's disease: Its relation to the dopamine dysregulation syndrome." Movement Disorders **19**(4): 397-405.
Fan, Z., H. Zhu, T. Zhou, S. Wang, Y. Wu and H. Hu (2019). "Using the tube test to measure social hierarchy in mice." Nature Protocols **14**(3): 819-831.
Farshim, P. P. and G. P. Bates (2018). Mouse Models of Huntington's Disease. Huntington's Disease. S. V. Precious, A. E. Rosser and S. B. Dunnett. New York, NY, Springer New York**:** 97-120.
Fatemi, S. H., T. D. Folsom and P. D. Thuras (2011). "Deficits in GABA(B) receptor system in schizophrenia and mood disorders: a postmortem study." Schizophr Res **128**(1-3): 37-43.
Fihl, P. and T. Moeslund (2007). Classification of gait types based on the duty-factor.
Fisher, S. P., S. I. Godinho, C. A. Pothecary, M. W. Hankins, R. G. Foster and S. N. Peirson (2012). "Rapid assessment of sleep-wake behavior in mice." J Biol Rhythms **27**(1): 48-58.
Floresco, S. B., A. R. West, B. Ash, H. Moore and A. A. Grace (2003). "Afferent modulation of dopamine neuron firing differentially regulates tonic and phasic dopamine transmission." Nature Neuroscience **6**(9): 968-973.

Flurkey, K., J. M. Currer and D. E. Harrison (2007). Chapter 20 - Mouse Models in Aging Research. The Mouse in Biomedical Research (Second Edition). J. G. Fox, M. T. Davisson, F. W. Quimby et al. Burlington, Academic Press**:** 637-672.
Furuta, Y., O. Lagutin, B. L. Hogan and G. C. Oliver (2000). "Retina- and ventral forebrain-specific Cre recombinase activity in transgenic mice." genesis **26**(2): 130-132.
Garcia-Esparcia, P., K. Hernández-Ortega, A. Koneti, L. Gil, R. Delgado-Morales, E. Castaño, M. Carmona and I. Ferrer (2015). "Altered machinery of protein synthesis is region- and stage-dependent and is associated with α-synuclein oligomers in Parkinson's disease." Acta Neuropathologica Communications **3**(1): 76.
Garrett, M. and P. Soares-da-Silva (1992). "Increased cerebrospinal fluid dopamine and 3, 4-dihydroxyphenylacetic acid levels in Huntington's disease: evidence for an overactive dopaminergic brain transmission." Journal of neurochemistry **58**(1): 101-106.
Gassmann, M. and B. Bettler (2012). "Regulation of neuronal GABAB receptor functions by subunit composition." Nature Reviews Neuroscience **13**(6): 380-394.
Glick, S. D., T. P. Jerussi and L. N. Fleisher (1976). "Turning in circles: The neuropharmacology of rotation." Life Sciences **18**(9): 889-896.
Goldstein, J. M., L. J. Seidman, J. M. Goodman, D. Koren, H. Lee, S. Weintraub and M. T. Tsuang (1998). "Are there sex differences in neuropsychological functions among patients with schizophrenia?" American Journal of Psychiatry **155**(10): 1358-1364.
Goldstein, J. M., L. J. Seidman, N. Makris, T. Ahern, L. M. O'Brien, V. S. Caviness Jr, D. N. Kennedy, S. V. Faraone and M. T. Tsuang (2007). "Hypothalamic abnormalities in schizophrenia: sex effects and genetic vulnerability." Biological psychiatry **61**(8): 935-945.
Grace, A. A. and F. V. Gomes (2019). "The Circuitry of Dopamine System Regulation and its Disruption in Schizophrenia: Insights Into Treatment and Prevention." Schizophr Bull **45**(1): 148-157.
Gudbjartsson, D. F., H. Holm, S. Gretarsdottir, G. Thorleifsson, G. B. Walters, G. Thorgeirsson, J. Gulcher, E. B. Mathiesen, I. Njolstad, A. Nyrnes, T. Wilsgaard, E. M. Hald, K. Hveem, C. Stoltenberg, G. Kucera, T. Stubblefield, S. Carter, D. Roden, M. C. Ng, L. Baum, W. Y. So, K. S. Wong, J. C. Chan, C. Gieger, H. E. Wichmann, A. Gschwendtner, M. Dichgans, G. Kuhlenbaumer, K. Berger, E. B. Ringelstein, S. Bevan, H. S. Markus, K. Kostulas, J. Hillert, S. Sveinbjornsdottir, E. M. Valdimarsson, M. L. Lochen, R. C. Ma, D. Darbar, A. Kong, D. O. Arnar, U. Thorsteinsdottir and K. Stefansson (2009). "A sequence variant in ZFHX3 on 16q22 associates with atrial fibrillation and ischemic stroke." Nat Genet **41**(8): 876-878.
Haaxma, C. A., B. R. Bloem, G. F. Borm, W. J. Oyen, K. L. Leenders, S. Eshuis, J. Booij, D. E. Dluzen and M. W. Horstink (2007). "Gender differences in Parkinson's disease." J Neurol Neurosurg Psychiatry **78**(8): 819-824.
Haery, L., B. E. Deverman, K. S. Matho, A. Cetin, K. Woodard, C. Cepko, K. I. Guerin, M. A. Rego, I. Ersing, S. M. Bachle, J. Kamens and M. Fan (2019). "Adeno-Associated Virus Technologies and Methods for Targeted Neuronal Manipulation." Frontiers in Neuroanatomy **13**.
Haggerty, D. L., G. G. Grecco, K. C. Reeves and B. Atwood (2020). "Adeno-Associated Viral Vectors in Neuroscience Research." Molecular Therapy - Methods & Clinical Development **17**: 69-82.
Hamilton (2019). Video: Priming a Neuroscience Injection Assembly. Syringe Knowledge Base. hamiltoncompany.com, Hamilton Lab Products.
Hasegawa, E., A. Miyasaka, K. Sakurai, Y. Cherasse, Y. Li and T. Sakurai (2022). "Rapid eye movement sleep is initiated by basolateral amygdala dopamine signaling in mice." Science **375**(6584): 994-1000.
Hawi, Z., T. D. R. Cummins, J. Tong, B. Johnson, R. Lau, W. Samarrai and M. A. Bellgrove (2015). "The molecular genetic architecture of attention deficit hyperactivity disorder." Molecular Psychiatry **20**(3): 289-297.

Hentosh, S., L. Zhu, J. Patino, J. W. Furr, N. P. Rocha and E. Furr Stimming (2021). "Sex Differences in Huntington's Disease: Evaluating the Enroll-HD Database." Movement Disorders Clinical Practice **8**(3): 420-426.
Herzog-Krzywoszanska, R. and L. Krzywoszanski (2019). "Sleep Disorders in Huntington's Disease." Front Psychiatry **10**: 221.
Hirst, J. (2013). "Mitochondrial complex I." Annu Rev Biochem **82**: 551-575.
Hirst, J., J. Carroll, I. M. Fearnley, R. J. Shannon and J. E. Walker (2003). "The nuclear encoded subunits of complex I from bovine heart mitochondria." Biochim Biophys Acta **1604**(3): 135-150.
Houser, M. C., J. Chang, S. A. Factor, E. S. Molho, C. P. Zabetian, E. M. Hill-Burns, H. Payami, V. S. Hertzberg and M. G. Tansey (2018). "Stool Immune Profiles Evince Gastrointestinal Inflammation in Parkinson's Disease." Mov Disord **33**(5): 793-804.
Howes, O. D. and S. Kapur (2009). "The dopamine hypothesis of schizophrenia: version III--the final common pathway." Schizophr Bull **35**(3): 549-562.
Huang, E. J. and L. F. Reichardt (2001). "Neurotrophins: roles in neuronal development and function." Annu Rev Neurosci **24**: 677-736.
Huang, S., Z. Zhang, E. Gambeta, S. C. Xu, C. Thomas, N. Godfrey, L. Chen, S. M'Dahoma, S. L. Borgland and G. W. Zamponi (2020). "Dopamine Inputs from the Ventral Tegmental Area into the Medial Prefrontal Cortex Modulate Neuropathic Pain-Associated Behaviors in Mice." Cell Reports **31**(12): 107812.
Ishii, Y., M. T. Kawaguchi, K , T. Oya, S. Nogami, A. Tamura, Y. Miura, A. Ido, N. H. T. Sakata, T , T. Kimura, T. Saito, T. Tamaoki and M. Sasahara (2003). "ATBF1-A protein, but not ATBF1-B, is preferentially expressed in developing rat brain." The Journal of Comparative Neurology **465**: 57-71.
Jenner, P. and C. W. Olanow (2006). "The pathogenesis of cell death in Parkinson's disease." Neurology **66**(10 suppl 4): S24-S36.
Johnson, K. R., C. Tian, L. H. Gagnon, H. Jiang, D. Ding and R. Salvi (2017). "Effects of Cdh23 single nucleotide substitutions on age-related hearing loss in C57BL/6 and 129S1/Sv mice and comparisons with congenic strains." Scientific Reports **7**(1): 44450.
Joseph, J. D., Y. M. Wang, P. R. Miles, E. A. Budygin, R. Picetti, R. R. Gainetdinov, M. G. Caron and R. M. Wightman (2002). "Dopamine autoreceptor regulation of release and uptake in mouse brain slices in the absence of D3 receptors." Neuroscience **112**(1): 39-49.
Jung, C. G., H. J. Kim, M. Kawaguchi, K. K. Khanna, H. Hida, K. Asai, H. Nishino and Y. Miura (2005). "Homeotic factor ATBF1 induces the cell cycle arrest associated with neuronal differentiation." Development **132**(23): 5137-5145.
Justice, J. N., C. S. Carter, H. J. Beck, R. A. Gioscia-Ryan, M. McQueen, R. M. Enoka and D. R. Seals (2014). "Battery of behavioral tests in mice that models age-associated changes in human motor function." Age (Dordr) **36**(2): 583-592.
Kadkhodaei, B., T. Ito, E. Joodmardi, B. Mattsson, C. Rouillard, M. Carta, S. Muramatsu, C. Sumi-Ichinose, T. Nomura, D. Metzger, P. Chambon, E. Lindqvist, N. G. Larsson, L. Olson, A. Björklund, H. Ichinose and T. Perlmann (2009). "Nurr1 is required for maintenance of maturing and adult midbrain dopamine neurons." J Neurosci **29**(50): 15923-15932.
Kaiser, R., A. Hofer, A. Grapengiesser, T. Gasser, A. Kupsch, I. Roots and J. Brockmöller (2003). "L -dopa-induced adverse effects in PD and dopamine transporter gene polymorphism." Neurology **60**(11): 1750-1755.
Kanehisa, M. (2019). "Toward understanding the origin and evolution of cellular organisms." Protein Sci **28**(11): 1947-1951.
Kanehisa, M., M. Furumichi, Y. Sato, M. Kawashima and M. Ishiguro-Watanabe (2023). "KEGG for taxonomy-based analysis of pathways and genomes." Nucleic Acids Res **51**(D1): D587-d592.
Kanehisa, M. and S. Goto (2000). "KEGG: kyoto encyclopedia of genes and genomes." Nucleic Acids Res **28**(1): 27-30.

Kang, S., J. Li, W. Zuo, P. Chen, D. Gregor, R. Fu, X. Han, A. Bekker and J. H. Ye (2019). "Downregulation of M-channels in lateral habenula mediates hyperalgesia during alcohol withdrawal in rats." Sci Rep **9**(1): 2714.
Kao, Y. H., J. C. Hsu, Y. C. Chen, Y. K. Lin, B. Lkhagva, S. A. Chen and Y. J. Chen (2016). "ZFHX3 knockdown increases arrhythmogenesis and dysregulates calcium homeostasis in HL-1 atrial myocytes." Int J Cardiol **210**: 85-92.
Kaplitt, M. G., P. Leone, R. J. Samulski, X. Xiao, D. W. Pfaff, K. L. O'Malley and M. J. During (1994). "Long-term gene expression and phenotypic correction using adeno-associated virus vectors in the mammalian brain." Nature Genetics **8**(2): 148-154.
Karler, R., L. D. Calder, L. H. Thai and J. B. Bedingfield (1995). "The dopaminergic, glutamatergic, GABAergic bases for the action of amphetamine and cocaine." Brain research **671**(1): 100-104.
Karlsson, M., C. Zhang, L. Méar, W. Zhong, A. Digre, B. Katona, E. Sjöstedt, L. Butler, J. Odeberg, P. Dusart, F. Edfors, P. Oksvold, K. von Feilitzen, M. Zwahlen, M. Arif, O. Altay, X. Li, M. Ozcan, A. Mardinoglu, L. Fagerberg, J. Mulder, Y. Luo, F. Ponten, M. Uhlén and C. Lindskog (2021). "A single-cell type transcriptomics map of human tissues." Sci Adv **7**(31).
Kaskie, R. E., B. Graziano and F. Ferrarelli (2017). "Schizophrenia and sleep disorders: links, risks, and management challenges." Nat Sci Sleep **9**: 227-239.
Kaspar, B., B. Vissel, T. Bengoechea, S. Crone, L. Randolph-Moore, R. Muller, E. Brandon, D. Schaffer, I. Verma, K.-F. Lee, S. Heinemann and F. Gage (2002). "Adeno-associated virus effectively mediates conditional gene modification in the brain." Proceedings of the National Academy of Sciences of the United States of America **99**: 2320-2325.
Kaspar, P., M. Dvoráková, J. Králová, P. Pajer, Z. Kozmik and M. Dvorák (1999). "Myb-interacting Protein, ATBF1, Represses Transcriptional Activity of Myb Oncoprotein." The Journal of Biological Chemistry **274**(20): 14422–14428.
Kataoka, H., T. Joh, Y. Miura, T. Tamaoki, K. Senoo, H. Ohara, T. Nomura, T. Tada, K. Asai, T. Kato and M. Itoh (2000). "AT motif binding factor 1-A (ATBF1-A) negatively regulates transcription of the aminopeptidase N gene in the crypt-villus axis of small intestine." Biochem Biophys Res Commun **267**(1): 91-95.
Kataoka, H., Y. Miura, T. Joh, K. Seno, T. Tada, T. Tamaoki, H. Nakabayashi, M. Kawaguchi, K. Asai, T. Kato and M. Itoh (2001). "Alpha-fetoprotein producing gastric cancer lacks transcription factor ATBF1." Oncogene **20**(7): 869-873.
Kawaguchi, M., N. Hara, V. Bilim, H. Koike, M. Suzuki, T. S. Kim, N. Gao, Y. Dong, S. Zhang, Y. Fujinawa, O. Yamamoto, H. Ito, Y. Tomita, Y. Naruse, A. Sakamaki, Y. Ishii, K. Tsuneyama, M. Inoue, J. Itoh, M. Yasuda, N. Sakata, C. G. Jung, S. Kanazawa, H. Akatsu, H. Minato, T. Nojima, K. Asai and Y. Miura (2016). "A diagnostic marker for superficial urothelial bladder carcinoma: lack of nuclear ATBF1 (ZFHX3) by immunohistochemistry suggests malignant progression." BMC Cancer **16**(1): 805.
Kebabian, J. W. and D. B. Calne (1979). "Multiple receptors for dopamine." Nature **277**(5692): 93-96.
Kedinger, C., M. Gniazdowski, J. Mandel Jr, F. Gissinger and P. Chambon (1970). "α-Amanitin: a specific inhibitor of one of two DNA-dependent RNA polymerase activities from calf thymus." Biochemical and biophysical research communications **38**(1): 165-171.
Keiser, M. S., Y. H. Chen and B. L. Davidson (2018). "Techniques for Intracranial Stereotaxic Injections of Adeno-Associated Viral Vectors in Adult Mice." Current Protocols in Mouse Biology **8**(4): e57.
Kelley, A. E. and K. C. Berridge (2002). "The neuroscience of natural rewards: relevance to addictive drugs." J Neurosci **22**(9): 3306-3311.
Kim, H. J., M. Kim, B. Kang, S. Yun, S. E. Ryeo, D. Hwang and J.-H. Kim (2019). "Systematic analysis of expression signatures of neuronal subpopulations in the VTA." Molecular Brain **12**(1): 110.
Kim, R., J. Lee, Y. Kim, A. Kim, M. Jang, H. J. Kim, B. Jeon, U. J. Kang and S. Fahn (2018). "Presynaptic striatal dopaminergic depletion predicts the later development of freezing of gait in

de novo Parkinson's disease: An analysis of the PPMI cohort." Parkinsonism Relat Disord **51**: 49-54.
Kincaid, A. E. (2001). "Spontaneous circling behavior and dopamine neuron loss in a genetically hypothyroid mouse." Neuroscience **105**(4): 891-898.
Kish, S. J., K. Shannak and O. Hornykiewicz (1987). "Elevated serotonin and reduced dopamine in subregionally divided Huntington's disease striatum." Annals of Neurology: Official Journal of the American Neurological Association and the Child Neurology Society **22**(3): 386-389.
Knie, B., M. T. Mitra, K. Logishetty and K. R. Chaudhuri (2011). "Excessive Daytime Sleepiness in Patients with Parkinson's Disease." CNS Drugs **25**(3): 203-212.
Konnova, E. S., M. (2018). Animal Models of Parkinson's Disease. Parkinson's Disease: Pathogenesis and Clinical Aspects [Internet]. G. J. Stoker TB. Brisbane (AU), Codon Publications.
Koopmans, F., P. van Nierop, M. Andres-Alonso, A. Byrnes, T. Cijsouw, M. P. Coba, L. N. Cornelisse, R. J. Farrell, H. L. Goldschmidt, D. P. Howrigan, N. K. Hussain, C. Imig, A. P. H. de Jong, H. Jung, M. Kohansalnodehi, B. Kramarz, N. Lipstein, R. C. Lovering, H. MacGillavry, V. Mariano, H. Mi, M. Ninov, D. Osumi-Sutherland, R. Pielot, K.-H. Smalla, H. Tang, K. Tashman, R. F. G. Toonen, C. Verpelli, R. Reig-Viader, K. Watanabe, J. van Weering, T. Achsel, G. Ashrafi, N. Asi, T. C. Brown, P. De Camilli, M. Feuermann, R. E. Foulger, P. Gaudet, A. Joglekar, A. Kanellopoulos, R. Malenka, R. A. Nicoll, C. Pulido, J. de Juan-Sanz, M. Sheng, T. C. Südhof, H. U. Tilgner, C. Bagni, À. Bayés, T. Biederer, N. Brose, J. J. E. Chua, D. C. Dieterich, E. D. Gundelfinger, C. Hoogenraad, R. L. Huganir, R. Jahn, P. S. Kaeser, E. Kim, M. R. Kreutz, P. S. McPherson, B. M. Neale, V. O'Connor, D. Posthuma, T. A. Ryan, C. Sala, G. Feng, S. E. Hyman, P. D. Thomas, A. B. Smit and M. Verhage (2019). "SynGO: An Evidence-Based, Expert-Curated Knowledge Base for the Synapse." Neuron **103**(2): 217-234.e214.
Krolewski, D. M., C. Bishop and P. D. Walker (2005). "Intrastriatal dopamine D1 receptor agonist-mediated motor behavior is reduced by local neurokinin 1 receptor antagonism." Synapse **57**(1): 1-7.
Kügler, S., E. Kilic and M. Bähr (2003). "Human synapsin 1 gene promoter confers highly neuron-specific long-term transgene expression from an adenoviral vector in the adult rat brain depending on the transduced area." Gene Ther **10**(4): 337-347.
Kul, M., F. Unal, H. Kandemir, B. Sarkarati, K. Kilinc and S. B. Kandemir (2015). "Evaluation of Oxidative Metabolism in Child and Adolescent Patients with Attention Deficit Hyperactivity Disorder." Psychiatry Investig **12**(3): 361-366.
Kumar, A. and R. R. Ratan (2016). "Oxidative Stress and Huntington's Disease: The Good, The Bad, and The Ugly." J Huntingtons Dis **5**(3): 217-237.
La-Vu, M., B. C. Tobias, P. J. Schuette and A. Adhikari (2020). "To Approach or Avoid: An Introductory Overview of the Study of Anxiety Using Rodent Assays." Frontiers in Behavioral Neuroscience **14**.
Leger, M. and J. C. Neill (2016). "A systematic review comparing sex differences in cognitive function in schizophrenia and in rodent models for schizophrenia, implications for improved therapeutic strategies." Neuroscience & Biobehavioral Reviews **68**: 979-1000.
Lein, E. S., M. J. Hawrylycz, N. Ao, M. Ayres, A. Bensinger, A. Bernard, A. F. Boe, M. S. Boguski, K. S. Brockway, E. J. Byrnes, L. Chen, L. Chen, T.-M. Chen, M. Chi Chin, J. Chong, B. E. Crook, A. Czaplinska, C. N. Dang, S. Datta, N. R. Dee, A. L. Desaki, T. Desta, E. Diep, T. A. Dolbeare, M. J. Donelan, H.-W. Dong, J. G. Dougherty, B. J. Duncan, A. J. Ebbert, G. Eichele, L. K. Estin, C. Faber, B. A. Facer, R. Fields, S. R. Fischer, T. P. Fliss, C. Frensley, S. N. Gates, K. J. Glattfelder, K. R. Halverson, M. R. Hart, J. G. Hohmann, M. P. Howell, D. P. Jeung, R. A. Johnson, P. T. Karr, R. Kawal, J. M. Kidney, R. H. Knapik, C. L. Kuan, J. H. Lake, A. R. Laramee, K. D. Larsen, C. Lau, T. A. Lemon, A. J. Liang, Y. Liu, L. T. Luong, J. Michaels, J. J. Morgan, R. J. Morgan, M. T. Mortrud, N. F. Mosqueda, L. L. Ng, R. Ng, G. J. Orta, C. C. Overly, T. H. Pak, S. E. Parry, S. D. Pathak, O. C. Pearson, R. B. Puchalski, Z. L. Riley, H. R. Rockett, S. A. Rowland, J. J. Royall, M. J. Ruiz, N. R. Sarno, K. Schaffnit, N. V. Shapovalova, T. Sivisay, C. R. Slaughterbeck, S. C. Smith, K. A. Smith, B. I. Smith, A. J. Sodt, N.

N. Stewart, K.-R. Stumpf, S. M. Sunkin, M. Sutram, A. Tam, C. D. Teemer, C. Thaller, C. L. Thompson, L. R. Varnam, A. Visel, R. M. Whitlock, P. E. Wohnoutka, C. K. Wolkey, V. Y. Wong, M. Wood, M. B. Yaylaoglu, R. C. Young, B. L. Youngstrom, X. Feng Yuan, B. Zhang, T. A. Zwingman and A. R. Jones (2007). "Genome-wide atlas of gene expression in the adult mouse brain." Nature **445**(7124): 168-176.
Lewis, M. H. and J. W. Bodfish (1998). "Repetitive behavior disorders in autism." Mental Retardation and Developmental Disabilities Research Reviews **4**: 80-89.
Lezak, K. R., G. Missig and W. A. Carlezon, Jr. (2017). "Behavioral methods to study anxiety in rodents." Dialogues Clin Neurosci **19**(2): 181-191.
Li, H., C. J. Huang and K. B. Choo (2002). "Expression of homeobox genes in cervical cancer." Gynecol Oncol **84**(2): 216-221.
Li, M., X. Fu, G. Ma, X. Sun, X. Dong, T. Nagy, C. Xing, J. Li and J. T. Dong (2012). "Atbf1 regulates pubertal mammary gland development likely by inhibiting the pro-proliferative function of estrogen-ER signaling." PLoS One **7**(12): e51283.
Lidow, M. S., P. S. Goldman-Rakic, D. W. Gallager and P. Rakic (1991). "Distribution of dopaminergic receptors in the primate cerebral cortex: quantitative autoradiographic analysis using [3H]raclopride, [3H]spiperone and [3H]SCH23390." Neuroscience **40**(3): 657-671.
Lindell, T. J., F. Weinberg, P. W. Morris, R. G. Roeder and W. J. Rutter (1970). "Specific inhibition of nuclear RNA polymerase II by α-amanitin." Science **170**(3956): 447-449.
Lisman, J. E., J.-M. Fellous and X.-J. Wang (1998). "A role for NMDA-receptor channels in working memory." Nature Neuroscience **1**(4): 273-275.
Low, M. (2003). "Stereotypies and behavioural medicine: confusions in current thinking." Australian Veterinary Journal **81**(4): 192-198.
Luchins, D. J., M. B. Goldman, M. Lieb and P. Hanrahan (1992). "Repetitive behaviors in chronically institutionalized schizophrenic patients." Schizophrenia Research **8**(2): 119-123.
MacDonald, M. E., C. M. Ambrose, M. P. Duyao, R. H. Myers, C. Lin, L. Srinidhi, G. Barnes, S. A. Taylor, M. James, N. Groot, H. MacFarlane, B. Jenkins, M. A. Anderson, N. S. Wexler, J. F. Gusella, G. P. Bates, S. Baxendale, H. Hummerich, S. Kirby, M. North, S. Youngman, R. Mott, G. Zehetner, Z. Sedlacek, A. Poustka, A.-M. Frischauf, H. Lehrach, A. J. Buckler, D. Church, L. Doucette-Stamm, M. C. O'Donovan, L. Riba-Ramirez, M. Shah, V. P. Stanton, S. A. Strobel, K. M. Draths, J. L. Wales, P. Dervan, D. E. Housman, M. Altherr, R. Shiang, L. Thompson, T. Fielder, J. J. Wasmuth, D. Tagle, J. Valdes, L. Elmer, M. Allard, L. Castilla, M. Swaroop, K. Blanchard, F. S. Collins, R. Snell, T. Holloway, K. Gillespie, N. Datson, D. Shaw and P. S. Harper (1993). "A novel gene containing a trinucleotide repeat that is expanded and unstable on Huntington's disease chromosomes." Cell **72**(6): 971-983.
Magen, I., S. M. Fleming, C. Zhu, E. C. Garcia, K. M. Cardiff, D. Dinh, K. De La Rosa, M. Sanchez, E. R. Torres, E. Masliah, J. D. Jentsch and M. F. Chesselet (2012). "Cognitive deficits in a mouse model of pre-manifest Parkinson's disease." Eur J Neurosci **35**(6): 870-882.
Malik, R., M. Traylor, S. L. Pulit, S. Bevan, J. C. Hopewell, E. G. Holliday, W. Zhao, P. Abrantes, P. Amouyel, J. R. Attia, T. W. Battey, K. Berger, G. B. Boncoraglio, G. Chauhan, Y. C. Cheng, W. M. Chen, R. Clarke, I. Cotlarciuc, S. Debette, G. J. Falcone, J. M. Ferro, D. M. Gamble, A. Ilinca, S. J. Kittner, C. E. Kourkoulis, R. Lemmens, C. R. Levi, P. Lichtner, A. Lindgren, J. Liu, J. F. Meschia, B. D. Mitchell, S. A. Oliveira, J. Pera, A. P. Reiner, P. M. Rothwell, P. Sharma, A. Slowik, C. L. Sudlow, T. Tatlisumak, V. Thijs, A. M. Vicente, D. Woo, S. Seshadri, D. Saleheen, J. Rosand, H. S. Markus, B. B. Worrall and M. Dichgans (2016). "Low-frequency and common genetic variation in ischemic stroke: The METASTROKE collaboration." Neurology **86**(13): 1217-1226.
Marié, R.-M. and G.-L. Defer (2003). "Working memory and dopamine: clinical and experimental clues." Current Opinion in Neurology **16**: S29-S35.
Martikainen, I. K., E. B. Nuechterlein, M. Peciña, T. M. Love, C. M. Cummiford, C. R. Green, C. S. Stohler and J. K. Zubieta (2015). "Chronic Back Pain Is Associated with Alterations in Dopamine Neurotransmission in the Ventral Striatum." J Neurosci **35**(27): 9957-9965.

Mathis, A., P. Mamidanna, K. M. Cury, T. Abe, V. N. Murthy, M. W. Mathis and M. Bethge (2018). "DeepLabCut: markerless pose estimation of user-defined body parts with deep learning." Nature Neuroscience **21**(9): 1281-1289.
Matsumoto, N., T. Hanakawa, S. Maki, A. M. Graybiel and M. Kimura (1999). "Nigrostriatal dopamine system in learning to perform sequential motor tasks in a predictive manner." Journal of neurophysiology **82**(2): 978-998.
McCown, T. J., X. Xiao, J. Li, G. R. Breese and R. Jude Samulski (1996). "Differential and persistent expression patterns of CNS gene transfer by an adeno-associated virus (AAV) vector." Brain Research **713**(1): 99-107.
McNeill Alexander, R. (2002). "Energetics and optimization of human walking and running: The 2000 Raymond Pearl memorial lecture." American Journal of Human Biology **14**(5): 641-648.
Meador-Woodruff, J. H., S. P. Damask, J. Wang, V. Haroutunian, K. L. Davis and S. J. Watson (1996). "Dopamine receptor mRNA expression in human striatum and neocortex." Neuropsychopharmacology **15**(1): 17-29.
Megat, S., S. Shiers, J. K. Moy, P. Barragan-Iglesias, G. Pradhan, R. P. Seal, G. Dussor and T. J. Price (2018). "A Critical Role for Dopamine D5 Receptors in Pain Chronicity in Male Mice." J Neurosci **38**(2): 379-397.
Mendes, C. S., I. Bartos, Z. Márka, T. Akay, S. Márka and R. S. Mann (2015). "Quantification of gait parameters in freely walking rodents." BMC Biol **13**: 50.
Merlot, E., E. Moze, A. Bartolomucci, R. Dantzer and P. J. Neveu (2004). "The rank assessed in a food competition test influences subsequent reactivity to immune and social challenges in mice." Brain, behavior, and immunity **18**(5): 468-475.
Michael-Titus, A., R. Bousselmame and J. Costentin (1990). "Stimulation of dopamine D2 receptors induces an analgesia involving an opiodergic but non enkephalinergic link." European Journal of Pharmacology **187**(2): 201-207.
Minamiya, Y., H. Saito, M. Ito, K. Imai, H. Konno, N. Takahashi, S. Motoyama and J. Ogawa (2012). "Suppression of Zinc Finger Homeobox 3 expression in tumor cells decreases the survival rate among non-small cell lung cancer patients." Cancer Biomark **11**(4): 139-146.
Mishra, A., S. Singh and S. Shukla (2018). "Physiological and Functional Basis of Dopamine Receptors and Their Role in Neurogenesis: Possible Implication for Parkinson's disease." J Exp Neurosci **12**: 1179069518779829.
Missale, C., S. R. Nash, S. W. Robinson, M. Jaber and M. G. Caron (1998). "Dopamine receptors: from structure to function." Physiol Rev **78**(1): 189-225.
Mitchell, P. (1975). "The protonmotive Q cycle: A general formulation." FEBS Letters **59**(2): 137-139.
Miura, Y., T. Tam, A. Ido, T. Morinaga, T. Miki and T. T. Hashimoto, T (1995). "Cloning and Characterization of an ATBF1 Isoform That Expresses in a Neuronal Differentiation-dependent Manner." Journal of Biological Chemistry **270**(45): 26840 –26848.
Mori, Y., H. Kataoka, Y. Miura, M. Kawaguchi, E. Kubota, N. Ogasawara, T. Oshima, S. Tanida, M. Sasaki, H. Ohara, T. Mizoshita, M. Tatematsu, K. Asai and T. Joh (2007). "Subcellular localization of ATBF1 regulates MUC5AC transcription in gastric cancer." Int J Cancer **121**(2): 241-247.
Morinaga, T., H. Yasuda, T. Hashimoto, K. Higashio and T. Tamaoki (1991). "A human alpha-fetoprotein enhancer-binding protein, ATBF1, contains four homeodomains and seventeen zinc fingers." Molecular and Cellular Biology **11**(12): 6041–6049.
Morrens, M., W. Hulstijn, P. J. Lewi, M. De Hert and B. G. C. Sabbe (2006). "Stereotypy in schizophrenia." Schizophrenia Research **84**(2): 397-404.
Morris, R. G. M., E. Anderson, G. S. Lynch and M. Baudry (1986). "Selective impairment of learning and blockade of long-term potentiation by an N-methyl-D-aspartate receptor antagonist, AP5." Nature **319**(6056): 774-776.

Mukai, J., E. Cannavò, G. W. Crabtree, Z. Sun, A. Diamantopoulou, P. Thakur, C. Y. Chang, Y. Cai, S. Lomvardas, A. Takata, B. Xu and J. A. Gogos (2019). "Recapitulation and Reversal of Schizophrenia-Related Phenotypes in Setd1a-Deficient Mice." Neuron **104**(3): 471-487.e412.
Murphy, K. P., R. J. Carter, L. A. Lione, L. Mangiarini, A. Mahal, G. P. Bates, S. B. Dunnett and A. J. Morton (2000). "Abnormal synaptic plasticity and impaired spatial cognition in mice transgenic for exon 1 of the human Huntington's disease mutation." Journal of Neuroscience **20**(13): 5115-5123.
Murphy, Michael P. (2008). "How mitochondria produce reactive oxygen species." Biochemical Journal **417**(1): 1-13.
Murray, A. J., J. C. Rogers, M. Z. U. H. Katshu, P. F. Liddle and R. Upthegrove (2021). "Oxidative Stress and the Pathophysiology and Symptom Profile of Schizophrenia Spectrum Disorders." Frontiers in Psychiatry **12**.
Murray, S. A., J. T. Eppig, D. Smedley, E. M. Simpson and N. Rosenthal (2012). "Beyond knockouts: cre resources for conditional mutagenesis." Mammalian Genome **23**(9): 587-599.
Nakatochi, M., S. Ichihara, K. Yamamoto, K. Naruse, S. Yokota, H. Asano, T. Matsubara and M. Yokota (2017). "Epigenome-wide association of myocardial infarction with DNA methylation sites at loci related to cardiovascular disease." Clin Epigenetics **9**: 54.
Nathanson, J. L., R. Jappelli, E. D. Scheeff, G. Manning, K. Obata, S. Brenner and E. M. Callaway (2009). "Short Promoters in Viral Vectors Drive Selective Expression in Mammalian Inhibitory Neurons, but do not Restrict Activity to Specific Inhibitory Cell-Types." Front Neural Circuits **3**: 19.
Nishio, E., Y. Miura, M. Kawaguchi and A. Morita (2012). "Nuclear translocation of ATBF1 is a potential prognostic marker for skin cancer." Acta Dermatovenerol Croat **20**(4): 239-245.
Niu, L., M. Matsui, S.-Y. Zhou, H. Hagino, T. Takahashi, E. Yoneyama, Y. Kawasaki, M. Suzuki, H. Seto and T. Ono (2004). "Volume reduction of the amygdala in patients with schizophrenia: a magnetic resonance imaging study." Psychiatry Research: Neuroimaging **132**(1): 41-51.
Nojiri, S., T. Joh, Y. Miura, N. Sakata, T. Nomura, H. Nakao, S. Sobue, H. Ohara, K. Asai and M. Ito (2004). "ATBF1 enhances the suppression of STAT3 signaling by interaction with PIAS3." Biochemical and Biophysical Research Communications **314**(1): 97-103.
Nolan, P. M., G. Banks, N. Bourbia, A. G. Wilcox, L. Bentley, L. Moir, L. Kent, R. Hillier, D. Wilson, P. Barrett and R. Dumbell (2022). "A missense mutation in zinc finger homeobox-3 (ZFHX3) impedes growth and alters metabolism and hypothalamic gene expression in mice." bioRxiv: 2022.2005.2025.493441.
Nolan, P. M., J. Peters, M. Strivens, D. Rogers, J. Hagan, N. Spurr, I. C. Gray, L. Vizor, D. Brooker, E. Whitehill, R. Washbourne, T. Hough, S. Greenaway, M. Hewitt, X. Liu, S. McCormack, K. Pickford, R. Selley, C. Wells, Z. Tymowska-Lalanne, P. Roby, P. Glenister, C. Thornton, C. Thaung, J. A. Stevenson, R. Arkell, P. Mburu, R. Hardisty, A. Kiernan, A. Erven, K. P. Steel, S. Voegeling, J. L. Guenet, C. Nickols, R. Sadri, M. Nasse, A. Isaacs, K. Davies, M. Browne, E. M. Fisher, J. Martin, S. Rastan, S. D. Brown and J. Hunter (2000). "A systematic, genome-wide, phenotype-driven mutagenesis programme for gene function studies in the mouse." Nat Genet **25**(4): 440-443.
Ohta, S., K. Goto, H. Arai and Y. Kagawa (1987). "An extremely acidic amino-terminal presequence of the precursor for the human mitochondrial hinge protein." FEBS Lett **226**(1): 171-175.
Oishi, Y. and M. Lazarus (2017). "The control of sleep and wakefulness by mesolimbic dopamine systems." Neuroscience Research **118**: 66-73.
Olney, J. W. and N. B. Farber (1995). "Glutamate Receptor Dysfunction and Schizophrenia." Archives of General Psychiatry **52**(12): 998-1007.
OpenStax. "Biology." OpenStax Retrieved 23/01/2024, 2024, from https://openstax.org/books/biology/pages/preface.
Orvoen, S., P. Pla, A. M. Gardier, F. Saudou and D. J. David (2012). "Huntington's disease knock-in male mice show specific anxiety-like behaviour and altered neuronal maturation." Neurosci Lett **507**(2): 127-132.

Orzelska-Górka, J., J. Mikulska, A. Wiszniewska and G. Biała (2022). "New Atypical Antipsychotics in the Treatment of Schizophrenia and Depression." International Journal of Molecular Sciences **23**(18): 10624.
Overton, P. and D. Clark (1992). "Iontophoretically administered drugs acting at the N-methyl-D-aspartate receptor modulate burst firing in A9 dopamine neurons in the rat." Synapse **10**(2): 131-140.
Oyanagi, K., S. Takeda, H. Takahashi, E. Ohama and F. Ikuta (1989). "A quantitative investigation of the substantia nigra in Huntington's disease." Annals of Neurology: Official Journal of the American Neurological Association and the Child Neurology Society **26**(1): 13-19.
Panaccione, A., Y. Zhang, Y. Mi, Y. Mitani, G. Yan, M. L. Prasad, W. H. McDonald, A. K. El-Naggar, W. G. Yarbrough and S. V. Ivanov (2017). "Chromosomal abnormalities and molecular landscape of metastasizing mucinous salivary adenocarcinoma." Oral Oncol **66**: 38-45.
Park, J., C. S. Lim, H. Seo, C. A. Park, M. Zhuo, B. K. Kaang and K. Lee (2015). "Pain perception in acute model mice of Parkinson's disease induced by 1-methyl-4-phenyl-1,2,3,6-tetrahydropyridine (MPTP)." Mol Pain **11**: 28.
Parker, W. D., Jr., S. J. Boyson and J. K. Parks (1989). "Abnormalities of the electron transport chain in idiopathic Parkinson's disease." Ann Neurol **26**(6): 719-723.
Parsons, Michael J., M. Brancaccio, S. Sethi, Elizabeth S. Maywood, R. Satija, Jessica K. Edwards, A. Jagannath, Y. Couch, Mattéa J. Finelli, Nicola J. Smyllie, C. Esapa, R. Butler, Alun R. Barnard, Johanna E. Chesham, S. Saito, G. Joynson, S. Wells, Russell G. Foster, Peter L. Oliver, Michelle M. Simon, A.-M. Mallon, Michael H. Hastings and Patrick M. Nolan (2015). "The Regulatory Factor ZFHX3 Modifies Circadian Function in SCN via an AT Motif-Driven Axis." Cell **162**(3): 607-621.
Passmore, G., J. Reilly, M. Thakur, V. Keasberry, S. Marsh, A. Dickenson and D. Brown (2012). "Functional significance of M-type potassium channels in nociceptive cutaneous sensory endings." Frontiers in Molecular Neuroscience **5**.
Paxinos, G. and K. B. J. Franklin (2012). Paxinos and Franklin's the Mouse Brain in Stereotaxic Coordinates, Academic Press.
Pfaffl, M. W. (2001). "A new mathematical model for relative quantification in real-time RT-PCR." Nucleic Acids Res **29**(9): e45.
Posner, J., V. Rauh, A. Gruber, I. Gat, Z. Wang and B. S. Peterson (2013). "Dissociable attentional and affective circuits in medication-naïve children with attention-deficit/hyperactivity disorder." Psychiatry Res **213**(1): 24-30.
Postuma, R. B., D. Berg, M. Stern, W. Poewe, C. W. Olanow, W. Oertel, J. Obeso, K. Marek, I. Litvan, A. E. Lang, G. Halliday, C. G. Goetz, T. Gasser, B. Dubois, P. Chan, B. R. Bloem, C. H. Adler and G. Deuschl (2015). "MDS clinical diagnostic criteria for Parkinson's disease." Movement Disorders **30**(12): 1591-1601.
Presti, M. F., H. M. Mikes and M. H. Lewis (2003). "Selective blockade of spontaneous motor stereotypy via intrastriatal pharmacological manipulation." Pharmacology Biochemistry and Behavior **74**(4): 833-839.
Prioni, S., V. Fetoni, F. Barocco, V. Redaelli, C. Falcone, P. Soliveri, F. Tagliavini, A. Scaglioni, P. Caffarra, L. Concari, S. Gardini and F. Girotti (2012). "Stereotypic behaviors in degenerative dementias." Journal of Neurology **259**(11): 2452-2459.
Qi, Y., J. A. Ranish, X. Zhu, A. Krones, J. Zhang, R. Aebersold, D. W. Rose, M. G. Rosenfeld and C. Carriere (2008). "Atbf1 is required for the Pit1 gene early activation." Proc Natl Acad Sci U S A **105**(7): 2481-2486.
Rajarethinam, R. P., J. R. DeQuardo, R. Nalepa and R. Tandon (2000). "Superior temporal gyrus in schizophrenia: a volumetric magnetic resonance imaging study." Schizophrenia Research **41**(2): 303-312.
Ramsay, R. R., J. I. Salach, J. Dadgar and T. P. Singer (1986). "Inhibition of mitochondrial NADH dehydrogenase by pyridine derivatives and its possible relation to experimental and idiopathic parkinsonism." Biochemical and Biophysical Research Communications **135**(1): 269-275.

Roffman, J. L. and L. A. Raskin (1997). "Stereotyped behavior: effects of d-amphetamine and methylphenidate in the young rat." Pharmacology Biochemistry and Behavior **58**(4): 1095-1102.
Roos, R. A. (2010). "Huntington's disease: a clinical review." Orphanet J Rare Dis **5**: 40.
Ruitenberg, M. F. L., T. Wu, B. B. Averbeck, K. L. Chou, V. Koppelmans and R. D. Seidler (2018). "Impulsivity in Parkinson's Disease Is Associated With Alterations in Affective and Sensorimotor Striatal Networks." Front Neurol **9**: 279.
Ruzankina, Y., C. Pinzon-Guzman, A. Asare, T. Ong, L. Pontano, G. Cotsarelis, V. P. Zediak, M. Velez, A. Bhandoola and E. J. Brown (2007). "Deletion of the developmentally essential gene ATR in adult mice leads to age-related phenotypes and stem cell loss." Cell Stem Cell **1**(1): 113-126.
Savitsky, K., A. Bar-Shira, S. Gilad, G. Rotman, Y. Ziv, L. Vanagaite, D. A. Tagle, S. Smith, T. Uziel and S. Sfez (1995). "A single ataxia telangiectasia gene with a product similar to PI-3 kinase." Science **268**(5218): 1749-1753.
Schapira, A. H. V., K. R. Chaudhuri and P. Jenner (2017). "Non-motor features of Parkinson disease." Nature Reviews Neuroscience **18**(7): 435-450.
Schindelin, J., I. Arganda-Carreras, E. Frise, V. Kaynig, M. Longair, T. Pietzsch, S. Preibisch, C. Rueden, S. Saalfeld, B. Schmid, J.-Y. Tinevez, D. J. White, V. Hartenstein, K. Eliceiri, P. Tomancak and A. Cardona (2012). "Fiji: an open-source platform for biological-image analysis." Nature Methods **9**(7): 676-682.
Schmidt, M. V. (2011). "Animal models for depression and the mismatch hypothesis of disease." Psychoneuroendocrinology **36**(3): 330-338.
Schobel, S. A., N. H. Chaudhury, U. A. Khan, B. Paniagua, M. A. Styner, I. Asllani, B. P. Inbar, C. M. Corcoran, J. A. Lieberman, H. Moore and S. A. Small (2013). "Imaging patients with psychosis and a mouse model establishes a spreading pattern of hippocampal dysfunction and implicates glutamate as a driver." Neuron **78**(1): 81-93.
Schwartz, T. L., S. Sachdeva and S. M. Stahl (2012). "Glutamate neurocircuitry: theoretical underpinnings in schizophrenia." Front Pharmacol **3**: 195.
Schwenk, J., M. Metz, G. Zolles, R. Turecek, T. Fritzius, W. Bildl, E. Tarusawa, A. Kulik, A. Unger, K. Ivankova, R. Seddik, J. Y. Tiao, M. Rajalu, J. Trojanova, V. Rohde, M. Gassmann, U. Schulte, B. Fakler and B. Bettler (2010). "Native GABA(B) receptors are heteromultimers with a family of auxiliary subunits." Nature **465**(7295): 231-235.
Seibenhener, M. L. and M. C. Wooten (2015). "Use of the Open Field Maze to measure locomotor and anxiety-like behavior in mice." Journal of visualized experiments : JoVE(96): e52434-e52434.
Seifart, K. and C. Sekeris (1969). "α Amanitin, a specific inhibitor of transcription by mammalian RNA-polymerase." Zeitschrift für Naturforschung B **24**(12): 1538-1544.
Sezen, H., H. Kandemir, E. Savik, S. Basmacı Kandemir, F. Kilicaslan, H. Bilinc and N. Aksoy (2016). "Increased oxidative stress in children with attention deficit hyperactivity disorder." Redox Rep **21**(6): 248-253.
Sibley, D. R. (1999). "New insights into dopaminergic receptor function using antisense and genetically altered animals." Annu Rev Pharmacol Toxicol **39**: 313-341.
Silva, L. M. and N. Stergiou (2020). Chapter 7 - The basics of gait analysis. Biomechanics and Gait Analysis. N. Stergiou, Academic Press**:** 225-250.
Silver, D. P. and D. M. Livingston (2001). "Self-excising retroviral vectors encoding the Cre recombinase overcome Cre-mediated cellular toxicity." Mol Cell **8**(1): 233-243.
Silverdale, M. A., C. Kobylecki, L. Kass-Iliyya, P. Martinez-Martin, M. Lawton, S. Cotterill, K. R. Chaudhuri, H. Morris, F. Baig, N. Williams, L. Hubbard, M. T. Hu and D. G. Grosset (2018). "A detailed clinical study of pain in 1957 participants with early/moderate Parkinson's disease." Parkinsonism Relat Disord **56**: 27-32.
Slobodin, O. and M. Davidovitch (2019). "Gender Differences in Objective and Subjective Measures of ADHD Among Clinic-Referred Children." Frontiers in Human Neuroscience **13**.

Steen, R. G., C. Mull, R. McClure, R. M. Hamer and J. A. Lieberman (2006). "Brain volume in first-episode schizophrenia: Systematic review and meta-analysis of magnetic resonance imaging studies." British Journal of Psychiatry **188**(6): 510-518.
Steimer, T. (2002). "The biology of fear- and anxiety-related behaviors." Dialogues Clin Neurosci **4**(3): 231-249.
Stein, D. J. and C. Bouwer (1997). "A neuro-evolutionary approach to the anxiety disorders." Journal of Anxiety Disorders **11**(4): 409-429.
Stępnicki, P., M. Kondej and A. A. Kaczor (2018). "Current concepts and treatments of schizophrenia." Molecules **23**(8): 2087.
Sun, S., W. Zhang, X. Chen, Y. Peng and Q. Chen (2015). "A complex insertion/deletion polymorphism in the compositionally biased region of the ZFHX3 gene in patients with coronary heart disease in a Chinese population." Int J Clin Exp Med **8**(5): 7890-7897.
Sun, S., W. Zhang, X. Chen and H. Song (2015). "The CAA repeat polymorphism in the ZFHX3 gene is associated with risk of coronary heart disease in a Chinese population." Tohoku J Exp Med **235**(4): 261-266.
Sun, X., H. F. Frierson, C. Chen, C. Li, Q. Ran, K. B. Otto, B. L. Cantarel, R. L. Vessella, A. C. Gao, J. Petros, Y. Miura, J. W. Simons and J. T. Dong (2005). "Frequent somatic mutations of the transcription factor ATBF1 in human prostate cancer." Nat Genet **37**(4): 407-412.
Sun, X., X. Fu, J. Li, C. Xing, D. W. Martin, H. H. Zhang, Z. Chen and J. T. Dong (2012). "Heterozygous deletion of Atbf1 by the Cre-loxP system in mice causes preweaning mortality." Genesis **50**(11): 819-827.
Sun, X., J. Li, G. Sica, S. Q. Fan, Y. Wang, Z. Chen, S. Muller, Z. G. Chen, X. Fu, X. Y. Dong, P. Guo, D. M. Shin and J. T. Dong (2013). "Interruption of nuclear localization of ATBF1 during the histopathologic progression of head and neck squamous cell carcinoma." Head Neck **35**(7): 1007-1014.
Szklarczyk, D., A. L. Gable, K. C. Nastou, D. Lyon, R. Kirsch, S. Pyysalo, N. T. Doncheva, M. Legeay, T. Fang, P. Bork, L. J. Jensen and C. von Mering (2021). "The STRING database in 2021: customizable protein-protein networks, and functional characterization of user-uploaded gene/measurement sets." Nucleic Acids Res **49**(D1): D605-d612.
Tang, D. L., Y. W. Luan, C. Y. Zhou and C. Xiao (2021). "D2 receptor activation relieves pain hypersensitivity by inhibiting superficial dorsal horn neurons in parkinsonian mice." Acta Pharmacol Sin **42**(2): 189-198.
Töle, J. (2014). Sagittal section of a mouse brain. https://commons.wikimedia.org/, Wikimedia.
Traynelis, S. F., L. P. Wollmuth, C. J. McBain, F. S. Menniti, K. M. Vance, K. K. Ogden, K. B. Hansen, H. Yuan, S. J. Myers and R. Dingledine (2010). "Glutamate Receptor Ion Channels: Structure, Regulation, and Function." Pharmacological Reviews **62**(3): 405-496.
Tsai, C. T., C. S. Hsieh, S. N. Chang, E. Y. Chuang, J. M. Juang, L. Y. Lin, L. P. Lai, J. J. Hwang, F. T. Chiang and J. L. Lin (2015). "Next-generation sequencing of nine atrial fibrillation candidate genes identified novel de novo mutations in patients with extreme trait of atrial fibrillation." J Med Genet **52**(1): 28-36.
Turcot, V., Y. Lu, H. M. Highland, C. Schurmann, A. E. Justice, R. S. Fine, J. P. Bradfield, T. Esko, A. Giri, M. Graff, X. Guo, A. E. Hendricks, T. Karaderi, A. Lempradl, A. E. Locke, A. Mahajan, E. Marouli, S. Sivapalaratnam, K. L. Young, T. Alfred, M. F. Feitosa, N. G. D. Masca, A. K. Manning, C. Medina-Gomez, P. Mudgal, M. C. Y. Ng, A. P. Reiner, S. Vedantam, S. M. Willems, T. W. Winkler, G. Abecasis, K. K. Aben, D. S. Alam, S. E. Alharthi, M. Allison, P. Amouyel, F. W. Asselbergs, P. L. Auer, B. Balkau, L. E. Bang, I. Barroso, L. Bastarache, M. Benn, S. Bergmann, L. F. Bielak, M. Bluher, M. Boehnke, H. Boeing, E. Boerwinkle, C. A. Boger, J. Bork-Jensen, M. L. Bots, E. P. Bottinger, D. W. Bowden, I. Brandslund, G. Breen, M. H. Brilliant, L. Broer, M. Brumat, A. A. Burt, A. S. Butterworth, P. T. Campbell, S. Cappellani, D. J. Carey, E. Catamo, M. J. Caulfield, J. C. Chambers, D. I. Chasman, Y. I. Chen, R. Chowdhury, C. Christensen, A. Y. Chu, M. Cocca, F. S. Collins, J. P. Cook, J. Corley, J. Corominas Galbany, A. J. Cox, D. S. Crosslin, G. Cuellar-Partida, A. D'Eustacchio,

J. Danesh, G. Davies, P. I. W. Bakker, M. C. H. Groot, R. Mutsert, I. J. Deary, G. Dedoussis, E. W. Demerath, M. Heijer, A. I. Hollander, H. M. Ruijter, J. G. Dennis, J. C. Denny, E. Di Angelantonio, F. Drenos, M. Du, M. P. Dube, A. M. Dunning, D. F. Easton, T. L. Edwards, D. Ellinghaus, P. T. Ellinor, P. Elliott, E. Evangelou, A. E. Farmaki, I. S. Farooqi, J. D. Faul, S. Fauser, S. Feng, E. Ferrannini, J. Ferrieres, J. C. Florez, I. Ford, M. Fornage, O. H. Franco, A. Franke, P. W. Franks, N. Friedrich, R. Frikke-Schmidt, T. E. Galesloot, W. Gan, I. Gandin, P. Gasparini, J. Gibson, V. Giedraitis, A. P. Gjesing, P. Gordon-Larsen, M. Gorski, H. J. Grabe, S. F. A. Grant, N. Grarup, H. L. Griffiths, M. L. Grove, V. Gudnason, S. Gustafsson, J. Haessler, H. Hakonarson, A. R. Hammerschlag, T. Hansen, K. M. Harris, T. B. Harris, A. T. Hattersley, C. T. Have, C. Hayward, L. He, N. L. Heard-Costa, A. C. Heath, I. M. Heid, O. Helgeland, J. Hernesniemi, A. W. Hewitt, O. L. Holmen, G. K. Hovingh, J. M. M. Howson, Y. Hu, P. L. Huang, J. E. Huffman, M. A. Ikram, E. Ingelsson, A. U. Jackson, J. H. Jansson, G. P. Jarvik, G. B. Jensen, Y. Jia, S. Johansson, M. E. Jorgensen, T. Jorgensen, J. W. Jukema, B. Kahali, R. S. Kahn, M. Kahonen, P. R. Kamstrup, S. Kanoni, J. Kaprio, M. Karaleftheri, S. L. R. Kardia, F. Karpe, S. Kathiresan, F. Kee, L. A. Kiemeney, E. Kim, H. Kitajima, P. Komulainen, J. S. Kooner, C. Kooperberg, T. Korhonen, P. Kovacs, H. Kuivaniemi, Z. Kutalik, K. Kuulasmaa, J. Kuusisto, M. Laakso, T. A. Lakka, D. Lamparter, E. M. Lange, L. A. Lange, C. Langenberg, E. B. Larson, N. R. Lee, T. Lehtimaki, C. E. Lewis, H. Li, J. Li, R. Li-Gao, H. Lin, K. H. Lin, L. A. Lin, X. Lin, L. Lind, J. Lindstrom, A. Linneberg, C. T. Liu, D. J. Liu, Y. Liu, K. S. Lo, A. Lophatananon, A. J. Lotery, A. Loukola, J. Luan, S. A. Lubitz, L. P. Lyytikainen, S. Mannisto, G. Marenne, A. L. Mazul, M. I. McCarthy, R. McKean-Cowdin, S. E. Medland, K. Meidtner, L. Milani, V. Mistry, P. Mitchell, K. L. Mohlke, L. Moilanen, M. Moitry, G. W. Montgomery, D. O. Mook-Kanamori, C. Moore, T. A. Mori, A. D. Morris, A. P. Morris, M. Muller-Nurasyid, P. B. Munroe, M. A. Nalls, N. Narisu, C. P. Nelson, M. Neville, S. F. Nielsen, K. Nikus, P. R. Njolstad, B. G. Nordestgaard, D. R. Nyholt, J. R. O'Connel, M. L. O'Donoghue, L. M. Olde Loohuis, R. A. Ophoff, K. R. Owen, C. J. Packard, S. Padmanabhan, C. N. A. Palmer, N. D. Palmer, G. Pasterkamp, A. P. Patel, A. Pattie, O. Pedersen, P. L. Peissig, G. M. Peloso, C. E. Pennell, M. Perola, J. A. Perry, J. R. B. Perry, T. H. Pers, T. N. Person, A. Peters, E. R. B. Petersen, P. A. Peyser, A. Pirie, O. Polasek, T. J. Polderman, H. Puolijoki, O. T. Raitakari, A. Rasheed, R. Rauramaa, D. F. Reilly, F. Renstrom, M. Rheinberger, P. M. Ridker, J. D. Rioux, M. A. Rivas, D. J. Roberts, N. R. Robertson, A. Robino, O. Rolandsson, I. Rudan, K. S. Ruth, D. Saleheen, V. Salomaa, N. J. Samani, Y. Sapkota, N. Sattar, R. E. Schoen, P. J. Schreiner, M. B. Schulze, R. A. Scott, M. P. Segura-Lepe, S. H. Shah, W. H. Sheu, X. Sim, A. J. Slater, K. S. Small, A. V. Smith, L. Southam, T. D. Spector, E. K. Speliotes, J. M. Starr, K. Stefansson, V. Steinthorsdottir, K. E. Stirrups, K. Strauch, H. M. Stringham, M. Stumvoll, L. Sun, P. Surendran, A. J. Swift, H. Tada, K. E. Tansey, J. C. Tardif, K. D. Taylor, A. Teumer, D. J. Thompson, G. Thorleifsson, U. Thorsteinsdottir, B. H. Thuesen, A. Tonjes, G. Tromp, S. Trompet, E. Tsafantakis, J. Tuomilehto, A. Tybjaerg-Hansen, J. P. Tyrer, R. Uher, A. G. Uitterlinden, M. Uusitupa, S. W. Laan, C. M. Duijn, N. Leeuwen, J. van Setten, M. Vanhala, A. Varbo, T. V. Varga, R. Varma, D. R. Velez Edwards, S. H. Vermeulen, G. Veronesi, H. Vestergaard, V. Vitart, T. F. Vogt, U. Volker, D. Vuckovic, L. E. Wagenknecht, M. Walker, L. Wallentin, F. Wang, C. A. Wang, S. Wang, Y. Wang, E. B. Ware, N. J. Wareham, H. R. Warren, D. M. Waterworth, J. Wessel, H. D. White, C. J. Willer, J. G. Wilson, D. R. Witte, A. R. Wood, Y. Wu, H. Yaghootkar, J. Yao, P. Yao, L. M. Yerges-Armstrong, R. Young, E. Zeggini, X. Zhan, W. Zhang, J. H. Zhao, W. Zhao, W. Zhao, W. Zhou, K. T. Zondervan, J. I. Rotter, J. A. Pospisilik, F. Rivadeneira, I. B. Borecki, P. Deloukas, T. M. Frayling, G. Lettre, K. E. North, C. M. Lindgren, J. N. Hirschhorn and R. J. F. Loos (2018). "Protein-altering variants associated with body mass index implicate pathways that control energy intake and expenditure in obesity." Nat Genet **50**(1): 26-41.

Turrens, J. F. (2003). "Mitochondrial formation of reactive oxygen species." The Journal of physiology **552**(2): 335-344.

Turunen, M., J. Olsson and G. Dallner (2004). "Metabolism and function of coenzyme Q." Biochimica et Biophysica Acta (BBA) - Biomembranes **1660**(1): 171-199.

Tzschentke, T. M. (2001). "Pharmacology and behavioral pharmacology of the mesocortical dopamine system." Progress in Neurobiology **63**(3): 241-320.

Ubhi, M., K. Achinivu, S. Seri and A. E. Cavanna (2020). "Motor stereotypies in adult patients with Tourette syndrome." Future Neurology **15**(2): FNL42.
Uhm, K. O., M. J. Kim, M. Kawaguchi, H. Akatsu, Y. Miura, S. Misumi, H. Hida, E. K. Choi, Y. S. Kim, M. Michikawa and C. G. Jung (2015). "ATBF1 is a novel amyloid-beta protein precursor (AbetaPP) binding protein that affects AbetaPP expression." J Alzheimers Dis **43**(1): 243-257.
Ujita, W., A. Kohyama-Koganeya, N. Endo, T. Saito and H. Oyama (2018). "Mice lacking a functional NMDA receptor exhibit social subordination in a group-housed environment." The FEBS journal **285**(1): 188-196.
van Duijn, E., E. M. Kingma and R. C. van der Mast (2007). "Psychopathology in verified Huntington's disease gene carriers." J Neuropsychiatry Clin Neurosci **19**(4): 441-448.
Vannini, A. and P. Cramer (2012). "Conservation between the RNA Polymerase I, II, and III Transcription Initiation Machineries." Molecular Cell **45**(4): 439-446.
Verma, P., A. Singh, D. N. Nthenge-Ngumbau, U. Rajamma, S. Sinha, K. Mukhopadhyay and K. P. Mohanakumar (2016). "Attention deficit-hyperactivity disorder suffers from mitochondrial dysfunction." BBA Clin **6**: 153-158.
Vinothkumar, K. R., J. Zhu and J. Hirst (2014). "Architecture of mammalian respiratory complex I." Nature **515**(7525): 80-84.
Volkow, N. D., G.-J. Wang, S. H. Kollins, T. L. Wigal, J. H. Newcorn, F. Telang, J. S. Fowler, W. Zhu, J. Logan, Y. Ma, K. Pradhan, C. Wong and J. M. Swanson (2009). "Evaluating Dopamine Reward Pathway in ADHD: Clinical Implications." JAMA **302**(10): 1084-1091.
Vonsattel, J.-P., R. H. Myers, T. J. Stevens, R. J. Ferrante, E. D. Bird and E. P. Richardson (1985). "Neuropathological classification of Huntington's disease." Journal of Neuropathology & Experimental Neurology **44**(6): 559-577.
Waddell, J., R. W. Morris and M. E. Bouton (2006). "Effects of bed nucleus of the stria terminalis lesions on conditioned anxiety: aversive conditioning with long-duration conditional stimuli and reinstatement of extinguished fear." Behav Neurosci **120**(2): 324-336.
Wajszilber, D., J. A. Santiseban and R. Gruber (2018). "Sleep disorders in patients with ADHD: impact and management challenges." Nat Sci Sleep **10**: 453-480.
Walker, C. J., M. A. Miranda, M. J. O'Hern, J. P. McElroy, K. R. Coombes, R. Bundschuh, D. E. Cohn, D. G. Mutch and P. J. Goodfellow (2015). "Patterns of CTCF and ZFHX3 Mutation and Associated Outcomes in Endometrial Cancer." J Natl Cancer Inst **107**(11).
Wang, J., Z. L. Liu and B. Chen (2001). "Association study of dopamine D2, D3 receptor gene polymorphisms with motor fluctuations in PD." Neurology **56**(12): 1757-1759.
Watanabe, M., Y. Miura, A. Ido, M. Sakai, S. Nishi, Y. Inoue, T. Hashimoto and T. Tamaoki (1996). "Developmental changes in expression of the ATBF1 transcription factor gene." Molecular Brain Research **42**(2): 344-349.
Weinmann, R. and R. G. Roeder (1974). "Role of DNA-dependent RNA polymerase III in the transcription of the tRNA and 5S RNA genes." Proceedings of the National Academy of Sciences **71**(5): 1790-1794.
Wilcox, A. G., R. S. Bains, D. Williams, E. Joynson, L. Vizor, P. L. Oliver, E. S. Maywood, M. H. Hastings, G. Banks and P. M. Nolan (2021). "Zfhx3-mediated genetic ablation of the SCN abolishes light entrainable circadian activity while sparing food anticipatory activity." iScience **24**(10): 103142.
Wilcox, A. G., L. Vizor, M. J. Parsons, G. Banks and P. M. Nolan (2017). "Inducible Knockout of Mouse Zfhx3 Emphasizes Its Key Role in Setting the Pace and Amplitude of the Adult Circadian Clock." Journal of biological rhythms **32**(5): 433-443.
Williams, O. O. F., M. Coppolino, S. R. George and M. L. Perreault (2021). "Sex Differences in Dopamine Receptors and Relevance to Neuropsychiatric Disorders." Brain Sci **11**(9).
Wolf, A., B. Bauer, E. L. Abner, T. Ashkenazy-Frolinger and A. M. Hartz (2016). "A Comprehensive Behavioral Test Battery to Assess Learning and Memory in 129S6/Tg2576 Mice." PLoS One **11**(1): e0147733.

Woodruff-Pak, D. S. (2010). Memory and Aging, Neural Basis of. Encyclopedia of Behavioral Neuroscience. G. F. Koob, M. L. Moal and R. F. Thompson. Oxford, Academic Press**:** 200-205.
Yaguchi, M., Y. Ohashi, T. Tsubota, A. Sato, K. W. Koyano, N. Wang and Y. Miyashita (2013). "Characterization of the properties of seven promoters in the motor cortex of rats and monkeys after lentiviral vector-mediated gene transfer." Hum Gene Ther Methods **24**(6): 333-344.
Yamaguchi, Y., Y. A. Lee, A. Kato and Y. Goto (2017). "The Roles of Dopamine D1 Receptor on the Social Hierarchy of Rodents and Nonhuman Primates." Int J Neuropsychopharmacol **20**(4): 324-335.
Yamaguchi, Y., Y. A. Lee, A. Kato, E. Jas and Y. Goto (2017). "The Roles of Dopamine D2 Receptor in the Social Hierarchy of Rodents and Primates." Sci Rep **7**: 43348.
Yan, L., I. Karatsoreos, J. LeSauter, D. Welsh, S. Kay, D. Foley and R. Silver (2007). Exploring spatiotemporal organization of SCN circuits. Cold Spring Harbor symposia on quantitative biology, Cold Spring Harbor Laboratory Press.
Yang, S. A. (2017). "Association study between ZFHX3 gene polymorphisms and obesity in Korean population." J Exerc Rehabil **13**(4): 491-494.
Yasuda, H., A. Mizuno, T. Tamaoki and T. Morinaga (1994). "ATBF1, a Multiple-Homeodomain Zinc Finger Protein, Selectively Down-Regulates AT-Rich Elements of the Human oL-Fetoprotein Gene." Molecular and Cellular Biology **14**(2): 1395-1401.
Youn, J. Y., J. Zhang, Y. Zhang, H. Chen, D. Liu, P. Ping, J. N. Weiss and H. Cai (2013). "Oxidative stress in atrial fibrillation: an emerging role of NADPH oxidase." J Mol Cell Cardiol **62**: 72-79.
Yung, W. H., M. A. Häusser and J. J. Jack (1991). "Electrophysiology of dopaminergic and non-dopaminergic neurones of the guinea-pig substantia nigra pars compacta in vitro." J Physiol **436**: 643-667.
Zangrossi, H., Jr. and S. E. File (1992). "Behavioral consequences in animal tests of anxiety and exploration of exposure to cat odor." Brain Res Bull **29**(3-4): 381-388.
Zhang, J., N. Zhou, A. Lin, P. Luo, X. Chen, H. Deng, S. Kang, L. Guo, W. Zhu and J. Zhang (2021). "ZFHX3 mutation as a protective biomarker for immune checkpoint blockade in non-small cell lung cancer." Cancer Immunol Immunother **70**(1): 137-151.
Zhang, K., C. J. Grady, E. M. Tsapakis, S. L. Andersen, F. I. Tarazi and R. J. Baldessarini (2004). "Regulation of Working Memory by Dopamine D4 Receptor in Rats." Neuropsychopharmacology **29**(9): 1648-1655.
Zhang, X., J. Q. Wan and X. P. Tong (2018). "Potassium channel dysfunction in neurons and astrocytes in Huntington's disease." CNS Neurosci Ther **24**(4): 311-318.
Zhang, Z., H. Yamashita, T. Toyama, H. Sugiura, Y. Ando, K. Mita, M. Hamaguchi, M. Kawaguchi, Y. Miura and H. Iwase (2005). "ATBF1-a messenger RNA expression is correlated with better prognosis in breast cancer." Clin Cancer Res **11**(1): 193-198.
Zhao, R. Z., S. Jiang, L. Zhang and Z. B. Yu (2019). "Mitochondrial electron transport chain, ROS generation and uncoupling (Review)." Int J Mol Med **44**(1): 3-15.
Zhou, T., H. Zhu, Z. Fan, F. Wang, Y. Chen, H. Liang, Z. Yang, L. Zhang, L. Lin and Y. Zhan (2017). "History of winning remodels thalamo-PFC circuit to reinforce social dominance." Science **357**(6347): 162-168.
Zhuang, X., J. Masson, J. A. Gingrich, S. Rayport and R. Hen (2005). "Targeted gene expression in dopamine and serotonin neurons of the mouse brain." J Neurosci Methods **143**(1): 27-32.
Zipursky, R. B., T. J. Reilly and R. M. Murray (2013). "The myth of schizophrenia as a progressive brain disease." Schizophr Bull **39**(6): 1363-1372.
Zylber, E. A. and S. Penman (1971). "Products of RNA polymerases in HeLa cell nuclei." Proceedings of the National Academy of Sciences **68**(11): 2861-2865.